

Review

One Stone, Three Birds: Innovations and Challenges of Layered Double Hydroxides in Batteries, Supercapacitors, and Hydrogen Production

Syed Shaheen Shah *, Manisha Das  and Takaya Ogawa *

Socio-Environmental Energy Science Department, Graduate School of Energy Science, Kyoto University, Yoshida-Honmachi, Sakyo-Ku, Kyoto 606-8501, Japan; nisha.ma.25s@st.kyoto-u.ac.jp

* Correspondence: shah.syedshaheen.3d@kyoto-u.ac.jp (S.S.S.); ogawa.takaya.8s@kyoto-u.ac.jp (T.O.)

Abstract: Layered double hydroxides (LDHs), notable for their unique two-dimensional layered structures, have attracted significant research attention due to their exceptional versatility and promising performance in energy storage and conversion applications. This comprehensive review systematically addresses the fundamentals and diverse synthesis strategies for LDHs, including co-precipitation, hydrothermal synthesis, electrochemical deposition, sol-gel processes, ultrasonication, and exfoliation techniques. The synthesis methods profoundly influence the physicochemical properties, morphology, and electrochemical performance of LDHs, necessitating a detailed understanding to optimize their applications. In this paper, the role of LDHs in batteries, supercapacitors, and hydrogen production is critically evaluated. We discuss their incorporation in various battery systems, such as lithium-ion, lithium–sulfur, sodium-ion, chloride-ion, zinc-ion, and zinc–air batteries, highlighting their structural and electrochemical advantages. Additionally, the superior pseudocapacitive behavior and high energy densities offered by LDHs in supercapacitors are elucidated. The effectiveness of LDHs in hydrogen production, particularly through electrocatalytic water splitting, underscores their significance in renewable energy systems. This review paper uniquely integrates these three pivotal energy technologies, outlining current innovations and challenges, thus fulfilling a critical need for the scientific community by providing consolidated insights and guiding future research directions.



Academic Editors: Kangyu Zou,
Tianjing Wu and Jiangmin Jiang

Received: 10 April 2025

Revised: 28 April 2025

Accepted: 9 May 2025

Published: 14 May 2025

Citation: Shah, S.S.; Das, M.; Ogawa, T. One Stone, Three Birds: Innovations and Challenges of Layered Double Hydroxides in Batteries, Supercapacitors, and Hydrogen Production. *Batteries* **2025**, *11*, 193. <https://doi.org/10.3390/batteries11050193>

Copyright: © 2025 by the authors. Licensee MDPI, Basel, Switzerland. This article is an open access article distributed under the terms and conditions of the Creative Commons Attribution (CC BY) license (<https://creativecommons.org/licenses/by/4.0/>).

1. Introduction

Layered double hydroxides (LDHs), known as hydrotalcite-like compounds or anionic clays, represent a versatile class of two-dimensional nanostructured materials characterized by their unique layered architecture and compositional tunability [1–4]. Structurally, LDHs are composed of positively charged metal hydroxide layers balanced by interlayer anions and water molecules, forming a stacked, sandwich-like configuration. The general chemical formula of LDHs is expressed as $[M(II)_{1-x}M(III)_x(OH)_2]^{x+}(A^{n-})_{x/n}\cdot mH_2O$, where M(II) and M(III) denote divalent and trivalent metal cations, respectively, and A^{n-} represents exchangeable interlayer anions [5]. This intrinsic flexibility in structure and composition has made LDHs attractive candidates for various scientific and industrial applications, especially in energy storage, conversion, and environmental remediation.

The urgent global demand for efficient, sustainable energy technologies has intensified research into materials that enhance performance in batteries, supercapacitors, and hydro-

gen production systems [4,6]. LDHs have emerged as promising materials due to their advantageous properties, including high specific surface area, tunable interlayer chemistry, rich redox-active sites, and robust electrochemical stability [7]. These features improve ion mobility, energy storage capacity, and catalytic efficiency. In battery technologies, especially those supporting electric vehicles and large-scale energy storage, materials with high energy density, long cycle life, and stable charge/discharge behavior are essential [8]. LDHs have demonstrated substantial potential to meet these requirements. Their layered structure facilitates efficient ion transport, while their ability to accommodate multiple metal cations and interlayer species enables tailored electrochemical properties. Moreover, the hybridization of LDHs with carbon-based materials such as graphene and carbon nanotubes (CNTs) further enhances electrical conductivity and structural integrity, thereby extending their practical utility in lithium-ion batteries (LIBs) and other emerging battery systems [9,10]. In addition to LIBs, LDHs have been applied in different battery chemistries, including lithium–sulfur batteries (LSBs), sodium-ion batteries (NIBs), chloride-ion batteries (CIBs), zinc-ion batteries (ZIBs), and zinc–air batteries (ZABs) [11–16]. In LSBs, LDHs help mitigate the polysulfide shuttle effect by effectively adsorbing and immobilizing dissolved polysulfides. Their high surface area and interlayer spacing also enhance sodium-ion diffusion in NIBs, which is critical for their energy storage performance. Furthermore, their incorporation into aqueous batteries, such as ZIB and ZAB systems, has improved rate capability and cyclic stability. LDHs also offer compelling advantages in supercapacitor applications, particularly due to their pseudocapacitive behavior [17]. Their electrochemical performance stems from fast and reversible surface redox reactions facilitated by the layered architecture that supports rapid ion transport. Consequently, LDHs exhibit high capacitance, fast charge/discharge rates, and long cycle life, making them suitable for high-power applications. Developing hybrid LDH materials, especially those combined with conductive polymers or carbon nanomaterials, has led to further energy and power density enhancements, expanding their practical viability in real-world devices [18,19]. Parallel to their electrochemical applications, LDHs have gained increasing recognition in hydrogen production, particularly through electrocatalytic water splitting [20]. Efficient and sustainable hydrogen generation depends on active, stable, and cost-effective catalysts for the hydrogen evolution reaction (HER) and oxygen evolution reaction (OER). LDHs, owing to their tunable composition and catalytic activity, have proven to be excellent candidates. Their performance can be further optimized by compositional modifications or integration with nanoparticles, semiconductors, or metal–organic frameworks (MOFs) to enhance electronic conductivity and surface reactivity [21–26].

The synthesis route plays a vital role in tailoring the physicochemical and electrochemical properties of LDHs. Conventional methods such as co-precipitation and hydrothermal synthesis have been widely adopted for their scalability and simplicity. Co-precipitation enables precise control over metal cation ratios and particle morphology, while hydrothermal methods offer improved crystallinity and uniform particle distribution [27]. Other advanced techniques, including electrochemical deposition, sol-gel processing, ultrasonication-assisted synthesis, and exfoliation, have shown promise in producing LDHs with higher surface areas, controlled nanoscale morphologies, and enhanced electrochemical behavior [28]. Furthermore, successfully doping various metal cations into LDH frameworks allows for the rational design of materials that address specific challenges in energy applications, such as conductivity limitations and ion diffusion barriers [29,30]. This adaptability highlights the strategic importance of synthesis optimization in maximizing LDH performance for targeted functionalities.

Beyond energy applications, LDHs also exhibit strong potential in environmental remediation due to their anion exchange capabilities and high chemical reactivity [31]. Recent advancements demonstrate that LDHs are pivotal in advancing circular economy principles and sustainable material practices. Researchers have significantly reduced environmental burdens while creating high-value functional materials by utilizing industrial by-products such as red mud, slag, and fly ash for LDH synthesis [32,33]. Waste-derived LDHs, particularly Ni-based variants, have shown remarkable efficiency in electrocatalysis for oxygen evolution reactions, simultaneously addressing waste valorization and promoting green hydrogen production [34]. In carbon capture, LDH-based photocatalysts facilitate CO₂ reduction to value-added chemicals under solar irradiation, supporting carbon circularity strategies [35]. Moreover, LDHs have been successfully applied in agriculture for controlled-release fertilizers, enhancing nutrient efficiency and minimizing environmental runoff [36]. These examples underscore the growing importance of LDHs in enabling resource recovery, pollution mitigation, and sustainable energy solutions, making them crucial materials in the transition toward greener technologies and closed-loop material systems. These characteristics make them effective in adsorbing pollutants, such as heavy metals and organic contaminants, from aqueous solutions. The dual functionality of LDHs as both energy materials and environmental agents underscores their relevance in supporting sustainability goals and circular economy models. In recent advancements, LDH-derived composite materials, especially those integrated with MOFs, have shown exceptional improvements in surface area, electron/ion transport pathways, and structural robustness [37]. These composites combine the best properties of both components, opening up new directions for multifunctional material systems capable of simultaneously addressing energy and environmental challenges.

LDHs have witnessed a significant surge in global research interest over the past decade due to their structural versatility and broad application potential. As of 2023, the global LDH market was valued at approximately USD 30.57 billion and is projected to reach USD 47.91 billion by 2032, growing at a compound annual growth rate (CAGR) of 5.12%. Research trends show that LDHs are extensively explored in biomedical fields (e.g., drug delivery, cancer therapy, and biosensors), environmental remediation (such as selenium and heavy metal removal from water), energy storage (as precursors for battery and supercapacitor electrodes), and catalytic applications. In the biomedical sector alone, there has been an average annual increase of ~8% in LDH-related publications between 2018 and 2024 [38]. Environmental applications are also expanding, with LDH-based materials achieving over 90% removal efficiencies for specific contaminants like selenium [39]. Research publications in LDH-based energy applications increased by over 250% between 2017 and 2023 (Scopus database). NiFe-LDHs are leading candidates for water splitting in electrocatalysis and hydrogen production with doping strategies (e.g., Co, Mn, Cr) and interlayer anion modifications significantly boosting activity and stability [40]. LDHs are also increasingly explored in supercapacitors, where their pseudocapacitive behavior and fast ion diffusion are enhanced through hybridization with graphene and carbon nanotubes; this field has seen a CAGR of approximately 10% in publications over the past five years. In photocatalysis, LDH-based heterostructures such as LDH/TiO₂ and LDH/g-C₃N₄ composites are under intense study for solar-driven water splitting and CO₂ reduction, with key focus areas including bandgap tuning and charge carrier separation [41]. Furthermore, due to their high surface area and redox-active sites, calcined LDH-derived mixed metal oxides are increasingly used for Li-ion and Zn-air batteries [42]. Novel research also advances LDHs as hosts for anion intercalation batteries and fuel cell electrocatalysts for the ORR [43]. LDHs are at the center of next-generation energy technologies, driven by their structural flexibility, high activity, and earth-abundant composition. Future research

directions focus on designing magnetic or structurally modified LDHs for easier recovery and enhanced performance, aiming to expand their role in advanced catalysis, CO₂ capture, and sustainable technologies.

Despite the vast promise of LDHs, several challenges hinder their widespread application. These include their relatively low intrinsic electronic conductivity, structural degradation under prolonged electrochemical cycling, and difficulties scaling up industrial synthesis techniques. To overcome these limitations, continued efforts are required to understand the fundamental relationships between LDH structure, composition, and electrochemical performance. Addressing these gaps will be crucial to unlocking the full potential of LDHs across diverse energy technologies. This review provides a comprehensive overview of the recent progress and emerging trends in applying LDHs in energy-related fields. By systematically discussing the role of LDHs in batteries, supercapacitors, and hydrogen production, alongside synthesis strategies and hybrid material developments, this work aims to consolidate fragmented research findings and provide an integrated perspective. Although several recent reviews have discussed the role of LDHs in electrochemical applications [44–49], most have focused on individual systems or narrowly defined topics. This review uniquely integrates the applications of LDHs across batteries, supercapacitors, and hydrogen production within a single framework, offering a comprehensive and comparative analysis that highlights interconnections, emerging challenges, and future research opportunities. The focus on batteries, supercapacitors, and hydrogen production as application areas for LDHs stems from their central role in advancing clean energy technologies. These three domains, although distinct, share critical commonalities in their underlying electrochemical processes, including charge storage, ion transport, and surface redox reactions, processes where LDHs exhibit remarkable properties such as tunable composition, high surface area, and excellent ion exchange capabilities. The synergy among them is evident via the advancements in LDH-based electrode materials for batteries, which often directly inform the design strategies for supercapacitors, given the need for high conductivity and cycling stability. Similarly, the catalytic properties of LDHs that enhance HER are closely tied to the electron and ion mobility mechanisms essential for energy storage devices. Thus, studying these three applications together allows a more integrated understanding of how LDH structural tuning can optimize performance across multiple energy technologies, paving the way for multifunctional materials that can simultaneously address storage and generation needs. The review also identifies existing challenges and future research directions, offering valuable insights for advancing LDH-based technologies toward scalable and sustainable energy solutions.

2. Fundamentals of LDHs

LDHs, often called anionic clays or hydrotalcite-like materials, represent a unique class of compounds characterized by their layered structure and variable ionic composition. These materials have attracted considerable attention across various fields, including catalysis, energy storage, and environmental remediation, owing to their distinctive properties and potential applications [23,50–52]. LDHs adopt a general structural formula of $[M_{1-x}^{2+}M_x^{3+}(OH)_2]^{x+}(A^{n-})_{x/n}\cdot mH_2O$, where M²⁺ and M³⁺ are metal cations (i.e., divalent (e.g., Fe²⁺, Mg²⁺, Ni²⁺) and trivalent (e.g., Al³⁺, Fe³⁺, Cr³⁺), while Aⁿ⁻ denotes interlayer anions (such as CO₃²⁻, NO₃⁻, or Cl⁻) [5,40,50,53,54]. The schematic representation for LDH basic structures is shown in Figure 1a,b. The octahedral sheets formed by metal hydroxides create anionic layers that house exchangeable anions and water molecules within their interlayer spaces [51,52]. This unique structural arrangement provides a large surface area for adsorption and allows for easy intercalation of various anions, making LDHs versatile for numerous applications. LDHs can form various morphologies, the most

prominent being flower-like structures [55], as illustrated in Figure 1c. Different types of LDHs have been synthesized, including those based on magnesium–aluminum (MgAl), nickel–aluminum (NiAl), nickel–cobalt (NiCo), and zinc–aluminum (ZnAl) combinations. The versatility of LDHs is primarily attributed to the variety of cations that can exist in the mixed metal sheets, leading to a diverse range of properties and functionalities. For instance, the intercalation of anionic species can significantly affect the catalytic activity, thermal stability, and solubility of LDHs, tailoring their usability in specific applications [56–58]. One notable property of LDHs is their hydrophilic nature, which enhances their interaction with water and biological systems, making them suitable for drug delivery and biocompatibility applications [58,59]. Furthermore, LDHs exhibit excellent acid–base characteristics, which can be optimized for processes such as CO₂ capture and adsorption of pollutants from aqueous solutions [60,61]. For example, studies have shown that LDHs can effectively remove azo dyes and other organic contaminants from water through adsorption mechanisms [57,62,63]. In energy storage applications, LDHs have emerged as promising candidates for electrode materials in supercapacitors and batteries. Their layered structure allows for easy ion diffusion, essential for charge/discharge processes [64,65]. Research has demonstrated that LDH-based composites incorporating materials such as graphene can significantly enhance the performance and efficiency of energy storage devices [56,66]. This dual functionality as ion storage matrices and conductive frameworks bolsters their application relevance in renewable energy systems. Another significant aspect of LDHs is their utility in hydrogen production, particularly in catalysis. LDHs, when modified with transition metals such as nickel or cobalt, can serve as highly efficient electrocatalysts for water splitting, an essential reaction to produce hydrogen [67,68]. Incorporating these metals into the LDH framework improves catalytic activity due to increased surface area and enhanced electronic properties. Studies have revealed that such modified LDHs can maintain stability and activity over prolonged periods, making them suitable candidates for industrial applications [66,69]. Several examples highlight the utility and properties of specific LDHs. The MgAl-LDH, often synthesized through coprecipitation methods, has shown remarkable adsorption capabilities for various pollutants due to its high surface area and effective ion exchange properties [70,71]. Similarly, ZnAl-LDH composites have been used for effective dye removal owing to their favorable ion exchange capacities and adsorptive kinetics, demonstrating high removal rates in wastewater treatments [72,73]. Additionally, NiFe-LDHs have been utilized as electrocatalysts for HER, achieving commendable efficiencies and stability in alkaline electrolytes [67,68]. LDHs are a vital material with extensive applications in various fields, such as water purification, energy storage, and catalysis. Their unique structural and compositional characteristics allow for adaptable performance based on specific application requirements. This adaptability, coupled with ongoing research to optimize their properties, ensures continued advancements in the functionality and applicability of LDHs in enhancing environmental sustainability and energy efficiency [74–76].

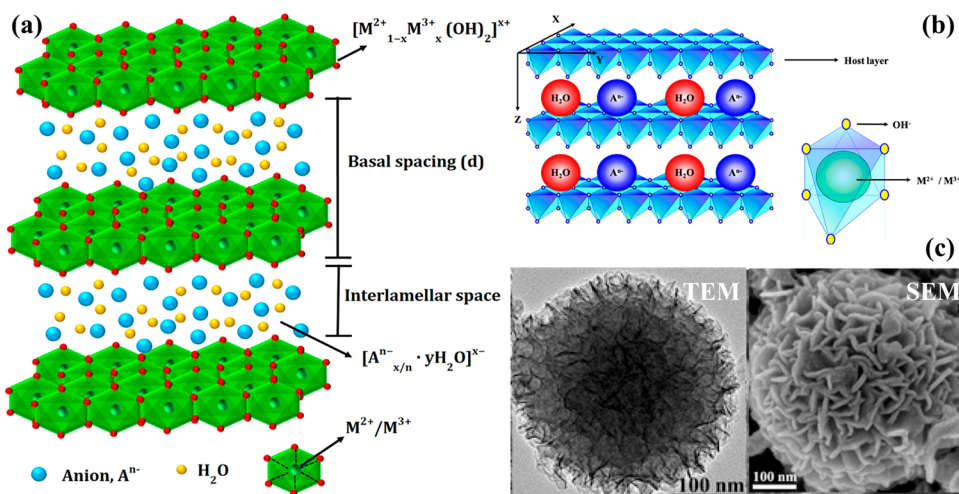


Figure 1. (a,b) Schematic representation for LDH structures. Reproduced with permission [77,78]. (c) TEM and FESEM images of LDH. Reproduced with permission [55].

The deployment of LDHs in practical applications faces several significant challenges, particularly when scaling up synthesis methods, ensuring stability during long-term operation, and addressing low intrinsic conductivity. These issues must be thoroughly examined and mitigated through ongoing research to realize the full potential of LDH-based materials in large-scale systems. One of the critical hurdles in deploying LDHs at scale is the synthesis methods employed. Traditional synthesis techniques often lack the efficiency required for large production. However, recent advancements, such as the “on-the-fly” synthesis method demonstrated by Mattera et al., utilize controlled microfluidic reaction/diffusion conditions to rapidly produce self-supported LDH hollow structures [79]. This technique not only enhances the scalability of production but also maintains the unique structural characteristics of LDHs, potentially overcoming current limitations in synthesis yields and uniformity. Furthermore, the separate nucleation and aging steps method has been explored, providing additional strategies for scalable synthesis while maintaining the structural integrity and performance of the resulting LDHs [80]. Stability under operational conditions represents another significant concern for the practical application of LDHs. The structural integrity of LDH materials can degrade over time in various environments, particularly in aqueous solutions, where traditional LDH configurations may disintegrate [81]. Research focusing on hybrid materials that combine LDHs with conductive carbon matrices has shown promising results. Integrating LDHs with conductive materials significantly enhances their electrochemical performance and stability over extended periods [82]. Moreover, innovative designs, such as incorporating porous structures into LDH composites, exhibit improved performance metrics, addressing the inherent limitations of LDHs regarding durability and efficiency [83]. The intrinsic low conductivity of LDHs is a well-documented limitation that impedes their performance in many electrochemical applications. Recent studies indicate that hybrid LDH composites, such as those combined with conductive polymers or carbon-based materials, can ameliorate these issues [84,85]. The enhancement of electric conductivity through these composites and the careful design of the pore structure allow for better electrolyte penetration and lower charge transfer resistance, significantly boosting the electrochemical activity of LDH-based systems [86]. Hybrid LDH–polymer membranes have also demonstrated substantial improvements in permeability and selectivity for CO_2 separation, showcasing their potential for real-world applications while addressing the conductivity concerns inherent to traditional LDH materials [87]. Significant strides have been made in addressing the challenges of deploying LDH-based materials. Innovations in synthesis techniques, material design,

and stability enhancements are crucial to overcoming these barriers. Continued research will be essential to refine these approaches further and ensure that LDHs can fulfil their promise in large-scale applications.

3. Synthesis Methods of LDHs

LDHs can be synthesized through various methods, each significantly influencing their structural, morphological, and functional properties. Common synthesis techniques include the co-precipitation method [88], valued for its simplicity and scalability, typically producing LDHs with uniform morphology and high purity; hydrothermal synthesis [89], favored for precise control over crystallinity and particle size, resulting in materials with enhanced thermal stability; and electrochemical deposition [90], advantageous for fabricating thin films with controllable thickness and adherence. Advanced techniques such as sol-gel, ultrasonication, and exfoliation offer further control over LDH structures; the sol-gel approach produces highly homogeneous and porous LDHs, ultrasonication facilitates smaller particle sizes and improved dispersion, while exfoliation allows isolation of single-layer nanosheets with exceptional surface activity [23]. Figure 2 depicts the structural framework of LDHs, highlighting common synthesis methods and their wide-ranging applications. Overall, the choice of synthesis method profoundly affects LDHs' properties, including crystallinity, surface area, porosity, interlayer spacing, and electrochemical performance, thus determining their suitability for diverse applications like batteries, supercapacitors, and catalysis.

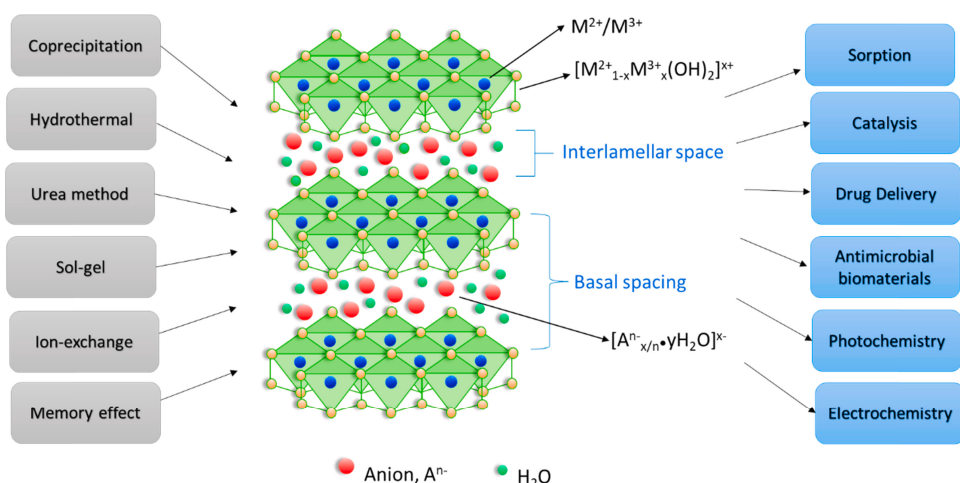


Figure 2. Schematic illustration of the synthesis methods, layered structure, and diverse applications of LDHs. Reproduced with permission [91].

3.1. Co-Precipitation

The co-precipitation method is a widely utilized synthesis technique for LDHs. This method involves the simultaneous precipitation of two or more metal salts from an aqueous solution in a specific pH-controlled environment. The goal is to create a solid precipitate comprising cations with differing oxidation states that can form a layered structure upon aging and further processing. The co-precipitation approach offers advantages such as simplicity, cost-efficiency, and the capability of producing homogeneous materials [92,93]. The fundamental mechanism underlying the co-precipitation of LDHs includes the generation of hydroxides by reacting an alkaline solution (e.g., sodium hydroxide) with metal salt solutions. When mixed, metal ions, typically divalent metals (M^{2+}) and trivalent metals (M^{3+}), condense to form brucite-like sheets, a precursor structure of LDHs. The excess positive charge of the brucite-like layers is balanced by the intercalation of anions within

the interlayer spacing, such as carbonate, nitrate, or organic molecules [94,95]. Thus, the co-precipitation method is fundamental for synthesizing LDHs with diverse properties suitable for various applications, including catalysis, ion exchange, and drug delivery systems [96,97].

Recent advancements in solid-state reactions have revealed numerous strategies for improving the structural and morphological qualities of LDHs synthesized via the co-precipitation method. For instance, a meticulous study by Wijitwongwan et al. [98] demonstrated that varying layer charge densities effectively alter the microstructure and performance of NiFe-LDH. Similarly, Zhang et al. [99] expounded on the preparation of chromium-modified ultrathin CoFe-LDH, noting that enhanced electrocatalytic performance can be attributed to its nanosheet structure, achieved efficiently through the co-precipitation route. Additionally, other research has indicated the potential for co-precipitation in the fabrication of ZnAl-LDH, particularly in enhancing the corrosion protection of steel-reinforced concrete. This study determined that the layering structure includes intercalated organic anions, which augment the protective qualities of the resulting material [88,98]. Their findings emphasize the importance of co-precipitation in producing multifunctional layered structures designed for specific engineering applications. In the domain of catalysis, the co-precipitation method allows for creating various catalytic layered materials with particular properties tailored for high activity. For example, NiAl-LDHs synthesized via the co-precipitation method exhibited significant electrochemical activity and stability, making them suitable candidates for application in batteries and supercapacitors [96,99]. The correlation between the morphology of LDHs and their catalytic behaviors has been systematically reviewed, indicating that factors such as particle size, crystallinity, and layering impact performance significantly [92,100]. Furthermore, approaches involving the hybridization of various LDH materials have emerged, expanding the range of applications and performance metrics of these materials. For instance, research has explored Co–Ni–Fe oxyhydroxide composites synthesized via co-precipitation, modifying their catalytic capabilities for various reactions [101]. These hybrid systems demonstrate that co-precipitation can yield single-component LDHs and complex multi-component systems with advanced functionality [97]. Ongoing studies focus on optimizing synthesis parameters to enhance performance metrics. Key considerations include the concentration of metal salts, pH level, temperature, and stirring conditions during synthesis. Attempts to generate various forms of zinc–Al LDHs have shown that altering these conditions can lead to significant variations in structural integrity and interlayer spacing, characterized through advanced spectroscopy techniques [93,102]. The versatility of the co-precipitation method is evident in its application; in a recent study exploring hybrid nanoparticles, the uniformity and dispersion of mesoporous ZnAl-LDHs were ensured by carefully controlling synthesis parameters [93,103]. Innovative adaptations of the co-precipitation method, including using surfactants and polymers as structure-directing agents, have progressively unlocked pathways for producing new LDH varieties with tailored layer spacing and enhanced chemical reactivity [96,104].

Thorough examinations have also been directed at using co-precipitation to produce nanostructured materials like mesoporous catalysts. For example, Zhang et al. [99] elucidated the synthesis of cobalt-LDH nanostructures displaying significant efficacy in HER. The nanosheet morphology achieved through co-precipitation allows for higher surface area and better catalytic performance than bulk materials [99,105]. The emergence of LDHs as effective adsorbents for environmental remediation has garnered considerable attention, with co-precipitation playing a critical role. Various authors have demonstrated the removal of toxic anionic contaminants such as fluoride and heavy metals using LDHs synthesized through this method [104,106]. The selective adsorption capabilities are primarily attributed

to the structural characteristics of LDHs, wherein the intercalated anions can be exchanged with environmental pollutants, applying this functionality in wastewater treatment [96,98]. The co-precipitation method is not limited to traditional LDH compositions; recent works have shown its viability in synthesizing more complex layered materials that integrate organic and inorganic components. Such multifunctional materials can effectively combine properties, enabling application in fields ranging from nanotechnology to biochemistry and medicine [107,108]. The co-precipitation method remains a powerful and versatile technique for synthesizing LDHs, allowing significant control over their structure and properties. The evolution and innovation in this methodology reflect ongoing academic and industrial pursuits toward developing sophisticated materials capable of addressing contemporary challenges in catalysis, energy storage, and environmental sustainability.

Flower-like NiCo-LDH nanoparticles were synthesized via the co-precipitation method using triethanolamine as the alkali source and hydrogen peroxide (H_2O_2) as the size-controlling reagent [109]. A subsequent heat treatment step (at 200 °C) was implemented to create a nanocrystal@amorphousness core/shell structure. This precise temperature-controlled process effectively induced amorphization at the surface of LDH crystals, significantly refining the grain size. As illustrated in Figure 3a, the LDH structure transforms with increasing temperature in an inert (Ar) atmosphere, leading to increased amorphous content and improved Li^+ diffusion channels due to the formation of disordered regions. Figure 3b presents the nitrogen adsorption/desorption isotherms of LDH samples treated at different temperatures. It can be observed that surface area increases significantly with temperature, reaching up to $178.9\text{ m}^2/\text{g}$ for LDH. In Figure 3c, the pore size distribution reveals that higher temperatures increase pore volume and broader pore distribution, which benefits ion transport and electrochemical performance. FESEM and TEM analyses revealed flower-like nanoparticles (~100 nm diameter) composed of small nanosheets (~20 nm × 5 nm), forming a unique nanocrystal@amorphous core/shell structure. The BET surface area measurement indicated a mesoporous structure with a specific surface area of approximately $76.6\text{ m}^2/\text{g}$, conducive to efficient electrolyte interaction and lithium-ion diffusion. The LDH amorphous-crystalline core/shell structure and enhanced surface area promote rapid lithium-ion transport, making it highly suitable for high-performance LIBs anodes.

The MgAl-LDH was synthesized via a straightforward co-precipitation method and incorporated with CNTs to form a hybrid composite [110]. This LDH@CNT hybrid was subsequently employed to create a sulfur composite cathode. The resulting material exhibited a well-dispersed morphology with nanoscale features and layered structure, a large surface area, and strong polysulfide adsorption characteristics. These features make the LDH highly suitable for LSB applications by effectively mediating polysulfide conversion and suppressing the shuttle effect. In another study, NiFe- NO_3 LDH was synthesized via a one-pot co-precipitation method by titrating a mixed nitrate solution of Ni and Fe with NaOH under an inert atmosphere, then aging at 70 °C for three days [111]. The obtained product was filtered, washed, dried, and ground to obtain the final LDH powder. The material revealed a typical hexagonal LDH structure with low crystallinity, turbostratic stacking, and a nanostructured surface. These structural features, combined with the high theoretical capacity (477 mAh/g) and dual redox/active metal centers (Ni^{2+}/Fe^{3+}), make the LDH highly suitable as an anode for NIB applications. The $Ni_3Mn_{0.7}Fe_{0.3}$ -LDH was synthesized via a co-precipitation method and subsequently activated electrochemically to introduce hydrogen vacancies, resulting in the $Hv-Ni_3Mn_{0.7}Fe_{0.3}$ -LDH [16]. The activation process involved CV in 1 M KOH to generate hydrogen-deficient lamellae that enhance zinc-ion accommodation. The reported LDH structure is highly suitable for ZIB applications due to its exposed terminal-O active sites and reduced Zn^{2+} diffusion barriers. NiFe

LDH nanosheets with varying interlayer spacings were synthesized through a simple co-precipitation method by intercalating different anionic species (Cl^- , $\text{C}_7\text{H}_5\text{O}_3^-$, and $\text{C}_{17}\text{H}_{25}\text{O}_3^-$) into the interlayer space [112]. The interlayer spacing was tuned from 7.695 Å to 24.114 Å by substituting the interlayer anions. The materials exhibited layered sheet-like morphology, preserved crystallinity, distinct interlayer anion fingerprints, uniform elemental distribution, consistent oxidation states, and enhanced interlayer water retention, all indicative of structural integrity and ion transport capacity. The expanded interlayer spacing and water facilitate rapid chloride ion diffusion, making these LDH materials highly suitable as cathodes in CIBs.

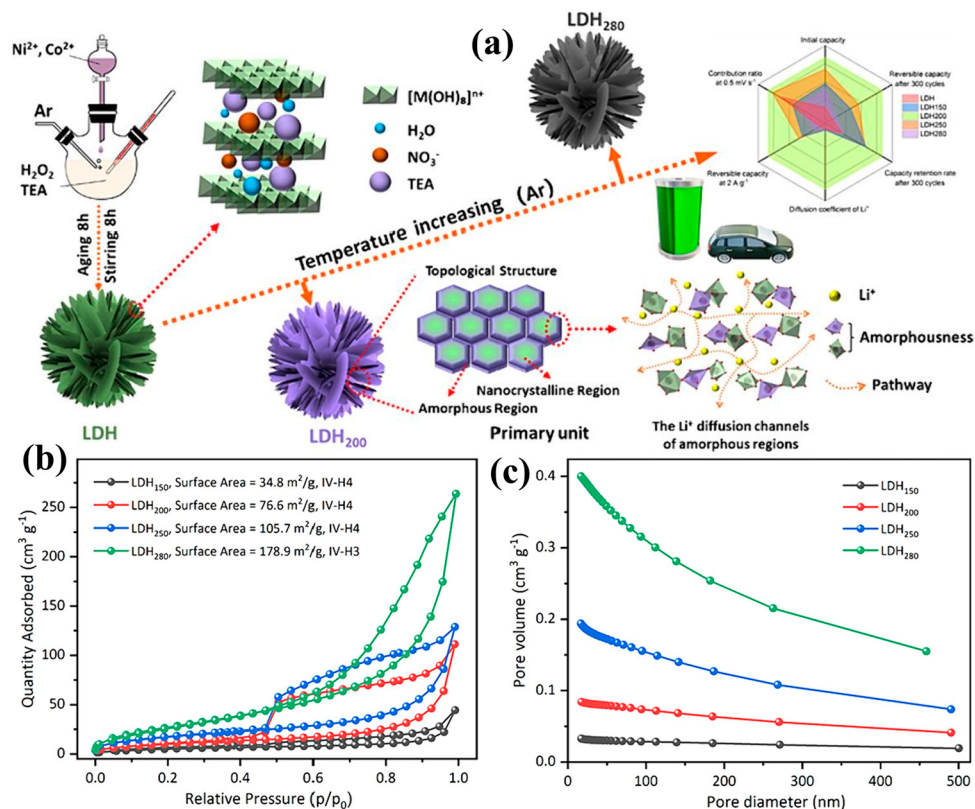


Figure 3. (a) Illustration of the synthesis pathway of temperature-regulated LDH and its transformation into an amorphous structure through thermal treatment. (b) Nitrogen adsorption/desorption curves and (c) pore size distribution profiles corresponding to the prepared samples. Reproduced with permission [109].

The NiMn-Cl LDH was synthesized via a co-precipitation method involving grafting NiMn-LDH nanosheets with chloride ion intercalation onto a CNT framework [113]. This process yielded a cross-linked network with a core/shell structure, enhancing ion transport and mechanical stability. These features make the material highly suitable for reversible chloride-ion storage in CIB applications. Similarly, $\text{Ni}_5\text{Ti}-\text{Cl}$ LDH was synthesized via a simple co-precipitation method using a high nickel-to-titanium molar ratio (5:1), followed by an anion exchange process in HCl/NaCl solution to replace interlayer carbonate with chloride ions [114]. This resulted in successful Cl^- intercalation, evidenced by XRD peak shifts and IR spectra indicating carbonate removal. Figure 4 highlights the structural and chemical characteristics of $\text{Ni}_5\text{Ti}-\text{Cl}$ LDH, designed to improve stability during cycling and enhance chloride ion adsorption. As seen in Figure 4a, the XRD analysis confirms the well-ordered layered structure. The FTIR results in Figure 4b show carbonate replacement with chloride, indicating successful ion exchange. Figure 4c presents a model structure of the LDH, showing expanded interlayer spacing favorable for Cl^- ion interaction. The TEM

image and elemental maps in Figure 4d reveal a uniform distribution of key elements and confirm nanosheet morphology. Figure 4e displays XPS spectra, verifying the oxidation states of Ni and Ti and supporting the material's chemical composition and structure. The high redox activity ($\text{Ni}^{2+}/\text{Ni}^{3+}$ and $\text{Ti}^{3+}/\text{Ti}^{4+}$) and excellent structural integrity with minimal volume change (~1.006%) make this LDH suitable for reversible chloride-ion intercalation in CIBs. The LDH was synthesized via a two-step method where ZIF-67 was first formed and then partially converted into Co-Fe-LDH by ion exchange and structural transformation under hydrothermal treatment at 80 °C for 48 h [115]. This Co-Fe-LDH was further hybridized with Fe-MOF and subsequently pyrolyzed at 900 °C under an argon atmosphere to yield the final CoFe/Fe₃C@CN heterojunction catalyst. The material possessed a nanosphere morphology with well-dispersed metal nanoparticles encapsulated by graphitic carbon layers, a high BET surface area of 247 m²/g, abundant mesoporosity, and a heterojunction structure. The resulting structure exhibits high surface area, abundant oxygen vacancies, and fast electron transfer, making it highly suitable as a bifunctional cathode catalyst in ZABs. Fe/Co LDH was synthesized via a simple in situ co-precipitation reaction over a cobalt-rich nitrogen-doped carbon framework (Co/N-C) derived by annealing ZIF-67 [116]. The resulting composite (CoL 2:1) was formed by varying mass ratios of LDH and Co/N-C precursors to optimize bifunctional catalytic performance. The material reveals a flaky LDH morphology on a porous carbon matrix with a high specific surface area of 230 m²/g and a meso/microporous structure. This structure enhances the availability of catalytic sites and is highly suitable for ZAB applications due to its excellent bifunctionality and electrochemical stability.

3.2. Hydrothermal Synthesis

Hydrothermal synthesis is a versatile method involving aqueous reactions at elevated temperatures and pressures, promoting controlled nucleation, dissolution/recrystallization, and growth of crystalline LDHs. This approach enables precise size, morphology, composition, and crystallinity tuning, making it highly effective for fabricating LDHs with tailored properties suitable for various applications, including catalysis and environmental remediation. Hydrothermal synthesis of LDHs typically involves an initial co-precipitation of metal salts with a base, followed by treatment under controlled temperature and pressure within an autoclave to enhance crystallinity and phase purity [117]. During hydrothermal processing, diffusion-controlled nucleation and growth mechanisms facilitate the oriented assembly of metal hydroxide layers and the systematic intercalation of anions, resulting in highly ordered and defect-minimized structures [118,119]. The precise regulation of synthesis parameters such as temperature, pressure, reaction time, and precursor concentration enables fine-tuning of LDH composition, morphology, and functional properties, optimizing them for catalytic, ion exchange, and environmental remediation applications [120,121]. The hydrothermal synthesis of LDHs involves an intricate balance between nucleation and growth, beginning with rapidly forming a gelatinous, disordered metal hydroxide precipitate. Under hydrothermal conditions, this initial phase undergoes a dissolution/reprecipitation cycle driven by thermodynamic stability, resulting in a well-ordered, defect-free lamellar structure through controlled alignment and stacking of hydroxide layers [122]. Furthermore, hydrothermal synthesis uniquely facilitates the incorporation of multiple metal cations into LDH frameworks, enabling the development of multi-cationic or high-entropy LDHs with distinct electronic and structural attributes [77]. These high-entropy LDHs exhibit superior electrocatalytic properties due to synergistic interactions among diverse cationic species, making them highly promising for advanced applications such as CO₂ methanation and other catalytic processes [123,124].

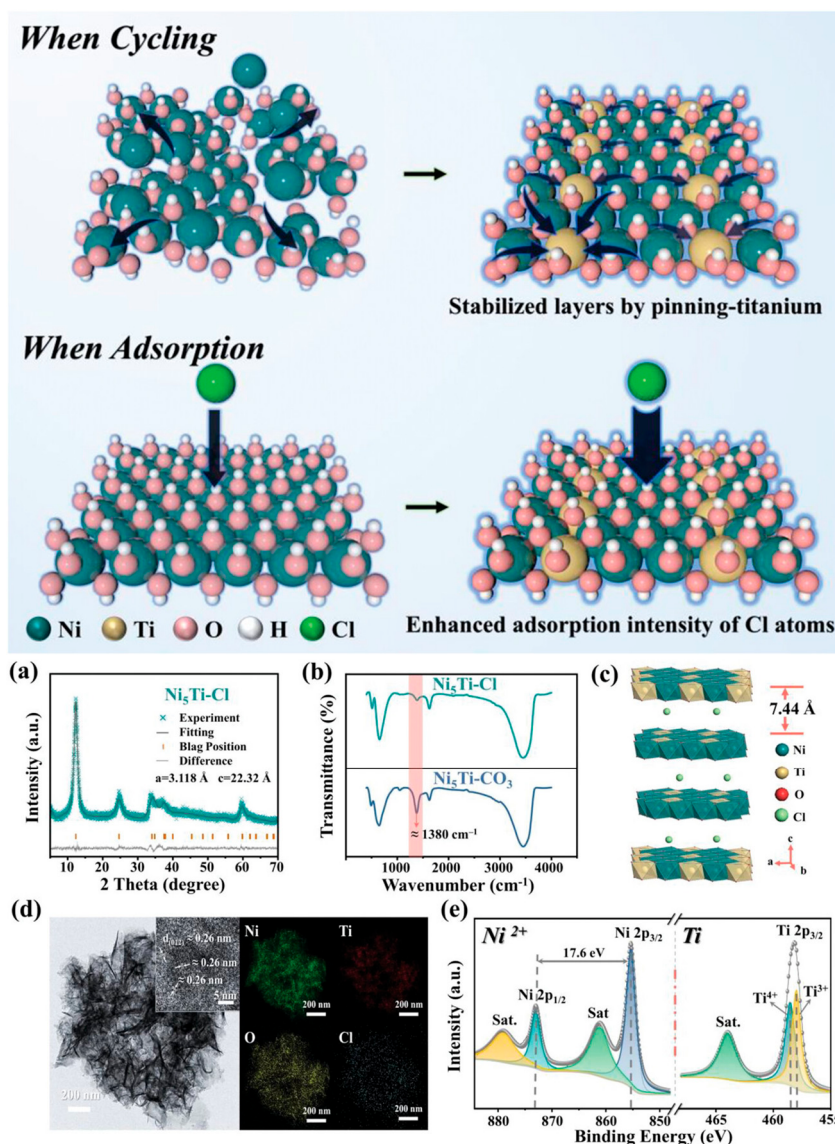


Figure 4. Demonstration of the structural stabilization and improved Cl adsorption in $\text{Ni}_5\text{Ti-Cl}$ LDH. (a) XRD pattern refined using the Rietveld method for $\text{Ni}_5\text{Ti-Cl}$ LDH. (b) FTIR spectra compare the $\text{Ni}_5\text{Ti-Cl}$ LDH and its carbonate-based precursor ($\text{Ni}_5\text{Ti-CO}_3$ LDH). (c) Structural model illustrating the layer arrangement in $\text{Ni}_5\text{Ti-Cl}$ LDH. (d) TEM image with SAED inset and elemental mapping showing distributions of Ni, Ti, O, and Cl. (e) Ni and Ti XPS profiles, confirming the oxidation states present in $\text{Ni}_5\text{Ti-Cl}$ LDH. Reproduced with permission [114].

Hydrothermal synthesis provides precise control over morphology, particle size, and structural ordering of LDHs, enabling the tailored formation of uniform nanosheets, nanorods, hierarchical architectures, and ultrathin nanosheets with large surface areas beneficial for catalytic, adsorption, and energy-related applications [125]. This method facilitates controlled intercalation of anions, defect healing through ion migration, incorporation of multiple cations, and utilization of structure-directing additives or surfactants, enhancing LDH crystallinity, phase purity, ion exchange capacities, and electrochemical performance [126]. Additionally, the adaptability and scalability of hydrothermal synthesis make it environmentally attractive and economically viable for industrial-scale production of multifunctional LDHs optimized for diverse applications, including catalysis, environmental remediation, sensors, and energy storage systems [127]. Recent advancements in hydrothermal synthesis have enabled the fabrication of compositionally complex and highly crystalline LDHs with tunable properties for advanced applications [128]. By precisely

controlling parameters such as temperature, pressure, pH, and precursor composition, this method facilitates the formation of defect-minimized, high-surface-area materials with tailored morphology, ion distribution, and interlayer characteristics [129]. High-entropy LDHs, multi-metallic composites, and nitrogen-doped structures synthesized hydrothermally demonstrate enhanced catalytic, adsorption, and electrochemical performance, particularly in environmental remediation and energy storage. The technique's scalability, energy efficiency, and use of water as a benign solvent further highlight its potential as a sustainable and industrially viable approach for producing multifunctional LDHs with minimal environmental impact [130]. Hydrothermal synthesis offers a highly versatile and controllable route for fabricating LDHs with tailored morphology, interlayer spacing, crystallinity, and multi-metal compositions [131]. Fine-tuning reaction parameters such as temperature, pressure, pH, and precursor concentration produces defect-minimized, thermally and chemically stable LDHs with enhanced ion exchange, catalytic, and electrochemical properties. The process supports *in situ* functionalization, hybridization with organic or carbonaceous materials, and integrating bulky anions or multiple cations [132]. It is ideal for diverse applications in catalysis, energy storage, environmental remediation, and advanced composites. Its scalability, reproducibility, and use of water as a benign solvent further establish hydrothermal synthesis as a sustainable and industrially viable strategy for developing high-performance, multifunctional LDH-based materials [133].

ZIF-67@NiCo-LDH heterostructures were synthesized using a straightforward one-pot hydrothermal method involving the reaction of cobalt and nickel nitrate precursors with 2-methylimidazole in methanol at 90 °C for 11 h [134]. This synthesis resulted in the formation of unique flower-shaped structures composed of ZIF-67 MOF cores uniformly decorated with NiCo-LDH nanosheets. The controlled reaction time allowed morphology tuning and ensured good dispersion and stability of the composite materials. Characterizations confirmed the heterostructures' flower-like morphology, high crystallinity, and uniform elemental distribution of Ni, Co, O, C, and N. The resulting porous structure exhibited enhanced electrolyte accessibility and improved electrical conductivity compared to the pristine LDH. The flower-shaped morphology and porous structure of ZIF-67@NiCo-LDH enhance ionic and electronic conductivity, making it suitable for LIB anode applications. NiFe₂O₄@NiCo-LDH was synthesized using a two-step hydrothermal process [135]. Initially, NiFe-MOF precursors were hydrothermally treated and annealed to obtain hollow NiFe₂O₄ nanocubes. Subsequently, NiCo-LDH nanosheets were hydrothermally grown onto the surface of these nanocubes, creating a hierarchical NiFe₂O₄@NiCo-LDH structure. The NiFe₂O₄@NiCo-LDH composite featured hollow hierarchical nanocubes with uniformly distributed NiCo-LDH nanosheets grown on NiFe₂O₄ surfaces. XRD and BET analyses revealed a crystalline structure with enhanced surface area (58.4 m²/g) and mesoporous characteristics (pore size 2–3 nm), advantageous for electrochemical reactions. Due to its hierarchical hollow structure, high surface area, and mesoporosity, the NiFe₂O₄@NiCo-LDH is highly suitable for batteries, facilitating rapid electron and ion transport and alleviating volumetric expansion during cycling. NiZn-LDH intercalated with dodecyl sulfate anions was synthesized using a facile hydrothermal method [136]. Nickel nitrate and zinc nitrate precursors were dissolved under an inert atmosphere, followed by a controlled addition of sodium dodecyl sulfate and sodium hydroxide solution. The mixture was then subjected to hydrothermal treatment at 100 °C for 4 h, centrifuged, washed, and freeze-dried. The synthesized LDH exhibited ultra-thin nanosheet morphology with significantly expanded interlayer spacing due to the intercalation of dodecyl sulfate anions. BET analysis revealed a mesoporous structure with a specific surface area of around 53.4 m²/g, indicating good accessibility and interaction sites for lithium ions. Due to its expanded interlayer spacing, ultra-thin nanosheet morphology, and favorable surface

area, the synthesized NiZn-LDH provides effective diffusion pathways for lithium ions, thus making it suitable for battery applications.

LDH was synthesized initially through a solvothermal process, creating NiFe glyceric acid precursors using $\text{Ni}(\text{NO}_3)_2 \cdot 6\text{H}_2\text{O}$ and $\text{Fe}(\text{NO}_3)_3 \cdot 9\text{H}_2\text{O}$ in glycerol/isopropanol solution [137]. These precursors were then coated with polydopamine and subjected to high-temperature carbonization and vulcanization, forming $\text{NiS}_2/\text{FeS}_2@\text{NC}$ structures. Finally, NiFe LDH/FeO(OH) nanosheets were grown on these structures via a hydrothermal reaction, resulting in hollow yolk/shell $\text{NiS}_2/\text{FeS}_2@\text{NC}@/\text{NiFe}$ LDH/FeO(OH) microspheres. The synthesized LDH exhibited a hollow yolk/shell structure with nanoflower morphology. The LDH's porous hollow yolk/shell structure and high specific surface area enable efficient ion transport and structural stability, making it highly suitable for battery applications. NiCo-LDH nanowires were synthesized using a simple one-step hydrothermal method [138]. Initially, MXene nanosheets were prepared by etching and delaminating Ti_3AlC_2 . Subsequently, NiCo-LDH nanowires were uniformly grown in situ onto MXene nanosheets, forming a hierarchical 1D/2D heterostructure [139]. The composite exhibited a 1D nanowire-on-2D nanosheet morphology with increased specific surface area ($14.50 \text{ m}^2/\text{g}$) and enhanced structural stability. The NiCo-LDH/MXene composite, with its hierarchical structure and enhanced conductivity, is highly suitable for battery applications as it ensures rapid lithium-ion diffusion and stable electrochemical cycling. MgAl LDH ($\text{Mg}_2\text{Al}_1-\text{CO}_3$ -LDH) was synthesized using a simple hydrothermal method [140]. Carbonate ions (CO_3^{2-}) were intercalated within Mg and Al layers as interlayer anions. The synthesized LDH exhibited a typical hexagonal flake-like morphology with uniform elemental distribution. The $\text{Mg}_2\text{Al}_1-\text{CO}_3$ -LDH reveals a well-defined hexagonal layered structure, a flake-like morphology, homogeneous elemental dispersion, and an interlamellar spacing of 7.45 \AA . These analyses confirmed its composition as $[\text{Mg}_{0.68}\text{Al}_{0.32}(\text{OH})_2](\text{CO}_3^{2-})_{0.16} \cdot 0.66\text{H}_2\text{O}$ with a high structural integrity. The $\text{Mg}_2\text{Al}_1-\text{CO}_3$ -LDH demonstrates suitable properties such as high specific surface area, structural stability, and active interlayer spaces, making it a promising candidate as an anode material for LIBs. The NiCo-LDH nanoflowers were synthesized via a hydrothermal method using nickel nitrate, cobalt nitrate, and CTAB, with in situ growth on either nickel foam (NF) or jute-derived AC (JAC-2) as substrates [89]. The optimal composite, NiCoLDH-1@JAC-2, was prepared by hydrothermally treating a mixture of Ni/Co in a 1:1 molar ratio with JAC-2 at 180°C for 12 h. Figure 5a,b presents the synthetic routes for preparing JAC and the subsequent in situ formation of NiCo-LDH@JAC nanoflowers. The resulting NiCoLDH nanostructures exhibit a hierarchical nanoflower morphology composed of ultrathin nanosheets ($\sim 10 \text{ nm}$) with high crystallinity and a well-defined layered structure confirmed by XRD and HRTEM. JAC-2 support contributed significantly with its nanosheet structure, high surface area ($\sim 2600 \text{ m}^2/\text{g}$), and rich micro/mesoporous texture, enhancing ion transport. These structural and morphological features make the composite highly suitable for supercapacitor applications by maximizing active surface area and minimizing ion diffusion resistance.

The CoLa-LDH (CL) was synthesized via a hydrothermal method followed by a second hydrothermal step to grow NiCoOOH (NC) onto the CL, forming a hierarchical NiCoOOH@CoLa-LDH (NC@CL) heterostructure [141]. The NC was tightly coated over the CL nanosheets, yielding a flower-like 3D nanosheet architecture. Morphologically, the NC@CL exhibited interconnected ultrathin nanosheets with a high BET surface area of $316.4 \text{ m}^2/\text{g}$ and mesoporous features (mainly 2–10 nm pores). Structural characterizations confirmed successful heterojunction formation and lattice deformation beneficial for ion/electron transport. The NC@CL structure provides abundant active sites and excellent electron/ion kinetics, making it highly suitable for ZIB applications. The NiCoMo LDH was

initially synthesized via a hydrothermal method, followed by an anion exchange reaction to replace interlayer carbonate ions with chloride ions [142]. Subsequent temperature-differential phosphorus doping using NaH_2PO_2 vapor at different controlled temperatures introduced P heteroatoms into the LDH structure. Morphologically, the LDH retained a sea urchin-like microsphere architecture composed of nanowires, while XRD, TEM, and XPS confirmed structural integrity and successful P-doping, with increased oxygen vacancies and enhanced electronic properties. These features collectively support its application in CIBs by improving conductivity and diffusion kinetics.



Figure 5. (a) Illustration of the JAC fabrication process involving a two-step pyrolysis method, and (b) detailed schematic of the in situ synthesis approach for growing NiCoLDH@JAC nanoflower structures. Reproduced with permission [89].

The NiAl-LDH was synthesized by first depositing Al_2O_3 on graphene using atomic layer deposition (ALD), followed by a hydrothermal transformation into NiAl-LDH@G [143]. This two-step process enabled the vertical growth of ultrathin LDH nanosheets on graphene, forming a nanoarray architecture. Characterization revealed a well-defined mesoporous structure with vertical LDH nanosheets (~3 nm thick), high surface area ($230.44 \text{ m}^2/\text{g}$), and a uniform elemental distribution. This architecture enhances electron/ion transport and structural stability, making it ideal for CIB cathode applications.

The NiCo-based LDH was synthesized via a hydrothermal method, and chloride ions were introduced through a post-synthesis ion exchange process by treating the carbonate-intercalated LDH with an NaCl/HCl solution [144]. This treatment replaced CO_3^{2-} ions

with Cl^- in the interlayer, enabling its function as a chloride host. The Mo-doped NiCo LDH exhibited a well-defined sea urchin-like morphology composed of ultrafine nanowires, with increased BET surface area ($74.6 \text{ m}^2/\text{g}$), preserved LDH structure confirmed by XRD, and homogenous elemental distribution. This structural configuration provides enhanced active surface area and diffusion pathways, making the material highly suitable as a CIB cathode. The CoFe–Cl-LDH/CNT composite was synthesized via a modified co-precipitation method followed by hydrothermal treatment under N_2 protection [145]. The process involved the preparation of a Co/Fe/CNT precursor solution, pH adjustment, and hydrothermal aging at 130°C , followed by Cl^- intercalation in NaCl/HCl solution. Characterizations revealed nanoflake-like LDH morphology with high crystallinity, uniform Cl^- intercalation, and improved conductivity due to CNTs. The material's layered structure, reversible Cl^- storage, and enhanced electrochemical performance make it suitable as an anode for CIBs. NiFe-LDH was synthesized on electrospun carbon nanofibers (CNFs) via hydrothermal treatment, followed by the in situ growth of conductive Ni-CAT nanorods using nickel acetate and HHTP at 85°C for 12 h [146]. This hierarchical assembly yielded a 3D Ni-CAT/NiFe-LDH/CNFs composite. The morphology revealed interconnected nanosheets and nanorods forming a porous architecture, while XRD and XPS verified structural and chemical composition. The BET surface area of Ni-CAT/NiFe-LDH/CNFs was significantly high at $258.84 \text{ m}^2/\text{g}$. This structure ensures high conductivity, active site exposure, and porosity, making it highly suitable for ZAB applications.

Using a two-step hydrothermal process, the NiMn-LDH was synthesized over a ZnCo_2O_4 (ZCO) nanowire array pre-grown on nickel foam [147]. The first step involved forming ZCO nanowires, followed by hydrothermal deposition of NiMn-LDH nanosheets with varied Ni/Mn precursor ratios, optimized at 2:1. Characterization revealed that the LDH formed a uniform core/shell structure with high crystallinity, a flower-like morphology, and a large surface area (BET: $57.91 \text{ m}^2/\text{g}$), along with favorable pore distribution, layered structure, and high electrochemical surface area. This tailored architecture with synergistic interactions and abundant electroactive sites renders the LDH ideal for use as an efficient air cathode catalyst in ZABs. The NiCo-LDH/NCM@NF catalyst was synthesized through a two-step process [148]. First, nitrogen-doped carbon nanosheets (NCMs) were formed via self-assembly and calcination of perylene tetracarboxylic dianhydride and dicyandiamide under hydrothermal conditions; subsequently, NiCo-LDH nanoplates were grown in situ on these NCM-modified nickel foam substrates using hydrothermal treatment. The incorporation of NCMs during LDH growth modulated the morphology into rough-edged, ultrathin nanoflakes and enhanced nucleation and dispersion. Characterization revealed a 2D flake morphology, enlarged interlayer spacing, a high BET surface area ($235.6 \text{ m}^2/\text{g}$ for NiCo-LDH/NCM vs. $140.3 \text{ m}^2/\text{g}$ for pristine NiCo-LDH), uniform elemental distribution, and rich oxygen vacancies. This LDH architecture ensures enhanced electron transport and more exposed catalytic sites, making it highly suitable for ZAB applications.

First, Co_9S_8 nanospheres synthesized $\text{NiFe-LDH}@\text{Co}_9\text{S}_8$ via hydrothermal treatment, were grown, followed by in situ growth of NiFe-LDH nanosheets on their surface [149]. Pt nanoparticles were then anchored onto the NiFe-LDH nanoflakes through a spontaneous redox reaction, exploiting cation vacancies in the LDH. NiFe-LDH nanosheet flowers were synthesized via a hydrothermal route [150], and two modified versions, CoNiFe-LDH (via one-step hydrothermal doping) and Co@NiFe-LDH (via two-step heterostructure formation with Co(OH)_2 nanoarrays) were developed. The morphology was characterized by FESEM and TEM, revealing spherical structures with smooth or flocculated surfaces; XRD, XPS, and SAED provided structural confirmation, while BET analysis showed Co@NiFe-LDH had the highest surface area ($34.14 \text{ m}^2/\text{g}$) and hierarchical porosity. These structural and

surface properties make the LDH, particularly Co@NiFe-LDH, well-suited for ZAB air cathode applications due to enhanced active site availability and electronic conductivity.

NiCo-LDH was synthesized via a one-step hydrothermal method by optimizing reaction temperature, time, and Ni/Co molar ratio, as shown in Figure 6a [119]. The resulting LDH showed a uniform sheet-like morphology with high porosity, well-defined crystalline structure, and the presence of $\text{Ni}^{2+}/\text{Ni}^{3+}$ and $\text{Co}^{2+}/\text{Co}^{3+}$ redox states, while FESEM revealed high surface area features favoring electrolyte diffusion and charge transport. Due to enhanced electron conductivity and electrochemical activity, these structural attributes make it an ideal candidate for supercapacitor applications. NiCo-LDH nanosheets were synthesized on nickel foam using a one-pot hydrothermal method involving nickel and cobalt nitrate precursors in the presence of HMTA at 110 °C [151]. As shown in Figure 6b, the basic structure of an LDH comprises stacked layers with positively charged metal hydroxides, separated by interlayer anions and water molecules. This layered structure is essential for the material's chemical and physical properties. Meanwhile, Figure 6c presents the hydrothermal synthesis approach for preparing NiCo-LDH nanosheets. It highlights how the morphology and structure of the nanosheets evolve depending on the duration of the hydrothermal treatment. Different reaction times can change sheet thickness, uniformity, and surface characteristics, significantly affecting the material's performance in various applications. The resulting LDH exhibited a binder-less, ultrathin, porous nanosheet morphology with high crystallinity and a large specific surface area of 46.8 m^2/g (for the optimized sample). These structural and morphological features facilitated rapid ion transport and abundant electroactive sites, rendering the material highly suitable for supercapacitor applications. The CoLa-LDH (CL) was synthesized via a hydrothermal method, followed by a secondary hydrothermal deposition of NiCoOOH (NC) to form the hierarchical NC@CL heterostructure [141]. As seen in Figure 6d, the process involves two hydrothermal steps. First, the CL nanosheets are synthesized at 120 °C for 5 h. Then, a second hydrothermal treatment at the same temperature for 3 h enables the formation of NC@CL, where a second layer is formed on top of the initial CL structure. Figure 6e–g presents FESEM images of the as-prepared CL nanosheets at different magnifications. These images reveal a highly porous, interconnected sheet-like structure that facilitates ion and electron transport. In comparison, Figure 6h–j displays the FESEM images of the NC@CL nanosheet arrays. The surface becomes more complex and flower-like, indicating the successful growth of the secondary NC layer. This hierarchical structure can enhance surface area and active sites, making it beneficial for energy storage or catalysis applications. The resulting NC@CL nanosheets displayed a 3D hierarchical flower-like morphology with a high BET surface area (316.4 m^2/g), mesoporous structure, and uniform elemental distribution; XRD and XPS analyses confirmed the formation of a mixed-phase structure with strong electronic interactions and lattice distortions beneficial for charge transport. These characteristics render the NC@CL heterostructure particularly advantageous for supercapacitor applications due to enhanced ion/electron transport and abundant electroactive sites.

The $\text{Ni}_2\text{Co}-\text{LDH}$ was synthesized via a simple co-precipitation method, where nickel and cobalt chloride precursors reacted with hexamethylenetetramine under reflux conditions at 80 °C for 8 h [152]. Expanded graphite (EG) was separately synthesized by rapid microwave irradiation of expandable graphite powder. Subsequently, $\text{Ni}_2\text{Co}-\text{LDH}/\text{EG}$ composites were prepared through an *in situ* growth technique, anchoring $\text{Ni}_2\text{Co}-\text{LDH}$ nanosheets onto the surface of EG. Structural and morphological characterizations revealed layered, crystalline nanosheets of $\text{Ni}_2\text{Co}-\text{LDH}$ anchored uniformly onto EG surfaces, with lattice spacings consistent with $\text{Ni}_2\text{Co}-\text{LDH}$. BET analysis indicated enhanced surface area from 26.1 m^2/g for pure LDH to 30.3 m^2/g for the composite, confirming effective integra-

tion with EG. The enhanced surface area and stable layered morphology confirmed by characterizations facilitate improved ionic and electronic transport, making Ni₂Co-LDH/EG composites suitable for battery electrode applications. NiAl LDH was synthesized via a one-pot hydrothermal reaction using nickel nitrate, aluminum nitrate, and urea dissolved in deionized water [153]. The solution was transferred to a Teflon-lined autoclave and heated at 100 °C for 24 h. The high surface area, porous nano-lamellar morphology, and structural stability of the synthesized NiAl LDH make it a promising candidate for LIB anodes. The CoNi-LDH/C composite was synthesized by first preparing ZIF-67 polyhedrons, which were then subjected to laser-induced carbonization to obtain porous Co/C structures [154]. These carbonized materials were reacted with Ni(NO₃)₂·6H₂O in ethanol under hydrothermal conditions at 90 °C to form the final CoNi-LDH/C composite. This process was optimized to retain polyhedral morphology while introducing amorphous carbon and catalytic metal sites. The resulting material exhibited a mesoporous structure with a high specific surface area (24.5 m²/g), tubular morphology, and crystalline CoNi-LDH domains enclosed by conductive carbon layers. Due to increased carbon content, structural characterizations confirmed the uniform distribution of Co/Ni, porous architecture, and enhanced conductivity. This hierarchical and conductive CoNi-LDH/C framework provides abundant active sites for LiPS adsorption and conversion, making it highly suitable for LSB cathodes. Li-Al LDH was synthesized via hydrothermal Al(OH)₃ and LiCl treatment at 90 °C for 24 h [155]. The LDH was exfoliated in formamide and reassembled with varying amounts of polystyrene sulfonate (PSS) to form LDH@PSS. The optimal composition (LDH/PSS = 1:1.5) was obtained through self-assembly under N₂ atmosphere and centrifugation. The notable structural and electrochemical properties render LDH@PSS highly suitable for stabilizing Li metal anodes in LSBs by suppressing polysulfide shuttling and dendrite formation.

The FeNi-LDH was synthesized hydrothermally by mixing NiCl₂·6H₂O, FeCl₂·6H₂O, and L-cysteine in water/ethanol, followed by ammonia addition, then heating in a Teflon-lined autoclave at 180 °C for 12 h [156]. The resulting cysteine-functionalized FeNi-LDH (Cys/FeNi-LDH) was further reacted with NaVO₃ in methanol under reflux to yield the ternary V₂O₅/Cys/FeNi-LDH (VCFN) composite. This process ensured the uniform decoration of V₂O₅ nanoparticles on the LDH disks through strong coordination with cysteine functional groups. This LDH-based composite, with its synergistic combination of polysulfide adsorption, catalytic conversion capability, and mesoporous framework, is highly suitable for suppressing the shuttle effect and enhancing sulfur redox kinetics in LSBs. The NiFe-LDH, NiAl-LDH, and ZnAl-LDH were synthesized via a hydrothermal method by co-dissolving respective metal nitrates and urea in deionized water, followed by heating under controlled temperatures for different durations [157]. Sulfur was incorporated into the LDHs using the classical melt/impregnation method at 155 °C, achieving ~75% sulfur loading. Characterization revealed that the LDHs had nanoflake morphology with a 3D network-like architecture, uniform sulfur distribution, and surface areas ranging from 52.6 to 54.8 m²/g. This structure with high surface area and interlayer spacing enabled strong interaction with polysulfides, making the LDHs suitable sulfur hosts for LSBs. NiCoAl-LDH nanosheets were synthesized on carbon cloth (CC) via a hydrothermal method [158]. Subsequently, vertical graphene was grown on the LDH/CC surface using plasma-enhanced chemical vapor deposition (PECVD), forming a 3D interconnected structure. The morphology showed uniformly distributed nanosheets and vertically aligned graphene, with lattice spacings confirming NiCo alloy and graphite planes. This nanocomposite offers strong polysulfide adsorption and fast redox kinetics, making it a suitable host for LSBs. The NiCr-Cl LDH/rGO composite was synthesized via a one-step hydrothermal method to produce NiCr-CO₃ LDH/rGO, followed by ion exchange in a NaCl/HCl solution to

replace CO_3^{2-} with Cl^- ions [159]. This approach involved urea-assisted hydrothermal reaction at 150 °C for 24 h, forming a well-dispersed LDH on GO sheets. Morphological and structural characterizations revealed flower-like nanosheet morphology, increased interlayer spacing after Cl^- exchange, and intense interaction between LDH and rGO; the BET surface area of the NiCr-CO₃ LDH/rGO composite was 170.44 m²/g, supporting good electrochemical performance. The resulting LDH composite demonstrated enhanced suitability for NIB applications due to its improved conductivity, mesoporous structure, and structural stability.

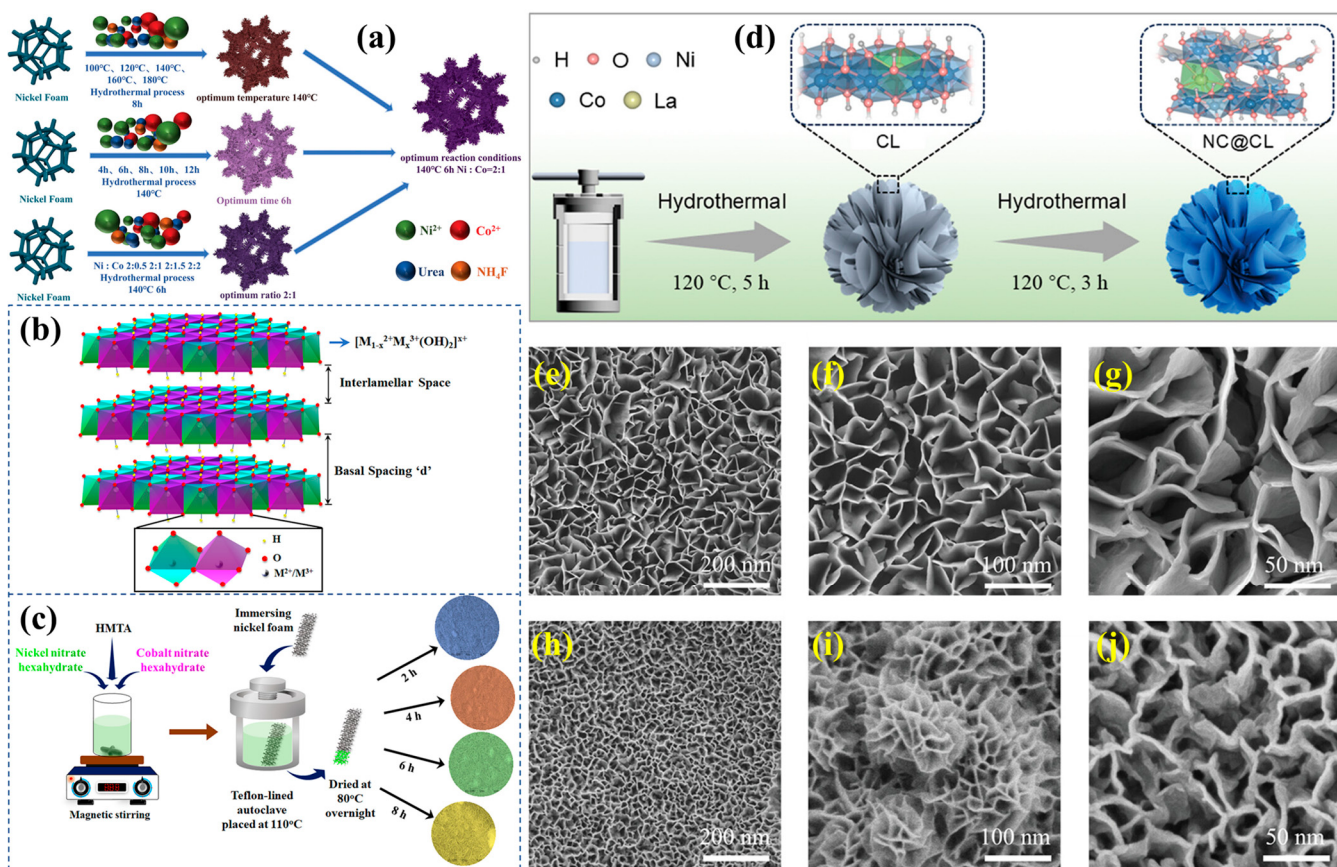


Figure 6. (a) Schematic representation for the NiCo-LDH synthesis. Reproduced with permission [119]. (b) Illustration showing the structural layout of an LDH material, and (c) diagram depicting the hydrothermal synthesis process of Ni-Co LDH nanosheets at various time intervals. Reproduced with permission [151]. (d) Conceptual diagram outlining the stepwise hydrothermal synthesis of NC@CL nanosheet arrays, beginning with CL formation and followed by growth of the NC layer. (e–g) FESEM images showing the surface morphology of the CL nanosheets at increasing magnifications. (h–j) FESEM images displaying the detailed nanostructure of the NC@CL hierarchical flower-like nanosheet arrays. Reproduced with permission [141].

The NiCo-LDH was synthesized via a hydrothermal method by immersing pre-treated sulfide-hollow ZIF-67 structures into a solution of $\text{Ni}(\text{NO}_3)_2$, $\text{Co}(\text{NO}_3)_2$, and hexamethylenetetramine at 90 °C for 24 h [160]. The resulting LDH featured a nanoflower-like morphology, layered structure, and a BET surface area of 266.76 m²/g with a mesoporous architecture, enhancing electron/ion transport and active surface sites. Due to its superior redox activity and efficient charge storage capability, these characteristics render the NiCo-LDH highly suitable for high-performance supercapacitor applications. NiFe-LDH/MnCO₃/MXene (NFMM) ternary composite was synthesized via a hydrothermal method by reacting Ni, Fe, and Mn nitrates with urea in the presence of MXene [161]. The resulting NFMM exhibited a layered and granular sandwich-like structure with uniformly dis-

tributed MnCO_3 and NiFe-LDH on MXene, showing a high BET surface area of $32.62 \text{ m}^2/\text{g}$ and a hierarchical mesoporous network with improved electronic conductivity. These properties make NFMM an ideal candidate for supercapacitor electrodes due to its enhanced ion/electron transport and abundant active sites. The FeCoNi-LDH nanosheets were synthesized via a secondary hydrothermal reaction onto pre-formed MnCo_2O_4 nanowires anchored on CC [162]. The resulting $\text{MnCo}_2\text{O}_4@\text{FeCoNi-LDH}$ exhibited a nanoflower-like, hierarchical morphology with high crystallinity, uniform nanosheet distribution, and a mesoporous structure, showing a specific surface area of $33.9 \text{ m}^2/\text{g}$ and distinct XRD and XPS signatures confirming multi-metal synergy. Figure 7 displays the synthesis steps and morphology changes of MnCo before and after FCN coating on CC, highlighting structural differences observed under SEM. This architecture enhances ion diffusion and redox activity, making it highly suitable for high-performance supercapacitor applications.

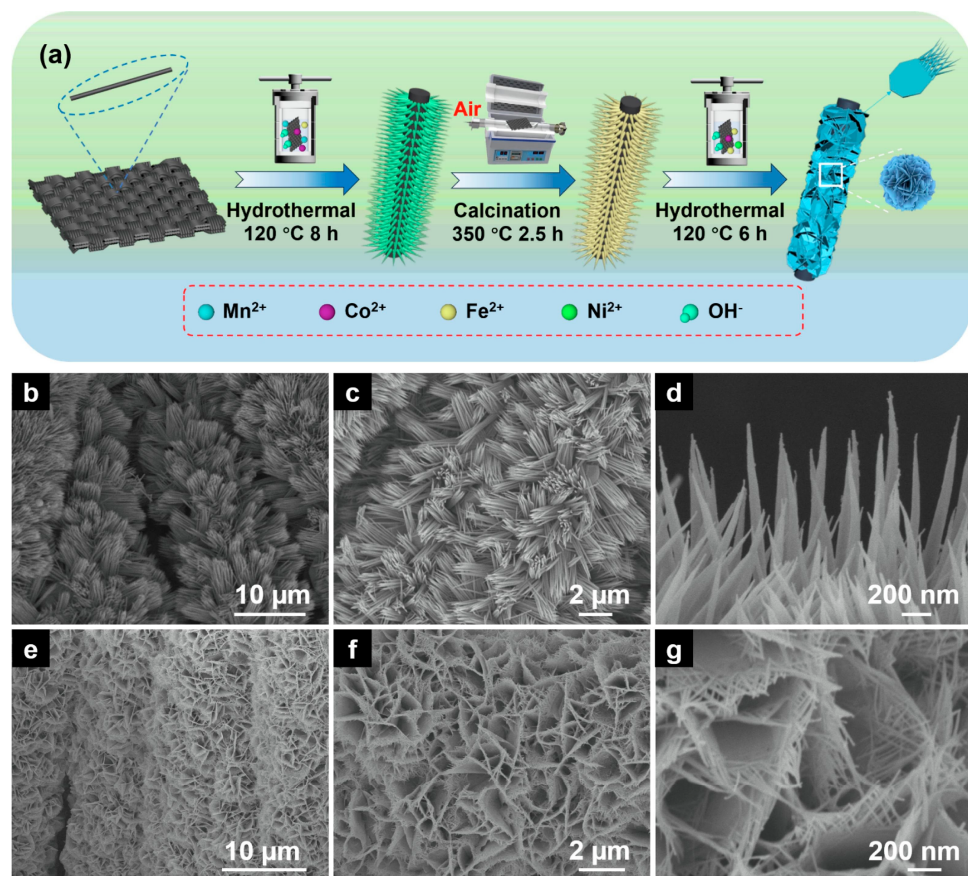


Figure 7. (a) Illustration of the step-by-step process to make MnCo@FCN on CC via hydrothermal synthesis. (b–d) FESEM images showing the surface of MnCo on CC at various zoom levels. (e–g) FESEM images of MnCo@FCN coated on CC under different magnifications. Reproduced with permission [162].

CoMo-LDH was synthesized via hydrothermal treatment of cobalt nitrate and sodium molybdate in the presence of urea, followed by coating with polydopamine (PDA) through a polymerization process and subsequent carbonization at 800°C to form CoMoLDH@C-PDA composites [163]. The duration of the hydrothermal and polymerization steps was optimized to achieve controlled morphology and appropriate carbon layer thickness. The carbon-coated CoMoLDH is considered suitable as an anode material for NIBs due to enhanced conductivity, structural stability, and sodium-ion diffusion. Co-Co LDH was synthesized via a hydrothermal method using ZIF-67 as the precursor and grown onto nitrogen-doped hollow carbon nanospheres (NHCNS) [164]. The resultant Co-Co LDH@NHCNS

was then selenized and coated with a carbon shell to obtain the final NHCNS@CoSe₂@C composite. The composite exhibited a nanoflower-like morphology with uniformly distributed CoSe₂ nanoparticles on the NHCNS surface. XRD validated the successful transformation to CoSe₂; XPS and Raman revealed the chemical states and defect structures, and TGA estimated a carbon content of 43.4%. This unique sandwich structure offers enhanced conductivity, stability, and sodium storage capability, making it highly suitable for NIB applications. The CoNi-LDH was synthesized via a two-step hydrothermal method, where cobalt phosphate (CP) was first grown on nickel foam, followed by in situ growth of molybdate-intercalated CoNi-LDH (MCN-LDH) on the CP surface [165]. Incorporating molybdate ions was achieved using urea and ammonium fluoride as structure-directing agents. The prepared LDH exhibited interconnected nanosheets on microsheets; XRD confirmed phase structure; BET analysis showed a surface area of 212.68 m²/g; Raman and XPS confirmed successful MoO₄²⁻ intercalation. These structural and textural improvements make the MCN-LDH highly suitable for high-performance ZIB cathode applications. ZnCo-LDH was synthesized via a hydrothermal process by dissolving CoCl₂·6H₂O, ZnCl₂, urea, and PVP in deionized water, then heating at 120 °C for 12 h [166]. The resulting product was collected, washed, and dried to obtain ZnCo-LDH microspheres. BET measurements showed a surface area of 37.1 m²/g with mesopores averaging 28.2 nm in diameter. These structural features, including high surface area and mesoporosity, make the material highly suitable for electrochemical applications in ZIBs.

NiAl LDH was synthesized using a one-step hydrothermal method [167]. The resulting LDH exhibited a porous nanosheet morphology with oxygen vacancies, high crystallinity, hierarchical nanostructures, and a BET surface area of up to 300 m²/g, promoting efficient ion transport and electron transfer. These features make it a suitable candidate for supercapacitor applications due to its enhanced redox activity, mechanical integrity, and electrochemical performance. MoB@NiCo-LDH was synthesized via a hydrothermal process by growing NiCo-LDH nanosheets on layered MoB templates derived from NaOH-etched MoAlB; subsequent phosphorization and NaBH₄ treatment introduced phosphorus vacancies, resulting in MP2 material [168]. The synthesized LDH exhibits an amorphous structure with a nanosheet-to-nanoparticle morphological transition, a layered architecture, uniform elemental distribution, enhanced electrical conductivity, and abundant surface-active sites due to phosphorus vacancies. These features contribute to fast charge transport, high redox activity, and structural stability, making the LDH ideal for supercapacitor applications.

The Te-doped NiMn LDH was synthesized via hydrothermal growth on CTAB-modified MXene-coated nickel foam, followed by tellurium doping through immersion in TeCl₄ ethanol solution [169]. The step-by-step design strategy and structural characterization of the Te-doped NiMn LDH system are illustrated in Figure 8. The CTAB-modified MXene coating on nickel foam (C-MXene/NF) is shown in Figure 8, which offers a rough, layered texture that supports better growth of the active material. Figure 8a,b shows the FESEM image of NiMn LDH directly grown on bare nickel foam, revealing a relatively smoother and flatter structure. With the addition of the MXene layer, Figure 8c shows that the NiMn LDH forms a more clustered, 3D nanostructure on C-MXene/NF, offering increased surface area and potential active sites. Figure 8d displays the final morphology after tellurium doping, which results in a highly porous, flower-like structure. This modification enhances electrochemical activity by introducing more redox-active centers and improving conductivity. XRD confirms the structural phases of the different samples in Figure 8e, where distinct peaks are observed for NiMn LDH/NF, NiMn LDH/C-MXene/NF, and Te-NiMn LDH/C-MXene/NF. Reference patterns for Ni(OH)₂ and Mn(OH)₂ are also compared, confirming the successful formation of the LDH phases and the influence of doping

and substrate modification. The prepared LDH displayed vertically aligned, nanosheet-like morphology with enhanced crystallinity, a significantly expanded interlayer spacing, increased surface roughness, and higher electrochemical surface area; BET analysis confirmed elevated surface area due to CTAB intercalation. Such morphological and structural characteristics, combined with improved conductivity from Te doping and MXene support, make this LDH ideal for high-performance supercapacitor applications.

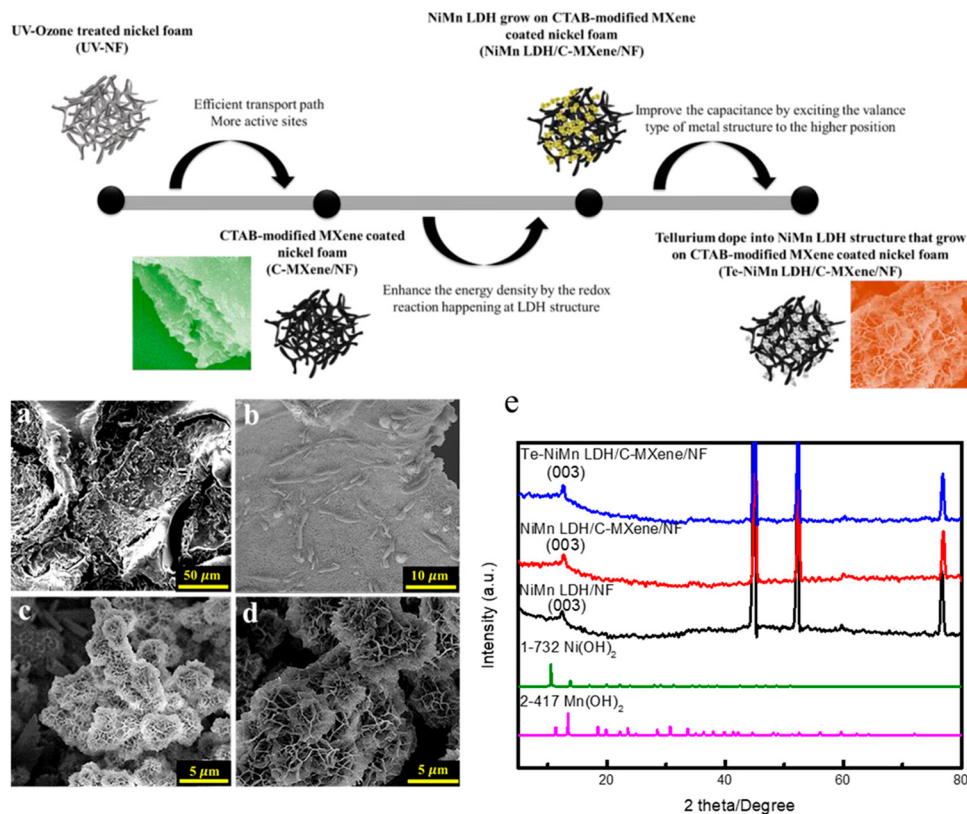


Figure 8. Overview of the synthesis process for Te-doped NiMn LDH on CTAB-modified MXene-coated nickel foam. FESEM images showing surface morphologies at various stages: (a) C-MXene/NF, (b) NiMn LDH on bare NF, (c) NiMn LDH on C-MXene/NF, and (d) Te-doped NiMn LDH on C-MXene/NF. (e) XRD patterns comparing NiMn LDH/NF, NiMn LDH/C-MXene/NF, and Te-NiMn LDH/C-MXene/NF, with standard reference peaks of Ni(OH)_2 and Mn(OH)_2 included for comparison. Reproduced with permission [169].

3.3. Electrochemical Deposition

Electrochemical deposition reduces metal ions from a solution with the potential to generate thin lamellar films on substrates for LDHs. Binders and post-treatment are unnecessary with this method [170–172]. Faradaic interactions at the electrode/electrolyte interface generate localized hydroxide ions, which combine with metal cations in solution to precipitate LDHs' layered structure [92,173]. This approach directly synthesizes LDHs with controlled composition and form by changing electrochemical parameters, making it a strong functional material creation tool. Electrochemical environments improve deposition kinetics, enabling fast nucleation for nanostructured coatings with high surface areas. Environmental friendliness and operational simplicity approach a viable alternative to existing chemical precipitation procedures. Electrochemical deposition for LDH synthesis reduces oxygen-containing species at the cathode, quickly raising local pH and forming metal hydroxide layers. Metal hydroxide layers form a lamellar structure held together by intercalated anions like carbonates or nitrates. The water reduction rate and hydroxide ion supply for LDH production rely on the applied voltage. Current density and deposition

duration can often change the LDHs' deposit shape and crystallinity. Researchers can tune LDH film performance for catalysis and energy storage.

Water electrolysis raises local hydroxide concentrations, which react with divalent and trivalent metal cations to synthesize LDHs by electrochemical deposition [174]. Metal hydroxide layers form *in situ* and stack into an organized array. The interaction between nucleation and growth controls deposition, ensuring uniform deposition across the electrode surface with controlled current or potential. The mechanism is complicated since deposition kinetics and ion transport compete to determine film structure. Understanding and regulating these parameters is necessary for making high-quality LDH films with desirable qualities. LDH film shape and crystallinity depend on electrodeposition parameters such as applied voltage, current density, and deposition time. Researchers can optimize these settings to create LDH deposits with consistent thickness and well-defined platelets [174]. Changing the electrolyte composition and pH controls LDH nanofilm deposition kinetics and structural evolution. These optimized conditions give synthesized films excellent electrochemical performance, which is helpful for catalytic applications and energy storage devices. Extensive parameter optimization is necessary to synthesize materials with specific functional properties [175]. Electrochemical deposition of LDHs commonly has hexagonal platelet-like formations after alkaline treatment, as documented in the literature [176]. Reorientation and crystallization of amorphous deposits under alkaline circumstances create an ordered lamellar pattern. Ion concentration and water decrease support platelet formation. Morphological aspects directly affect functional properties like ion intercalation and film catalytic activity. Optimizing LDH-based electrode performance requires precise control over deposition and post-treatment. Alternating metal hydroxide layers and intercalated anions or water molecules give LDHs their lamellar structure. Recent research confirms this tendency [93]. The systematic stacking of LDHs is caused by metal cations reacting with hydroxide ions during electrochemical deposition. Interlayer anions balance the positive charge of metal hydroxide layers and improve structural stability and functionality. The deposition environment can also be modified to these intercalated species, further controlling material characteristics. The deposition method naturally forms highly structured, anion-rich structures, enabling rapid ion exchange and high specific surface areas.

When comparing electrodeposition with traditional synthesis methods, such as co-precipitation or hydrothermal techniques, it becomes evident that electrochemical deposition offers significant advantages for the fabrication of LDHs [177]. This technique enables the direct deposition of LDHs onto conductive substrates, thereby eliminating the need for binder agents and enhancing electron transfer efficiency. In addition, the *in situ* formation of hydroxide films during electrodeposition leads to rapid synthesis and improved uniformity relative to conventional methods. Such direct synthesis is crucial in applications where interface quality between the active material and the substrate determines overall device performance. Consequently, electrochemical deposition has become a preferred method for preparing LDH films in many high-performance electrochemical systems. Electrochemical deposition presents several notable advantages, including precise control over film thickness, composition, and morphology, which are critical factors for optimizing the properties of LDHs [174,177]. This approach may change reactant concentration and deposition rate by carefully adjusting the applied voltage and current. This control guarantees uniform nucleation density across the substrate, decreasing flaws and improving electrode performance. Electrodeposition also makes LDH integration on metal foams and carbon-based electrodes easy. These tunable characteristics allow researchers to customize LDHs' physical and chemical features for energy storage and electrocatalysis applications. Recent studies have exemplified the successful application of electrodeposi-

tion in synthesizing NiCo-LDH films directly onto nickel foam substrates, a configuration that significantly enhances electrocatalytic performance [174,178]. Direct development of LDHs on structured substrates provides excellent electrical connection and a high electrochemically active surface area for effective catalytic reactions. Interconnected nanosheets in the hierarchical microstructure enable quick charge transfer and mechanical stability under operational conditions. The substrate/active LDH material synergy boosts device performance, making them attractive for water splitting and supercapacitor electrodes. Electrodeposition helps synthesize improved composite electrodes for energy conversion and storage. Pulse electrodeposition, a variant of the traditional electrochemical deposition technique, involves applying cyclic pulses of current or potential, which are sometimes interspersed with reverse pulses [179]. Incorporating pauses between deposition pulses alleviates the local depletion of metal ions, thereby allowing a more uniform ion concentration to be maintained across the deposition zone. This technique effectively enhances the morphological quality of the deposited LDH films, leading to more homogeneous structures with reduced defects. Additionally, reverse pulses can help remove undesirable surface charges that may otherwise impede further deposition or lead to non-uniform film growth. As a result, pulse electrodeposition is a valuable method for fine-tuning the properties of LDH films in various electrochemical applications.

Recent research using *in situ* techniques, such as atomic force microscopy, has revealed the dynamic morphological evolution of Co-based LDH nanosheets during electrodeposition [180]. These studies have shown that the initial nucleation step is critical in establishing the eventual sheet-like structure and that subsequent growth is susceptible to the applied deposition parameters. The evolution process is characterized by the formation of nanoscale features that promote efficient charge transport and ion diffusion. Moreover, the real-time observation of the growth process has provided critical insights into the nucleation and growth mechanisms, enabling further optimization of deposition protocols. This understanding is vital for designing LDHs with enhanced electrocatalytic or supercapacitive properties, as the nanosheet structure is key to their high surface area and functionality. The impact of deposition time and current density is well documented, with studies demonstrating that prolonged deposition or increased current can significantly enhance the crystallinity and overall quality of LDH films [181]. Longer deposition times allow for gradually reorganising initially amorphous deposits into highly ordered, crystalline platelets suitable for various electrochemical applications. Similarly, higher current densities can accelerate hydroxide ion generation, boosting nucleation rates and leading to finer nanostructures. However, excessive current may also lead to inhomogeneities; thus, optimizing these parameters is crucial to maintaining the lattice structure. Therefore, systematic studies that vary these factors are essential for mapping the optimal conditions that yield LDHs with superior structural and electrochemical characteristics.

A significant body of work has centered on the electrochemical deposition of NiFe and NiCo LDHs, which have been shown to provide high performance for water oxidation and other electrocatalytic reactions [182,183]. In these systems, the deposition process is optimized to ensure the formation of ultrathin nanosheets, whose abundant active sites contribute to enhanced catalytic activity. The simultaneous incorporation of two types of metal ions in the LDH structure is particularly beneficial, as it facilitates synergistic effects that lower overpotentials and improve reaction kinetics. Moreover, such bimetallic systems benefit from the tunability offered by electrodeposition, allowing researchers to balance the composition and morphology for maximum efficiency. These studies provide compelling evidence that electrodeposited LDHs can meet the rigorous demands of modern electrocatalytic applications.

In another compelling example, the synthesis of CoNi-LDH films via electrodeposition onto copper substrates has been reported for high-performance supercapacitor applications [184]. Direct deposition promotes strong adhesion between the active material and substrate, improving device stability and charge/discharge cycling. Hierarchical nanostructures created by electrodeposition improve accessible surface area, boosting pseudocapacitive performance, according to researchers. Active sites are evenly distributed over the electrode surface, enabling fast ion transport and energy storage. According to such studies, electrodeposition methods are widely applicable and work well in LDH-based energy storage devices. The pulsed deposition methods, as discussed earlier, also play a critical role in refining LDH film morphology by allowing for periodic replenishment of metal ions and the removal of excessive surface charge [179]. This controlled deposition method produces uniform, defect-free coatings with outstanding adhesion and electrochemical characteristics. The intermittent deposition approach slows reactant depletion near the cathode, assuring film growth. Such methods benefit complex multimetal systems that require homogeneous distribution for desirable electrical properties. Thus, pulse electrodeposition provides a versatile and practical approach for synthesizing improved LDH materials.

Electrochemical deposition has also been extended to synthesizing CoFe and CoNi LDH catalysts, which show superior OER performance owing to their enhanced conductivity and abundant active sites [177,185]. In these studies, precise control over the deposition conditions results in ultrathin films that maximize the exposure of catalytically active sites while maintaining excellent adherence to the substrate. The voltage and current parameters are optimized to balance the nucleation and growth processes, ensuring the resulting film is uniform and highly porous. Such optimization is key to reducing the overpotential required for OER and enhancing overall catalytic efficiency. The resulting electrode architectures, therefore, present a promising route for developing cost-effective and efficient water splitting systems. Consistent with the critical role of processing parameters, numerous experimental studies have underscored that the nucleation rate and the growth kinetics during electrodeposition are pivotal in determining the overall quality of LDH films [174]. Optimal equilibrium between these elements ensures continuous, defect-free, nanostructured deposited layers. Furthermore, systematic modification of deposition time and applied voltage has greatly affected film shape and crystallinity. Finely tailored deposition techniques increase electrochemical performance and reproducibility across substrate materials. Optimizing the electrodeposition process is necessary to produce high-quality LDH films for advanced energy and catalytic applications.

The versatility of electrodeposition has allowed for the synthesis of LDH films on various substrates, including metal alloys and conductive carbon materials, thereby broadening the scope of potential applications [186,187]. Growth on substrates like titanium and aluminum alloys has been demonstrated to improve corrosion resistance and enhance the material's durability in aggressive environments. Similarly, deposition on carbon-based substrates offers benefits such as improved conductivity and flexibility, which are crucial for fabricating next-generation electrodes. The inherent adaptability of the electrochemical deposition process accommodates modifications to suit various substrate types while retaining high film quality and consistency. Thus, the method's applicability to various substrates significantly expands potential applications for LDH-based materials. The electrodeposition method inherently facilitates the formation of binder-free LDH films, thereby eliminating potential interference from insulating binders and enhancing electrical connectivity between the active material and the substrate [188,189]. This direct deposition onto conductive substrates results in improved electron transfer and overall device performance, which is particularly beneficial in electrochemical sensing and energy storage devices. With-

out additional processing steps, the simplicity and efficiency of the process are markedly enhanced, leading to lower production costs and higher material uniformity. Moreover, the direct interface formed by binder-free deposition ensures intimate contact between the catalyst and the electrode, a crucial factor for high-performance devices. Therefore, electrodeposition is an efficient route to achieving high-quality, binder-free LDH films with optimized properties.

The fundamental mechanism driving the electrochemical deposition of LDHs pivots on the local generation of hydroxide ions from water reduction, which quickly interact with dissolved metal cations to create precipitated hydroxide layers [175]. This process is initiated at the cathode and progresses by the continuous supply of hydroxide ions, resulting in sustained growth of the layered structure as long as the applied potential is maintained. The reaction environment is finely tuned so that the concentration gradients created during deposition facilitate the uniform nucleation of the LDH phase across the electrode surface. Additionally, the ease of ion migration and fluid dynamics within the electrolyte further contributes to the modernization of the deposition front. Thus, the coupling between electrochemical reactions and diffusive transport is essential in establishing the layered architecture characteristic of LDHs. Under optimized electrochemical deposition conditions, it is possible to generate LDH films exhibiting diverse morphologies, including nanosheets, nanoframes, and porous networks [180,183]. Deposition parameters, including current density, pulse duration, and electrolyte composition, can be adjusted to control these morphological differences to match the application. Rapid nucleation and anisotropic growth in the substrate plane produce ultrathin nanosheets with excellent lateral connectivity. Slower deposition rates and higher ion diffusion can create a more porous network, which is helpful for quick ion transport applications. Thus, controlling the deposition environment allows researchers to construct LDH films with unique morphologies for specific functional tasks.

The deposition process is susceptible to external parameters like pH and temperature, which influence the reaction kinetics and the structural outcome of the synthesized LDH films [190]. High pH levels enhance nucleation by increasing hydroxide ion concentration, forming hydroxide layers that assemble into lamellar structures quickly. Temperature also helps constituent ions move, enabling rearrangement to create a crystal lattice. This sensitivity to deposition circumstances requires rigorous experimental control because even small variations might impact material characteristics. The interaction between pH, temperature, and applied voltage is crucial for regulated deposition and high-quality LDH films. The overall synthesis of LDHs by electrodeposition has been widely employed in developing electrocatalysis and energy storage device catalysts [181,182]. The layered structure of LDHs, alternating metal hydroxide sheets intercalated with anions, provides many active sites and improved ion transport routes in various applications. These functional applications require accurate film thickness and composition control, which the deposition process offers. Electrodeposited LDHs adhere well to substrates, making them stable under high-current or long-term operation. In addition to being a straightforward synthetic pathway, the technology allows the integration of high-performance LDH materials in innovative technological applications [191]. Structural and electrochemical analyses have indicated that the LDH films produced through electrodeposition feature a unique lamellar morphology and highly porous structure, essential for rapid ion transport and high surface reactivity [177,192]. These materials have large interlayer spacing because the deposition process creates loosely packed layers intercalated by anions or solvent molecules. Electrocatalysis and supercapacitors require rapid ion diffusion and high charge storage capacities, making porosity favorable. The films' wide pore channels minimize ion transport resis-

tance, improving electrochemical performance. The structure of electrodeposited LDHs allows for adequate charge storage and robust catalytic processes.

Recent examples in the literature have demonstrated that strategic modulation of the pulse deposition sequence, by incorporating rest periods and reverse pulses, can significantly enhance the quality of LDH films [174,179]. Incorporating pauses between active deposition pulses allows for the equilibrium re-establishment of metal ion concentration near the electrode surface, thereby avoiding depletion effects and promoting uniform growth. Furthermore, reverse pulses help remove excess charge accumulation on the surface, which can otherwise lead to undesirable side reactions or film defects. The precise control over these deposition parameters enables the creation of LDH films with highly uniform thicknesses and minimized defect densities, both of which are crucial for ensuring high electrochemical performance. Therefore, advanced pulse modulation strategies have emerged as indispensable tools in the electrodeposition synthesis of high-quality LDH materials.

Certain studies have highlighted the deposition of MnCo-based films, where incorporating cobalt into the electrodeposited film significantly affected the electrocatalytic performance of OERs [175,193]. This research demonstrated that by varying the deposition parameters, the crystallinity and morphology of the LDH films could be tailored to enhance their catalytic activity. In these cases, the presence of cobalt was shown to improve the films' electronic conductivity and redox capabilities, thereby reducing the overpotential required for catalysis. Additionally, the synergistic effect of the mixed metal composition resulted in enhanced nucleation rates and more uniform film formation during deposition. These findings underscore the importance of compositional tuning in the electrodeposition process to optimize the functional properties of LDHs [175,193].

The transformation of precursor materials such as MOFs into LDHs via electrochemical deposition is another emerging avenue that broadens the synthesis strategies available for these materials [190,194]. In this approach, the MOF serves as a sacrificial template, which, upon exposure to an alkaline environment and an applied potential, is converted into an LDH. This method offers the advantage of controlling the porosity and morphology of the final product by precisely tuning the conversion process. The reconstruction of MOFs into LDH structures simplifies the synthetic steps and results in materials with enhanced catalytic and electrochemical properties. As a result, this technique has garnered attention as a promising strategy for producing advanced LDHs with tailored features for diverse applications. In a related innovation, the reconstruction of Prussian blue analogs into thin LDHs has been meticulously demonstrated, offering a pathway toward synthesizing efficient electrocatalysts [194,195]. One of the foremost benefits of electrodeposition is the direct integration of LDH films onto conductive substrates, eliminating the need for nonconductive binders that might hinder electron transport [177,196]. The resulting electrodes exhibit excellent electrical connectivity and reduced interfacial resistance by depositing LDHs directly onto substrates such as titanium carbide or nickel foam. This direct synthesis approach enhances electrochemical performance, particularly in applications requiring high-rate charge transport, such as supercapacitors and electrolysis cells. Moreover, the robust interface formed through electrodeposition contributes significantly to the devices' mechanical stability and operational longevity. Consequently, the method provides a streamlined route to high-performance electrodes by ensuring that the active material is directly and intimately connected with the current collector.

The inherent precision of the electrodeposition method allows for exceptional tunability in the thickness, composition, and morphology of the resulting LDH films, which is essential for correlating structure with performance [174,177]. Researchers have effectively exploited this precision to fabricate films optimized for specific applications, whether en-

hanced catalytic activity or improved storage capacity. By adjusting parameters such as deposition potential and electrolyte concentration, the process can be customized to yield films with distinct microstructures ranging from smooth continuous layers to highly porous networks. This level of control is particularly beneficial in energy-related applications, where the surface area and active site accessibility largely dictate the device's performance. Therefore, electrodeposition remains a desirable method due to its flexibility and effectiveness in producing high-quality LDH films tailored to meet specific performance criteria. In addition to conventional electrodeposition, recent advancements have illustrated how integrated deposition strategies can further enhance the functional properties of LDH films [197,198]. During LDH electrodeposition, nanostructured carbon materials can increase the composite electrode's electrical conductivity and surface area. This synergistic combination creates an electrode with better charge transport and effective capacitance, which is ideal for energy storage. Dual nanocarbon supports ensure structural integrity and excellent catalytic reactivity of deposited LDHs. Such hybrid structures emphasize the need for multifarious deposition techniques to generate integrated materials with improved performance.

Advanced methodologies also include the *in situ* formation of NiAl-LDHs within confined microreactor environments, where tunable interlayer spacing can be achieved by adjusting the impinging jet parameters during deposition [186]. Microreactor-assisted electrodeposition enables precise nanoscale control of LDH structures, enhancing their electrochemical performance for energy applications. The unique design of deposition setups, including pauses between deposition pulses, further ensures the uniform regeneration of metal ion concentrations near the electrode surface [173,179]. Pulse-controlled electrodeposition enhances LDH film uniformity and structural order, yielding high-performance electrodes with reduced defects and improved interlayer connectivity.

Electrodeposition techniques have also been highly effective in synthesizing uniformly mixed LDH films incorporating multimetal systems, such as NiCo-LDH, which are critical for high-performance electrocatalysis [174,196]. Electrodeposition enables uniform multimetal integration in LDH films, enhancing conductivity, redox activity, and catalytic performance for advanced energy applications. Detailed interfacial analyses have shown that the layer-by-layer growth achieved during the electrodeposition of LDHs results in exceptional interfaces crucial for efficient electron transport and ion accessibility [183,192]. The well-organized lamellar structure in these systems ensures that charge carriers can traverse the electrode with minimal impedance due to the abundant and organized active sites. The formation of these homogeneous interfaces is critical in reducing the electrode's internal resistance and enhancing the overall electrochemical performance. Furthermore, the intimate contact facilitated by the direct deposition method minimizes potential interfacial delamination issues, thereby contributing to the longevity and robustness of the device. Consequently, the layer-by-layer growth mechanism achieved through electrodeposition is a key feature that reinforces the practical viability of LDHs in complex electrochemical applications.

The electrodeposition synthesis strategy is strongly influenced by the competition between nucleation and growth processes, which are both sensitive to the deposition parameters set during the process [193]. A higher applied potential can increase the nucleation rate, leading to a greater density of small nuclei, which eventually merge to form a continuous film. However, if the growth process is not carefully managed, rapid nucleation can lead to the formation of overly rough and non-uniform surfaces. Therefore, selecting the appropriate deposition conditions, such as current density and pulse duration, is essential to achieve the desired balance between nucleation and growth.

This delicate balance is fundamental for synthesizing high-quality LDH films with optimal microstructural characteristics [181,193].

Among the innovative examples in recent literature are ternary LDH composites that have been synthesized via electrodeposition, demonstrating significantly improved OER performance [199,200]. The introduction of a third metal component not only enhances the electronic structure of the LDH but also introduces a new level of active sites that facilitate more efficient catalytic processes. Detailed electrochemical studies have revealed that such ternary systems lower the overpotential required for OER and improve reaction kinetics due to the synergistic interactions among the incorporated metal species. Moreover, these composite materials were obtained by adjusting the deposition parameters to ensure uniformity and high dispersion of the active species across the electrode. Therefore, the evolution of electrodeposition techniques to include multimetal systems represents a significant advancement toward developing next-generation catalysts for clean energy applications.

An intriguing dimension of electrodeposition is its adaptability in fabricating flexible energy storage devices. LDH films are deposited onto flexible substrates to yield electrodes with outstanding mechanical integrity and high capacitance [189,201]. Such flexible electrodes not only sustain large mechanical deformations but also maintain excellent electrochemical performance during long-term cycling. The direct growth of LDHs onto flexible substrates ensures that the interface is robust and the ion transport channels remain unimpeded despite mechanical bending or stretching. In addition, the combination of electrodeposited LDHs with flexible conductive materials opens up new possibilities for wearable energy storage devices and portable electronics. This innovative approach underscores the versatility of electrochemical deposition in producing advanced electrodes that combine mechanical flexibility with exceptional electrochemical properties.

The careful selection of deposition parameters, such as electrolyte composition and deposition time, is essential to unlocking the theoretical structural advantages of LDHs, including high surface areas, accessible interlayer spaces, and controlled redox properties [196,202]. For instance, tuning the electrolyte composition can promote the selective intercalation of specific anions, thereby optimizing the interlayer spacing and significantly enhancing the electrochemical performance. Similarly, adjusting the deposition time allows for precise control over film thickness, directly impacting the electron and ion transport kinetics within the LDH film. These controlled modifications enable the synthesis of LDHs that exhibit tailored properties for applications ranging from water splitting to supercapacitors. In this context, the electrodeposition technique stands out for its flexibility and effectiveness in producing materials with finely tuned structural and functional characteristics.

Numerous studies have demonstrated the advantages of pulsed electrodeposition, wherein reverse pulses are utilized to mitigate the accumulation of surface charges and to ensure a steady state of deposition ion concentration [174]. By carefully calibrating the pulse duration and the intervals between pulses, the deposition process can be optimized to yield smoother, more uniform LDH films with reduced defect densities. This method also minimizes undesirable side reactions, thereby enhancing the deposited materials' chemical integrity and electrochemical stability. The resulting improvement in uniformity is directly related to improved device performance, as fewer defects translate to fewer pathways for unwanted charge recombination or degradation. As such, pulsed electrodeposition represents a sophisticated synthesis strategy well-suited for preparing high-quality LDHs for advanced electrochemical applications.

The high degree of tunability in electrodeposition also permits the fabrication of LDH films with diverse morphologies, ranging from densely packed continuous layers to highly porous, exfoliated nanosheets [180,183]. By systematically adjusting deposition conditions,

researchers have induced a controlled exfoliation of the layered structure, thereby exposing more active sites and increasing the effective surface area. These morphological features are particularly beneficial for supercapacitors and electrocatalysts, where rapid ion diffusion and extensive charge storage are critical. Moreover, synthesizing distinct nanostructures within a single processing technique allows for integrating materials with complementary properties, further enhancing device performance. Consequently, the tunability of the electrodeposition process serves as a key advantage in the strategic design and synthesis of advanced LDH-based materials.

Complementary to the direct electrodeposition approach, *in situ* reconstruction methodologies have emerged as powerful strategies to convert existing compounds into LDH structures with desired morphologies and enhanced functionalities [92,194]. Such methods involve transforming precursor materials under the influence of applied potential and alkaline conditions, leading to the formation of LDH structures from an initially non-layered phase. This reconstruction process streamlines the overall synthesis and results in LDH materials with improved crystallinity and increased active surface areas. Integrating reconstruction techniques with electrodeposition offers additional control over the deposition kinetics and final structure. As a result, these coupled strategies enable the fabrication of high-performance LDH-based electrodes suitable for an array of advanced applications [92].

These advanced synthesis strategies have been further refined by incorporating design templates that direct the formation of hierarchical LDH structures with enhanced catalytic and energy storage properties [178,197]. Whether sacrificial or permanent, templates allow the growth of LDH films with controlled porosity, uniform layer thickness, and precisely engineered interlayer distances. Such templated electrodeposition enhances the material's electrochemical performance by increasing the effective surface area, improving ion transport, and imparting mechanical robustness to the composite electrode. Moreover, the templating approach facilitates the formation of multidimensional architectures tailored to specific functional requirements. Consequently, these design strategies underscore the critical role of electrodeposition in synthesizing advanced LDH materials with tailored structure/property relationships for various applications. The electrochemical deposition and synthesis mechanism for LDHs embodies a multifaceted process that leverages controlled faradaic reactions to generate well-defined, nanostructured films with tunable compositions and morphologies [173,181,193]. By meticulously adjusting parameters such as deposition potential, current density, ionic concentration, and pulse duration, researchers can achieve high-quality LDH films that are directly integrated with conductive substrates, making them readily applicable in electrocatalysis, energy storage, and corrosion protection [177,184,196]. Recent advances have further demonstrated that innovative approaches, ranging from pulsed electrodeposition to reconstruction of precursor materials, significantly enhance the performance attributes of LDH films by optimizing the exposure of active sites and ensuring efficient ion transport. The versatility and scalability of the electrochemical deposition technique promise to further advance the field of nanostructured material synthesis and are expected to play a pivotal role in developing next-generation devices. Thus, this synthesis process's robust and adaptable nature ultimately underscores its importance and potential for future applications in various scientific and technological domains.

NiCo LDH was synthesized via an electrodeposition method, enhanced by incorporating $Ti_3C_2T_x$ MXene on the nickel foam (NF) substrate and in the plating solution [203]. This dual role of MXene improved interfacial contact and conductivity, facilitating the deposition of ultrathin LDH nanosheets with high areal loading ($\sim 65 \text{ mg/cm}^2$). Characterization revealed a porous nanosheet morphology, polycrystalline hexagonal structure

via HRTEM, uniform Ni and Co distribution, and MXene confirmed through XRD and XPS analyses. These features collectively make the MXene-enhanced LDH electrode highly suitable for high-performance ZIB cathodes. The CoNi-LDH was synthesized on flexible CC via in situ electrochemical deposition from a $\text{Co}^{2+}/\text{Ni}^{2+}$ precursor, followed by electrochemical activation (ECA) in aqueous KOH to induce H-vacancy formation, resulting in CoNi-LDH(v) [204]. Figure 9a outlines the two-step process used to create the CoNi-LDH electrode. First, CoNi-LDH is deposited onto CC via electrochemical deposition, then it undergoes electrochemical activation to introduce hydrogen vacancies, forming CoNi-LDH(v)@CC. As shown in Figure 9b, the deposition occurs in a solution containing Co^{2+} , Ni^{2+} , and OH^- ions. The corresponding CV curve shows redox behavior, and the resulting material has a layered crystal structure with nitrate ions. Figure 9c illustrates the activation step, where CoNi-LDH is treated under an applied voltage to create hydrogen vacancies. The CV plot shows enhanced electrochemical activity after activation, and the structure model confirms the formation of H vacancies that improve the material's electrochemical properties. The morphology revealed vertically aligned nanosheets forming a porous 3D network; structural analysis via XRD and TEM confirmed partial amorphization and reduced interlayer spacing due to NO_3^- extravasation. BET surface area was not directly stated, but the induced H vacancies and 2D open channels significantly increased the active surface and conductivity. These features enhanced Zn^{2+} diffusion and intercalation, making the LDH highly suitable for Zn-ion battery applications.

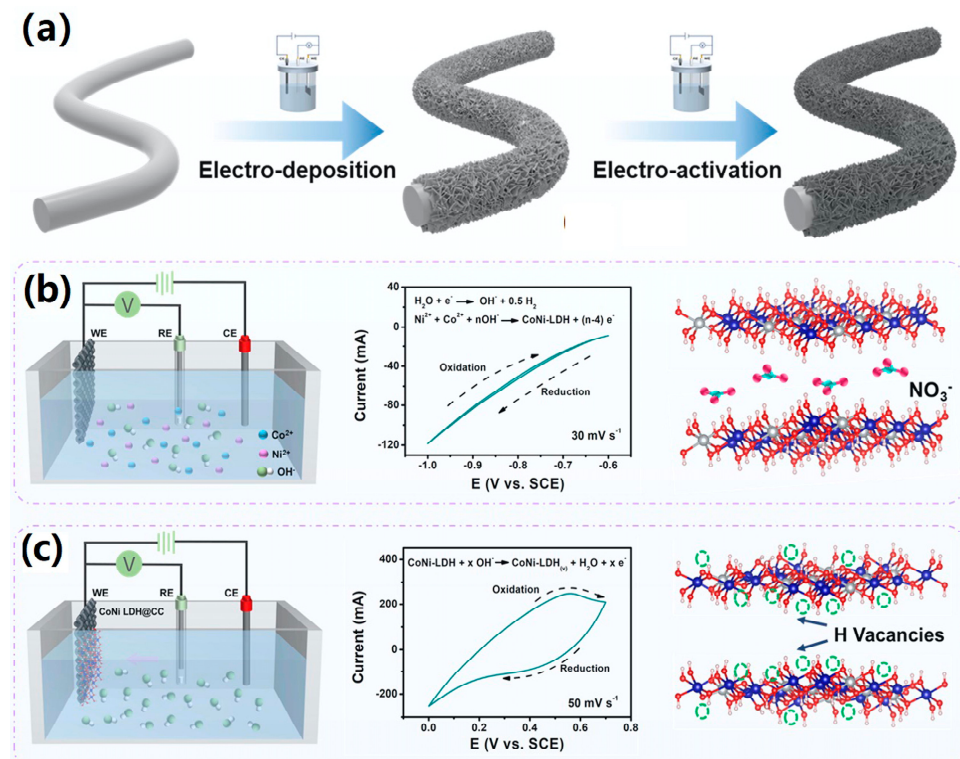


Figure 9. (a) Illustration of the fabrication steps involving electrochemical deposition of CoNi-LDH on CC (CoNi-LDH@CC), followed by electrochemical activation to generate hydrogen-deficient CoNi-LDH(v)@CC. (b) Diagram of the deposition setup (left), corresponding CV curve (middle), and the crystal structure of the as-prepared CoNi-LDH (right). (c) Electrochemical activation process (left), CV curve under optimized activation conditions (middle), and structural model showing hydrogen vacancies in CoNi-LDH(v) (right). Reproduced with permission [204].

A novel synthesis pathway involves the reconstruction of MOFs or Prussian blue analogs into LDHs, which can also be achieved through an electrochemical deposition

process [190,194]. This approach uses the structural change of a precursor molecule in an alkaline environment under an applied voltage to create an LDH. The reconstruction method simplifies synthesis and increases product surface area and reactivity. Using MOFs as sacrificial templates also allows fine control over the LDH structure's porosity and shape. This comprehensive technique shows how electrochemical deposition can synthesize customized LDHs with enhanced functional characteristics. Adjusting the deposition parameters enables the production of ultrathin LDH films with exceptional surface area and catalytic activity, which are crucial for their application in sensors and energy devices. By fine-tuning factors such as ionic strength, deposition time, and pulse frequency, researchers can achieve controlled growth that yields films with homogeneous thickness and low defect densities [173]. The resulting LDHs exhibit enhanced electron mobility and rapid ion diffusion, vital for high-performance catalytic and supercapacitor applications. Furthermore, the deposition technique provides a direct route to engineering the film architecture, which supports efficient charge storage and transfer. As a result, the method stands out for its ability to customize nanostructured films for a wide range of electrochemical applications.

The formation of hexagonal platelets, a hallmark of well-crystallized LDHs, is significantly influenced by the alkaline treatment following electrodeposition, during which an initial disordered film is reorganized into an ordered lamellar structure [93]. This transition is attributed to the enhanced mobility of constituent ions within the deposit, which facilitates the rearrangement into a thermodynamically favorable configuration. The development of hexagonal platelets indicates high crystallinity and correlates with improved functional properties, such as ion exchange capacity and catalytic performance. Therefore, the post-deposition treatment must be carefully controlled to maximize these desirable features. Consequently, combining electrodeposition with subsequent alkaline treatment forms a robust strategy for synthesizing ordered and functional LDH films. Control over interlayer composition during the synthesis of LDHs via electrodeposition can be effectively achieved by modulating the electrolyte composition and deposition parameters [190]. Selecting electrolyte anions affects LDH charge balance, interlayer spacing, and structural stability. This process is useful when improved conductivity or selective adsorption is needed. The deposition potential also affects intercalating species production and integration, fine-tuning the final layered structure [186]. Thus, deliberate control over the ionic environment during deposition is essential for crafting LDHs with tailored interlayer characteristics and optimized performance. Co-deposition techniques have been effectively employed in more complex systems to synthesize hierarchical LDH structures by concurrently depositing multiple metal ions, which leads to synergistic enhancements in electrocatalytic performance [182,205]. The simultaneous incorporation of different metal species into the LDH framework generates a material with a multifaceted electronic structure that supports rapid redox kinetics. This hierarchical organization improves not only the catalytic activity but also the mechanical stability of the electrode under rigorous operational conditions. The co-deposition strategy thus enables fine control over the relative concentrations and spatial distribution of the metal ions, ensuring that each contributes efficiently to the overall performance. Such advanced synthesis techniques highlight the power of electrodeposition in crafting multifunctional LDH catalysts tailored for high-demand electrochemical processes.

The ZnAl-LDH coating layer was synthesized on commercial Zn foil using a galvanostatic electrochemical deposition method in a nitrate aqueous solution [172]. Optimized parameters included a current density of 3 mA/cm^2 for 2 min and a $\text{Zn}^{2+}/\text{Al}^{3+}$ molar ratio of 2:1. The LDH layer exhibited a smooth and uniform morphology with a hydrotalcite-like structure. The coating had a thickness of $\sim 1.5\text{ }\mu\text{m}$ and displayed excellent wettability

(contact angle $\sim 5.96^\circ$) and strong zincophilicity, indicating its suitability as an artificial interfacial layer. This tailored ZnAl-LDH effectively stabilizes Zn plating/stripping and inhibits dendrite growth, making it highly suitable for ZIB anode protection. Figure 10a–c illustrates the critical balance between zincophilicity and zincophobicity in stabilizing Zn anodes [206], a concept highly relevant to LDH-based strategies where their tunable surface chemistry and layered structures can be engineered to regulate Zn^{2+} deposition and electrolyte interactions in both ZIBs and ZABs. The CoNi LDH was synthesized via *in situ* electrochemical deposition on an exfoliated graphite (EG) substrate, followed by CV-based electrochemical activation in KOH to introduce hydrogen vacancies [207]. During activation, interlayer anions (NO_3^-) were removed, and O–H bonds in the hydroxide lattice were cleaved to form a defect-rich CoNi LDH(v) structure. The resulting material exhibited ultrathin mesoporous nanosheets (~ 5 nm thick), a hierarchically porous architecture, increased surface area (from 28.3 to $40.7\text{ m}^2/\text{g}$), and good elemental distribution and crystallinity. These structural and surface properties make this LDH well-suited for Zn-ion battery cathode applications due to enhanced ion accessibility, conductivity, and defect-driven cation adsorption.

The synthesis of NiCo-LDH involved a two-step process [208]. Initially, NiCoS nanotubes were formed on nickel foam using hydrothermal sulfidation, followed by constant potential electrodeposition of ultrathin NiCo-LDH nanosheets to construct a core/shell heterostructure. Characterization through FESEM and TEM confirmed a 3D nanotube@nanosheet architecture, XRD and Raman verified phase composition, and XPS analyzed valence states; the morphology provided abundant active sites and fast ion/electron pathways. This architecture is particularly suitable for ZIB cathodes due to its enhanced conductivity and electrochemical kinetics. The LDH-based composite was synthesized by first hydrothermally growing Ni_3S_2/NiS hetero-nanowire arrays on nickel foam, followed by electrodeposition of NiCo-LDH nanosheets to form a hierarchical core/shell structure [209]. This two-step process enables intimate interfacial contact between the conductive sulfide core and the active LDH shell. The resulting composite exhibited a 3D nanoarray morphology and chemical states characterized by XPS. The uniform architecture and rich surface functionalities render this LDH ideal for rapid ion/electron transport and structural stability, making it highly suitable for ZIB applications.

NiFe LDH was synthesized via a multi-step electrochemical approach where $Cu(OH)_2$ nanowires were first electroplated onto Cu foam, converted to CuO by annealing, reduced to Cu nanowires, and, finally, used as a scaffold for the electrochemical deposition of NiFe LDH nanosheets [210]. This process formed a 3D hierarchical core/shell structure of Cu@Cu NWs@LDH. The morphology presents uniform vertical nanosheet growth; XRD verified the crystalline structure, and XPS confirmed the elemental composition and valence states. The high surface area, strong bonding, and excellent electron conductivity make this LDH suitable for ZAB applications. CuCo LDH was synthesized by potentiostatic electrodeposition on nickel foam, followed by CV-based electrodeposition of Ni_3S_2 to form the CuCo LDH@ Ni_3S_2 composite [211]. The resulting composite featured a tremella-like interconnected nanosheet morphology, exhibited a layered LDH structure confirmed by XRD, weak crystallinity with abundant active sites, and had a high electrochemical double-layer capacitance ($C_{dl} = 2.74\text{ mF/cm}^2$), indicating excellent charge storage potential. This unique architecture provided enhanced conductivity, lower diffusion resistance, and increased redox sites, making it highly suitable for high-performance supercapacitor applications.

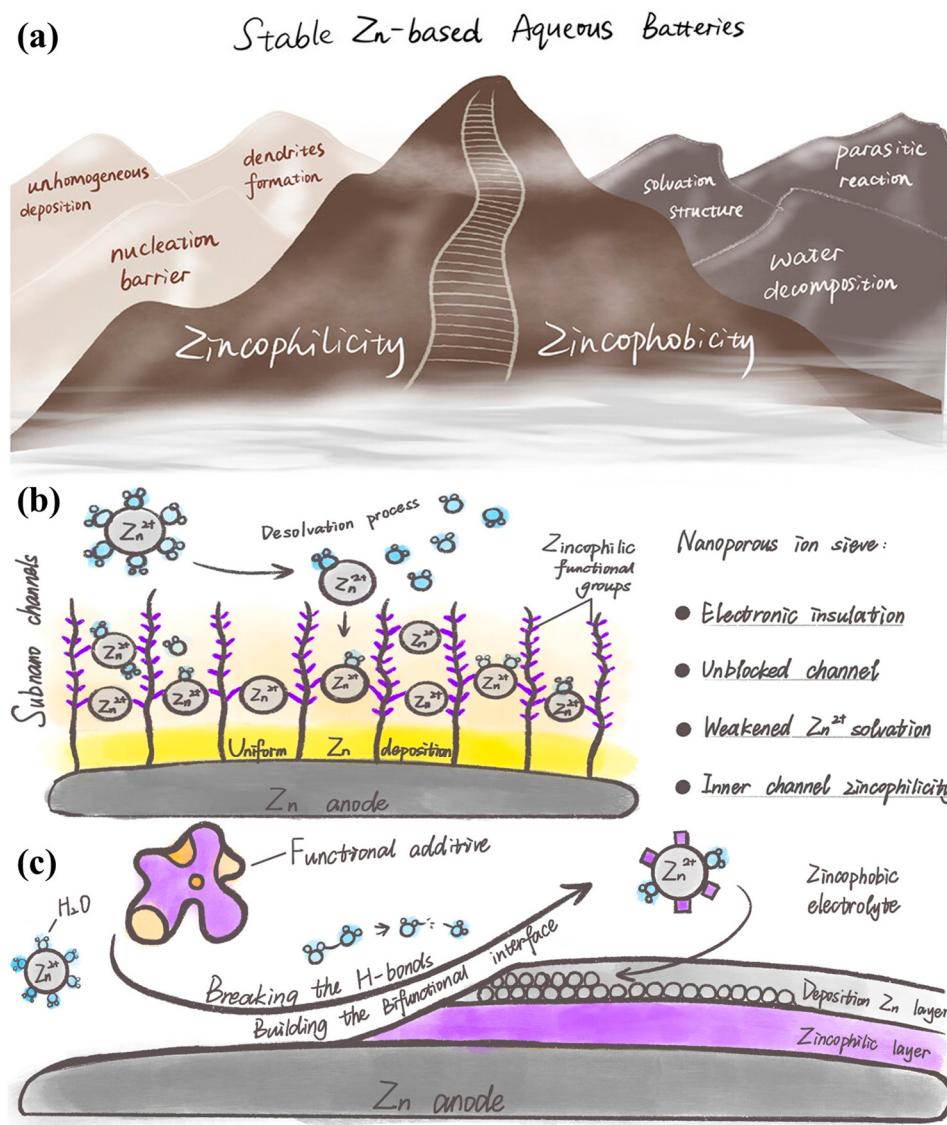


Figure 10. (a) Schematic illustration of the trade-off between zincophilicity and zincophobicity in achieving stable Zn-based aqueous batteries. (b) Design of a nanoporous ion sieve with zincophilic functional groups to enable uniform Zn deposition through controlled Zn^{2+} desolvation and selective ion transport. (c) Formation of a bifunctional interface using functional additives to simultaneously break water hydrogen bonds and construct zincophilic/zincophobic regions on the Zn anode. Reproduced with permission [206].

NiCo-LDH was synthesized via a simple electrochemical deposition process onto CC, followed by CV activation at various scan rates to induce hydrogen vacancies [212]. The as-prepared LDH retained its nanosheet morphology with a polycrystalline layered structure, showed reduced interlayer spacing (from 0.71 to 0.60 nm), preserved elemental homogeneity (Ni, Co, O), and exhibited enhanced M–O bonding indicative of H vacancy formation. These structural features, particularly the vacancy-rich domains, significantly improved the redox kinetics and ion diffusion, making this LDH highly suitable for supercapacitor applications. Khalafallah et al. [213] presented a low-cost, binder-free Zn-doped cobalt/lanthanum LDH (Zn/CoLa LDH) nanoarray-on-nanoarray electrode fabricated via a two-step electrodeposition method (Figure 11a), demonstrating superior electrochemical performance and durability for high-energy, high-power supercapacitor applications. NiAl-LDH was synthesized by a single-step electrochemical deposition on AC cloth using a chronoamperometry method at -1.0 V for 15 min [214]. Figure 11b depicts the stepwise

electrochemical strategy to grow NiAl-LDH nanosheets on a CC substrate. The resulting NiAl-LDH@CC composite exhibited a porous, vertically aligned nanosheet array structure with a high BET surface area of $437.5\text{ m}^2/\text{g}$, crystalline hydrotalcite-like layered structure, well-distributed elements (Ni, Al, O), and uniform coating thickness of $\sim 1.11\text{ }\mu\text{m}$. This combination of high surface area, structural integrity, and improved electron/ion transport characteristics renders the LDH highly suitable for supercapacitor applications. LDH was synthesized via *in situ* electrochemical deposition of nickel and cobalt nitrates onto carbon felt at -1 V for 10 min using a chronoamperometry technique [215]. The prepared NiCo-LDH formed a coral reef-inspired ultrathin mesoporous nanosheet architecture vertically aligned on the carbon felt, displaying a high BET surface area of $14.56\text{ m}^2/\text{g}$ and a narrow average pore diameter of 5.52 nm , with enhanced structural features confirmed by SEM, FTIR, and XRD analyses. This morphology, porosity, and strong electronic interaction between Ni and Co make the LDH ideal for efficient ion diffusion and redox kinetics, which is suitable for high-performance supercapacitor applications.

3.4. Other Advanced Synthesis Techniques (*e.g.*, Sol-Gel, Ultrasonication, Exfoliation)

Various other methods have been reported for synthesizing LDHs, which are anionic materials characterized by a unique layered structure of hydroxides intercalated with anions. Among these methods, sol-gel synthesis, ultrasonication, and exfoliation stand out due to their distinct advantages in producing LDHs with controlled morphology and composition. The sol-gel method is a widely employed technique for synthesizing LDHs because of its ability to control the chemical composition, morphology, and crystallinity of the resultant materials. This method involves the hydrolysis and polycondensation of metal alkoxides or salts, forming a gel that can then be converted into an oxide or hydroxide material upon thermal treatment. For instance, Klydziute et al. [216] highlighted the capacity of the sol-gel approach to yield MgAl-LDHs with tunable properties, emphasizing its versatility across different metal compositions and operating conditions. Additionally, Valente et al. [217] reported that the sol-gel method allows for precise control over parameters such as pH and temperature during synthesis, which facilitates particle size and distribution adjustments, making it suitable for various applications in catalysis and environmental remediation. Ultrasonication is another promising synthesis technique that has gained popularity for preparing LDHs due to its ability to enhance reaction rates and promote homogeneous nucleation. This method employs high-frequency sound waves to create cavitation bubbles, which, upon collapsing, generate localized high temperatures and pressures conducive to the chemical reactions needed to form LDHs. Mallakpour et al. [218] demonstrated that using ultrasonic waves shortened reaction times and improved the characteristics of the synthesized LDHs. Further, Sokol et al. [219] showcased that ultrasonication could accelerate the formation of Mg-Al-phosphate LDHs, signifying the method's effectiveness in synthesizing complex layered structures. Exfoliation refers to methods to produce nanosheets or dispersed layers from bulk LDH materials, enhancing their surface area and accessibility for various applications. This technique often involves delining layered structures in suitable solvents or via chemical treatments. According to Ibrahimova [92], several methods, including exfoliation, can alter the interlayer spacing of LDHs, facilitating the intercalation of functional anions. Additionally, Butenko et al. [220] provided evidence for the potential of exfoliated LDHs as effective adsorbents for environmental contaminants like phenols, thereby highlighting the practical implications of such synthesized materials. Specific examples of LDH synthesis using these advanced techniques are abundant in the literature. For instance, research by Mahjoubi et al. [221] employed sol-gel synthesis to produce ZnAl-LDHs intercalated with various anionic species, affirming the method's capability in tailoring materials for

specific functionalities such as dye removal. In the context of ultrasonication, the study by Mallakpour [218] emphasized the synthesis of bioactive intercalated LDHs with accelerated reaction rates and enhanced functional properties, which can significantly improve material performance in biomedical applications. Furthermore, the application of exfoliation in generating high-surface-area LDHs has been validated in environmental science, where these materials demonstrated promising performances in adsorbing toxic pollutants [220]. Sol-gel synthesis, ultrasonication, and exfoliation represent significant advancements in producing LDHs, allowing for tailored properties and functionalities. Each method contributes unique benefits that enhance the applicability of LDHs in diverse fields such as catalysis, environmental remediation, and materials science, leading to growing interest and research in this area.

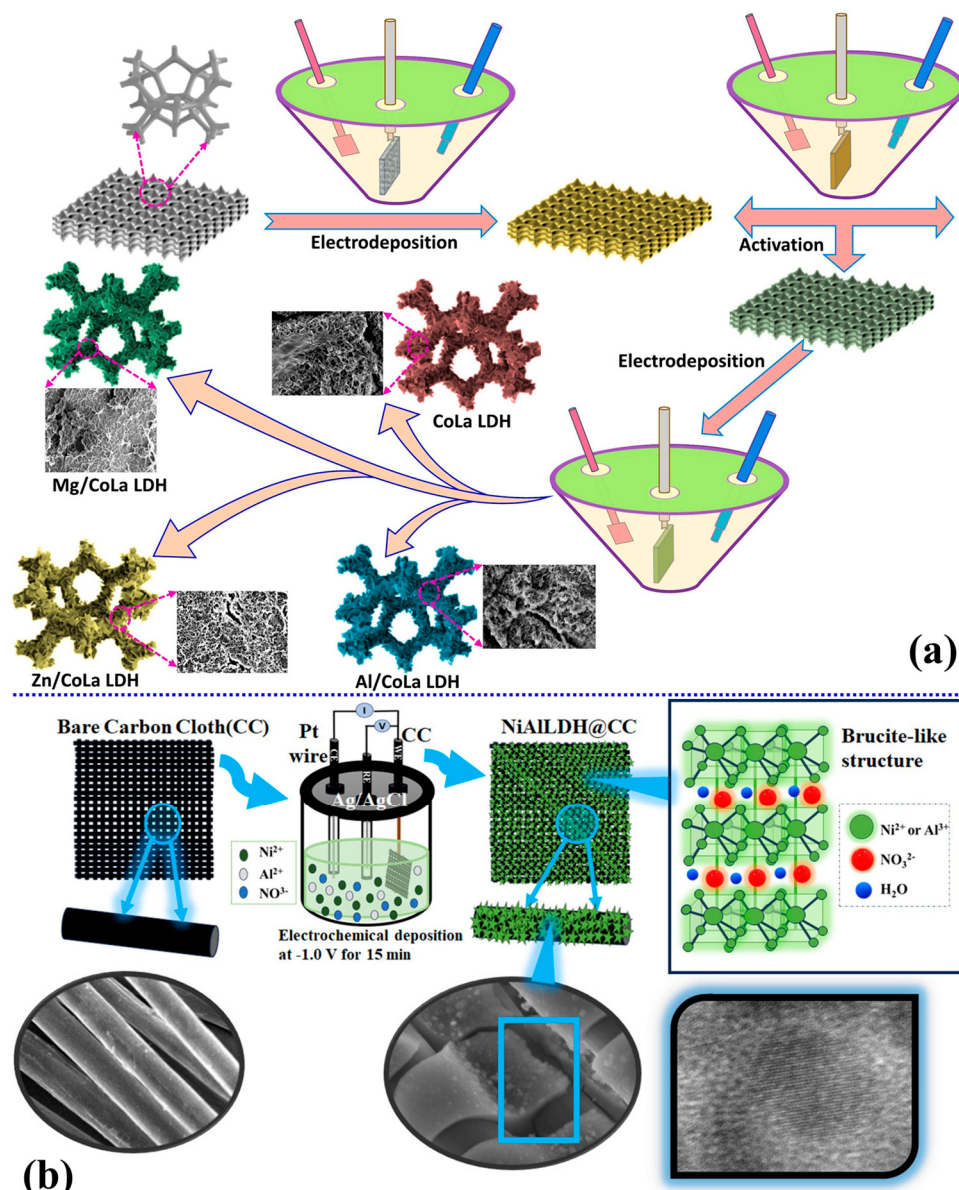


Figure 11. (a) Schematic illustration of the electrodeposition-based synthesis of binder-free CoLa LDH nanoarray-on-nanoarray networks doped with Zn^{2+} , Mg^{2+} , and Al^{3+} ions. Reproduced with permission [213]. (b) Illustration of the electrochemical synthesis procedure for fabricating NiAl-LDH nanosheets directly on CC (NiAl-LDH@CC). Reproduced with permission [214].

The nickel microwire aerogel (NMWAs) was synthesized via a sol-gel method under a magnetic field, followed by vacuum drying to obtain a porous and flexible aerogel

structure [222]. Subsequently, ultrathin NiCo-LDH nanosheets were grown *in situ* on the NMWAs surface via a solvothermal route, resulting in a core/shell NMWAs@NiCo-LDH architecture. The sulfur was then infused into the composite to form NMWAs@NiCo-LDH/S via a melt/diffusion method. Characterization revealed a 3D porous network of aligned nickel microwires coated with ultrathin LDH nanosheets (~6.8 nm thick). BET analysis showed mesopores (4–10 nm) and high surface area, while XRD, Raman, and XPS confirmed the phase purity and the presence of active functional groups like hydroxyls. This core/shell structure with high porosity, hydrophilicity, and strong chemical affinity for polysulfides makes it highly suitable for LSB applications by enhancing electrolyte access, trapping LiPSs, and promoting redox kinetics.

NiCo-LDHs were synthesized via a self-growth aging method in the presence of Ti_3C_2 -MXene [156]. Initially, few-layered MXene nanosheets were prepared through LiF/HCl etching of Ti_3AlC_2 , followed by ultrasonic exfoliation. These MXene sheets then served as substrates for the *in situ* growth of NiCo-LDHs through the reaction of Ni^{2+} and Co^{2+} with $NH_3 \cdot H_2O$ under an inert atmosphere, resulting in Vo-LDHs-MXenes with abundant oxygen vacancies. Morphologically, TEM and FESEM revealed a homogeneous 2D nanosheet structure, while BET analysis showed a high surface area ($35.22\text{ m}^2/\text{g}$) with mesoporosity, ideal for electrolyte access and sulfur redox reaction sites. XRD, XPS, and EPR further confirmed structural integration, oxygen vacancies, and electronic synergy between LDHs and MXenes. These features collectively enhance the immobilization of polysulfides and facilitate faster redox kinetics, making Vo-LDHs-MXenes highly suitable for LSB applications.

The NiCo-LDH was first synthesized by refluxing a mixed aqueous solution of $Ni(NO_3)_2 \cdot 6H_2O$, $Co(NO_3)_2 \cdot 6H_2O$, hexamethylenetetramine, and oxalic acid at $100\text{ }^\circ C$ for 6 h [223]. This precursor was then converted into NiCo-MOF/LDH nanorods through a solvothermal reaction with 2,5-dihydroxyterephthalic acid (DHTA) in a DMF/ethanol/water mixture at $140\text{ }^\circ C$ for 24 h. The synthesized NiCo-MOF/LDH nanorods exhibit a rod-like morphology with homogeneous elemental distribution, a high surface area ($512.3\text{ m}^2/\text{g}$), meso/microporosity, and coexisting crystalline (NiCo-MOF) and amorphous (NiCo-LDH) phases. These features make the material ideal for LSB applications by combining strong polysulfide adsorption and electrocatalytic conversion properties.

NiCo-LDH was synthesized by etching ZIF-67 nanocrystals using $Ni(NO_3)_2 \cdot 6H_2O$ in ethanol at elevated temperature, which led to the formation of hollow NiCo-LDH nanostructures [224]. Sulfur was subsequently incorporated into the LDH via a melt/diffusion process. The composite exhibited a hollow polyhedral morphology, confirmed by SEM/TEM, with a high BET surface area of $76.089\text{ m}^2/\text{g}$, mesoporosity (2–8 nm), and phase purity validated by XRD and XPS. This structural design, featuring abundant active sites and high sulfur content (~71.9%), is highly beneficial for Li-S batteries due to enhanced polysulfide confinement and catalytic redox behavior.

Ni-Co LDH was synthesized by ion-exchanging Co from ZIF-67 nanocubes with Ni^{2+} ions in ethanol, forming ZIF-67@LDH nanoboxes [225]. These were subsequently carbonized and sulfided at $400\text{ }^\circ C$ to form $NiCo_2S_4$ - NiS_2 nano-heterostructures embedded in hollow carbon boxes. Characterization using SEM, TEM, and XRD confirmed well-maintained nanobox morphology, distinct lattice spacings for $NiCo_2S_4$ and NiS_2 , and uniform elemental distribution; BET analysis showed a high surface area of $111.5\text{ m}^2/\text{g}$. The resulting LDH-derived nano-heterostructure offers abundant catalytic sites and strong lithium polysulfide (LiPS) adsorption capabilities, making it ideal for LSB applications. The CuCo-LDH was synthesized via a chemical etching strategy, where ZIF-67 (a cobalt-based MOF) acted as a sacrificial template and was treated with $Cu(NO_3)_2 \cdot 3H_2O$ in ethanol to form a hollow and hierarchical structure composed of vertically aligned LDH

nanosheets [226]. Figure 12 shows the synthesis process and morphological evolution of CuCo-LDH materials used in lithium–sulfur batteries. The structure is derived from ZIF-67 by introducing copper nitrate, forming a CuCo-LDH composite that enhances sulfur redox kinetics and polysulfide adsorption. FESEM images in Figure 12A–G reveal how particle morphology changes with different Co/Cu ratios. As the Co content decreases, the structure becomes less defined and more fragmented, indicating that the metal ratio significantly influences the material’s architecture, which, in turn, may affect its electrochemical performance. The optimal Co/Cu ratio (0.7) facilitated complete etching and formation of well-defined CuCo-LDH polyhedrons. Characterization results revealed that the synthesized LDH has a hollow dodecahedral morphology, layered nanosheet microstructure, mesoporous texture (BET surface area: $104.1\text{ m}^2/\text{g}$), and a mixed $\text{Cu}^{2+}/\text{Co}^{3+}$ oxidation state. CuCo-LDH is highly suitable for LSBs due to its strong polysulfide anchoring capability and catalytic activity.

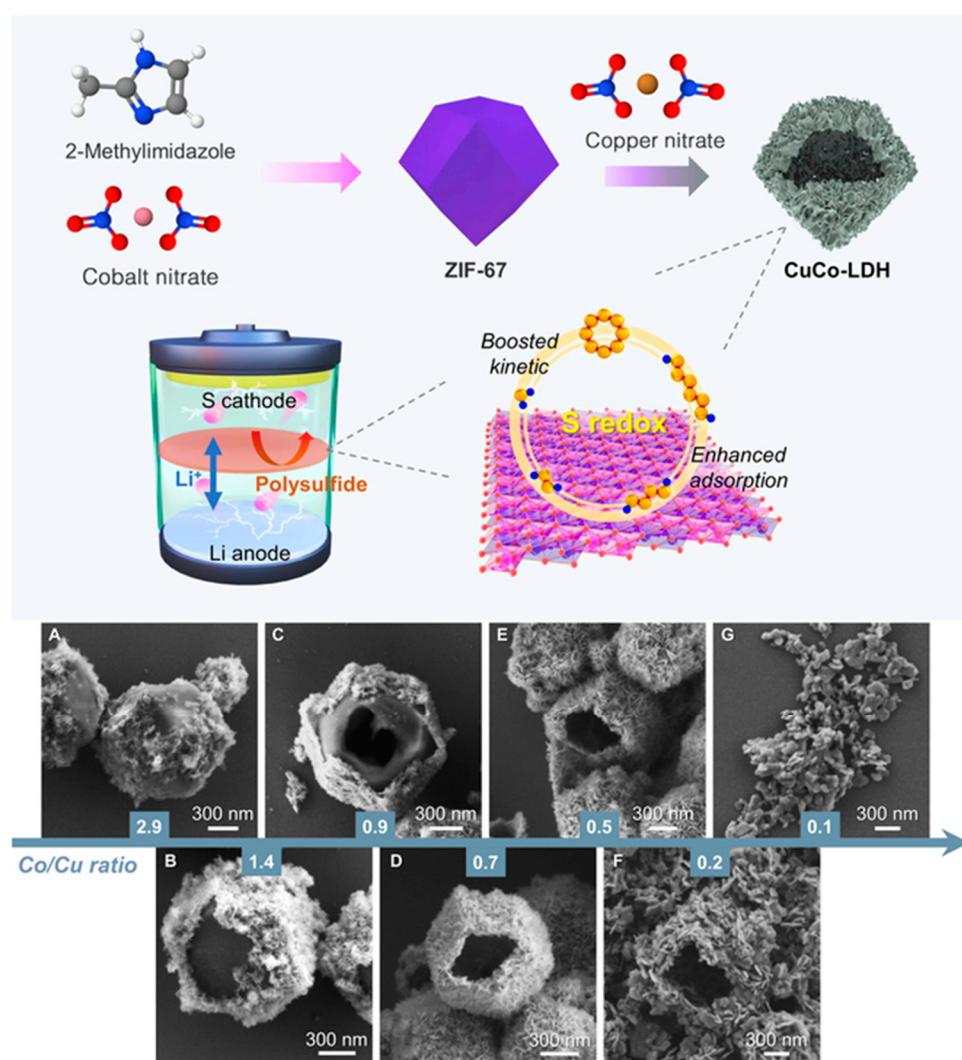


Figure 12. Schematic representation of the synthesis route for CuCo-LDH derived from ZIF-67 and its role in LSBs, highlighting its ability to accelerate redox reactions and trap polysulfides. FESEM images show the morphology of CuCo-LDH synthesized at various Co/Cu molar ratios: (A) 2.9, (B) 1.4, (C) 0.9, (D) 0.7, (E) 0.5, (F) 0.2, and (G) 0.1. Reproduced with permission [226].

The synthesis of PPy@LDH-S involved a multi-step process beginning with the formation of ZIF-67 nanocrystals, which were then transformed into hollow NiCo-LDH through a nickel ion exchange process [227]. Subsequently, sulfur was infiltrated via the solid-state melting method, and finally, a thin polypyrrole (PPy) film was polymerized onto the LDH-S composite. BET analysis showed a progressive reduction in surface area from $135.4\text{ m}^2/\text{g}$ (LDH) to $3.3\text{ m}^2/\text{g}$ (PPy@LDH-S) due to sulfur loading. The structural and chemical features—such as strong polysulfide adsorption, mesoporosity, and catalytic activity—make PPy@LDH-S a highly effective sulfur host for LSBs. The $\text{N}_{x}\text{Ca}_{2-x}\text{Al}-\text{Cl}$ LDH and $\text{CoyCa}_{2-\gamma}\text{Al}-\text{Cl}$ LDH were synthesized through a simple one-step ion exchange method, using $\text{Ca}_2\text{Al}-\text{Cl}$ LDH derived from chlorine-containing wastewater as a precursor [228]. Ni^{2+} and Co^{2+} ions replaced Ca^{2+} ions under ambient conditions with stirring and sonication, followed by filtration and drying. The resulting LDHs exhibited a thin, porous, tunnel-like morphology with abundant surface folds; XRD confirmed the layered structure, BET indicated high surface area ($\sim 4\times$ compared to the precursor), and XPS verified successful $\text{Ni}^{2+}/\text{Co}^{2+}$ substitution. Due to improved conductivity, active sites, and ion diffusion kinetics, this structural and electronic modification makes the LDHs highly suitable as anode materials for NIBs. CoSn-LDH@MXene nanocomposites were synthesized via a one-step solvothermal process where $\text{Co}(\text{NO}_3)_2 \cdot 6\text{H}_2\text{O}$ and $\text{SnCl}_2 \cdot 2\text{H}_2\text{O}$ were reacted in a mixture of isopropanol and glycerol at 180°C , followed by ultrasonic treatment with few-layer Ti_3C_2 MXene in ethanol [229]. The CoSn-LDH microspheres self-assembled and anchored onto the MXene nanosheets through hydrogen bonding and electrostatic interactions, forming a uniform hybrid structure. BET analysis showed a high surface area ($44.15\text{ m}^2/\text{g}$) and mesoporous structure, and XPS confirmed successful chemical integration. This architecture facilitates electron/ion transport and suppresses agglomeration, making it well-suited for Na-ion battery applications. $\text{Ni}_3\text{Ti}-\text{CO}_3$ LDH was synthesized via a urea precipitation method, whereas $\text{Ni}_3\text{Cr}-\text{CO}_3$ LDH was prepared using a conventional hydrothermal method [230]. Both were further converted into Cl^- -intercalated LDHs through an anion exchange process using HCl/NaCl solution. The developed LDHs exhibit high Cl^- insertion capacity and structural integrity, making them well-suited for CIB applications.

The CoMn-LDH/NPGA was synthesized via a combined cross-linking gelation, hydrothermal self-assembly, and freeze-drying process [231]. Vertically grown CoMn-LDH nanosheets were anchored onto a 3D hierarchical porous N,P co-doped graphene aerogel framework (NPGA). Characterizations revealed a lamellar morphology, well-defined crystalline structure, mesoporous nature with a BET surface area of $105.8\text{ m}^2/\text{g}$, and a high degree of N,P doping. This configuration provides high surface area, exposed active sites, and effective charge/mass transport, making it well-suited for ZAB applications. CoNi LDH nanoflowers (NFs) and nanosheets (NSs) were synthesized via a simple solvothermal method using a mixed solvent of deionized water and ethylene glycol in varying ratios [232]. The nanoflowers exhibited a hierarchical flower-like morphology with high crystallinity, a mesoporous structure, and a large BET surface area of $101.28\text{ m}^2/\text{g}$ (vs. $38.54\text{ m}^2/\text{g}$ for NSs), with XRD confirming α -phase $\text{Co}(\text{OH})_2$ and $\text{Ni}(\text{OH})_2$, and XPS revealing mixed oxidation states of $\text{Co}^{2+}/\text{Co}^{3+}$ and Ni^{2+} . These structural and surface characteristics endow the CoNi LDH, especially the NFs, with abundant active sites, good charge transport properties, and superior suitability for high-performance supercapacitor applications. NiCo-MOF@LDH hybrid nanosheets were synthesized via a one-step solvothermal method using 1,4-terephthalic acid and urea [233]. The resulting material displayed ultrathin, interconnected nanosheet morphology with high porosity, alongside the presence of Ni, Co, O, and C through EDS and XPS; the XRD patterns confirmed a hybrid structure of NiCo-MOF and LDH, and the

sample exhibited high surface area and abundant active sites. These structural features enhance ion diffusion and electron transfer, making the material highly suitable for supercapacitor applications.

NiCo-LDH nanosheets were synthesized by transforming Co-based MOFs on AC cloth (ACC) using a simple room-temperature ion exchange method in a mixed water and ethylene glycol solution [234]. The resulting material exhibited vertically aligned ultrathin amorphous nanosheets interconnected in a 3D mesoporous network, with a surface area of $25.8\text{ m}^2/\text{g}$ and a pore diameter of 3.9 nm. This unique structure and amorphous nature facilitate high electrochemical activity and ion transport, making it highly suitable for high-performance supercapacitor applications. Co-Ni LDH was synthesized through a facile cation exchange reaction between $\text{Mg}(\text{OH})_2$ and $\text{Co}^{2+}/\text{Ni}^{2+}$ ions, followed by a controlled anion exchange sulfurization using Na_2S [235]. The resulting CoNi LDH displayed a nanosheet morphology, layered crystal structure, and a BET surface area of $58\text{ m}^2/\text{g}$, progressively decreasing with sulfurization. These structural and chemical features, coupled with improved conductivity due to sulfur incorporation, make the material well-suited for high-performance supercapacitor applications. $\text{NiCo}_2\text{S}_4@\text{CoAl-LDH}$ (NCS@CA) heterojunction nanosheets were synthesized on nickel foam using a two-step solvothermal process [236]. The resulting material exhibited a unique flower-like core/shell nanosheet morphology with high crystallinity and a well-defined layered structure; it also showed enhanced light absorption (bandgap $\sim 2.23\text{ eV}$) and high redox-active surface area ideal for electrochemical applications. This rationally designed nanostructure facilitates fast ion diffusion and superior redox activity, making it highly suitable for supercapacitor applications. The NiCo-LDH was synthesized via a one-step microwave hydrothermal co-assembly method using tannin-derived carbon microspheres as a substrate [237]. The resulting LDH exhibited a well-defined sea urchin-like morphology with a core/shell nanostructure composed of uniformly distributed NiCo-LDH nanoneedles anchored on smooth carbon microspheres, possessing mesoporous features and a BET surface area of $56\text{ m}^2/\text{g}$. This structured design provides a high active surface area and improved charge transport, making it highly suitable for supercapacitor applications.

3.5. Impact of Synthesis Methods on LDH Properties

The synthesis methods employed significantly influence the structural, morphological, and functional characteristics of LDHs, directly impacting their performance in batteries, supercapacitors, and hydrogen production applications. Co-precipitation, a widely adopted synthesis method, excels due to its simplicity, scalability, and cost-efficiency. It typically results in LDHs with uniform morphology, high purity, and controllable interlayer spacing. These attributes are particularly beneficial in battery applications, where homogeneity and controlled particle size ensure efficient ion diffusion and high electrochemical stability. Recent advancements, such as incorporating surfactants, polymers, and organic anions during co-precipitation, have enabled further refinement of LDHs, enhancing their corrosion protection capabilities in reinforced concrete, boosting electrochemical activity, and improving stability in NIB and LIB systems. Furthermore, co-precipitated LDHs demonstrate remarkable adsorption characteristics, making them suitable for environmental remediation, a critical supplementary property in battery and supercapacitor electrodes where impurity management is crucial.

Hydrothermal synthesis, characterized by elevated temperatures and pressures, provides precise control over the crystallinity, particle size, and hierarchical architectures of LDHs, yielding materials with enhanced thermal stability and defect-free structures. This technique is particularly advantageous in synthesizing high-entropy LDHs and multi-metallic systems, where synergistic interactions among multiple cationic species significantly improve electrocatalytic performance. Hydrothermally synthesized LDHs display superior catalytic activities for hydrogen production applications due to their high surface area, controlled porosity, and finely tuned morphology, collectively facilitating efficient HER. Hybridization approaches combining LDHs with MOFs or carbonaceous substrates via hydrothermal methods further enhance their suitability for energy storage and catalytic processes by improving conductivity, structural integrity, and electrolyte accessibility.

Electrochemical deposition offers direct, binder-free growth of LDH films onto conductive substrates, thereby improving electron transport, adherence, and structural stability crucial for high-performance supercapacitors and catalytic electrodes. The tunability of electrochemical parameters enables precise control over film thickness, crystallinity, and porosity, directly correlating with enhanced electrochemical and catalytic performance. Techniques such as pulsed electrodeposition provide superior morphological control, reducing defects and optimizing the exposure of catalytic active sites, which is significantly beneficial for hydrogen production and supercapacitor applications.

Advanced synthesis methods such as sol-gel, ultrasonication, and exfoliation further expand the potential of LDHs. Sol-gel synthesis enables highly homogeneous and porous structures with tailored compositions, significantly enhancing electrode performance in supercapacitors and batteries due to improved ion transport pathways and increased active sites. Ultrasonication accelerates LDH formation, yielding finer particle sizes and improved dispersion, which critically benefits applications requiring rapid charge/discharge capabilities and high surface reactivity. Exfoliation methods generate ultrathin LDH nanosheets with exceptional surface area, which is crucial for enhancing catalytic activities in hydrogen production by maximizing exposed active sites and facilitating efficient electron transfer. Collectively, the meticulous selection and optimization of LDH synthesis methodologies are essential for tailoring materials with targeted functional properties, ensuring optimal performance across energy storage and catalytic applications.

LDHs are a class of materials characterized by a unique double-layered structure formed by two distinct metallic cations and an interlayer of anions, typically hydroxides or organic moieties. They exhibit properties that make them suitable for energy storage and hydrogen production applications. This response categorizes LDHs based on structural composition, defect engineering, and their composites, examining their properties relevant to energy applications. LDHs can be broadly classified based on their cationic composition. Common cations include transition metals such as nickel, cobalt, magnesium, aluminum, and iron, which can form various configurations [44,238]. Synthesis methods, such as hydrothermal and co-precipitation techniques, can induce defects like vacancies and irregular stacking, significantly influencing their electrochemical properties [239,240]. For instance, NiFe-LDHs exhibit enhanced OER activity when defects are strategically engineered, allowing for improved electronic conductivity and catalytic performance [241,242]. Structural modifications enable tailoring LDHs for specific application requirements. For example, engineering heterostructures, combining LDHs with other materials (such as carbon or metal oxides), can enhance catalytic activity and stability for water-splitting applications [242,243]. Using pulsed laser ablation or ion intercalation can produce nanosheets that provide a larger surface area for ion exchange, which is crucial for efficient energy storage systems like supercapacitors [244,245].

LDHs can also be integrated into composite matrices, enhancing their performance in energy applications. For instance, composites of LDHs with conductive polymers or carbonaceous materials show improved capacitance and energy density relative to their standalone counterparts [243,246]. The synergistic effects observed in such composites lead to enhanced electrochemical performance, making them suitable candidates for hybrid supercapacitors and batteries [247].

LDHs stand out due to their impressive electrochemical properties relevant to energy storage and hydrogen production. LDHs demonstrate significant catalytic activity toward the OER and HER due to their tunable electronic structures and high specific surface areas [248–250]. The presence of transition metals in their structure allows them to participate actively in redox reactions, enhancing their functionality as electrocatalysts [241,251]. The layered structure of LDHs contributes to their stability under operational conditions. They can maintain structural integrity during cycling in energy devices, making them reliable choices for applications in supercapacitors and batteries [240,252]. Furthermore, proper intercalation and defect engineering can improve their ionic conductivity and structural resilience, leading to a prolonged lifespan and consistent performance [251,253]. The unique interlayer space in LDHs permits the exchange of various anions to enhance energy storage capabilities. For instance, LDHs can be intercalated with anions suited for specific electrochemical applications, improving overall electrochemical properties [40,254]. The classification of LDHs into structural categories, the strategic use of defects and engineering approaches, and the development of composite materials are pivotal in leveraging their properties for enhanced energy storage and hydrogen production. Ongoing research continues to explore this fascinating class of materials, further unlocking their potential across various applications.

Among various synthesis strategies for LDHs, hydrothermal synthesis has emerged as the most widely employed method, particularly for energy-related applications. The hydrothermal route allows for precise control over crystallinity, morphology, and composition, enabling the fabrication of highly ordered LDH nanostructures with tailored porosity and surface area, properties that are critical for high-performance battery electrodes, supercapacitors, and electrocatalysts for water splitting and CO₂ reduction. Co-precipitation methods remain popular for producing LDHs at large scales, especially for supercapacitor electrodes and lithium-ion batteries, due to their simplicity and compositional flexibility. Electrodeposition techniques are increasingly favored for directly growing LDH thin films on conductive substrates, particularly in water-splitting electrocatalysis and flexible energy devices, where strong substrate adhesion and tunable thickness are desirable. Emerging methods such as spray pyrolysis, microemulsion synthesis, and mechanochemical activation are being explored for large-scale production of LDH-derived oxides for HER and carbon dioxide reduction reactions (CO₂RR). Ultimately, the choice of synthesis method critically influences the structural features, ion transport properties, and overall electrochemical performance of LDHs, thereby determining their suitability for specific energy storage and conversion applications. Figure 13 highlights the key advantages of various synthesis methods for LDHs, emphasizing how each technique offers unique benefits such as compositional flexibility, controlled morphology, high purity, and structural tailoring.

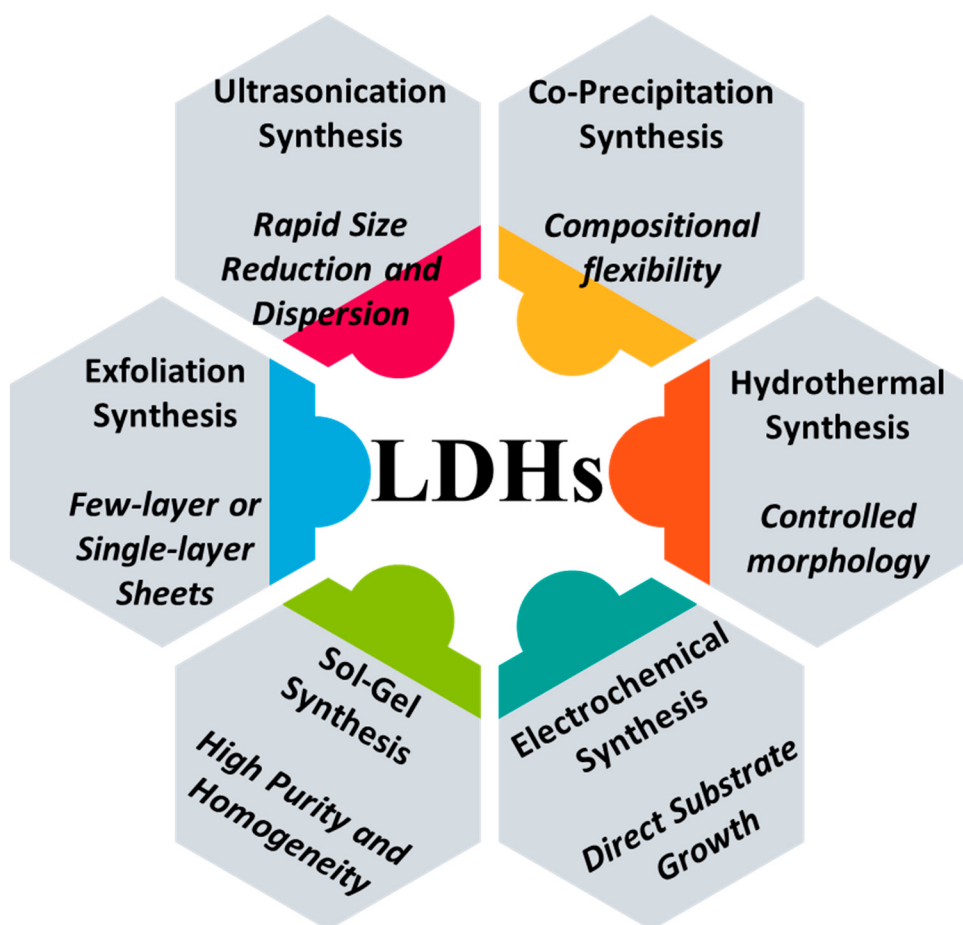


Figure 13. Schematic illustration of the advantages associated with different synthesis methods for LDHs.

4. LDHs in Batteries

LDHs have garnered significant interest in recent years due to their unique structural properties and wide-ranging applications, particularly in batteries. Composed of positively charged metal hydroxide layers interleaved with charge-compensating anions, LDHs can host a variety of cations and anions, which endow them with tunable electrochemical properties essential for battery technologies. Optimizing LDH materials for battery applications involves enhancing their structural integrity, electrochemical performance, and conductivity. Several strategies have emerged in recent studies. Incorporating high-valence metal ions, such as molybdenum, into LDH structures can stimulate lattice oxygen and improve stability and performance in applications such as CIBs [144]. Adjusting the metal/ion ratio within LDHs can optimize charge storage capabilities and reduce phase instability, enhancing electrochemical properties [255]. Research has also shown that hybridizing LDHs with conductive materials, such as graphene or carbon nanotubes, further enhances electrical conductivity and facilitates electron transport, providing superior performance in high-capacity batteries [256]. Furthermore, computational models for high-throughput screening of LDHs enable the identification of optimal stoichiometric ratios and structures, streamlining the development process [230]. Collectively, these strategies represent a multifaceted approach to optimizing LDH materials for next-generation battery technologies.

4.1. Lithium-Ion Batteries

In LIBs, LDHs exhibit promising behavior as cathode materials. For instance, nickel-cobalt LDHs have been shown to provide higher capacity and stability than conventional materials. Research by Bai et al. [257] highlights that these LDHs achieve about 160 mAh/g capacities at high current densities, showcasing excellent rate capability and cycling stability, which are crucial for practical applications. Furthermore, the study emphasizes how the layered structure and the ability to intercalate lithium ions enhance ionic conductivity and electron transport, improving overall battery performance. ZIF-67@NiCo-LDH was utilized as an anode material in LIBs, displaying high electrochemical performance [134]. Initially, the composite delivered a high discharge capacity of 1997.1 mAh/g at 100 mA/g and maintained a stable reversible capacity of 807.9 mAh/g after 100 cycles. It demonstrated excellent rate capability, achieving capacities of approximately 1303.9, 931.5, 601.3, and 445.0 mAh/g at current densities of 100, 200, 500, and 1000 mA/g, respectively. The excellent cyclic stability, high specific capacity, and superior rate performance were attributed to the synergistic effect between ZIF-67 MOF and NiCo-LDH nanosheets and the unique heterostructure morphology's enhanced conductivity and structural integrity. NiFe₂O₄@NiCo-LDH was utilized as an anode in LIBs [135], exhibiting superior electrochemical performance characterized by a high specific capacity of 636.9 mAh/g after 100 cycles at 0.3 A/g, along with high coulombic efficiency (~98%). The composite anode demonstrated good rate performance, maintaining stable capacities at various current densities and temperatures (−10 °C, 25 °C, 50 °C), thus confirming its robustness. Electrochemical impedance and galvanostatic intermittent titration techniques indicated that the NiFe₂O₄@NiCo-LDH possessed significantly lower internal resistance and higher conductivity, resulting in efficient ion/electron transfer and improved cyclic stability compared to pristine NiFe₂O₄. The synthesized NiZn-LDH, intercalated with DS– anions, was employed as an anode material for LIBs [136]. Specifically, the optimized LDH (NZDS-20) demonstrated superior electrochemical performance, delivering a high specific capacity of 850 mAh/g at a current density of 0.5 A/g, which remained stable after 400 cycles. Furthermore, the material showed excellent rate capability, maintaining a capacity of approximately 473.5 mAh/g at a higher current density of 3 A/g. EIS and galvanostatic intermittent titration technique (GITT) measurements further confirmed improved lithium-ion diffusivity and reduced reaction resistance, highlighting the beneficial effects of DS– intercalation. Moreover, a significant pseudocapacitance contribution was observed, underscoring rapid reaction kinetics and enhanced electrochemical stability. The hollow yolk/shell NiS₂/FeS₂@NC@NiFe LDH/FeO(OH) microspheres were utilized as an anode in LIBs, demonstrating excellent electrochemical performance [137]. At 0.2 A/g, the LDH electrode delivered a specific 709.9 mAh/g capacity after 200 cycles, highlighting robust cycling stability. Furthermore, at a higher current density (1.0 A/g), it maintained a capacity of 403.3 mAh/g even after 500 cycles, showcasing superior cyclic and rate stability compared to individual NiS₂/FeS₂ or NiFe LDH/FeO(OH) electrodes. The improved performance is attributed to the hollow yolk/shell structure, N-doped carbon layer, and enhanced conductivity and stability. The NiCo-LDH/MXene composite was used as an anode material for LIBs, showing excellent electrochemical performance [138]. It achieved a high specific capacity of 1081 mAh/g after 100 cycles at 100 mA/g and demonstrated outstanding rate capability, retaining 439 mAh/g even at a high current density of 1000 mA/g. Additionally, the material exhibited superior cycling stability, with minimal capacity fading, demonstrating the effectiveness of the 1D/2D structure in enhancing battery performance. Mg₂Al₁–CO₃-LDH was utilized as an anode in LIBs [140], exhibiting an impressive initial discharge-specific capacity of 814 mAh/g at a current density of 200 mA/g. Despite initial capacity fading, the material recovered significantly, stabilizing at 203.8 mAh/g after 300 cycles. Additionally, it

demonstrated reasonable rate capabilities (up to 61.3 mAh/g at 2000 mA/g), attributing electrochemical performance primarily to reversible Li⁺ storage through valence change of Mg and conversion reactions involving LiOH and LiH/Li₂O.

An LDH material (LDH200) was employed as an anode material for LIBs, demonstrating exceptional electrochemical properties [109]. Specifically, the LDH anode delivered a high specific capacity of 1821.3 mAh/g at a current density of 0.1 A/g. Impressively, the material maintained a robust cyclic stability, retaining a reversible capacity of about 687.7 mAh/g after 500 cycles at 0.5 A/g, corresponding to a very low capacity attrition rate of 0.092%. Figure 14A shows the CV curves of LDH200, where the redox peaks remain stable after the first few cycles, indicating good electrochemical reversibility. In Figure 14B, the charge/discharge profiles of LDH200 over various cycles at 0.5 A/g show consistent voltage plateaus, demonstrating stable cycling behavior. Figure 14C compares the long-term cycling performance of LDH200 with other samples. LDH200 shows the highest capacity retention and coulombic efficiency over 500 cycles. Figure 14D presents rate performance data, where LDH200 retains superior capacity across different current densities compared to the other LDH samples. Figure 14E provides a radar plot comparing all electrode types across six performance parameters. LDH200 shows balanced and enhanced electrochemical behavior, confirming it as the most promising candidate among the studied materials. Additionally, this material exhibited a significantly improved lithium-ion diffusion coefficient of approximately 4.08×10^{-11} cm²/s, indicative of its excellent rate capability and suitability for practical high-performance battery applications.

The synthesized Ni₂Co-LDH/EG composite served as an anode material for LIBs [152], demonstrating superior electrochemical performance compared to pristine Ni₂Co-LDH. It exhibited a high specific capacity of 1880 mAh/g at 0.05 A/g and maintained an excellent specific capacity of 919 mAh/g at a high current density of 1 A/g. Additionally, it showed remarkable cyclic stability with minimal capacity fading, retaining a specific capacity of approximately 973 mAh/g after 100 cycles at 1 A/g. The integration of expanded graphite significantly enhanced electronic conductivity and effectively suppressed volume expansion during the lithiation/delithiation process, supported by reduced charge transfer resistance measured through EIS. NiAl-LDH was used as a negative electrode (anode) material for LIBs and tested with two types of binders: sodium alginate (SA) and PVDF [153]. The SA-based electrode exhibited a remarkable initial discharge capacity of 2586 mAh/g at 0.05 A/g with a reversible 1578 mAh/g capacity. After 400 cycles at 0.5 A/g, the capacity retained was 697 mAh/g (42.2%), and at 1.0 A/g, it remained 388 mAh/g after 1400 cycles (27.6% retention). In contrast, the PVDF-based electrode showed significantly lower retention, indicating the superior performance of the SA binder. The conversion-type mechanism involving Ni²⁺ to Ni⁰ and forming a stable SEI layer (rich in Li₂O and LiOH) contributed to the enhanced cycling stability and rate capability.

4.2. Lithium–Sulfur Batteries

In LSBs, utilizing LDHs helps mitigate the polysulfide dissolution issue, which is crucial for improving cycling stability [258]. Bai et al. [257] demonstrated that a NiCo-LDH-based cathode effectively retains capacity over 500 cycles, outperforming conventional sulfur cathodes. The LDH structure helps configure polysulfide species, thus facilitating a more stable electrochemical reaction environment during charge/discharge cycles, addressing a significant challenge in LSBs [202]. LDH@PSS was applied as an artificial solid electrolyte interphase (ASEI) on lithium metal anodes in LSBs [155]. The composite SEI was fabricated via spin-coating, providing mechanical robustness and ionic selectivity. Li || Li symmetric cells with LDH@PSS-Li electrodes demonstrated an ultra-long cycle life of over 3100 h at 1 mA/cm² with significantly reduced overpotential. When paired with sulfur

cathodes, the full Li–S cells showed excellent performance: an initial specific capacity of 1247.2 mAh/g and a reversible capacity of 1032.6 mAh/g after 200 cycles at 0.2 C, with a minimal capacity decay of 0.086% per cycle. At higher rates (1 C), the cell retained 65.2% of its capacity after 1000 cycles. Additionally, the system exhibited suppressed shuttle currents, lower self-discharge, enhanced Li⁺ transference numbers ($t\text{Li}^+ = 0.81$), and improved charge transfer kinetics, highlighting its potential for stable, high-performance LSBs.

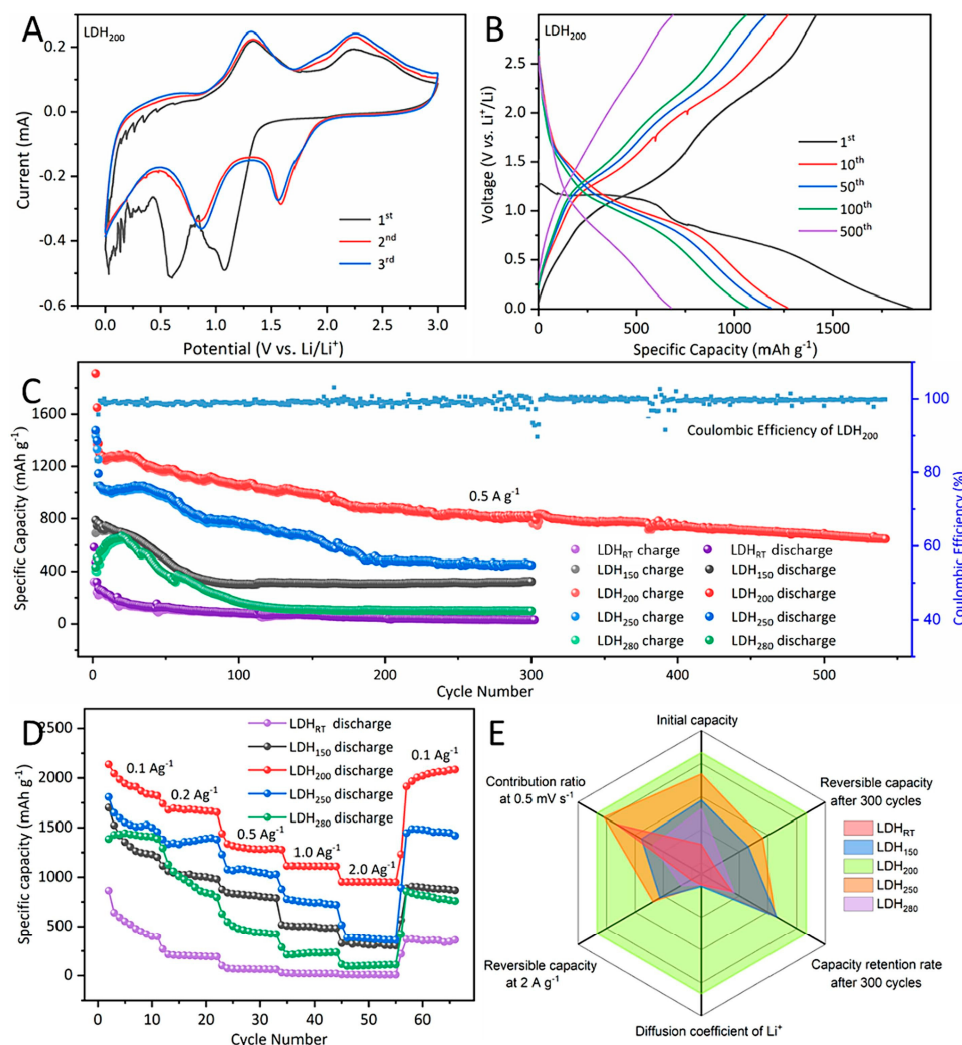


Figure 14. (A) CV curves of the LDH sample recorded at 0.1 mV/s within a voltage range of 0.01–3.0 V vs. Li/Li⁺. (B) Charge/discharge voltage profiles of LDH at a current density of 0.5 A/g over multiple cycles. (C) Long-term cycling performance and coulombic efficiency of LDH₂₀₀ compared to other LDH-based electrodes at 0.5 A/g. (D) Rate capability comparison for different samples under various current densities. (E) The radar chart displays normalized electrochemical metrics, including initial capacity, rate performance, and capacity retention, for all LDH variants. Reproduced with permission [109].

NiCo-LDH-based material was used as a freestanding cathode (NMWAs@NiCo-LDH/S) in LSBs [222]. It demonstrated exceptional electrochemical performance, with an initial specific capacity of 1238.4 mAh/g at 0.1 C, and 805.8 mAh/g at 5.0 C, reflecting excellent rate capability. Over 700 cycles at 5.0 C, it retained 647.1 mAh/g with a minimal capacity decay rate of 0.018% per cycle. The unique structure facilitated effective sulfur confinement, rapid Li⁺ diffusion, and robust redox kinetics while alleviating volume expansion and suppressing the polysulfide shuttle effect. This makes NMWAs@NiCo-LDH/S a competitive candidate for high-rate and long-life LSB cathodes. The Vo-LDHs-MXenes were

employed as a functional separator coating in LSBs [156]. The heterostructure significantly improved the electrochemical performance through enhanced adsorption and catalytic conversion of lithium polysulfides. The assembled LSBs exhibited an initial specific capacity of 1549 mAh/g at 0.1 C and retained 701 mAh/g after 300 cycles at 1.0 C, with a minimal capacity decay rate of 0.084% per cycle. Under high sulfur loading (6.7 mg/cm^2) and a low electrolyte/sulfur ratio (6 $\mu\text{L}/\text{mg}$), the areal capacity reached 6.09 mAh/cm^2 . The cell demonstrated superior rate capability, ranging from 1530 to 342.9 mAh/g across 0.1 C to 3.0 C. These results underscore the effectiveness of the V₂O₅-LDHs-MXenes in suppressing shuttle effects and enhancing redox kinetics in LSBs.

A VCFN composite was employed not as a cathode or anode material but as a separator modification layer (VCFN/SP/PVDF) on a glass fiber (GF) separator in LSBs [156]. The modified separator enabled superior polysulfide confinement and redox kinetics due to the synergistic effects of V₂O₅ catalysis, LDH's high surface area, and cysteine's functional linkage. The battery exhibited a high initial specific capacity of 1035.2 mAh/g at 0.5 C and retained 920.1 mAh/g after 300 cycles, demonstrating excellent cycling stability with a minimal capacity decay of 0.039% per cycle. Even at elevated sulfur loadings (up to 4.5 mg/cm^2), the system maintained stable capacities above 900 mAh/g, highlighting its scalability. Moreover, the cell exhibited improved Li-ion diffusion, reduced charge/transfer resistance (15.3Ω), high ionic conductivity ($4.1 \times 10^{-2} \text{ S/cm}$), and minimized polarization, underlining the role of the VCFN-modified separator in promoting efficient electrochemical performance.

In LSBs, NiCo-MOF/LDH was applied as a functional interlayer between the sulfur cathode and separator [223]. The cell delivered remarkable electrochemical performance when used with a sulfur cathode composed of sulfur-encapsulated nitrogen-doped carbon nanocages (S@hNCNC). Specifically, it exhibited a high specific capacity of 950 mAh/g after 200 cycles at 1 C with a minimal capacity decay of 0.033% per cycle. It also maintained 982 mAh/g at 0.5 C after 200 cycles and 633 mAh/g over 1000 cycles at 1 C. The rate capability was also excellent, achieving 640 mAh/g at 5 C and returning to 1103 mAh/g when the current returned to 0.1 C. The interlayer significantly reduced polarization and enhanced polysulfide conversion, which was further validated by CV, Tafel plots, and EIS. These enhancements are attributed to the synergistic effect of NiCo-LDH's strong chemisorption and NiCo-MOF's catalytic activity.

In LSBs, the synthesized NiCo-LDH was used as a cathode host after sulfur loading [224]. The S/NiCo-LDH cathode delivered a high initial specific capacity of 1540 mAh/g at 0.1 C and retained 485 mAh/g even at 5 C, showing excellent rate performance. At 0.2 C, the electrode retained a stable 650 mAh/g capacity over 100 cycles with nearly 100% coulombic efficiency. Most notably, after 500 cycles at 1 C, the capacity remained at 475 mAh/g with 78% retention, indicating robust cycling stability. The synergistic effect of strong chemical polysulfide adsorption and catalytic activity of NiCo-LDH significantly improved the redox kinetics and suppressed shuttle effects, validating its potential as a high-performance cathode host in LSB systems.

The synthesized L-CoNi-LDH/C was employed as a sulfur host in the cathode (S@L-CoNi-LDH/C) of LiSB [154]. The composite enabled high sulfur loading (~66.4 wt.%) and delivered a high initial discharge capacity of 1574 mAh/g, retaining 1097 mAh/g after 100 cycles at 0.1 C with nearly 100% coulombic efficiency. At a high rate of 2 C, the electrode exhibited a stable capacity of 503 mAh/g after 200 cycles. Additionally, it showed excellent rate capability, sustaining 486 mAh/g at 5 C and recovering to 730 mAh/g when returned to 0.2 C. Figure 15 highlights the electrochemical performance and mechanism of the S@L-CoNi-LDH/C cathode for LSBs. As shown in Figure 15a, the charge/discharge profiles at 0.1 C indicate that the S@L-CoNi-LDH/C electrode delivers a higher capacity than the

S@CoNi-LDH/C, confirming enhanced redox activity and sulfur utilization. Figure 15b demonstrates the superior cycling stability of S@L-CoNi-LDH/C at 0.1 C, while Figure 15c shows its high capacity retention even at 2 C, along with excellent coulombic efficiency. The performance at various current densities is displayed in Figure 15d, and the rate capability in Figure 15e confirms the electrode's ability to recover its capacity when the current is returned to a lower value. Figure 15f presents EIS measurements at different voltages, illustrating the charge transfer behavior and confirming the effective catalytic role of the CoNi-LDH/C framework in promoting polysulfide conversion. This performance is attributed to the enhanced catalytic activity, conductivity, and strong LiPS confinement offered by the L-CoNi-LDH/C composite. In applying LSBs, the NiCo₂S₄-NiS₂ nano-heterostructure was used as a sulfur host in the cathode [225]. The designed cathode exhibited an outstanding initial specific capacity of 1207 mAh/g at 0.2 C and excellent rate capability with 766 mAh/g at 2 C. Under high sulfur loading conditions (5.0 mg/cm²) and lean electrolyte usage (E/S ratio of 8.0 mL/g), the system achieved a high areal capacity of 6.09 mAh/cm². Long-term cycling at 1 C showed a capacity retention of 60.23% after 450 cycles (fading rate of 0.089% per cycle), and further tests confirmed suppression of LiPS shuttle and lithium dendrite formation, validating its superior electrochemical stability and catalytic effect. CuCo-LDH was utilized as a separator modifier rather than a direct cathode or anode material [226]. Its hollow, mesoporous architecture provided a strong barrier against polysulfide shuttle and enhanced sulfur redox kinetics via metal–sulfur interactions. As a result, the CuCo-LDH-modified separator enabled high reversible specific capacities (~1262.8 mAh/g initially at 0.2 C and ~697.0 mAh/g after 500 cycles at 1 C), excellent rate capability up to 5 C, and an extremely low capacity decay of 0.049% per cycle over 500 cycles. Under practical conditions with high sulfur loading (4.2 mg/cm²) and lean electrolyte (E/S = 6 mL/g), a remarkable areal capacity of 4.39 mAh/cm² was achieved and retained 3.42 mAh/cm² after 200 cycles. These results highlight its dual-functionality as a physical barrier and a chemical catalyst in improving LSB performance. MgAl-LDH@CNT was utilized as a cathode component in Li–S batteries, combined with sulfur to form a composite cathode and paired with a dual-functional graphene/PP/Al₂O₃ (DF-GPA) separator [110]. This system significantly enhanced the electrocatalytic conversion of polysulfides and stabilized the redox kinetics. As a result, the Li–S cell delivered a high specific capacity and showed excellent cycling performance with minimal capacity decay over 200 cycles at 1 C. With a high sulfur loading of 4.0 mg/cm², the battery exhibited stable operation and high coulombic efficiency, making it a promising design for high-energy-density sulfur cathodes in practical applications.

LDHs were used as sulfur host materials in the cathode [157]. Among the variants, NiFe-LDH@S demonstrated superior electrochemical performance due to the stronger coordination between Ni/Fe sites and lithium polysulfides, facilitating better adsorption and catalytic conversion. It delivered an initial 676 mAh/g capacity at 0.2 C and maintained 503 mAh/g after 100 cycles. At a higher rate of 2 C, it still retained 386 mAh/g after 500 cycles. In contrast, NiAl-LDH@S and ZnAl-LDH@S showed poorer capacity retention and higher polarization, highlighting the critical role of transition metal composition in tuning LDH performance. Moreover, NiFe-LDH@S exhibited the lowest charge transfer resistance (4.9 Ω) and the highest polysulfide adsorption capacity, reinforcing its effectiveness as a high-performance sulfur host.

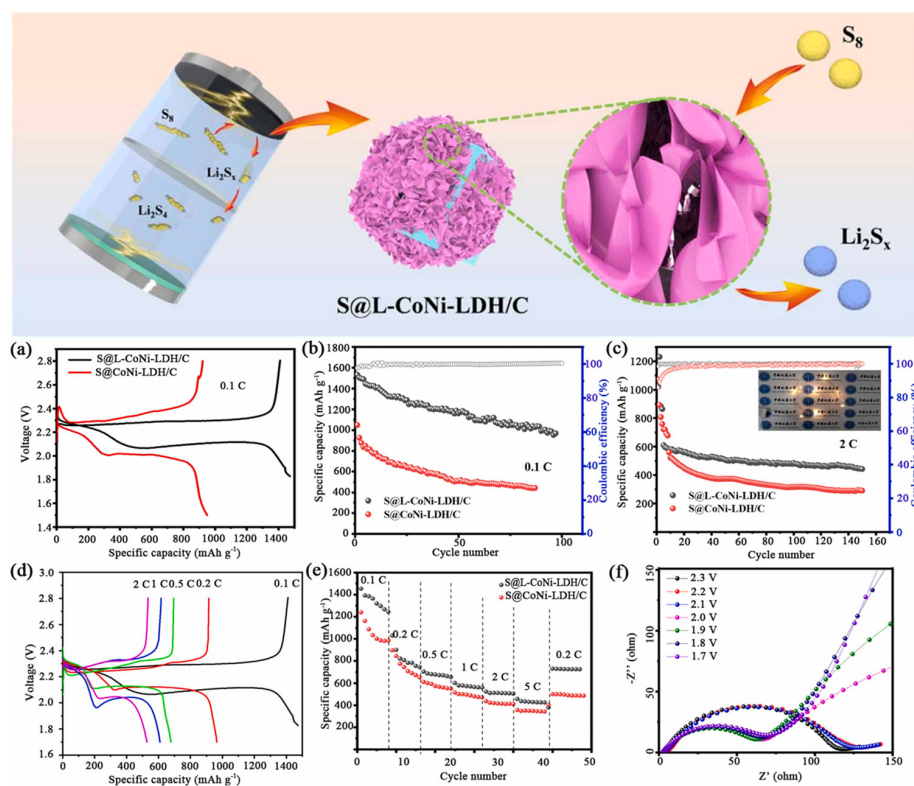


Figure 15. Illustration showing the role of S@CoNi-LDH/C in enhancing polysulfide adsorption and catalytic conversion. (a) Charge/discharge voltage profiles of S@L-CoNi-LDH/C and S@CoNi-LDH/C electrodes tested at 0.1 C. (b) Cycling stability at 0.1 C and (c) high-rate cycling at 2 C for both cathodes, including coulombic efficiency. (d) GCD curves at various current rates, and (e) corresponding rate capability of S@L-CoNi-LDH/C. (f) Nyquist plots of S@L-CoNi-LDH/C cathode collected at different voltage stages [154].

The PPy@LDH-S was employed as a cathode in LSBs [227], demonstrating superior performance due to its unique multi-functional architecture. The composite cathode delivered a high initial discharge capacity of 907.2 mAh/g at 1 C. It retained 633.4 mAh/g after 500 cycles with a minimal fading rate of 0.06% per cycle, maintaining ~99% coulombic efficiency. At various rates from 0.2 C to 5 C, the electrode exhibited excellent rate capability and reversible capacity up to 983.2 mAh/g when returned to 0.2 C. It also achieved a reversible areal capacity of 535.7 mAh/g (3.5 mg/cm² sulfur loading) and 416.9 mAh/g (5.2 mg/cm²) after 500 cycles. The flexible pouch cell configuration further validated its mechanical robustness and suitability for wearable electronics, maintaining functionality under bending and twisting conditions. In the LSB configuration, the VG@LDH/CC composite was used as a sulfur host for the cathode [158]. This structure provides both physical confinement and chemical adsorption of polysulfides, minimizing shuttle effects and improving reaction kinetics. The battery delivered a high specific capacity of 1182.4 mAh/g at 0.1 C, and retained 441.3 mAh/g after 750 cycles at 0.5 C, with a very low capacity decay rate of 0.0755% per cycle. The rate performance was also excellent, sustaining 780.8 mAh/g at 3 C, and maintaining capacity recovery upon returning to lower rates. The design supports high-rate and high-capacity operation, even under high sulfur loading conditions (e.g., 547.7 mAh/g after 300 cycles at 3.5 mg/cm² loading at 1 C).

4.3. Sodium-Ion Batteries

For NIBs, LDHs have shown notable electrochemical performance. Research indicates that ZnAl-LDHs can be effective anode materials, exhibiting around 200 mAh/g capacities with good cycling stability over extended periods [102]. The ability to intercalate sodium

ions while maintaining structural integrity enhances energy storage capabilities. The intrinsic layered structure also allows for efficient ion diffusion and electron transport, leading to faster charge/discharge rates than traditional anode materials. The synthesized NiCr-Cl LDH/rGO was utilized as an anode material in NIBs [159]. Electrochemical tests revealed a high initial discharge capacity of 632 mAh/g, with a reversible capacity of 218 mAh/g after 200 cycles at 100 mA/g, indicating good cyclic stability. Moreover, it delivered 219 mAh/g at a high rate of 2 A/g, highlighting its excellent rate capability. The improved electrochemical performance is attributed to the expanded interlayer spacing, enhancing Na^+ ion diffusion, and the rGO matrix, which boosts conductivity and buffers volume changes. EIS confirmed the lowest charge transfer resistance among the compared samples, supporting fast kinetics. Capacitive contribution analysis showed dominant pseudocapacitive behavior, with 55.1% capacitive contribution at 0.2 mV/s, confirming its favorable kinetic profile for high-rate applications.

The CoMoLDH@C-PDA material was evaluated as an anode in NIBs [163]. The composite synthesized with 6-h PDA polymerization (CoMoLDH-24@C-PDA-6) exhibited superior electrochemical performance among various samples. This anode delivered an initial specific capacity of 779.9 mAh/g at 0.05 A/g and maintained 310.9 mAh/g after 100 cycles at 0.1 A/g, with a 70% capacity retention. High rate capability and long-term stability were attributed to the formation of $\alpha\text{-CoMoO}_4$ and conductive carbon coating, which improved Na^+ diffusion and minimized charge transfer resistance. Figure 16a presents the fabrication steps for CoMoLDH-based materials with and without carbon and PDA modifications. The composite CoMoLDH-24@C-PDA-6 is prepared by combining polymerized dopamine with carbonized CoMoLDH. The electrochemical behavior of these electrodes is shown in Figure 16b,c. The CoMoLDH-24@C-PDA-6 electrode exhibits more stable and extended charge/discharge profiles, indicating enhanced capacity and reaction reversibility. In Figure 16d, cycling performance over 100 cycles at 0.1 A/g shows that CoMoLDH-24@C-PDA-6 retains 70% of its capacity, significantly outperforming the unmodified CoMoLDH-24 (43.7%). Nyquist plots in Figure 16e,f demonstrate reduced charge transfer resistance for the modified electrode, both before and after cycling, confirming improved conductivity and electrochemical stability. Further, EIS and GITT analysis confirmed a lower R_{ct} and higher Na^+ diffusion coefficient for the coated material, reinforcing its viability for high-performance NIB applications.

In NIB applications, both $\text{Ni}_{0.8}\text{Ca}_{1.2}\text{Al-Cl}$ LDH and $\text{Co}_{0.6}\text{Ca}_{1.4}\text{Al-Cl}$ LDH were evaluated as anode materials in CR2032 coin-type cells [228]. These materials demonstrated promising electrochemical properties, with initial discharge capacities of 819.2 and 746.6 mAh/g and coulombic efficiencies of 65.2% and 56.8%, respectively. $\text{Ni}_{0.8}\text{Ca}_{1.2}\text{Al-Cl}$ LDH delivered a stable specific capacity of 256.9 mAh/g, and $\text{Co}_{0.6}\text{Ca}_{1.4}\text{Al-Cl}$ LDH achieved 292.8 mAh/g at 0.2 A/g after 200 cycles. Notably, they maintained 102 and 118.1 mAh/g after 600 cycles at 2 A/g, demonstrating excellent cycling stability. Both materials exhibited enhanced rate capability and reduced impedance, attributable to the porous structure and bimetallic synergies, and their performance was comparable to that of conventional hard carbon. The sodium storage mechanism involved both diffusion-controlled intercalation and surface capacitive effects, supported by ex situ XRD and XPS analyses. NHCNS@CoSe₂@C was employed as an anode material. It demonstrated an initial discharge capacity of 465.6 mAh/g at 0.1 A/g, and retained 373.8 mAh/g after 100 cycles, with a coulombic efficiency of 59.7% in the first cycle [164]. Even at a high current density of 5 A/g, the electrode retained a specific capacity of 314.2 mAh/g, reflecting outstanding rate capability. Additionally, long-term cycling at 0.5 A/g for 1000 cycles showed stabilized performance at 325 mAh/g, despite some capacity fade due to volume expansion. The hybrid's superior performance is attributed to its high conductivity, abundant active sites, and structural robustness against sodium insertion/extraction.

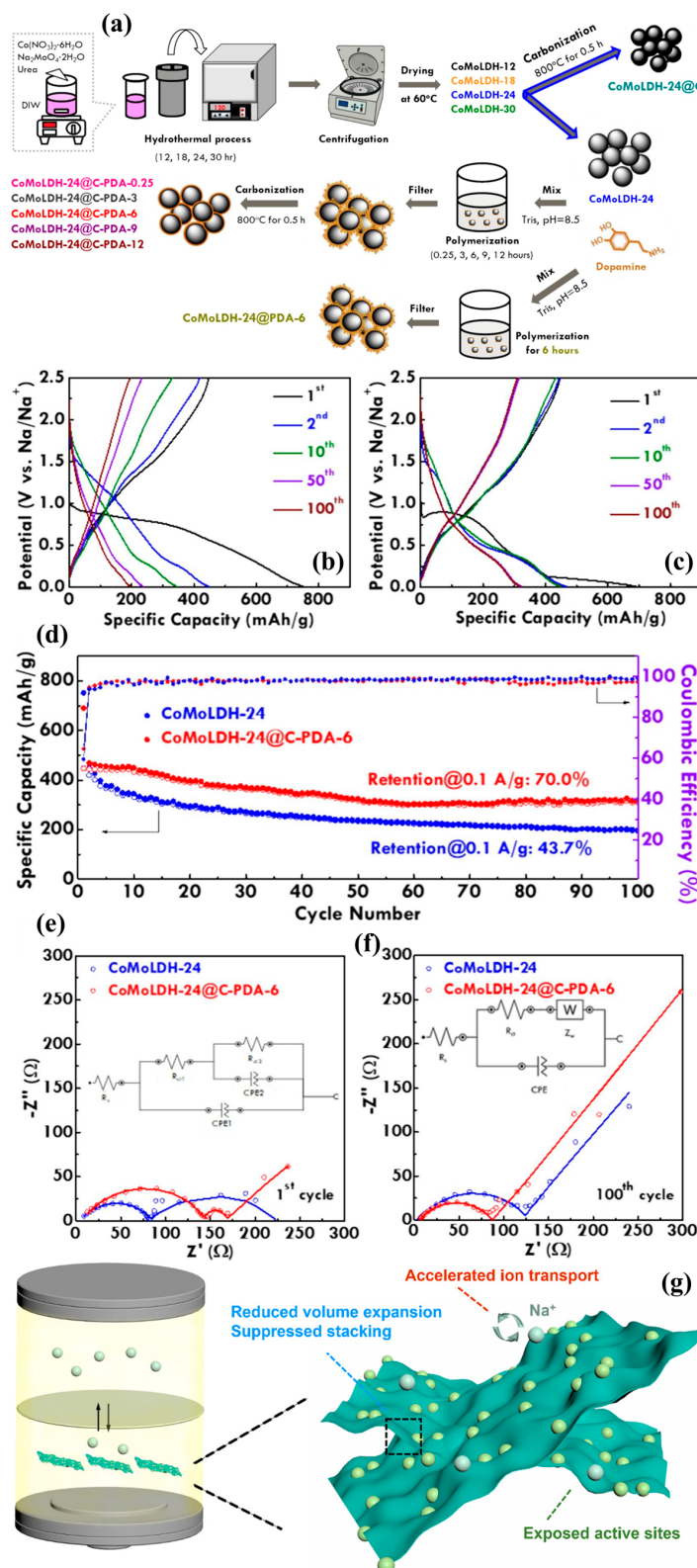


Figure 16. (a) Schematic of the synthesis procedure for CoMoLDH, CoMoLDH-24@C, CoMoLDH-24@PDA-6, and CoMoLDH-24@C-PDA composites. (b,c) GCD profiles of CoMoLDH-24 and CoMoLDH-24@C-PDA-6 electrodes, respectively. (d) Cycling performance comparison at 0.1 A/g over 100 cycles for both electrodes. (e,f) Nyquist plots obtained before cycling and after 100 cycles. Reproduced with permission [163]. (g) Diagram illustrating how the electrode design enhances sodium-ion storage by improving ion transport, limiting volume expansion, and increasing active site exposure. Reproduced with permission [229].

NiFe-NO₃ LDH was employed as a conversion-type anode material in a sodium metal half-cell configuration [111]. During electrochemical testing, the electrode demonstrated an impressive initial sodiation capacity of ~972 mAh/g, though with a significant first-cycle irreversibility (~60% coulombic efficiency). Upon cycling at 50 mA/g, it stabilized at ~388 mAh/g after 60 cycles, maintaining over 95% coulombic efficiency. High-rate cycling (500 mA/g) over 500 cycles yielded a final capacity of 122 mAh/g. Rate capability studies showed the electrode retained a reversible capacity of 430 mAh/g when the current returned to 50 mA/g after high-rate steps. Operando XAS and magnetic measurements revealed a hybrid intercalation–conversion mechanism, with Fe³⁺ reducing to Fe²⁺ and forming Fe₃O₄, while Ni partially transitions to NiO_x. This complex, partially reversible mechanism contributed to the sustained capacity despite an initial irreversible structural transformation.

CoSn-LDH@MXene was employed as an anode material in 2032-type coin cells [229]. The hybrid electrode demonstrated remarkable sodium storage performance due to its synergistic structure combining redox-active CoSn-LDH and highly conductive MXene. At a current density of 0.1 A/g, the material delivered an initial specific capacity of 976.1 mAh/g and retained 504 mAh/g after 100 cycles with 97.29% retention. At a higher current density of 0.5 A/g, it maintained 387.4 mAh/g after 100 cycles and still showed 419.3 mAh/g after 1000 cycles, highlighting excellent long-term stability. Rate capability was outstanding, with capacities ranging from 532.2 to 187.1 mAh/g across 0.05–5 A/g. The electrode exhibited strong pseudocapacitive behavior (up to 95% at high scan rates), excellent reversibility, and low charge/transfer resistance (574.5 Ω), positioning it among the top-performing LDH-based anodes for SIBs. Figure 16g visually summarizes the key functional advantages of the electrode structure, such as faster Na⁺ ion transport, reduced stacking, enhanced structural integrity, and greater exposure to active sites.

4.4. Chloride-Ion Batteries

Though less explored, the application of LDHs in CIBs presents exciting opportunities. Research indicates that chloride-intercalated LDHs can exhibit promising electrochemical behavior, including good cycling stability and capacity retention [102]. The favorable ion exchange capacity of LDHs facilitates chloride ion intercalation, opening pathways for improved conductivity and performance in battery applications. The ability of these materials to accommodate diverse anions while maintaining structural stability makes them suitable candidates for next-generation battery technologies. NiFe LDH nanosheets with different interlayer spacings were used as cathode materials in Li-based CIBs, where Li sheets served as the anode and 0.5 M 1-butyl 1-methylpyrrolidinium chloride (Bpy14Cl) in propylene carbonate as the electrolyte [112]. Among the three samples, the NiFe-C₁₇H₂₅O₃ LDH with the most significant interlayer spacing (24.114 Å) demonstrated superior electrochemical performance, delivering a specific discharge capacity of 64.2 mAh/g after 200 cycles at 300 mA/g, and maintaining 52.4 mAh/g even at 1 A/g. The electrode exhibited a high diffusion coefficient (~10⁻¹⁰ cm²/s), significantly reduced charge transfer resistance (48.9 Ω), and enhanced redox activity of Ni²⁺/Ni³⁺ and Fe²⁺/Fe³⁺ couples during Cl⁻ intercalation. These features enabled improved rate capability, cycling stability, and ion transport kinetics, establishing the interlayer-engineered NiFe LDH as a promising high-rate cathode for CIBs. Ni₃Ti-Cl and Ni₃Cr-Cl LDHs were employed as cathodes in CIBs paired with lithium metal anodes [230]. The Ni₃Ti-Cl LDH delivered a high initial discharge capacity of 346.4 mAh/g and retained a stable reversible capacity of ~131.8 mAh/g over 200 cycles at a current density of 200 mA/g, showcasing excellent cycling stability and coulombic efficiency (~100%). Ni₃Cr-Cl LDH, exhibiting a slightly lower maximum capacity of 182.6 mAh/g, maintained a competitive capacity of 111.3 mAh/g after 200 cycles. The performance validates theo-

cal predictions, highlighting $\text{Ni}_3\text{Ti-Cl}$ LDH as a superior cathode material due to its high specific capacity, excellent cyclic stability, and favorable Cl^- insertion dynamics.

Phosphorus-doped NiCoMo-P150 LDH was employed as the cathode material in a CIB configuration with a lithium metal anode and ionic liquid electrolyte [142]. This cathode delivered a high initial discharge capacity of 363.4 mAh/g and maintained a stable 150.2 mAh/g capacity over 800 cycles at 300 mA/g. It exhibited superior cycling stability and coulombic efficiency (~100%), with enhanced Cl^- diffusion coefficients ($\sim 10^{-10}\text{--}10^{-12} \text{ cm}^2/\text{s}$). The redox activity of Ni, Co, and Mo across multiple oxidation states ($\text{Ni}^{10}/^{2+}/^{3+}$, $\text{Co}^{0}/^{2+}/^{3+}$, $\text{Mo}^{4+}/^{6+}$) facilitated efficient chloride ion intercalation and de-intercalation, resulting in high energy and power performance metrics suitable for long-cycle chloride-ion storage.

In the CIB application, the Mo-doped $\text{NiCo}_2\text{-Cl}$ LDH was employed as a cathode material [144]. Among various Mo doping levels, $\text{Mo}_{0.3}\text{NiCo}_2\text{Cl}$ LDH exhibited optimal performance. This material delivered an initial specific capacity of 278.5 mAh/g and maintained a reversible discharge capacity of 159.7 mAh/g after 300 cycles at 150 mA/g, demonstrating remarkable cyclic stability. The electrode also showed enhanced chloride-ion diffusion coefficients ($10^{-11}\text{--}10^{-12} \text{ cm}^2/\text{s}$), and its energy storage involved multiple reversible redox couples ($\text{Ni}^0/\text{Ni}^{2+}/\text{Ni}^{3+}$, $\text{Co}^0/\text{Co}^{2+}/\text{Co}^{3+}$, and $\text{Mo}^{4+}/\text{Mo}^{6+}$). The material's high performance is attributed to Mo-induced oxygen vacancies and reduced bandgap, promoting superior electronic conductivity, fast Cl^- transport, and low-strain structural stability (volume change <3%). These features result in high energy density and power capability, outperforming many previously reported CIB cathodes.

NiMn-Cl LDH/CNT was employed as a cathode material in the CIB application [113]. The hybrid architecture facilitated efficient chloride-ion intercalation and deintercalation during cycling. The composite electrode delivered a stable specific capacity of approximately 130 mAh/g over 150 cycles, demonstrating good cyclic durability. The enhanced structure ensured prolonged operational performance and mitigated degradation, key metrics for practical CIB deployment. $\text{Ni}_5\text{Ti-Cl}$ LDH was employed as a cathode material, exhibiting remarkable electrochemical performance in CIB applications [114]. At 300 mA/g, it delivered an initial discharge capacity of 374.6 mAh/g and retained 193.3 mAh/g after 200 cycles. Notably, even under a high current density of 1000 mA/g, it maintained a stable reversible capacity of 127.9 mAh/g over 1000 cycles, showcasing excellent long-term cycling stability. The $\text{Ni}_5\text{Ti-Cl}$ LDH also demonstrated high-rate capabilities with capacities of 264.9 to 104 mAh/g across increasing current densities (100–1000 mA/g), with capacity recovering when the rate was lowered again. EIS confirmed low charge/transfer resistance (37.44Ω), and diffusion coefficients ranged from 10^{-10} to $10^{-13} \text{ cm}^2/\text{s}$. Figure 17a shows the charge/discharge behavior of the $\text{Ni}_5\text{Ti-Cl}$ LDH electrode. Structural evolution during cycling is captured by the XRD data in Figure 17b, with a detailed view of the (003) peak in Figure 17c and related volume changes in Figure 17d. Chemical states of Ni and Ti are analyzed through XPS in Figure 17e,f, while Figure 17g,h displays the corresponding oxidation state ratio shifts with voltage. Figure 17i illustrates the Cl^- transport mechanism across the battery. Additionally, density functional theory (DFT) calculations revealed favorable Cl^- adsorption energies and low diffusion barriers (0.045–0.091 eV), correlating with high-rate performance and fast Cl^- transport kinetics. These attributes make the $\text{Ni}_5\text{Ti-Cl}$ LDH cathode one of the most promising candidates for next-generation CIBs. In the CIB application, CoFe-Cl-LDH/CNT was utilized as the anode, paired with an AgCl/CNT cathode in a neutral aqueous NaCl electrolyte [145]. The cell exhibited an impressive initial capacity of ~190 mAh/g at 200 mA/g and maintained ~125 mAh/g after 200 cycles, highlighting excellent cyclic stability. At higher current densities (400 mA/g), the capacity remained around 120 mAh/g, demonstrating robust rate capability. The

energy density reached 165 Wh/kg and power density up to 140 W/kg depending on the current rate and voltage range. The outstanding performance is attributed to reversible Cl^- intercalation/deintercalation, stable layered structure, and enhanced electron transfer facilitated by CNTs, making it a promising anode for aqueous CIBs.

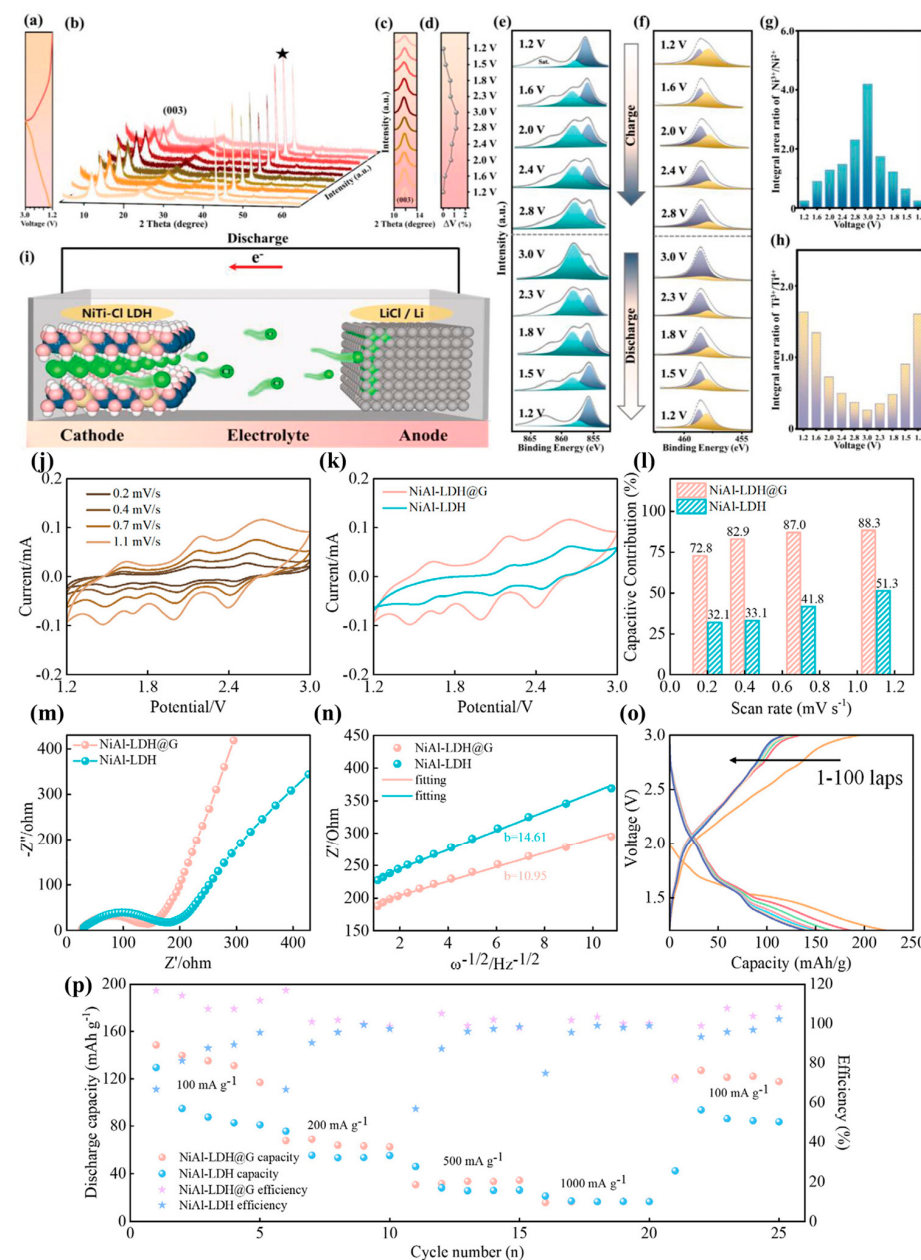


Figure 17. (a) Charge/discharge profiles of $\text{Ni}_5\text{Ti-Cl LDH}$. (b) In situ XRD patterns during full cycling, showing structural changes; the peak at $2\theta = 43.17^\circ$ corresponds to the current collector. (c) Enlarged view of the (003) reflection peak. (d) Volume variation across charge/discharge states. (e,f) Ex situ XPS spectra of Ni 2p and Ti 2p regions during different stages of the cycle. (g,h) Peak area ratio changes of $\text{Ni}^{3+}/\text{Ni}^{2+}$ and $\text{Ti}^{3+}/\text{Ti}^{4+}$ with voltage. (i) Schematic of Cl^- ion transport mechanism in $\text{Li}^+|\text{Ni}_5\text{Ti-Cl LDH}$ battery. Reproduced with permission [114]. (j) CV curves at various scan rates for NiAl-LDH@G electrode. (k) CV comparison of NiAl-LDH and NiAl-LDH@G at 1.1 mV/s. (l) Capacitance contribution at different scan rates. (m,n) Nyquist plots and low-frequency Z' vs. $\omega^{-1/2}$ plots for NiAl-LDH and NiAl-LDH@G. (o) Charge/discharge voltage curves over 100 cycles. (p) Rate performance of NiAl-LDH and NiAl-LDH@G at various current densities. Reproduced with permission [143].

NiAl-LDH@G was employed as a cathode material in CIBs. Compared to pure NiAl-LDH, the NiAl-LDH@G cathode demonstrated significantly enhanced electrochemical performance [143]. It delivered a high specific capacity of 223.3 mAh/g during the first discharge and a stable reversible capacity of 107 mAh/g over 500 cycles at 100 mA/g with a coulombic efficiency of ~96%. It also retained 72 mAh/g after 120 days, indicating low self-discharge and excellent long-term stability. The composite exhibited good rate capability with capacities of 148.5, 67.8, 30.9, and 15.9 mAh/g at increasing current densities, recovering to 120.8 mAh/g when returned to 100 mA/g. EIS showed reduced charge transfer resistance and higher chloride ion diffusion coefficients (up to $3.22 \times 10^{-12} \text{ cm}^2/\text{s}$), confirming improved conductivity and ion mobility. Electrochemical properties of NiAl-LDH@G are shown in Figure 17j to Figure 17n, with CV and impedance tests confirming improved charge storage and ion diffusion compared to NiAl-LDH. Long-term cycling behavior is presented in Figure 17o, and rate capability at different current densities is plotted in Figure 17p, showing the superior performance of the NiAl-LDH@G composite. These results underscore the superiority of the nanoarray structure in facilitating fast redox kinetics and durable performance in CIBs.

4.5. Zinc-Ion Batteries

ZIBs also benefit from LDH incorporation. Studies have shown that LDH compounds like Zn-Al serve as structural promoters and improve charge storage capabilities, achieving specific capacities upward of 300 mAh/g [259]. Furthermore, their layered structure contributes to the selective intercalation of zinc ions, which further optimizes battery performance and longevity [260]. This characteristic is particularly advantageous in developing versatile and efficient energy storage solutions. Hv-Ni₃Mn_{0.7}Fe_{0.3}-LDH was employed as a cathode material in aqueous ZIBs (AZIBs) [16]. The modified LDH displayed exceptional performance, delivering a high specific capacity of 328 mAh/g at 50 mA/g and maintaining 122 mAh/g over 500 cycles at 1 A/g with 85% capacity retention. The enhanced electrochemical behavior stems from introducing hydrogen vacancies that expose terminal oxygen atoms, promoting Zn²⁺ intercalation and diffusion. The material also exhibited robust rate capability and reversible Zn²⁺/H⁺ intercalation mechanism. The synergy among Ni, Mn, and Fe contributed to conductivity and redox activity and effectively suppressed Jahn-Teller distortion, ensuring structural stability during long-term cycling. The Ragone plot revealed competitive energy and power densities, positioning this LDH among the top-performing ZIB cathodes.

The synthesized NiCo LDH, supported with MXene and electrodeposited on nickel foam, served as a high-performance cathode in alkaline Zn || NiCo batteries [203]. The battery exhibited a remarkable areal specific capacity of 20.2 mAh/cm² (equivalent to 311.7 mAh/g), with exceptional rate capabilities maintaining 9.6 mAh/cm² at 120 mA/cm² (148 mAh/g). It also delivered ultrahigh areal and gravimetric energy densities of 31.2 mWh/cm² and 465 Wh/kg, respectively, alongside a peak power density of 80 mW/cm² (2752 W/kg). The electrode retained 88.6% of its capacity after 10,000 cycles, demonstrating outstanding long-term cycling stability, fast kinetics, and high ion diffusion coefficients due to the unique MXene-assisted structure. MCN-LDH@CP was used as the cathode in an aqueous CoNi//Zn battery [165]. The hybrid electrode exhibited a high areal specific capacity of 1.74 mAh/cm², an areal energy density of 2.89 mWh/cm², and a peak power density of 111.22 mW/cm². It demonstrated excellent cycling stability, maintaining 97.8% capacity retention after 7000 cycles at 40 mA/cm². These superior performances are attributed to the molybdate-induced increase in surface area, interlayer spacing, and improved diffusion kinetics. The battery also showed outstanding mechanical resilience and safety in quasi-solid-state form, maintaining functionality under physical damage.

The ZnCo-LDH was employed as a cathode material in Zn-ZnCo batteries, using Ni foam as the current collector and a 6 M KOH + 0.2 M Zn(CH₃COO)₂ electrolyte [166]. The batteries exhibited a linear increase in specific capacity with increased ZnCo-LDH loading, reaching up to 2.5 mAh/cm² at a 60 mg/cm² loading. Remarkable rate performance was maintained across various current densities, with over 75% capacity retention at high rates and full recovery upon returning to lower current densities. The ZnCo-LDH cathode demonstrated exceptional cycling stability, retaining 86% of its capacity after 5000 cycles at 30 mg/cm² loading. Additionally, hybrid Zn batteries incorporating an air-accessible Pt/C-coated gas diffusion layer alongside ZnCo-LDH delivered dual-stage voltage plateaus, enabling a combination of Zn–ZnCo and Zn-air functionalities. The hybrid cell exhibited stable cycling over 270 cycles and enhanced Zn–ZnCo segment capacity due to improved electrode wettability.

The H-vacancy-rich CoNi-LDH(v) was used as a cathode in aqueous and flexible solid-state Zn-ion batteries (ZIBs), paired with Zn@CC as the anode [204]. The aqueous CoNi-LDH(v)@CC//Zn@CC battery delivered a high specific capacity of 225 mAh/g at 0.5 A/g, with energy and power densities of 353.62 Wh/kg and 3056.51 W/kg, respectively. It retained 53.9% capacity after 900 cycles, significantly outperforming the non-activated CoNi-LDH. Figure 18a shows the layered structure of the flexible CoNi-LDH(v)@CC//Zn@CC solid-state battery. Electrochemical behavior is displayed in Figure 18b, where the GCD curves demonstrate good performance at different current rates. The corresponding specific capacity and coulombic efficiency over cycling are shown in Figure 18c. Figure 18d presents the cycling stability, with the battery maintaining 47.22% of its capacity after 1000 cycles. Mechanical flexibility is evaluated in Figure 18e, where the battery retains over 85% capacity even when bent at 150°. Figure 18f shows it remains functional after 100 bending cycles with 74.82% capacity retention. Figure 18g–i visually demonstrates the battery's robustness: it powers a digital device while bent, continues operating even after being cut, and maintains output for over 80 h in an open environment. Moreover, a flexible, solid-state version of the battery demonstrated excellent deformability and stability under mechanical stress and sustained operation over 80 h without encapsulation, underlining its promise for wearable electronics.

ZnAl-LDH was applied as an artificial interface layer on Zn anodes (SZ/LDH@Zn) to enhance the performance of aqueous ZIBs [172]. The SZ/LDH@Zn||SZ/LDH@Zn symmetric cell delivered an ultra-long cycling lifespan of 5500 h at 1 mA/cm² with low voltage hysteresis (16.4 mV). In asymmetric Zn||Cu cells, it achieved a high average coulombic efficiency of 99.85% over 3800 cycles, outperforming bare Zn and ZnAl-LDH@Zn. Furthermore, in an entire cell with NaV₃O₈·xH₂O cathode and a low N/P ratio of 3.62, the SZ/LDH@Zn||NVOH cell exhibited a specific capacity of 251.45 mAh/g, an areal capacity of 5.36 mAh/cm², and stable cycling over 1500 cycles at 1 A/g. These results confirm the superior reversibility, capacity retention, and anti-corrosion performance of SZ/LDH@Zn in practical ZIB systems.

H-vacancy-enriched CoNi LDH (denoted as CoNi LDH(v)) was employed as a cathode material for aqueous ZIBs in a mild ZnSO₄ electrolyte (pH ≈ 4) [207]. The electrode demonstrated a high specific capacity of 185 mAh/g at 1.2 A/g, with an average discharge voltage of 1.6 V (vs. Zn²⁺/Zn), leading to an excellent energy density of 296.2 Wh/kg at a power density of 1894 W/kg. Even at a high current density of 12 A/g, it maintained a 103 mAh/g capacity, indicating good rate performance. Furthermore, the electrode showed impressive cyclic stability with 80% capacity retention over 1000 cycles at 6 A/g. The superior performance was attributed to the Zn²⁺/H⁺ co-intercalation mechanism enabled by the introduced hydrogen vacancies, which improved ion diffusion and electronic conductivity.

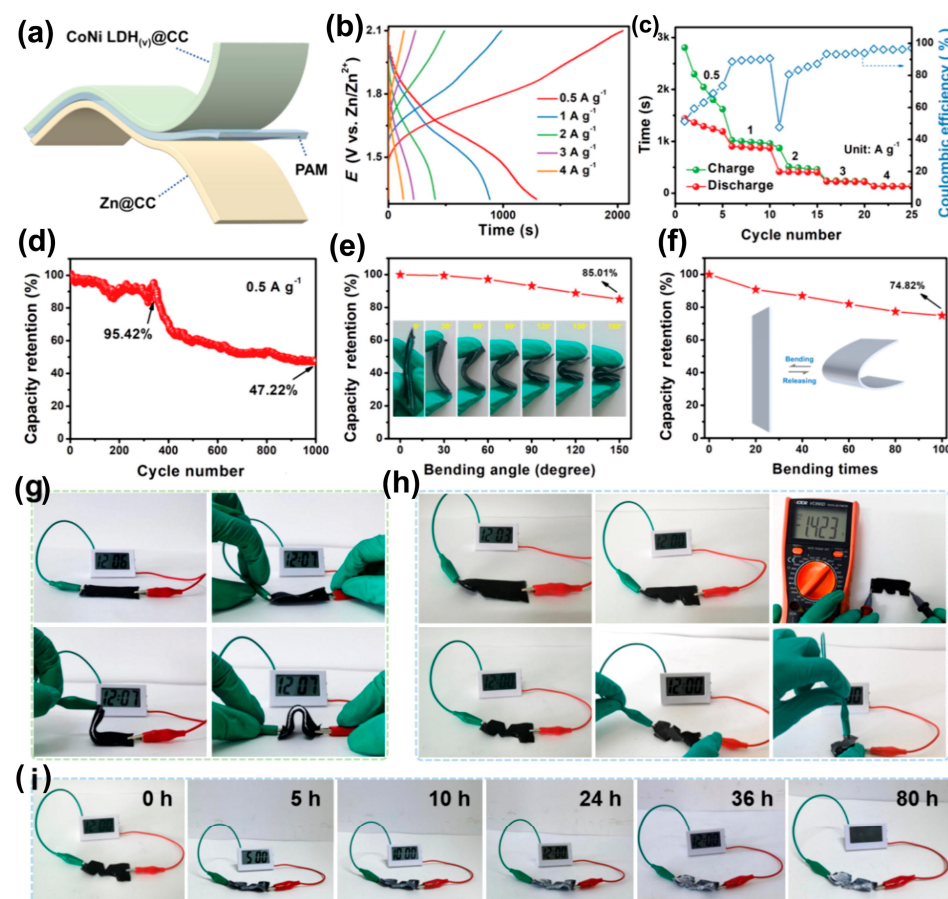


Figure 18. Design and performance of a flexible solid-state battery based on a CoNi-LDH(v)@CC//Zn@CC layered configuration. (a) Schematic of the battery's structural composition. (b) Charge/discharge profiles at various current densities. (c) Specific capacity and coulombic efficiency during charge/discharge cycling. (d) Long-term cycling performance at 0.5 A/g. (e) Capacity retention under different bending angles. (f) Capacity retention after multiple bending cycles. (g) Photographs showing operation under various bending and twisting states. (h) Device functionality after being cut. (i) Duration of continuous power output to a digital watch in open-air conditions. Reproduced with permission [204].

In the alkaline ZIB configuration, NC@CL was employed as the cathode against a Zn anode in an aqueous electrolyte (1 M KOH + 5 mM ZnO) [141]. The NC@CL//Zn battery demonstrated outstanding electrochemical performance with a high specific capacity of 381.1 mAh/g at 0.5 A/g, maintaining 243.4 mAh/g even at 10 A/g, confirming excellent rate capability. The device showed a robust energy density of 66.56 Wh/kg and power density of 15,375 W/kg, with superior cyclic stability—retaining 98% capacity over 2000 cycles at 5 A/g. These performances are attributed to the hierarchical nanosheet morphology, heterostructure-induced interfacial charge redistribution, and enhanced OH⁻ adsorption facilitated by La-doping and NC-CL synergism. The synthesized NiCoS@NiCo-LDH was utilized as the cathode in aqueous alkaline zinc-based batteries (AAZBs), assembled in a full cell with zinc foil as the anode [208]. The device delivered an impressive specific capacity of 312 mAh/g at 2 mA/cm². Moreover, it achieved a high energy density of 435.3 Wh/kg at a power density of 4.1 kW/kg, maintaining 95.9% capacity retention over 3000 cycles at 20 mA/cm². These values highlight excellent rate capability and stability and surpass the performance of many previously reported nickel-based cathode materials, showcasing its potential for high-performance, long-life ZIBs.

The synthesized NF\Ni₃S₂/NiS@NiCo-LDH was employed as the cathode in an aqueous alkaline Ni-Zn battery, paired with a zinc anode and a mixed KOH/Zn(CH₃COO)₂

electrolyte [209]. The battery delivered a high specific capacity of 434.5 mAh/g at 3 mA/cm², showcasing excellent rate performance with capacities ranging from 317.9 to 100.3 mAh/g across 2–15 A/g. The device achieved a maximum energy density of 556.3 Wh/kg and a peak power density of 26.3 kW/kg. The cycling stability was outstanding, retaining 116.7% of its original capacity after 5000 cycles at 60 mA/cm², highlighting its activation behavior and robust long-term performance.

4.6. Zinc–Air Batteries

In the context of ZABs, LDHs demonstrate exceptional catalytic activity for OER. Yan et al. [261] highlighted the efficiency of Ni–Fe LDHs as bifunctional electrocatalysts, achieving low overpotentials that significantly enhance the performance of ZABs. Their superior activity can be attributed to the highly active sites the layered structure provides, which facilitate oxygen reduction and evolution reactions. Consequently, integrating LDHs in air battery systems can lead to enhanced energy densities and improved operational lifetimes. In the ZAB application, Co@NiFe-LDH was employed as the air cathode catalyst, while a zinc plate was used as the anode [150]. The battery demonstrated outstanding performance metrics, surpassing even Pt/C + RuO₂-based systems. Specifically, Co@NiFe-LDH achieved a specific capacity of 652 mAh/g, power density of 165 mW/cm², and an open circuit voltage of 1.44 V. It exhibited excellent cyclic stability over 90 h of continuous GCD cycling with a minor voltage gap increase (from 0.78 V to 0.80 V), maintaining about 59.5% round-trip efficiency. These results confirm Co@NiFe-LDH's promise as a cost-effective and efficient catalyst for rechargeable ZABs.

The Pt-anchored NiFe-LDH@Co₉S₈ was used as a bifunctional air cathode catalyst in both liquid-state and flexible quasi-solid ZABs [149]. The catalyst demonstrated superior electrocatalytic performance with a high specific capacity of 796.6 mAh/g and a 164.3 mW/cm² peak power density in liquid-state ZABs. It also exhibited an energy density of 76.4 Wh/kg and excellent cyclic stability, maintaining performance over 240 cycles (80 h) in flexible ZABs. Figure 19a presents the structural design of the flexible ZAB, which includes an air cathode and a NiFe-LDH@Co₉S₈ electrocatalyst that supports both OER and ORR processes. Figure 19b compares the impedance of three different polymer electrolytes, showing that the PANA-CMC-IL hydrogel offers the lowest resistance. Figure 19c confirms its superior water retention over time, supporting stable operation. The practical application of the battery is shown in Figure 19d, where it successfully powers an LED display. The discharge and power density performance are detailed in Figure 19e, showing a peak power density of 78.4 mW/cm². Figure 19f illustrates the battery's ability to maintain high capacities across different current densities, and Figure 19g confirms cycling durability through stable voltage over repeated charge/discharge cycles. Figure 19h demonstrates excellent mechanical flexibility, as the device retains stable output after multiple bending cycles. The catalyst outperformed commercial Pt/C and RuO₂ references, attributed to its synergistic core/shell architecture, high electrochemical surface area (28.2 mF/cm²), and enhanced ORR/OER activity. The NiCo-LDH/NCM@NF was employed as a bifunctional air cathode in ZABs [148]. It demonstrated a high open-circuit voltage (1.374 V), a peak power density of 158 mW/cm², and a specific capacity of 685 mAh/g at 10 mA/cm², outperforming commercial Pt/C + IrO₂ catalysts. The catalyst also showed excellent cycling stability, maintaining consistent charge/discharge voltage profiles over 500 cycles and sustaining high round-trip efficiency (~62%) with minimal voltage gap increase. The four-electron ORR pathway, high ECSA (194 cm²), and low OER overpotential (0.352 V at 50 mA/cm²) contribute to its robust and durable ZAB performance, attributed to the synergistic integration of NCM and LDH structures enriched with oxygen vacancies.

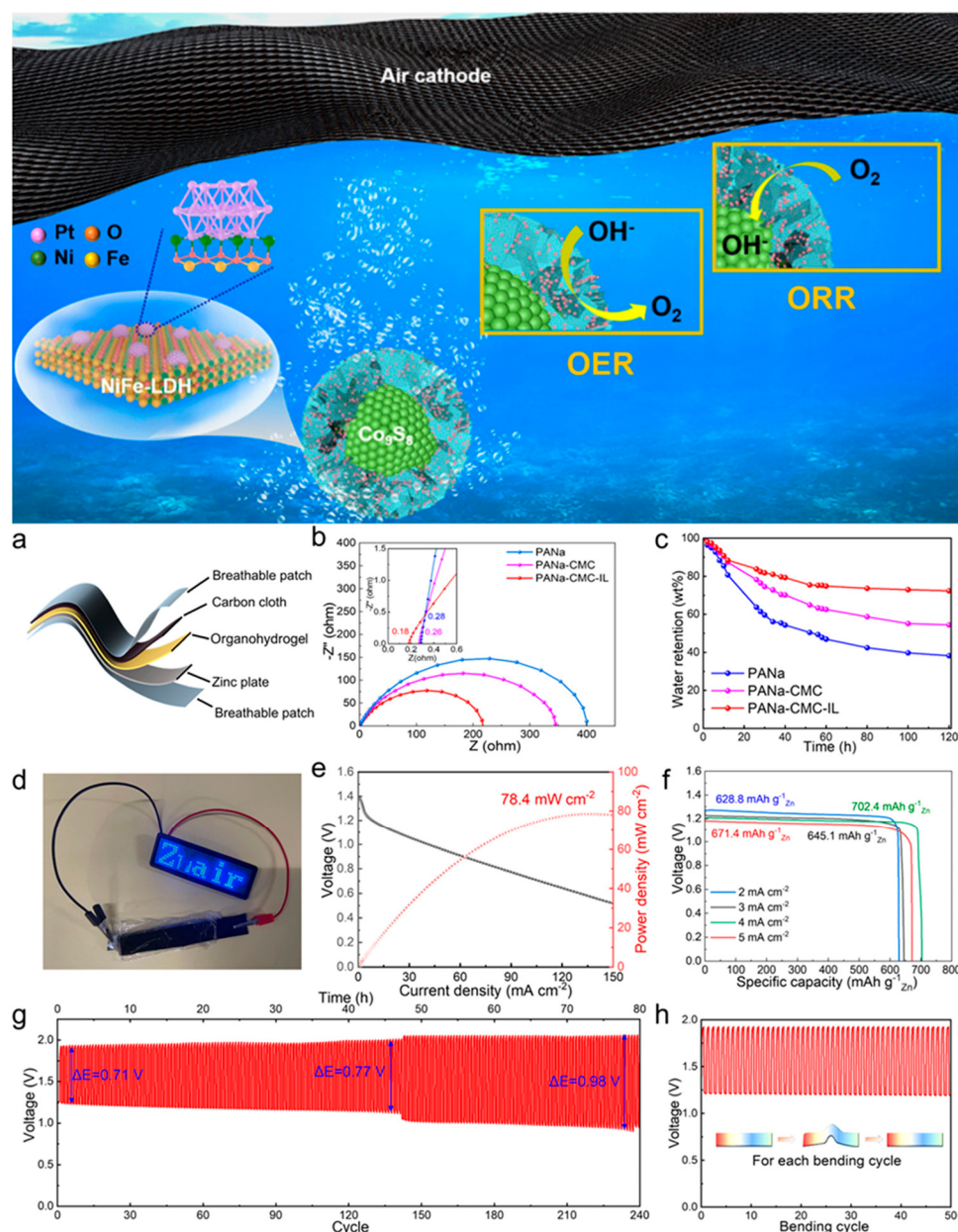


Figure 19. Design and performance of a flexible quasi-solid ZAB using NiFe-LDH@Co₉S₈ nanoflowers with Pt nanocrystals as bifunctional electrocatalysts. (a) Schematic of the overall FZAB configuration and its air cathode mechanism involving OER and ORR. (b) Nyquist plots comparing PANa, PANa-CMC, and PANa-CMC-IL hydrogels. (c) Water retention characteristics over time for each hydrogel type. (d) Photograph showing the FZAB powering an LED panel. (e) Discharge polarization curve and power density output of the battery. (f) Discharge profiles of the device at varying current densities. (g) Charge/discharge cycling stability at 2 mA/cm². (h) Charge/discharge behavior after repeated bending cycles, highlighting mechanical flexibility. Reproduced with permission [149].

In the ZAB application, the synthesized ZnCo₂O₄@NiMn-LDH (2:1) was employed as the air cathode [147]. It demonstrated a significantly lower overpotential of 390 mV at a current density of 50 mA/cm², outperforming pristine ZnCo₂O₄. The battery exhibited a peak power density of 43 mW/cm² and delivered a high specific capacity of 639 mAh/g. Notably, it maintained excellent stability, operating continuously for up to 200 h under repeated charge/discharge cycling. These results highlight the material's suitability for long-term and efficient OER catalysis in ZABs. The optimized Fe/CoLDH-based composite (CoL 2:1) was employed as a bifunctional cathode catalyst in a rechargeable ZAB [116].

The assembled battery exhibited a high open-circuit voltage (OCV) of 1.503 V and delivered a peak power density of 161 mW/cm^2 . It achieved a specific discharge capacity of 804 mAh/gZn at 5 mA/cm^2 and a calculated energy density of 965 Wh/kg . Notably, the device maintained stable operation over 200 h with a minimal voltage gap of 0.76 V at 10 mA/cm^2 , corresponding to a high voltage efficiency of 96%. Even under high current densities (up to 50 mA/cm^2), the system exhibited remarkable rate capability and durability, highlighting the catalyst's robustness and practical viability in real-world ZAB systems.

In application, the CoFe/Fe₃C@CN-900 served as the air cathode catalyst in both aqueous and all-solid-state ZABs [115]. The aqueous ZAB delivered a specific 795 mAh/g capacity, an energy density of 982 Wh/kg , and a maximum power density of 190 mW/cm^2 , outperforming the benchmark Pt/C + RuO₂ catalyst. Additionally, it retained 96.5% current after 10 h in stability tests and displayed excellent charge/discharge cycling performance with minimal voltage hysteresis at 5 and 10 mA/cm^2 . Solid-state ZABs also demonstrated competitive performance, with a specific capacity of 750 mAh/g and energy density of 929 Wh/kg , along with robust cycling stability, confirming their strong potential for practical applications. The Ni-CAT/NiFe-LDH/CNFs composite was used as a bifunctional catalyst at the air cathode of both liquid and solid-state ZABs [146]. Liquid ZABs demonstrated a high peak power density of 292.1 mW/cm^2 , with an open-circuit voltage of 1.407 V , and superior cyclic stability up to 66 h with a low voltage gap. In solid-state flexible ZABs, it retained structural integrity under bending. It showed even better performance, reaching a power density of 299.48 mW/cm^2 and a cycle life of 30 h at a current density of 1 mA/cm^2 . These results highlight its promising bifunctional catalytic activity and robust mechanical flexibility for advanced energy storage systems.

In applying ZABs, the Cu@Cu NWs@LDH composite was employed as the air cathode [210]. The assembled battery exhibited a high open-circuit potential of 1.336 V and achieved a peak power density of 179.3 mW/cm^2 . It showed superior charge/discharge performance with a low potential gap of 0.852 V at 50 mA/cm^2 . The battery maintained stable cycling performance for over 250 h at 10 mA/cm^2 with negligible voltage decay. The NiFe LDH coating on Cu nanowires offered high catalytic activity for OER and ORR, attributed to its enhanced surface area, conductivity, and corrosion resistance. The synthesized CoMn-LDH/NPGA was used as the air cathode in a rechargeable liquid ZAB, where it demonstrated outstanding bifunctional catalytic activity for both ORR and OER [231]. The ZAB showed an open-circuit voltage of 1.514 V and delivered a maximum power density of 206 mW/cm^2 at 226 mA/cm^2 , surpassing the performance of Pt/C + IrO₂. It also achieved a high energy density and excellent rate capability, maintaining a discharge voltage of $\sim 1.37 \text{ V}$ across varied current densities. Impressively, it exhibited exceptional cycling stability over 72 h (432 cycles) with minimal voltage decay, attributed to the structural robustness of the 3D NPGA framework and uniform CoMn-LDH dispersion.

LDHs have emerged as highly versatile and tunable materials across a wide spectrum of battery chemistries, including LIBs, LSBs, NIBs, CIBs, ZIBs, and ZABs. Their unique 2D lamellar structures, high surface area, compositional flexibility, and anion exchange capacity enable exceptional electrochemical performance through enhanced ion diffusion, redox activity, and structural integrity. In LIBs and NIBs, LDH-based electrodes exhibit high specific capacities, excellent rate performance, and long-term cycling stability due to their ability to accommodate lithium or sodium ions via intercalation and conversion mechanisms. In LSBs, LDHs serve as cathode hosts, interlayers, and separator coatings, effectively suppressing polysulfide shuttling and catalyzing redox reactions, leading to outstanding capacity retention and coulombic efficiency. Their role in CIBs is expanding, with interlayer-engineered LDHs showing promising Cl⁻ transport properties and structural robustness. Similarly, in ZIBs, LDHs contribute to superior zinc ion intercalation

kinetics, energy density, and mechanical resilience, particularly in flexible and high-loading configurations. Moreover, in ZABs, LDHs, often combined with conductive or catalytic materials, act as efficient bifunctional electrocatalysts for oxygen evolution and reduction, offering low overpotentials, high power densities, and extended cycle life. Collectively, the multifunctional role of LDHs across these systems underscores their transformative potential in advancing next-generation, high-performance, and sustainable energy storage technologies. A comprehensive comparison of LDH-based materials in diverse battery systems, including their synthesis methods and electrochemical performance, is presented in Table 1.

Table 1. Summary of various LDH-based electrode materials, their synthesis methods, and electrochemical performance parameters for battery applications.

LDH Name	Synthesis Procedure	Battery Type	Electrolyte	Specific Capacity (mAh/g)	Stability	Ref.
Hv-Ni ₃ Mn _{0.7} Fe _{0.3} -LDH	Co-precipitation + Electrochemical Activation	ZIB	0.2 M ZnSO ₄	328	85% capacity retention over 500 cycles at 1 A/g	[16]
NiCo-LDH nanocrystall@amorphousness core/shell structure (LDH200)	Co-precipitation followed by heat treatment at 200 °C	LIB	1.0 M LiPF ₆	1821.3 (0.1 A/g)	~687.7 mAh/g at 0.5 A/g after 500 cycles (attrition rate: 0.092%)	[109]
MgAl-LDH@CNT	Co-precipitation	LSB	Li ₆ PS ₅ Cl	...	Stable over 200 cycles at 1 C with 4.0 mg/cm ² S loading	[110]
NiFe-NO ₃ LDH	Co-precipitation	NIB	1 M NaClO ₄	972 (initial); 388 (60 cycles at 50 mA/g); 122 (500 cycles at 500 mA/g)	388 mAh/g after 60 cycles; 122 mAh/g after 500 cycles	[111]
NiFe-Cl LDH	Co-precipitation	CIB	0.5 M Bpy ₁₄ Cl/PC	27.1	64.2 mAh/g after 200 cycles	[112]
Ni ₅ Ti-Cl LDH	Co-precipitation + anion exchange	CIB	0.5 M Bpy ₁₄ Cl	257.8	127.9 mAh/g after 1000 cycles @1 A/g	[114]
CoFe/Fe ₃ C@CN-900	MOF-derived + Co-precipitation	ZAB	0.1 M KOH	795	96.5% current retention after 10 h discharge	[115]
Fe/Co LDH (CoL 2:1)	Co-precipitation	ZAB	0.1 M KOH	804	200 h (307 cycles)	[116]
ZIF-67@NiCo-LDH	One-pot hydrothermal synthesis	LIB	1 M LiPF ₆	1997.1 (initial), 807.9 (after 100 cycles)	Stable up to 100 cycles, excellent rate capability	[134]
NiFe ₂ O ₄ @NiCo-LDH	Two-step hydrothermal method (MOF-derived)	LIB	1 M LiPF ₆	636.9	Stable after 100 cycles (636.9 mAh/g at 0.3 A/g), coulombic efficiency ~98%	[135]
Ni-Zn LDH intercalated with DS ⁻	Hydrothermal synthesis	LIB	1 M LiPF ₆	850 at 0.5 A/g	850 mAh/g over 400 cycles	[136]
NiS ₂ /FeS ₂ @NC@NiFe LDH/FeO(OH)	Solvothermal followed by hydrothermal synthesis	LIB	1 M LiPF ₆	709.9	709.9 mAh/g at 0.2 A/g after 200 cycles; 403.3 mAh/g at 1.0 A/g after 500 cycles	[137]
NiCo-LDH/MXene	Hydrothermal	LIB	1 M LiPF ₆	1081 (at 100 mA/g)	100 cycles at 0.1 A/g with excellent capacity retention	[138]
Mg ₂ Al ₁ -CO ₃ -LDH	Hydrothermal synthesis	LIB	1 M LiPF ₆	814	203.8 mAh/g after 300 cycles	[140]
NiCoOOH@CoLa-LDH (NC@CL)	Hydrothermal synthesis (2-step)	ZIB	1 M KOH + 5 mM ZnO	381.1	98% capacity retention after 2000 cycles	[141]

Table 1. Cont.

LDH Name	Synthesis Procedure	Battery Type	Electrolyte	Specific Capacity (mAh/g)	Stability	Ref.
NiCoMo-P150 LDH	Hydrothermal + Anion exchange + Temperature-differential phosphorus doping	CIB	0.5 M Bpy14Cl	363.4 (initial), 150.2 (stable)	800 cycles at 300 mA/g	[142]
NiAl-LDH@G	Atomic layer deposition + Hydrothermal	CIB	0.5 M Bpy14Cl	223.3	107 mAh/g after 500 cycles; 72 mAh/g after 120 days	[143]
Mo _{0.3} NiCo ₂ -Cl LDH	Hydrothermal synthesis + Ion exchange	CIB	0.5 M Bpy14Cl	352.5	159.7 mAh/g (after 300 cycles)	[144]
CoFe-Cl-LDH/CNT	Co-precipitation + Hydrothermal synthesis	CIB	1.0 M NaCl	190	125 mAh/g after 200 cycles	[145]
Ni-CAT/NiFe-LDH/CNFs	Hydrothermal synthesis + in situ MOF growth	ZAB	6 M KOH	...	66 h (liquid)/30 h (solid)	[146]
ZnCo ₂ O ₄ @NiMn-LDH (2:1)	Two-step hydrothermal	ZAB	6 M KOH	639	200 h cycling	[147]
NiCo-LDH/NCM@NF	Hydrothermal synthesis	ZAB	1 M KOH	685	Stable over 500 cycles	[148]
Pt-NiFe-LDH@Co ₉ S ₈	Hydrothermal + Spontaneous-redox strategy	ZAB	6.0 M KOH/0.2 M Zn(OAc) ₂	796.6	240 cycles (80 h, flex)	[149]
Co@NiFe-LDH	Two-step hydrothermal	ZAB	0.2 M Zn(OAc) ₂ + 6 M KOH	652	90 h cycling with minor degradation	[150]
Ni ₂ Co-LDH/EG composites	Co-precipitation and Microwave irradiation	LIB	1 M LiPF ₆	1880 (0.05 A/g); 919 (1 A/g)	~973 mAh/g after 100 cycles at 1 A/g	[152]
NiAl LDH	Hydrothermal	LIB	1 M LiPF ₆	2586 (initial), 697 (400th cycle @ 0.5 A/g)	27.6% after 1400 cycles @ 1.0 A/g	[153]
L-CoNi-LDH/C	Laser-induced + Hydrothermal synthesis	LSB	1.0 M LiTFSI	1574 (initial), 1097 (100th)	503 mAh/g after 200 cycles @ 2 C	[154]
LDH@PSS (1:1.5)	Hydrothermal + Exfoliation + Self-assembly	LSB	1 M LiTFSI	1247.2 (initial), 1032.6 (after 200 cycles @ 0.2 C)	0.086% capacity decay per cycle over 200 cycles (0.2 C); 65.2% retention after 1000 cycles (1 C)	[155]
Vo-LDHs-MXenes	Self-growth aging	LSB	1.0 M LiTFSI	1549 (initial), 701 (after 300 cycles at 1 C)	300 cycles at 1.0 C, 0.084% decay/cycle	[156]
V ₂ O ₅ /Cys/FeNi-LDH	Hydrothermal + Reflux	LSB	1.0 M LiTFSI	1035.2 (initial), 920.1 (after 300 cycles)	88.9% retention after 300 cycles; 0.039% decay per cycle	[156]
NiFe-LDH@S	Hydrothermal	LSB	1 M LiTFSI	676 (initial), 386 (after 500 cycles at 2 C)	386 mAh/g after 500 cycles @ 2 C	[157]
NiAl-LDH@S	Hydrothermal	LSB	1 M LiTFSI	432 (initial), 238 (after 500 cycles at 2 C)	238 mAh/g after 500 cycles @ 2 C	[157]
ZnAl-LDH@S	Hydrothermal	LSB	1 M LiTFSI	357 (initial), 198 (after 500 cycles at 2 C)	198 mAh/g after 500 cycles @ 2 C	[157]

Table 1. Cont.

LDH Name	Synthesis Procedure	Battery Type	Electrolyte	Specific Capacity (mAh/g)	Stability	Ref.
NiCoAl-LDH	Hydrothermal + PECVD (for VG growth)	LSB	1.0 M LiTFSI with 1 wt.% LiNO ₃	1182.4 (initial), 441.3 (after 750 cycles at 0.5 C)	0.0755% capacity decay per cycle (750 cycles at 0.5 C)	[158]
NiCr-Cl LDH/rGO	Hydrothermal + Ion Exchange	NIB	1 M NaCF ₃ SO ₃	218 (200 cycles @ 100 mA/g)	34.5% capacity retention after 200 cycles	[159]
CoMoLDH@C-PDA-6	Hydrothermal + Polymerization + Carbonization	NIB	1 M NaClO ₄	779.9 (initial); 310.9 (after 100 cycles)	70% retention after 100 cycles at 0.1 A/g	[163]
Co-Co LDH-derived CoSe ₂ @NHCNS@C	Hydrothermal synthesis + selenization + carbon coating	NIB	1 M NaClO ₄	465.6 (initial), 373.8 (after 100 cycles)	373.8 mAh/g after 100 cycles; 325 mAh/g after 1000 cycles at 0.5 A/g	[164]
MCN-LDH@CP	Two-step hydrothermal	ZIB	3.0 M KOH	1.74 mAh/cm ²	97.8% @ 7000 cycles	[165]
ZnCo-LDH	Hydrothermal	Zn-ZnCo/Hybrid Zn	6 M KOH + 0.2 M Zn(AC) ₂	2.5 mAh/cm ²	86% after 5000 cycles	[166]
NiCo LDH/MXene@NF	Electrodeposition	ZIB	1 M KOH	311.7	capacity retention of 88.6% after 10,000 cycles at 2 A/g	[203]
CoNi-LDH(v)	Electrochemical deposition + Electrochemical activation (ECA)	Aqueous and Solid-state ZIB	3 M ZnSO ₄	225	53.9% after 900 cycles (aqueous); 47.22% after 1000 cycles (solid-state)	[204]
ZnAl-LDH@Zn	Electrochemical deposition	ZIB	3 M ZnSO ₄	251.45	Stable after 1500 cycles	[172]
CoNi LDH(v)	Electrochemical deposition + CV activation	ZIB	1 M ZnSO ₄	185	80% retention after 1000 cycles	[207]
NiCoS@NiCo-LDH	Hydrothermal + Electrodeposition	ZIB	6 M KOH	312	95.9% after 3000 cycles @ 20 mA/cm ²	[208]
Ni ₃ S ₂ /NiS@NiCo-LDH	Hydrothermal + Electrochemical deposition	ZIB	6 M KOH	434.5	116.7% after 5000 cycles	[209]
NiFe LDH on Cu NWs	Electrochemical deposition	ZAB	6 M KOH and 0.2 M zinc acetate	...	>250 h @ 10 mA/cm ²	[210]
NiCo-LDH	Sol-gel (Ni aerogel) + Solvothermal	LSB	1.0 M LITFSI	1238.4 (0.1 C); 805.8 (5.0 C)	647.1 mAh/g after 700 cycles at 5.0 C (0.018% decay/cycle)	[222]
NiCo-MOF/LDH	Solvothermal synthesis	LSB	1 M LITFSI	950 (after 200 cycles @ 1 C)	0.033% capacity decay per cycle; 633 mAh/g after 1000 cycles @ 1 C	[223]
NiCo-LDH	ZIF-67 template etching + melt-diffusion with sulfur	LSB	1.0 M LiTFSI	1540 @ 0.1 C, 485 @ 5 C	475 mAh/g after 500 cycles @ 1 C (78%)	[224]
NiCo ₂ S ₄ -NiS ₂ NH@C	Ion exchange + in situ transformation	LSB	5 mM Li ₂ S ₆	1207 at 0.2 C; 766 at 2 C	60.23% retention after 450 cycles at 1 C; 6.09 mAh/cm ² at 5 mg/cm ² sulfur loading	[225]
CuCo-LDH	Chemical etching (ZIF-67 template)	LSB	1 M LiTFSI	1262.8 (initial), 697.0 (after 500 cycles at 1 C)	500 cycles, 0.049% capacity decay per cycle	[226]
PPy@LDH-S	Ion exchange + solid-state melting + polymerization	LSB	1 M LiTFSI with 1% LiNO ₃	907.2 (initial, 1 C); 633.4 after 500 cycles	0.06% capacity fading per cycle over 500 cycles	[227]

Table 1. Cont.

LDH Name	Synthesis Procedure	Battery Type	Electrolyte	Specific Capacity (mAh/g)	Stability	Ref.
Ni _{0.8} Ca _{1.2} Al-Cl LDH	Ion exchange	NIB	1.0 M NaPF ₆	256.9 (200 cycles at 0.2 A/g)	102 mAh/g after 600 cycles at 2 A/g	[228]
Co _{0.6} Ca _{1.4} Al-Cl LDH	Ion exchange	NIB	1.0 M NaPF ₆	292.8 (200 cycles at 0.2 A/g)	118.1 mAh/g after 600 cycles at 2 A/g	[228]
CoSn-LDH@MXene	Solvothermal + Ultrasonic	NIB	1 M NaClO ₄	976.1 (0.1 A/g)	87.6% retention after 1000 cycles	[229]
Ni ₃ Ti-Cl LDH	Urea precipitation + anion exchange	CIB	0.5 M PP ₁₄ Cl	346.4	131.8 mAh/g over 200 cycles	[230]
CoMn-LDH/NPGA	Cross-linking gelation + Hydrothermal self-assembly + Freeze drying	ZAB	1 M KOH	...	72 h (~432 cycles) stable operation	[231]

5. LDHs in Supercapacitors

LDHs have attracted significant attention in electrochemical energy storage, particularly as electrode materials in supercapacitors, owing to their tunable chemical composition, two-dimensional layered structure, and abundant redox-active sites [18,182]. The distinctive crystal structure of LDHs features divalent and trivalent metal cations coordinated by hydroxyl groups with intercalated anions and water molecules. This architecture offers multiple pathways for charge storage through both surface redox reactions (pseudocapacitance) and ion intercalation mechanisms, as well as enabling the formation of the electric double layer (EDLC) at the electrode/electrolyte interface [262]. In particular, the exchangeable interlayer anions and the expansive interlayer spacing facilitate rapid diffusion of electrolyte ions, which is critical for achieving high-rate capabilities in supercapacitor applications. Structural modifications and composite strategies have been extensively exploited to enhance the electrochemical performance of LDH-based electrodes. Chemical modifications, such as doping with different metal ions (e.g., Ni, Co, Al, Mn) and anion intercalation, allow precise tuning of the redox properties and electrical conductivity [18,263]. For example, constructing NiCo-LDH microspheres derived from MOFs (Ni-MOFs) has significantly enhanced ion transport kinetics, reduced the charge transfer resistance, and increased the accessible electroactive surface area. Moreover, the integration of LDHs with conductive carbonaceous materials (e.g., graphene, CNTs) or conductive polymers has emerged as a promising strategy to overcome the intrinsic low electronic conductivity of LDHs, thereby improving the overall charge storage efficiency and cycling durability [264,265]. These composite strategies involve synergistic effects whereby the carbon matrix provides an effective conductive network while the LDH component contributes high pseudocapacitance from its Faradaic reactions [18,266].

Electrochemical performance metrics such as capacitance, cycling stability, and rate capability have been a primary focus in assessing the viability of LDH-based supercapacitors. High specific capacitances have been achieved by designing nanostructured LDH architectures that maximize ion diffusion and electron transfer; for example, ultrathin LDH nanosheets demonstrate significantly enhanced pseudocapacitive behavior due to the exposure to a high density of active sites [267]. The cycling stability of these materials is also improved by engineering composite structures that mitigate the typically observed volume changes and agglomeration during charge/discharge cycles [268,269]. Additionally, the rate capability, crucial for high-power applications, is enhanced when LDHs are integrated with conductive scaffolds, resulting in faster charge/transfer kinetics and high capacitance retention at increased current densities [263,266].

Hybrid LDH-based supercapacitors represent a sophisticated approach to delivering high energy and power density by synergistically combining materials that exhibit EDLC and pseudocapacitive behaviors. In hybrid devices, incorporating LDHs as pseudocapacitive components in conjunction with high-conductivity materials (such as MXenes, CNTs, or metal tellurides) has demonstrated promising improvements in energy and power performance [270,271]. For instance, the fabrication of hybrid architectures involving CuCo LDHs coated on conductive substrates, as well as the assembly of molecular-level heterostructures between titanium carbide MXene and Ni-Co-Al-LDH nanosheets, has led to devices capable of delivering rapid charge/discharge cycles while maintaining high specific capacitance and excellent cyclic stability [271,272]. These hybrid systems effectively leverage the ultrafast redox reactions of LDHs and the robust electrical conductivity of the secondary phases, making them attractive for applications in portable electronics and electric vehicles where both high energy and power demands are critical [270,271].

The application of LDHs in supercapacitors is underpinned by their unique layered structures that facilitate efficient charge storage via EDLC and pseudocapacitive mechanisms. The evolution of structural modifications and composite strategies, including the integration with conductive carbonaceous materials and the formation of hybrid heterostructures, has advanced the electrochemical performance of LDH-based devices in terms of high capacitance, improved cycling stability, and superior rate capability. These innovations pave the way for the next generation of high-energy and high-power supercapacitors. Shah et al. [89] reported that NiCoLDH-1@JAC-2 served as the positive electrode, while JAC-2 was employed as the negative electrode in an all-solid-state asymmetric HSC, using a PVA/KOH gel as the solid electrolyte. Figure 20a,b outlines the design and assembly of both symmetric and ASC devices based on JAC and NiCoLDH@JAC materials. The device demonstrated a specific capacitance of 750 F/g, with a specific capacity of 209 mAh/g at a current density of 0.5 A/g. Figure 20c–f demonstrates the electrochemical behavior of the NiCoLDH-1@JAC-2 // JAC-2 HSC under different scan rates, potential windows, and current densities. It achieved a maximum energy density of 100 Wh/kg at a power density of 250 W/kg, significantly outperforming many conventional systems. The supercapacitor maintained excellent cyclic stability, with negligible performance degradation over repeated cycles. The synergistic interaction between the high surface area carbon scaffold and the electroactive LDH nanoflowers contributed to the remarkable electrochemical behavior.

The synthesized NiCo-LDH was employed as the positive electrode in an ASC with AC as the negative electrode, using PVA-KOH gel as the electrolyte [119]. Under optimal conditions (140 °C, 6 h, Ni/Co = 2:1), the device demonstrated a high specific capacitance of 400.2 C/g at 1 A/g. The ASC exhibited a maximum energy density of 51.59 µWh/cm² at a power density of 1.125 mW/cm². GCD profiles were highly symmetric, and impedance analysis revealed low internal resistance (0.861–0.915 Ω), indicating efficient charge transport. Furthermore, the device maintained 70% of its initial capacitance after 10,000 cycles, highlighting excellent cycling stability and long-term operational reliability. The CoNi LDH materials were employed as positive electrodes in HSC devices, with AC as the negative electrode and 2 M KOH as the electrolyte [232]. The CoNi LDH nanoflowers (NFs) demonstrated superior performance, delivering a specific capacity of 768.3 C/g at 1 A/g and maintaining 643.1 C/g at 10 A/g, compared to 669.3 C/g for nanosheets (NSs). The HSC assembled with CoNi LDH NFs // AC exhibited a high energy density of 37.1 Wh/kg at a power density of 748.0 W/kg while retaining 21.6 Wh/kg even at 7.12 kW/kg. Both HSCs showed excellent long-term cyclic stability, maintaining over 93% capacity retention after 4000 cycles at 10 A/g, demonstrating their strong potential as advanced battery-type materials in energy storage devices.

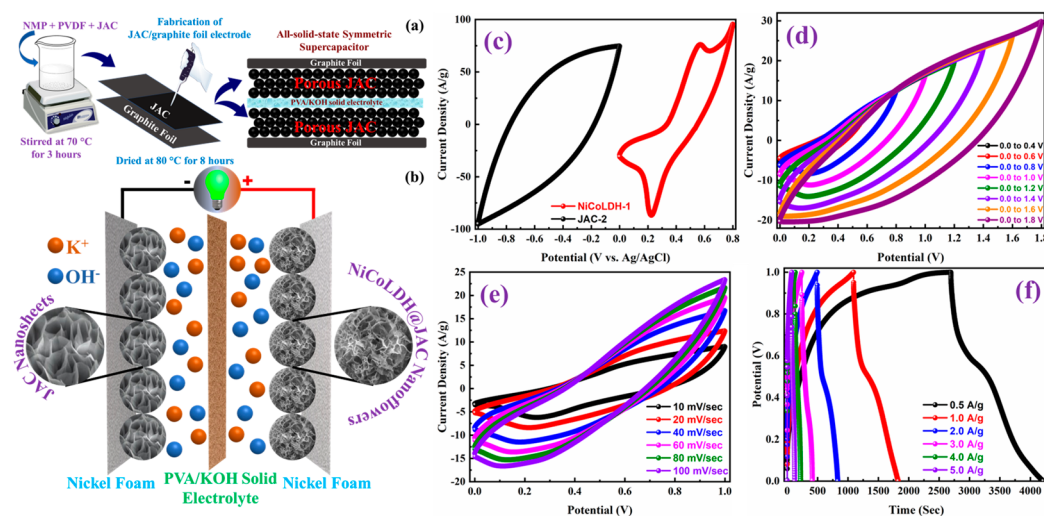


Figure 20. (a) Schematic overview of the fabrication process for JAC-based electrodes and assembly of the corresponding all-solid-state symmetric supercapacitor. (b) Diagram illustrating the configuration of the asymmetric HSC constructed using NiCoLDH@JAC and JAC electrodes. (c) CV curves of JAC-2 and NiCoLDH-1 electrodes measured in a three-electrode setup at a scan rate of 50 mV/s, (d) CV responses of the NiCoLDH-1@JAC-2//JAC-2 HSC at different operating potential windows (OPWs) at 50 mV/s, (e) CV curves of the same HSC recorded at various scan rates, and (f) GCD profiles of the HSC at different current densities. Reproduced with permission [89].

The electrochemical performance of the synthesized NiCo-LDH/NF (NCL3 for the optimized 6 h synthesis) was assessed in three-electrode and asymmetric two-electrode configurations [151]. In the three-electrode system with 1 M KOH, the NiCo-LDH served as the positive electrode, demonstrating a high specific capacitance of 1577 F/g at 1 mA/cm², with an energy density of 107.34 Wh/kg and a power density of 159.09 W/kg. Excellent cyclic stability was observed, with 96.17% retention after 5000 cycles. For the asymmetric device (NiCo-LDH/NF as positive and AC as negative electrode), the assembled AHSC device delivered an energy density of 38 Wh/kg and a power density of 1702 W/kg, retaining 76% capacitance after 2000 cycles, highlighting its practical viability for high-performance supercapacitor applications.

The synthesized NiCo-MOF@LDH-2 was employed as the positive electrode in an ASC device, with AC serving as the negative electrode and 2 M KOH as the electrolyte [233]. Electrochemical tests revealed excellent pseudocapacitive behavior with a high specific capacitance of 1873.9 F/g at 0.5 A/g and a maintained capacitance of 694.5 F/g at 20 A/g, indicating good rate capability. The ASC device (NiCo-MOF@LDH-2//AC) delivered an energy density of 49.8 Wh/kg at a power density of 422.4 W/kg and retained 21 Wh/kg even at 9318 W/kg, demonstrating superior energy/power performance. Furthermore, the device exhibited impressive cyclic stability with 83% capacitance retention after 10,000 cycles at 5 A/g, and coulombic efficiency of 99.3%, confirming its durability and practical viability. The synthesized NiCo-LDH/ACC composite was employed as a bifunctional electrode (cathode and anode) in a symmetric aqueous supercapacitor configuration with 1 M KOH as the electrolyte [234]. As a cathode, it achieved a high areal capacitance of 3770 mF/cm² at 1 mA/cm² and retained 79.5% of its capacity at 50 mA/cm² with 88% capacitance retention after 5000 cycles. As an anode, the electrode showed 1480 mF/cm² at 1 mA/cm², retaining 80% at 50 mA/cm² and demonstrating 100% stability after 10,000 cycles. The symmetric device delivered a high areal energy density of 0.352 mWh/cm² and a volumetric energy density of 5.61 mWh/cm³, with a maximum power density of 559.5 mW cm⁻³, maintaining performance over 15,000 cycles, indicating exceptional durability and fast ion/electron transport due to the amorphous, ultrathin architecture.

The synthesized NiCo-LDH-based heterostructure (S-NCCO) was employed as the positive electrode in an ASC, paired with AC as the negative electrode and PVA/KOH gel as the solid-state electrolyte [160]. The ASC device, configured as S-NCCO//AC, demonstrated exceptional performance, achieving a high specific capacitance of 3744.4 F/g at 1 A/g. It delivered an energy density of 92.3 Wh/kg and a power density of 750 W/kg, significantly outperforming comparable materials. Moreover, the device retained 87% of its capacitance after 5000 cycles at 10 A/g, indicating excellent long-term cycling stability and practical viability in energy storage applications. In supercapacitor applications, the CuCo LDH@Ni₃S₂ composite (specifically the CCNS-15 sample) was used as the positive electrode, while AC served as the negative electrode in an ASC configuration [211]. The device demonstrated exceptional areal capacitance (11.24 F/cm² at 5 mA/cm²), an impressive energy density of 0.62 mWh/cm², and a power density of 8 mW/cm². Even after 6000 charge/discharge cycles, the ASC retained 72.2% of its initial capacitance, highlighting excellent cyclic stability. The superior electrochemical behavior was attributed to the composite's tremella-like structure and the synergistic interaction between CuCo LDH and Ni₃S₂, which enhanced charge transfer and ion diffusion pathways.

In the application section, the NFMM composite was used as a positive electrode in an ASC, paired with AC as the negative electrode and 6 M KOH as the electrolyte [161]. The device exhibited battery-type behavior with a remarkable specific capacitance of 2079.6 F/g at 1 A/g, and retained 85% of its capacitance after 5000 cycles. The assembled NFMM//AC ASC delivered a high energy density of 67.3 Wh/kg at a power density of 750.9 W/kg, and maintained 89% capacitance retention after 5000 cycles, showcasing excellent cycling stability. The synergistic interaction between NiFe-LDH, MnCO₃, and MXene enhanced conductivity, charge storage, and structural stability, affirming NFMM's suitability for high-performance supercapacitor applications. The MnCo₂O₄@FeCoNi-LDH/CC was used as the positive electrode and AC/CC as the negative electrode in an all-solid-state ASC device, with a PVA/KOH gel as the electrolyte [162]. The device exhibited exceptional electrochemical performance with a high specific capacitance of 145.2 F/g at 1 A/g, an energy density of 51.66 Wh/kg at a power density of 890.81 W/kg, and outstanding cyclic stability, retaining 90.3% capacitance after 10,000 charge/discharge cycles. Figure 21 demonstrates the electrochemical performance and practical application of the MnCo@FCN-LDH/CC//AC/CC ASC device, including stability, energy storage capability, and its ability to power an LED. These results highlight the material's potential in flexible and high-energy-density supercapacitor applications.

The vacancy-rich NiCo-LDH (designated as AL-LDH) was employed as the positive electrode in a magnesium-ion HSC (Mg-HSC), with VS₂ as the negative electrode and MgSO₄ as the electrolyte [212]. The AL-LDH electrode delivered a specific capacitance of 47.70 mAh/g (\approx 238.5 F/g) at 1 A/g in a two-electrode setup. The device achieved a high energy density of 48.44 Wh/kg and a power density of 937.49 W/kg, demonstrating excellent rate capability by retaining 4 mAh/g at 20 A/g. After 500 cycles, the device retained ~42% of its capacity, indicating moderate stability. These results highlight the effectiveness of defect engineering (via H vacancy formation) in boosting charge storage and delivery performance in LDH-based supercapacitor systems. The electrochemical performance of NiAl-LDH was explored by constructing an ASC with NiAl-LDH@CC as the positive electrode and AC cloth as the negative electrode, using 1 M KOH as the electrolyte [214]. The ASC exhibited excellent pseudocapacitive behavior with a high specific capacitance of 310 mF/cm², corresponding to an energy density of 51.67 μ Wh/cm² and a power density of 913.84 μ W/cm² at a current density of 0.2 mA/cm², maintaining a stable operating voltage of 1.6 V. The device demonstrated outstanding long-term durability with 90% capacitance retention over 10,000 cycles and an average coulombic efficiency

of 98.9%, emphasizing the suitability of NiAl-LDH@CC for high-performance, flexible energy storage systems. NiAl LDH was employed as the positive electrode in an ASC configuration, paired with AC or graphene as the negative electrode [167]. The ASC devices demonstrated excellent performance, such as a specific capacitance of 214.4 F/g, energy density of up to 76.23 Wh/kg, and power density of 1127.03 W/kg, depending on the configuration. These devices maintained outstanding cycling stability, retaining 91.4% to 95.84% of their original capacitance after 5000–10,000 cycles at high current densities, showcasing the LDH's potential for long-term energy storage applications.

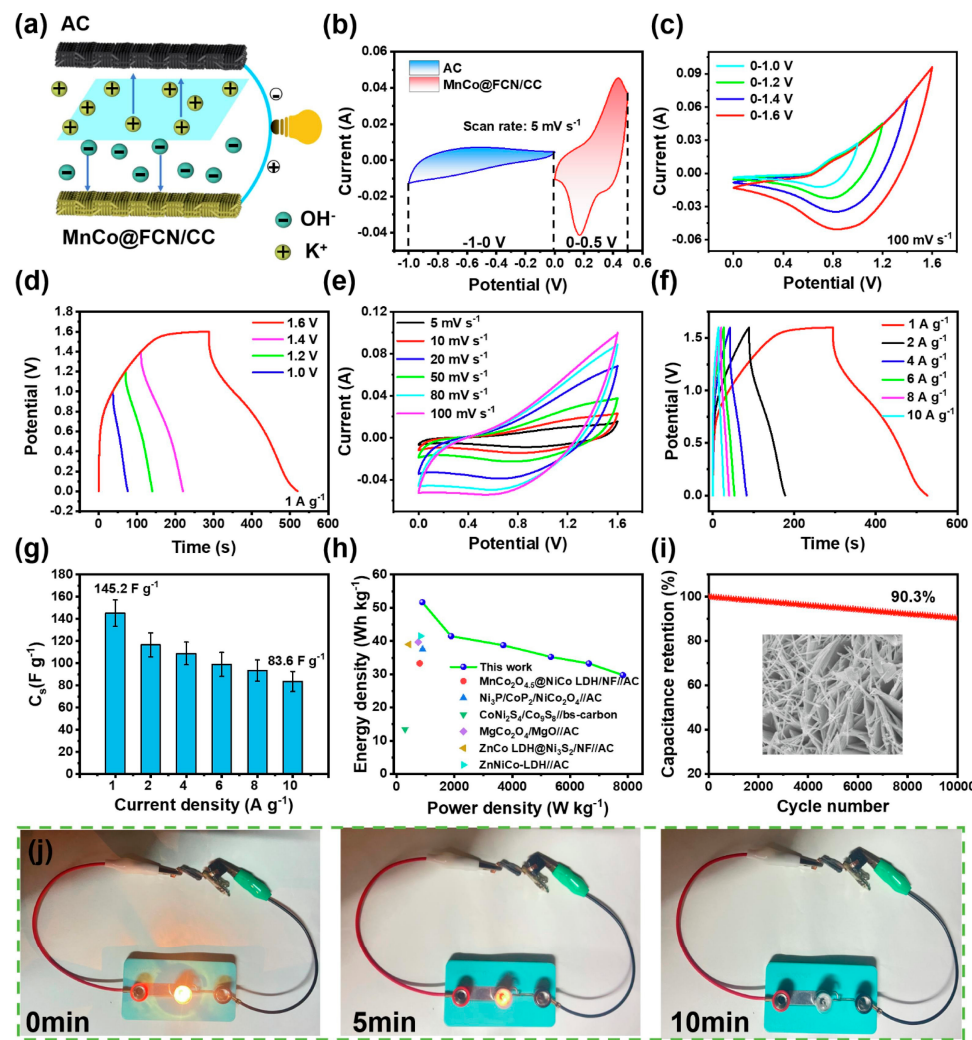


Figure 21. (a) Illustration of the MnCo@FCN-LDH//AC/CC ASC setup. (b) CV comparison of AC and MnCo@FCN-LDH/CC electrodes at 5 mV/s. (c) CV curves of the ASC device at various voltages from 0–1.0 V to 0–1.6 V at 100 mV/s. (d) GCD curves at 1 A/g under the same voltage range. (e,f) CV and GCD performance of the device at 0–1.6 V. (g) Specific capacitance at different current densities. (h) Ragone plot comparing energy and power density with previous reports. (i) Cycling stability over 10,000 cycles at 1 A/g. (j) Digital photographs showing the device powering an LED for different durations. Reproduced with permission [162].

The optimized MP2 material, phosphorized MoB@NiCo-LDH with phosphorus vacancies, was employed as the positive electrode in an ASC device, with AC used as the negative electrode and 3 M KOH as the electrolyte [168]. The device exhibited outstanding electrochemical performance, including a high specific capacitance of 112.52 F/g at 1 A/g (two-electrode configuration), a maximum energy density of 39.91 Wh/kg at a power density of 948.25 W/kg, and an excellent power density of 7876.76 W/kg at 20.62 Wh/kg.

Furthermore, the device maintained 78.76% of its capacitance after 5000 cycles, demonstrating excellent cycling stability. These results highlight the synergistic effect of heterojunction formation and phosphorus vacancy engineering in enhancing charge transport kinetics and redox reactivity, thereby boosting the practical application potential of LDH-based electrodes in advanced energy storage systems. The NCS@CA heterojunction was employed as the positive electrode in a light-assisted ASC, with AC as the negative electrode and 3 M KOH as the electrolyte [236]. Under illumination, the device exhibited a remarkable specific capacitance of 112.2 F/g, a high energy density of 35.1 Wh/kg at a power density of 751.2 W/kg, and maintained 97.7% of its initial capacitance after 10,000 cycles, demonstrating excellent cyclic stability. Due to the semiconductor nature of NCS and LDH, the synergistic photoelectrochemical effect further enhanced charge separation and electrochemical kinetics, leading to substantial performance improvement over non-illuminated conditions.

In supercapacitor applications, the synthesized Te-NiMn LDH was employed as the positive electrode in a hybrid device, with AC as the negative electrode [169]. The resulting Te-NiMn LDH/C-MXene/NF//AC device achieved an impressive specific capacitance of 202.6 F/g at 2 A/g in a two-electrode configuration, along with a high energy density of 52.3 Wh/kg and a maximum power density of 6452 W/kg. Long-term cycling stability tests demonstrated excellent performance, with 77.3% capacitance retention after 10,000 cycles. The electrochemical performance of the Te-NiMn LDH/C-MXene/NF//AC device is illustrated in Figure 22. As shown in Figure 22a, the CV curves reveal that the Te-NiMn LDH/C-MXene/NF electrode exhibits a significantly higher current response than the AC electrode, indicating better electrochemical activity. Figure 22b presents CV measurements under different voltage ranges, showing that the area under the curve increases with higher potential windows, which reflects enhanced energy storage capacity. Figure 22c shows CV curves at various scan rates (5 to 50 mV/s) for a fixed voltage window of 1.5 V. The shapes of the curves remain consistent, suggesting good rate capability and reversibility. Figure 22d shows the GCD curves at different current densities, where the discharge time decreases with increasing current, typical of pseudocapacitive behavior. Long-term cycling performance is assessed in Figure 22e, with the device retaining 77.3% of its initial capacitance after 10,000 cycles at 5 A/g, indicating excellent stability. Finally, Figure 22f compares GCD curves before and after cycling. The slight change in shape further confirms the material's durability over extended use. These results highlight the synergistic enhancement due to CTAB-modified MXene conductivity and Te doping, which collectively facilitate improved redox kinetics, higher charge storage, and structural integrity over prolonged cycling.

The NC@CL nanosheet electrode was employed as the positive electrode in an ASC with AC as the negative electrode in a 2 M KOH electrolyte [141]. The NC@CL electrode delivered a high specific capacitance of 213 F/g at 0.2 A/g in the two-electrode device configuration, showcasing superior electrochemical performance due to its hierarchical nanostructure. The device achieved an energy density of 66.56 Wh/kg at a power density of 148.83 W/kg, maintaining 88.1% capacitance retention over 20,000 cycles, indicating excellent stability and reversibility. The enhanced performance is attributed to the synergistic interaction between NC and CL, large surface area, and efficient ion diffusion through the mesoporous framework.

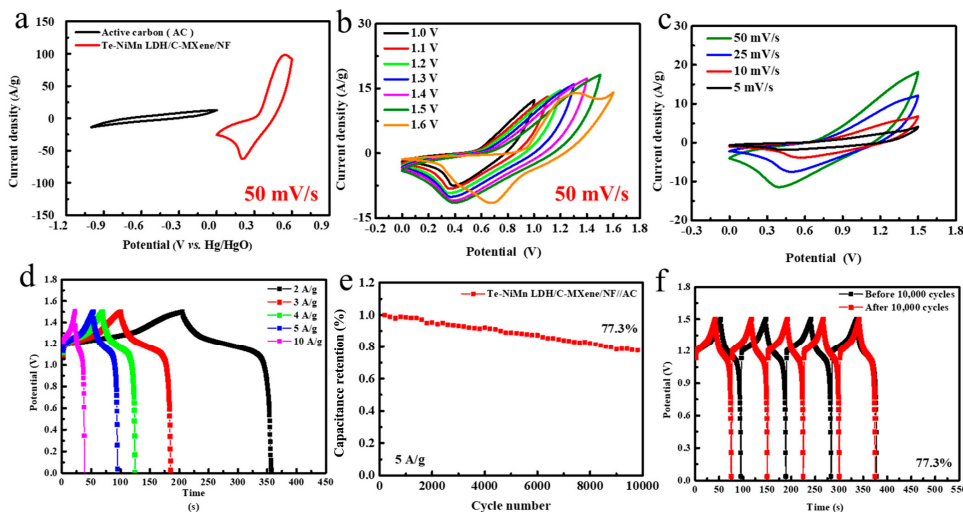


Figure 22. (a) CV comparison of Te-NiMn LDH/C-MXene/NF and AC electrodes at a scan rate of 50 mV/s. (b) CV profiles of Te-NiMn LDH/C-MXene/NF//AC device recorded under varying potential windows. (c) CV curves at different scan rates within a fixed voltage range of 1.5 V. (d) GCD curves at multiple current densities. (e) Cycling stability test showing capacitance retention after 10,000 cycles at 5 A/g. (f) GCD comparison before and after 10,000 charge/discharge cycles to evaluate long-term durability. Reproduced with permission [169].

The synthesized CF/CRBI-NiCo-LDH was employed as the positive electrode, while AC-coated carbon felt (CF/AC) was the negative electrode in an ASC [215]. The device utilized a cellulose separator and 6 M KOH aqueous electrolyte. In a two-electrode configuration, the supercapacitor achieved an impressive specific capacitance of 167.85 F/g at 0.5 A/g, with a high energy density of 57.2 Wh/kg and power density of 820 W/kg. Furthermore, the device retained 89% of its capacitance after 3000 cycles, highlighting excellent cycling stability and mechanical integrity. Figure 23a illustrates the coral reef-inspired structure of the CF/CRBI-NiCo-LDH electrode, promoting strong binding and fast redox transitions. CV curves (Figure 23b) confirm pseudocapacitive behavior with good rate capability, while GCD profiles (Figure 23c) show high coulombic efficiency across current densities. The specific capacitance trend (Figure 23d) indicates excellent rate performance, and the Ragone plot (Figure 23e) highlights the device's superior energy and power densities. The vertically grown nanoflake structure enhanced the charge storage through efficient ion transport and minimal resistance, confirmed by EIS and CV.

In the application as a supercapacitor, NiCo-LDH@TAC600-0 composite was used as the positive electrode, and tannin-derived AC (TAC600-2) served as the negative electrode in an ASC configuration with 6 M KOH as the electrolyte [237]. The device achieved a specific capacitance of 1250 F/g (three-electrode) and excellent performance in a two-electrode system, delivering a maximum energy density of 30.8 Wh/kg at a power density of 800 W/kg. Moreover, it demonstrated a stable cycle life with 72.5% capacitance retention after 5000 cycles at a high current density of 10 A/g. The sea urchin-like morphology contributed to a high rate of performance (82.8%) and facilitated fast ion/electron transport, validating its effectiveness in high-performance energy storage devices. In ASC configuration, CoNi LDH and its sulfurized derivatives were used as the positive electrode, while commercial AC was the negative electrode [235]. Figure 24a presents the synthesis and performance of the CoNiS-50-based electrode, highlighting its formation via sequential cation and anion exchange reactions to produce a flower-like CoNiS nanostructure. Among the synthesized materials, CoNiS-50 exhibited the most promising electrochemical performance, achieving a high specific capacitance of 150 F/g in the two-electrode configuration. The device delivered a maximum energy density of 37.8 Wh/kg at a power density of

750 W/kg. Furthermore, as shown in Figure 24a, the CoNiS-50-based ASC demonstrated excellent cycling stability, retaining 92.2% of its initial capacitance after 10,000 cycles at 10 A/g, attributed to the stabilized microstructure facilitated by residual Mg(OH)₂ and improved intrinsic conductivity from sulfur doping. Jia et al. [273] engineered NiCo-LDH/NiCo₂S₄ nanotube arrays modified with BPQDs, achieving an ultra-high specific capacitance of 2938.2 F/g, energy density of 133.7 Wh/kg at 800 W/kg, and 76.5% retention after 10,000 cycles. Figure 24b provides a visual overview of the energy storage mechanism. It outlines how charge is stored and transferred during electrochemical reactions, typically involving a combination of surface adsorption, redox reactions, and ion diffusion. This mechanism plays a key role in determining the overall performance of the electrode material, including its capacity, rate capability, and cycling stability. Figure 24c presents the design of the NiCo-LDH/NiCo₂S₄/BPQD//AC ASC. The electrochemical behavior of each electrode is shown in Figure 24d, where the CV curves confirm that the positive electrode has significantly higher redox activity than the AC negative electrode. Figure 24e displays CV curves at various voltage windows, indicating the device can operate stably up to 1.7 V. Figure 24f shows how the CV shape changes with increasing scan rates, suggesting good rate capability. The GCD curves in Figure 24g confirm that the device delivers longer discharge times at lower current densities. Finally, Figure 24h shows that the specific capacitance decreases as the current density increases, which is a typical trend in supercapacitor behavior.

Khalafallah et al. [213] developed Zn/CoLa LDH nanoarray-on-nanoarray electrodes using electrodeposition, achieving a specific capacitance of 269.4 F/g, an energy density of 59.9 Wh/kg at 800 W/kg, and a stability of 86.4% over 12,000 cycles in an ASC device. Liu et al. [162] synthesized MnCo₂O₄@FeCoNi-LDH on CC, achieving a high specific capacitance of 2235 F/g, an energy density of 51.66 Wh/kg at 890.81 W/kg, and 92.9% retention after 10,000 cycles in an ASC device. Luo et al. [274] prepared N-doped ZnNi-LDH via one-step hydrothermal synthesis, demonstrating a specific capacitance of 1265.7 C/g (~351.6 F/g), energy density of 64.6 Wh/kg at 850 W/kg, and excellent long-term cycle life when used with AC. Wei et al. [275] developed BPQD-embedded NiCoCu-LDH with a porous structure, reaching a specific capacitance of 1810.6 F/g, an outstanding energy density of 202.2 Wh/kg at 800 W/kg, and retained 81.4% capacity after 10,000 cycles. Moradi et al. [276] created a partially sulfurized CoMn-LDH/CoMn-S heterostructure, showing a capacity of 792.4 C/g (~220 F/g), energy density of 82.63 Wh/kg, power density up to 10,998 W/kg, and 94% stability over 6000 cycles. Wang et al. [277] introduced Ce into NiCo LDH@PBAs multi-core/shell structure, yielding a specific capacitance of 1847 F/g, energy density of 99.8 Wh/kg at 1283 W/kg, and 95.7% stability over 10,000 cycles.

Optimization strategies for LDH cathode materials in supercapacitors involve several synergistic approaches. Firstly, element doping, such as scandium doping, has promoted a superlong activation process and enhanced cycling durability while modifying the intrinsic electronic properties [278]. Secondly, tailoring the synthesis conditions to control the nanoscale morphology, including the design of hollow and quantum-layered structures, significantly improves ion diffusion and charge storage capability [119,243]. Modifying the intercalated anions and integrating LDHs with conductive substrates further optimizes electron transfer and overall capacitance performance [119,279]. These optimization methods, thus, address the challenges of moderate energy density and rate capability by enhancing both the redox activity and structural stability of LDH cathodes, ensuring improved electrochemical outcomes for supercapacitor applications [243,279].

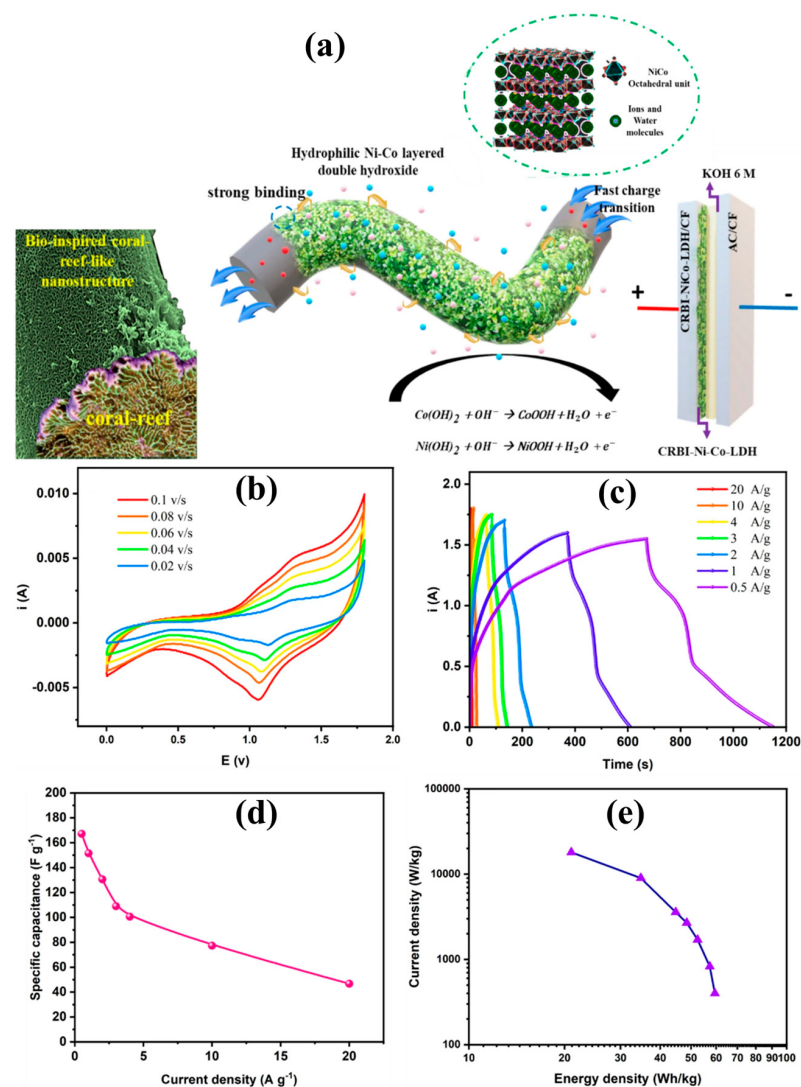


Figure 23. (a) Schematic illustration of the enhanced electrochemical charge storage mechanism in the electrosynthesized CF/CRBI-NiCo-LDH electrode, featuring a coral reef-inspired nanostructure that promotes strong binding, fast charge transfer, and redox reactions of Ni and Co hydroxides. (b) CV curves and (c) GCD profiles of the CF/CRBI-NiCo-LDH||CF//AC HSC at various scan rates and current densities. (d) Specific capacitance as a function of current density, and (e) Ragone plot comparing energy and power densities of the hybrid device. Reproduced with permission [215].

LDHs have emerged as highly effective electrode materials for supercapacitors, owing to their unique two-dimensional structure, tunable composition, and abundance of electroactive redox sites that support both pseudocapacitive and electric double-layer charge storage mechanisms. Their exceptional electrochemical behavior is attributed to the synergistic effects of compositional tailoring, such as metal-ion doping and anion intercalation, and advanced structural engineering, including nanosheet design, hierarchical porosity, and vacancy modulation. Integration with conductive matrices like carbon nanotubes, graphene, MXenes, and conductive polymers has been pivotal in mitigating LDHs' intrinsic low conductivity while enhancing rate capability, specific capacitance, and cycling durability. Particularly in asymmetric and hybrid supercapacitor configurations, LDHs paired with carbon-based or sulfide materials have demonstrated remarkable energy and power densities, extended cycle life, and mechanical robustness. Recent innovations such as heterostructures, phosphorization, photoelectrochemical enhancement, and defect engineering have pushed LDH-based devices toward practical viability in flexible, wearable,

and high-performance energy storage systems. The continued development of LDH-based composites is central to advancing next-generation supercapacitors with superior energy density, fast charge/discharge kinetics, and long-term stability. A detailed summary of LDH-based materials applied in supercapacitor devices, highlighting their fabrication methods, device architecture, and electrochemical performance, is provided in Table 2.

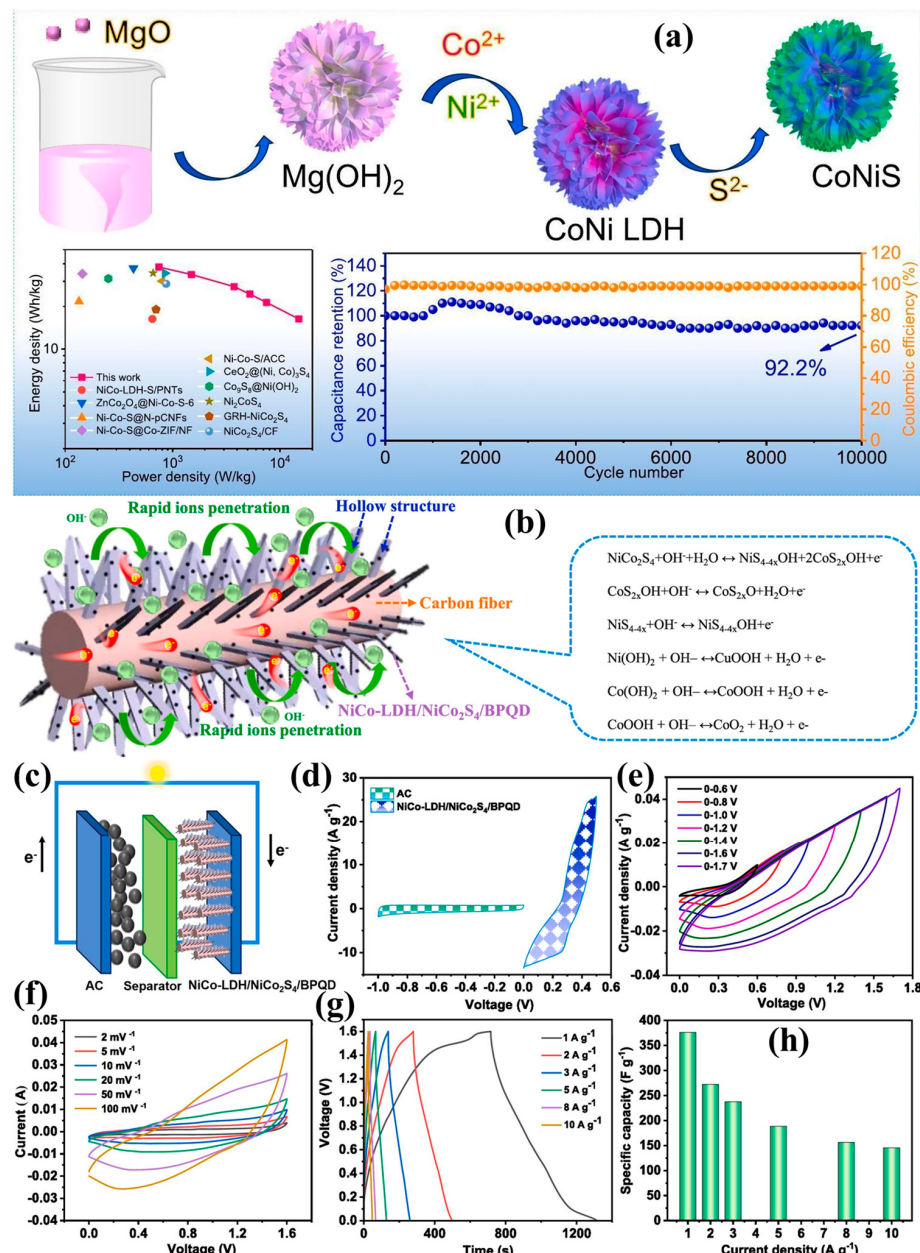


Figure 24. (a) An illustration shows the stepwise synthesis of CoNiS via combined cation and anion exchange, along with the energy and power density comparison of the CoNiS-50-based ASC and its cycling performance at 10 A/g. Reproduced with permission [235]. (b) Schematic representation illustrating the energy storage mechanism involved in the electrochemical process. (c) Schematic representation of the assembled NiCo-LDH/NiCo₂S₄/BPQD//AC ASC device. (d) CV curves of the NiCo-LDH/NiCo₂S₄/BPQD positive electrode and AC negative electrode measured at 2 mV/s. (e) CV profiles of the full device at varying voltage windows recorded at 100 mV/s. (f) CV curves at different scan rates ranging from 2 to 100 mV/s. (g) GCD curves at different current densities. (h) Specific capacitance values derived from the GCD results at various current densities. Reproduced with permission [273].

Table 2. Overview of LDH-based supercapacitor electrode materials with corresponding synthesis techniques, electrode configurations, and electrochemical performance metrics.

LDH Synthesis Procedure	Positive Electrode	Negative Electrode	Electrolyte	Specific Capacitance (F/g)	Energy Density (Wh/kg)	Power Density (W/kg)	Stability (%), No. of Cycles	Ref.
Hydrothermal synthesis	NiCoLDH-1@JAC-2	JAC-2	PVA/KOH	750	100	250	95%, 10,000	[89]
Hydrothermal synthesis	NC@CL nanosheets	AC	1 M KOH	213	66.56	148.83	88%, 20,000	[141]
Hydrothermal synthesis	NiCo-LDH	AC	PVA/KOH	400.2 C/g	51.59 μ Wh/cm ²	1.125 mW/cm ²	70%, 10,000	[119]
Hydrothermal synthesis	Ni–Co LDH/NF (NCL3)	AC	1 M KOH	107	38	1702	76%, 2000	[151]
Hydrothermal + TA etching + sulfurization	S-NCCO (NiCo-LDH on S-ZIF-67)	AC	PVA/KOH	295	92.3	750	87%, 5000	[160]
Hydrothermal	NiFe-LDH/MnCO ₃ /MXene	AC	6 M KOH	215	67.3	750.9	89%, 5000	[161]
Hydrothermal synthesis	MnCo ₂ O ₄ @FeCoNi-LDH/CC	AC/CC	6 M KOH	145.2	51.66	890.81	90.3%, 10,000	[162]
Electrodeposition	NiAl LDH-rGO	Fe ₂ O ₃ -rGO	2 M KOH	214.4	76.23	800	95%, 5000	[167]
Hydrothermal synthesis + Phosphorization + NaBH ₄ reduction	MP2 (MoB@NiCoP)	AC	3 M KOH	112.52	39.91	948.25	78.76%, 5000	[168]
Hydrothermal + Te soaking	Te-NiMn LDH/C-MXene/NF	AC	6 M KOH	202.6	52.3	6452	77.3%, 10,000	[169]
Two-step electrodeposition	CuCo LDH@Ni ₃ S ₂	AC	3 M KOH	11.24 F/cm ²	0.62 mWh/cm ²	8 mW/cm ²	72.2%, 6000	[211]
Electrodeposition + Electrochemical Activation	Hv-rich NiCo-LDH	VS ₂	1 M KOH	238.5 F/g	48.44	937.49	42%, 500	[212]
Electrodeposition of CoLa LDH nanoarrays followed by Zn ²⁺ doping	Zn/CoLa LDH	AC	3 M KOH	269.4	59.9	800	86.4%, 12,000	[213]
Electrochemical deposition	NiAl-LDH@CC	CC	1 M KOH	310	51.67	913.84	90%, 10,000	[214]
Electrochemical deposition	CF/CRBI-NiCo-LDH	CF/AC	6 M KOH	167.85	57.2	820	89%, 3000	[215]
Solvothermal synthesis	CoNi LDH nanoflowers	AC	2 M KOH	768.3 C/g @ 1 A/g	37.1	748.0	93.7%, 4000	[232]
Solvothermal	NiCo-MOF@LDH-2 nanosheets	AC	2 M KOH	1873.9	49.8	422.4	83%, 10,000	[233]
Ion exchange	NiCo-LDH/ACC	NiCo-LDH/ACC	3 M KOH	876 mF/cm ²	0.352 mWh/cm ²	559.5 mW/cm ³	94.9%, 15,000	[234]
Cation/anion exchange	CoNiS-50	AC	6 M KOH	150	37.8	750	92.2%, 10,000	[235]
Two-step solvothermal	NCS@CoAl-LDH	AC	3 M KOH	112.2	35.1	751.2	97.7%, 10,000	[236]
Microwave hydrothermal synthesis	NiCo-LDH@TAC600-0	TAC600-2	6 M KOH	1250 (3-electrode)	30.8	800	72.5%, 5000	[237]

Table 2. *Cont.*

LDH Synthesis Procedure	Positive Electrode	Negative Electrode	Electrolyte	Specific Capacitance (F/g)	Energy Density (Wh/kg)	Power Density (W/kg)	Stability (%), No. of Cycles	Ref.
Solvothermal synthesis followed by BPQD modification and hydrothermal sulfidation	NiCo-LDH/NiCo ₂ S ₄ /BPQD	AC	6 M KOH	376.1	133.7	800	76.5%, 10,000	[273]
Hydrothermal synthesis using 2-methylimidazole for N-doping	N-doped ZnNi-LDH	AC	3 M KOH	351.6	64.6	850	85.6%, 10,000	[274]
Precipitation and hydrothermal method with BPQD anchoring on CC	NiCoCu-LDH/BPQD	AC	6 M KOH	568.7	202.2	800	81.4%, 10,000	[275]
Electrochemical deposition followed by partial hydrothermal sulfidation	CoMn-LDH/CoMn-S	AC	3 M KOH	201	82.63	985	94%, 6000	[276]
Core/shell formation using Ce bridging between NiCo LDH and PBAs	NiCo-Ce@PBAs	AC	1 M KOH	222.3	99.8	1283	95.7%, 10,000	[277]

6. LDHs in Electrochemical Hydrogen Production

Hydrogen is a key clean energy carrier in the shift toward sustainable, low-carbon systems due to its high energy density, zero-emission profile, and broad applicability across sectors [280]. Efficient and affordable hydrogen production, particularly via water electrolysis, relies on effective catalysts for the HER and OER [281]. While noble metals like Pt, RuO₂, and IrO₂ offer excellent performance, their cost and scarcity limit widespread use [282]. LDHs have emerged as promising alternatives, thanks to their tunable brucite-like layered structure, high surface area, and rich active sites [283]. Their general formula, $[M^{2+}]_{1-x} [M^{3+}]_x (OH)_2]^{x+} (A^{n-})_{x/n} \cdot yH_2O$, reflects their compositional flexibility, allowing precise control over layer charge, interlayer spacing, and anion content. LDHs also exhibit favorable redox behavior and surface characteristics, while modifications such as metal doping or hybridization with conductive materials can overcome their low intrinsic conductivity [284]. These properties make LDHs strong candidates for next-generation electrocatalysts in hydrogen production.

Pt-based catalysts are widely regarded as the benchmark for HER due to their exceptionally low overpotentials and high exchange current densities across a broad pH range. However, advanced LDH-based catalysts, particularly NiFe-LDH and CoFe-LDH, have emerged as competitive alternatives, especially under alkaline conditions. These LDHs can achieve overpotentials within 50–100 mV of Pt/C at a current density of 10 mA/cm², showcasing promising catalytic efficiency at a significantly reduced material cost [20,285,286]. In terms of stability, LDH catalysts exhibit excellent durability in alkaline electrolytes, maintaining over 90% of their initial performance after extended testing periods exceeding 50–100 h, whereas Pt-based catalysts, although stable in acidic environments, are prone to degradation in alkaline media. Furthermore, the use of earth-abundant and low-cost transition metals in LDHs provides a major economic advantage over expensive and scarce platinum. Nevertheless, LDHs still face limitations such as relatively lower electrical conductivity and reduced HER kinetics in acidic media, which currently limit their direct

application in proton exchange membrane (PEM) electrolyzers [287]. Various strategies, including hybridization with conductive materials and defect engineering, are actively being explored to overcome these challenges [288].

6.1. Fundamentals of Electrochemical Hydrogen Production

Hydrogen production via water electrolysis involves passing an electric current through electrodes immersed in an electrolyte, triggering two key half-reactions: the HER at the cathode and the OER at the anode. Thermodynamically, water splitting requires a minimum of 1.23 V at standard conditions (25 °C, 1 atm), but in practice, a higher voltage (typically 1.8–2.0 V) is needed due to kinetic barriers and system resistances [289,290]. This additional energy input is known as the overpotential (η), caused by factors like charge transfer resistance, bubble formation, and ion diffusion limitations. Lowering η is critical for enhancing efficiency, often achieved by using advanced electrocatalysts that optimize interactions with H⁺ or H₂O molecules. HER is a multi-step, pH-dependent process influenced by electrolyte type. In acidic media, H⁺ ions are reduced via the Volmer (adsorption), Heyrovsky (electrochemical desorption), or Tafel (recombination) steps. In basic conditions, water molecules act as proton sources, undergoing similar steps but with a higher energy barrier due to stronger H–O bonds [291]. The general HER mechanism is described by Equations (1)–(6) and illustrated in Figure 25.

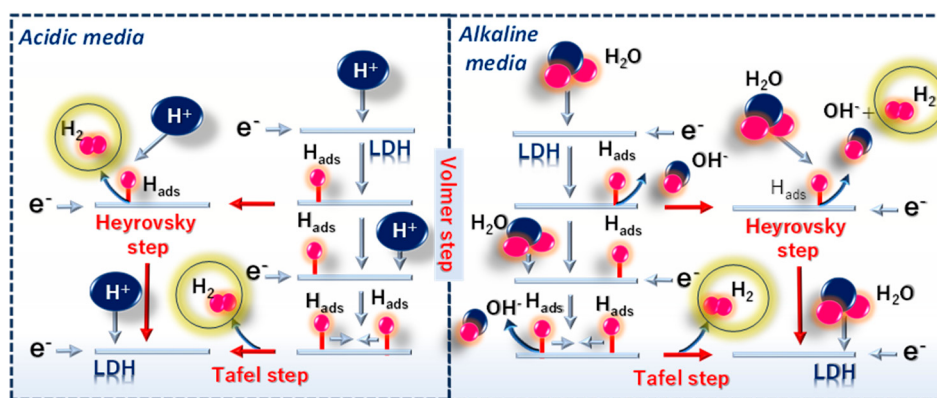


Figure 25. Schematic illustration of Volmer, Tafel, and Heyrovsky steps for HER in acidic and alkaline media.

Acidic HER:



Alkaline HER:



Due to slower kinetics in alkaline media, developing efficient electrocatalysts, such as composition/doping/interfacial engineering, etc., in LDHs is vital to lower overpotentials and enhance reaction rates, especially under non-acidic conditions [284,292]. Consequently, extensive research has turned toward low-cost, earth-abundant alternatives. Strategies such as carbon integration have improved conductivity and charge transfer, enhancing HER performance. Non-noble metal-based materials, including phosphides, sulfides, nitrides,

borides, oxides, hydroxides, and especially LDHs, have gained prominence as bifunctional catalysts. Tailoring the composition, morphology, and electronic structure of LDHs through doping, defect engineering, and heterostructure construction has proven highly effective in enhancing their intrinsic activity and charge transfer efficiency for HER.

6.2. Mechanistic Role of LDHs Catalysts in Electrochemical HER

LDHs play a critical mechanistic role in HER due to their unique lamellar structure and tuneable composition. The brucite-like layers composed of divalent and trivalent metal cations create a high density of active sites and favorable charge environments that facilitate proton adsorption and electron transfer during HER. The metal composition significantly influences the catalytic behavior; for instance, incorporating transition metals like Ni, Co, or Fe enhances redox activity and electron conductivity, while synergistic interactions between metal centers modulate the hydrogen binding energy. Additionally, the interlayer anions and hydration layers contribute to ion transport and surface reactivity. HER performance of LDHs is strongly pH-dependent. In acidic media, LDHs often face stability challenges but can support HER through proton reduction if properly engineered. In neutral or alkaline environments, LDHs exhibit better structural durability, and the HER mechanism proceeds via water dissociation, making the Volmer step rate-limiting. Modifying the metal layers or coupling with conductive supports improves activity across all pH ranges. Among various electrocatalysts developed for water splitting, LDHs have gained considerable attention due to their tuneable composition, abundant active sites, and structural versatility [7]. While traditionally more active toward OER, several LDH systems have been tailored to exhibit excellent HER performance, especially in alkaline media [293,294]. Binary LDHs such as NiCo-LDH, NiMn-LDH, and CoMn-LDH have shown promising HER activity due to their redox flexibility and enhanced conductivity [295–297]. NiFe-LDH, though more renowned for OER, can be modified to support HER when integrated with conductive or catalytically active phases [298]. Ternary and doped LDHs, including NiCoFe-LDH, NiFeMn-LDH, and NiMo/NiFe-LDH, further enhance HER performance through synergistic electronic effects and optimized adsorption of intermediates [299–301]. Doping with elements like Cu, Mo, and W modulates the electronic structure, increases conductivity, and facilitates water dissociation [302–304]. Additionally, heterostructures such as NiFe-LDH@NiCoP, NiFe-LDH/NiS₂/VS₂, and LDH hybrids with MXene or graphene provide an ideal platform by coupling HER-active phases with conductive supports, promoting rapid charge transfer and improved stability [185,305,306]. These tailored LDH-based materials collectively demonstrate strong potential as noble metal-free HER electrocatalysts for efficient and scalable hydrogen production.

Another effective strategy involves combining LDHs with carbon-based materials such as graphene, CNTs, or reduced graphene oxide through the intercalation/exfoliation method. These LDH/carbon hybrids not only improve electrical conductivity but also provide a high surface area scaffold that prevents layer restacking and promotes better dispersion of active sites. The conductive carbon matrix facilitates rapid charge transport and enhances overall electrocatalytic kinetics. Exfoliation and intercalation of bulk NiFe LDHs into ultrathin nanosheets have proven to be powerful strategies for improving HER activity, primarily by enlarging surface area, enhancing charge transport, and exposing more active sites. Several advanced techniques, such as ultrasonic exfoliation, laser irradiation, and solid-phase assembly, have been employed to tailor their structure and electrochemical properties. For instance, Yao et al. fabricated a NiFe LDH nanosheet–defective graphene hybrid (NiFe LDH-NS@DG10) [307]. The synthesis of NiFe LDH@DG nanocomposite is successfully achieved through a straightforward electrostatic assembly of positively charged exfoliated NiFe LDH nanosheets with negatively charged defective graphene (Figure 26a).

Structural analyses confirm the formation of a well-dispersed hybrid architecture. XRD and AFM results validate the effective exfoliation into single-layer nanosheets (Figure 26b–e), while TEM and SAED demonstrate the preservation of crystallinity and uniform anchoring on the graphene support (Figure 26f,g). The EDS and HAADF mapping further confirm the homogeneous distribution of key elements, underscoring the intimate coupling between the LDH and DG components, as depicted in Figure 26h. This layered heterostructure achieved outstanding bifunctional performance with HER and OER overpotentials of 115 mV and 210 mV, respectively, at 10 mA/cm^2 . This approach allows the coupling of diverse catalytic materials, creating junctions that foster synergistic interactions and facilitate more efficient charge transport. Such tailored interfaces can significantly lower the energy barriers for intermediate species and improve their adsorption behavior, thereby addressing the performance limitations typically observed in single-phase catalysts.

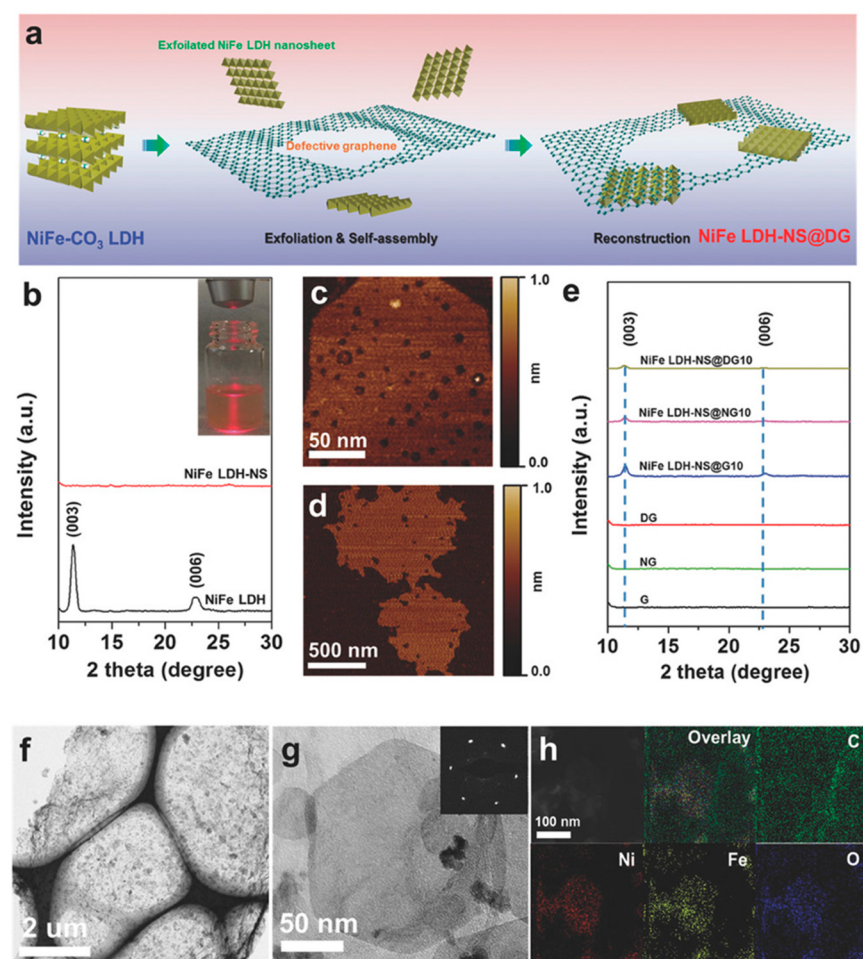


Figure 26. (a) Schematic depicting the synthesis pathway for the NiFe LDH-NS@DG hybrid, starting from bulk NiFe --CO_3 LDH, followed by exfoliation and integration with defective graphene, leading to the reconstructed nanocomposite. (b) XRD profiles comparing the bulk NiFe LDH and its exfoliated nanosheet form. (c,d) Atomic force microscopy (AFM) images showing the morphology of the exfoliated NiFe LDH nanosheets and defective graphene sheets, respectively. (e) XRD patterns of NiFe LDH nanosheets combined with various graphene types, including defective (DG), nitrogen-doped (NG), and pristine graphene (G). (f) Low-magnification TEM image displaying the overall morphology of the NiFe LDH-NS@DG10 composite. (g) High-resolution TEM highlighting the anchoring of NiFe LDH nanosheets on defective graphene, with the corresponding SAED pattern shown in the inset. (h) Elemental mapping via STEM-HAADF and EDS, confirming the uniform distribution of Ni, Fe, O, and C within the hybrid structure. Reproduced with permission [307].

LDH–metal composites, particularly those incorporating transition metals like Ni or Co, exhibit improved electron transfer and catalytic activity due to strong metal/metal interactions and enhanced redox behavior. These bimetallic or multimetallic systems often benefit from synergistic effects that optimize hydrogen adsorption and lower activation energy barriers. For example, Yao et al. developed a hierarchical heterostructured electrocatalyst, NiTe@CoFe LDH, by coupling conductive NiTe nanorods with amorphous CoFe-LDH via hydrothermal synthesis followed by electrodeposition [308]. This 3D architecture promotes rapid electron transfer, enhanced mass diffusion, and abundant active sites due to its large surface area and synergistic interfacial interactions. As a result, the catalyst exhibits excellent HER performance in alkaline media, requiring an overpotential of only 103 mV for HER at a current density of 10 mA/cm^2 . The catalyst also demonstrates remarkable durability, maintaining stable performance for over 50 h. When used as both anode and cathode in a two-electrode configuration, the NiTe@CoFe LDH system achieves efficient overall water splitting at a low cell voltage of 1.56 V at 10 mA/cm^2 , with admirable stability, indicating its strong potential for practical hydrogen production applications, as shown in Figure 27a–e. In addition, NiCo LDHs are promising electrocatalysts for hydrogen production due to their tunable redox properties, hydrophilicity, and structural flexibility. However, their HER performance is limited by poor conductivity and sluggish water dissociation kinetics. To address this, Xia et al. developed a hierarchical heterostructure comprising Cu-doped NiCo LDH grown on NiCo alloy (Cu-NiCo LDH/NiCo@CC) via a two-step electrodeposition process as shown in Figure 27f [285]. The NiCo alloy substrate enhanced conductivity, while Cu doping introduced oxygen vacancies and modulated the electronic structure. This optimized architecture delivered superior HER performance, achieving an overpotential of just 73 mV at 10 mA/cm^2 and a Tafel slope of 78.5 mV/dec in 1.0 M KOH. Electrochemical impedance spectroscopy showed a low charge transfer resistance of 1.48Ω , and the catalyst also exhibited high surface capacitance ($C_{dl} = 10.3 \text{ mF/cm}^2$) and excellent long-term stability. DFT calculations confirmed that Cu doping and interface effects enhanced water adsorption and charge transport, making this a promising strategy for efficient alkaline hydrogen evolution. Wang et al. developed a CoNiN@NiFe LDH hybrid electrocatalyst by electrodepositing NiFe-LDH onto NH₃-treated CoNiN grown on CC [309]. This structure combines the high conductivity of CoNiN with the catalytic activity of NiFe-LDH, enhancing charge transfer and active site exposure. In 1.0 M KOH, it delivered a low HER overpotential of 150 mV at 10 mA/cm^2 , a Tafel slope of 169 mV/dec, and a charge/transfer resistance of 1.5Ω , with excellent stability over 50 h. The synergy between components makes it a promising bifunctional catalyst for alkaline water splitting.

Furthermore, hybrid systems LDH with MOFs have shown great promise. MOFs offer a porous structure and high surface area that can be leveraged to host LDHs, creating hierarchical architectures with tailored pore channels and improved mass transport. For example, Huo et al. developed a novel strategy to fabricate monodispersed platinum (Pt) sites supported on NiFe-LDH via a targeted-anchoring and spontaneous-redox approach [286]. By engineering a MOF/LDH heterostructure, they introduced abundant defect sites that enabled the uniform dispersion and stabilization of Pt atoms. The synthesis of Pt@LDH-4h involves a stepwise strategy beginning with the formation of Fe-soc-MOF nanocubes, which serve as a structural scaffold, as shown in Figure 28a,b. Through urea-assisted hydrolysis in the presence of Ni²⁺ ions, a partial transformation occurs, generating a NiFe-LDH layer on the MOF surface and forming a MOF/LDH heterostructure rich in interfacial defects. These defects act as anchoring sites for Pt²⁺ ions introduced via K₂PtCl₄. A spontaneous redox reaction between Fe²⁺ in the MOF and Pt²⁺ leads to the in situ reduction of Pt to a lower valence state (~+0.96), resulting in the formation of monodispersed Pt sites, including both single atoms and nanoparticles (~4–5 nm). This process not only stabilizes the Pt species

but also enhances electron transfer and active site exposure. The resulting Pt@LDH-4h catalyst demonstrated remarkable bifunctional activity for overall water splitting in alkaline media, achieving an impressively low overpotential of 58 mV for HER at 10 mA/cm². Among various LDH-based materials, NiAl-LDHs are attractive for their structural stability and tunable composition, and recent strategies have explored noble metal incorporation to enhance their catalytic performance. In this context, Kalusulingam et al. synthesized Pd-integrated NiAl-LDH nanosheets via a simple coprecipitation method, where Pd²⁺ was embedded into the brucite layer of NiAl-LDH to enhance electronic interactions and surface activity [310]. Pd-NiAl-LDH exhibited significantly improved HER performance in 1.0 M KOH, delivering an overpotential of 189 mV at 10 mA/cm² and a Tafel slope of 133.2 mV/dec, outperforming the pristine NiAl-LDH (258 mV, 137.4 mV/dec). The catalyst also showed a TOF of 40.37 s⁻¹ at -0.4 V, indicating high intrinsic activity as depicted in Figure 29a–f. Moreover, the Pd-NiAl-LDH retained stability over 48 h of continuous HER operation, confirming its potential as a durable and efficient bifunctional catalyst for alkaline water electrolysis. The remarkable HER performance of Pd-NiAl-LDH in 1.0 M KOH is primarily attributed to its facilitation of the Volmer–Heyrovsky mechanism, enabling efficient hydrogen generation at reduced overpotentials, as shown in Figure 29g.

Transition metal compounds such as phosphides, oxides, and hydroxides are widely studied for water splitting, with phosphides like Ni₂P showing excellent HER activity due to their high conductivity and strong hydrogen affinity [311–313]. Coupling phosphides with LDHs enhances HER kinetics by improving water adsorption and proton transfer [185,314]. Ge et al. synthesized a Ni₂P/NiFe-LDH heterostructure featuring p-d orbital coupling P–Fe heterosites, which promoted O–H bond cleavage and improved charge transfer [315]. The catalyst achieved an HER overpotential of 230 mV at 100 mA/cm² and a Tafel slope of 47.43 mV/dec in 1.0 M KOH. DFT calculations revealed a significantly reduced Gibbs free energy (0.55 eV) for H₂O dissociation at the interface, confirming the synergistic effect of the heterostructure.

Zheng et al. developed a series of hybrid crystalline/amorphous electrocatalysts by decorating amorphous CoM LDHs (M = Mn, Fe, Ni, Cu, Zn) with crystalline CoMP nanostructures directly on nickel foam through partial dehydroxylation and phosphidation [316]. Among the variants, c-CoMnP/a-CoMn LDH/NF exhibited the best HER activity in 1.0 M KOH, requiring overpotentials of 170.3 mV and 254.9 mV to reach current densities of 100 and 500 mA/cm², respectively, with an onset potential of -0.134 V vs. RHE and a Tafel slope of 73.7 mV/dec. The enhanced performance was attributed to the synergistic effects between crystalline CoP domains and the amorphous LDH matrix, which increased active site density and improved charge transfer. The catalyst also demonstrated excellent stability over 60 h of continuous operation, positioning it as a promising candidate for high-rate alkaline hydrogen evolution.

Optimization of LDH cathode materials for hydrogen production focuses on tailoring composition, morphology, and surface properties to boost HER. Recent strategies include engineering 2D structures such as nanosheets or nanosheet arrays to increase the active surface area and thereby enhance charge transfer [317]. Additionally, compositional modifications, such as doping with transition metals or atomic platinum deposition, can tune the electronic structure, reduce reaction barriers, and promote efficient hydrogen adsorption [318]. Structural modulation via controlled annealing or anisotropic strain has also been shown to optimize phase evolution and lower water dissociation energy barriers, which further accelerates the HER kinetics [319,320]. Finally, surfactant-assisted exfoliation techniques help to overcome intrinsic conductivity limitations by exposing internal active sites and facilitating electron mobility [321]. These collective approaches contribute to

the design of high-performance, stable, and cost-effective LDH cathodes for sustainable hydrogen production.

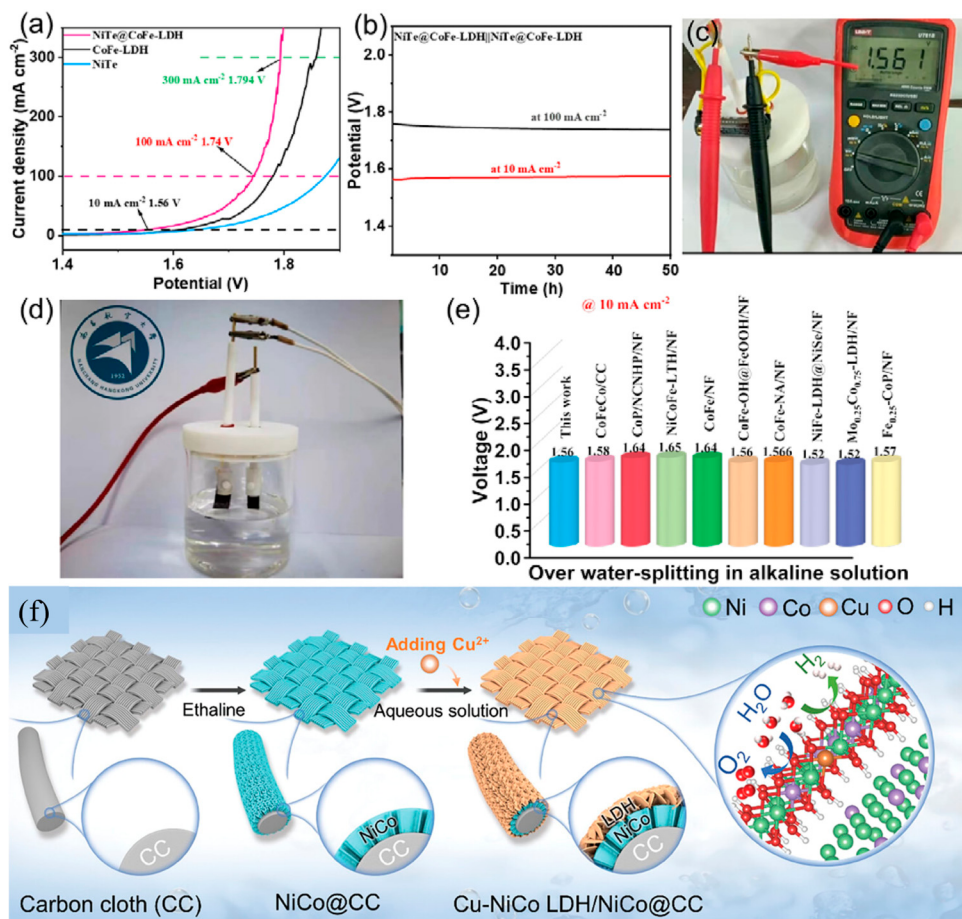


Figure 27. (a) Polarization curves of different electrocatalysts for overall water splitting recorded in 1.0 M KOH using a two-electrode setup at a scan rate of 1 mV/s. (b) Durability evaluation of NiTe@CoFe-LDH electrodes operated at current densities of 10 and 100 mA/cm^2 over a 50-h period. (c) Visual representation of the water-splitting device powered by a single battery, with a digital voltmeter showing the applied cell voltage. (d) Photograph of the assembled full-cell system under operation. (e) Comparative analysis of the cell voltages at 10 mA/cm^2 for NiTe@CoFe-LDH and other recently reported bifunctional catalysts in alkaline conditions. Reproduced with permission [308]. (f) Illustration of the synthetic strategy for constructing 3D hierarchical Cu-doped NiCo LDH nanosheets on NiCo alloy substrate and their deployment in overall water splitting applications. Reproduced with permission [285].

Integrating LDHs with MXenes significantly enhances catalytic performance by improving conductivity, preventing aggregation, and increasing exposure of active metal sites. This synergy accelerates gas evolution kinetics and boosts redox efficiency [306,322]. MXenes also offer corrosion resistance and mechanical reinforcement, improving overall catalyst durability. Though still emerging, LDH–MXene hybrids show great promise for water splitting applications. Xi et al. reported a CoFe-LDH-based catalyst synthesized via a partial *in situ* transformation of Co-MOF on a modified 3D MXene substrate (N-MXene), followed by the introduction of cationic vacancy defects to boost electrocatalytic activity [323]. The modified MXene provided a porous, conductive scaffold, while the vacancies tuned the electronic structure and enhanced active site exposure. The resulting hybrid, d-MLN (MOF-d-CoFe LDH@N-MXene), delivered excellent HER performance, requiring an overpotential of only 206 mV at 10 mA/cm^2 in 1 M KOH. It also showed a Tafel slope of 113 mV/dec,

high electrochemical surface area ($C_{dl} = 13.07 \text{ mF/cm}^2$), and charge transfer resistance as low as 1.72Ω , confirming its fast kinetics and efficient electron transfer. Stability tests revealed minimal performance degradation over 60 h, highlighting its practical potential for sustainable hydrogen production. In one study, Shen et al. designed a 3D interwoven architecture combining $\text{Ti}_3\text{C}_2\text{T}_x$ MXene, reduced graphene oxide (RGO), and NiFe-LDH nanosheets via a hydrothermal co-assembly method. This structure, denoted as LDH (60%)/MX-RGO, featured a meso/macroporous network with a large BET surface area of $254.7 \text{ m}^2/\text{g}$, enhanced charge transfer, and strong electronic interactions among components. The optimized composite exhibited outstanding HER performance in 1 M KOH, with an overpotential of only 326 mV at 10 mA/cm^2 and a Tafel slope of 100 mV/dec . It also showed a high electrochemical double-layer capacitance ($C_{dl} = 8.3 \text{ mF/cm}^2$) and a low charge/transfer resistance (2.7Ω), indicating improved intrinsic activity and conductivity. The catalyst maintained excellent stability over 40 h of continuous operation and 2000 CV cycles, establishing its robustness and practical potential in alkaline HER systems. Table 3 presents a comparative overview of recent LDH-based HER electrocatalysts, highlighting the diversity in synthesis approaches and their corresponding electrocatalytic performances, including overpotential, stability, and Tafel slope.

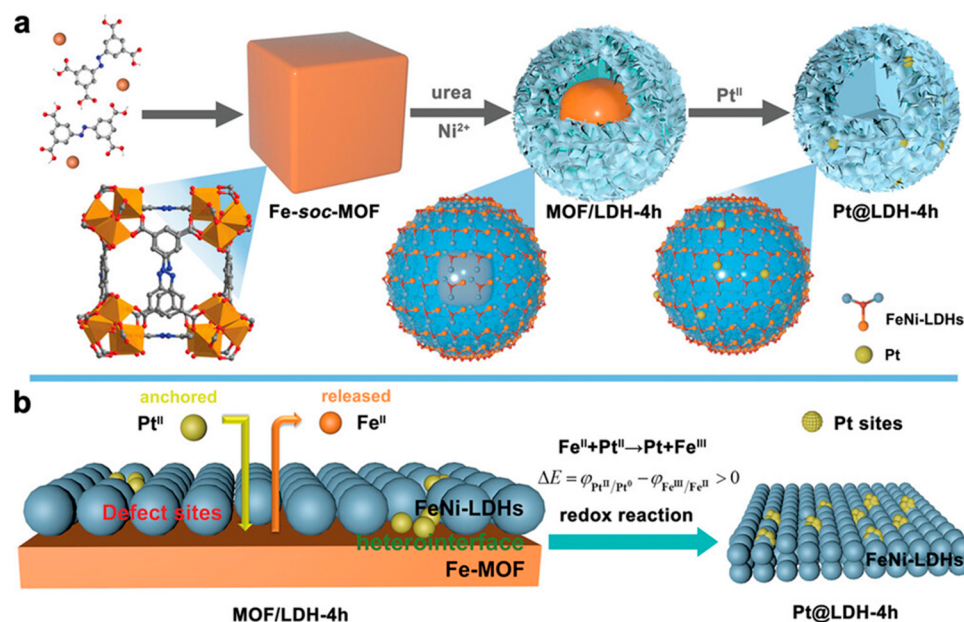


Figure 28. (a,b) Schematic representation of the strategic stepwise synthesis of Pt@LDH-4h catalysts tailored for efficient overall water splitting. Reproduced with permission [286].

Table 3. Summary of various LDH-based electrocatalysts for HER.

LDH Name	Synthesis Procedure	Electrolyte	HER Overpotential ($\eta/\text{mV}, \text{j/mA/cm}^2$)	Stability (Retention %, Time/h)	Tafel Slope (mV/dec), FE (%)	Ref.
NiFe LDH-NS@DG10	Exfoliation method	1 M KOH	115, 10	~100%, 5.5 h	110, 97.3%	[307]
NiTe@CoFe-LDH	Hydrothermal and electrodeposition	1 M KOH	103, 10	~100%, 50 h	20, 100%	[308]
Cu-NiCo LDH/NiCo@CC	Electrodeposition process	1 M KOH	73, 10	..., 100 h	78.5, ...	[285]
CoNiN@NiFe	Co-deposition	1 M KOH	150, 10	..., 60 h	167, 100%	[309]

Table 3. Cont.

LDH Name	Synthesis Procedure	Electrolyte	HER Overpotential (η /mV, $j/\text{mA/cm}^2$)	Stability (Retention %, Time/h)	Tafel Slope (mV/dec), FE (%)	Ref.
Pt@LDH-4h	Hydrolysis reaction	1 M KOH	58, 10	~100%, 24 h	43.6, 95%	[286]
Pd-NiAl-LDH	Chemical precipitation	1 M KOH	189, 10	~100%, 48 h	133.2, ...	[310]
Ni ₂ P/NiFe-LDH	Hydrothermal	1 M KOH	230, 100	~100%, 32 h	47.43, ...	[315]
c-CoMnP/a-CoMn LDH/NF	Chemical and thermal route	1 M KOH	170, 100	99%, 60 h	73.7, ...	[316]
MOF-d-CoFe LDH@N-MXene	Hydrothermal and electrophoretic deposition	1 M KOH	206, 10	..., 60 h	113, 93%	[323]
LDH(60%)/MX-RGO	Hydrothermal co-assembly	1 M KOH	326, 10	..., 40 h	100, ...	[324]

LDH: Layered double hydroxide, HER: Hydrogen evolution reaction, FE: Faradaic efficiency

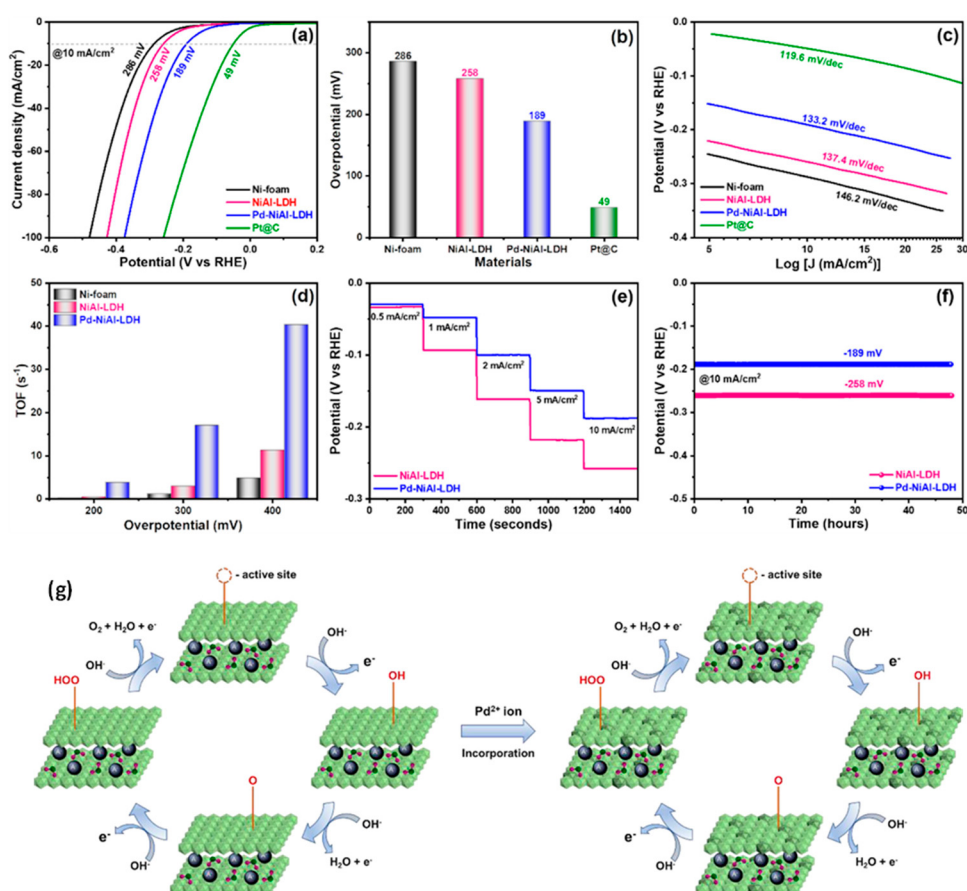


Figure 29. Evaluation of hydrogen evolution performance in 1.0 M KOH for NiAl-LDH, Pd-NiAl-LDH, Pt@C, and bare nickel foam: (a) Linear sweep voltammetry (LSV) profiles without iR compensation, (b) comparative HER overpotentials at 10 mA/cm², (c) Tafel plots indicating reaction kinetics, (d) TOF analysis, (e) stepwise chronopotentiometry tests across current densities from 0.5 to 10 mA/cm² with 300-s intervals for NiAl-LDH and Pd-NiAl-LDH, and (f) long-term stability test of Pd-NiAl-LDH at a constant current density of 10 mA/cm² over 48 h. (g) Illustration of the HER pathway involving two-electron transfer steps on NiAl-LDH and Pd-NiAl-LDH surfaces. Reproduced with permission [310].

6.3. Challenges in Catalytic Activity, Stability, and Practical Deployment

Despite their considerable promise, LDH-based electrocatalysts face several challenges that limit their widespread deployment in practical hydrogen production systems. A primary issue is their relatively modest intrinsic catalytic activity compared to noble metals, which stems from suboptimal hydrogen binding energies and sluggish electron transfer kinetics. While compositional tuning, doping, and heterostructure engineering have improved activity, achieving a balance between stability, conductivity, and catalytic efficiency remains complex. Durability under continuous operation is another major concern. Prolonged electrolysis can lead to structural disintegration, metal ion leaching, and the collapse of layered architectures, particularly under acidic or high-current conditions. These degradation mechanisms compromise long-term performance and hinder reliability. Scalability also presents significant hurdles. Many advanced LDH synthesis routes, such as hydrothermal growth, exfoliation, or electrodeposition, are challenging to scale due to batch limitations, material inconsistency, and the need for controlled environments. Moreover, integrating LDH materials into commercial electrolyzers and ensuring compatibility with system architectures and operational demands requires further development. To address these limitations, future efforts should focus on developing scalable and green synthesis methods that allow precise control over morphology and composition and enhancing interfacial engineering strategies, such as LDH–MXene, LDH–MOF, or LDH–graphene composites, to improve stability and charge transfer, *in situ*/operando characterization to uncover dynamic structural and electronic transformations under reaction conditions, and computational screening and machine learning approaches to accelerate the discovery of optimized compositions and architectures. Ultimately, advancing LDH-based electrocatalysts will require interdisciplinary strategies combining materials science, electrochemistry, and engineering design to bridge the gap from laboratory innovation to commercial application.

The utilization of LDHs in electrochemical hydrogen production presents several notable challenges related to their catalytic activity, stability, and practical deployment. This delves into these challenges, emphasizing the current understanding shaped by multiple academic explorations. One of the primary challenges in leveraging LDHs for electrochemical hydrogen production is their catalytic activity. Despite demonstrated potential, the efficiency of LDHs as electrocatalysts for HER remains limited when compared to noble metal counterparts. Transition metal-based LDHs exhibit favorable properties such as tunable composition and layered structures, yet often show inferior electrocatalytic efficiency. For instance, Wang et al. state that the catalytic performance is significantly influenced by the crystallographic phase and morphology of LDHs, where variations can lead to diverse electrochemical activities under identical conditions [314]. Luo et al. emphasize the necessity for adequately designed LDHs to provide more active sites while reducing reaction energy barriers [325]. Moreover, specific LDH compositions reveal limitations in their electrocatalytic performance; for instance, NiFe-based LDHs have been recognized as effective but still face challenges regarding the balance of active sites and reaction kinetics [326]. Optimizing the density of active sites while managing charge transfer efficiency is critical. Research by Liu et al. articulates that enhancing the uniform distribution of catalytic sites is vital for improving overall catalytic performance [327]. Ultimately, the ability of LDHs to function under diverse electrochemical conditions remains an area demanding further exploration and innovation.

In addition to catalytic activity, stability is a crucial concern regarding the performance of LDHs in practical applications. The intrinsic structure of LDHs is often susceptible to degradation under harsh electrochemical conditions, leading to a diminished operational lifetime [328]. For instance, during prolonged electrolysis, corrosion can occur, particularly in saline environments, resulting in the dissolution of components and loss of

functionality. Research has demonstrated that specific compositions, such as $\text{CoCO}_3/\text{CoFe}$ LDHs, show improved electrochemical stability, yet widespread stability challenges remain. Furthermore, Zhao highlights that ion leaching and structural collapse under continuous operational stress compromise the sustainable use of LDHs [329]. This instability limits their practical applications, especially in environments subjected to varying pH and current densities. Thus, integrating robust structural mechanisms capable of withstanding electrochemical stress while maintaining active sites is crucial for the successful deployment of LDHs in hydrogen evolution technologies.

In considering the practical deployment of LDHs in industry, several logistical and economic factors arise. The synthesis of LDHs must strike a balance between cost, scalability, and reproducibility. Current methods for producing LDHs, such as coprecipitation and hydrothermal techniques, may not be sufficiently scalable for industrial application, which is underscored by Chen et al., who point to the need for more efficient synthesis protocols that minimize costs and resource usage [330]. Additionally, the integration of LDHs into existing systems presents challenges regarding compatibility with associated materials, such as electrodes and supporting substrates [331]. Adjusting the physical and chemical properties of LDHs to facilitate optimal interaction with other components of electrochemical cells is critical [332]. The demand for multifunctional applications frames LDHs not merely as catalysts but as composite materials requiring structural and functional harmonization with other energy storage technologies. Moreover, environmental considerations, regulatory compliance, and societal acceptance play vital roles in deploying LDHs within commercial settings. As the push toward sustainable energy production intensifies, the environmental footprint of LDH processes must be carefully evaluated. Balancing lifecycle impacts while achieving functional deployment is an ongoing challenge faced by researchers and engineers [13].

Addressing the challenges of catalytic activity, stability, and deployment of LDHs in hydrogen production processes necessitates innovative strategies. Incorporating advanced synthesis methodologies can enhance the uniformity and availability of active sites within LDHs, as supported by various studies highlighting the effectiveness of nanosheet morphologies [314,333]. Additionally, engineering techniques such as doping and structural modification can enhance both the electrocatalytic performance and stability of LDHs [334]. Promising advancements include integrating LDHs with conductive substrates or hybrid materials that leverage the beneficial properties of both materials, thereby improving charge transfer and catalyst stability [89,335]. Achieving a harmonious integration of LDHs with materials such as MXenes or incorporating them into composite structures may offer pathways to overcome existing challenges [332]. Moreover, ongoing research focused on tailoring LDH compositions to optimize their electrochemical characteristics, stability, and economic viability is crucial. A deeper understanding of structure/performance relationships is fundamental to innovating LDH-based systems for hydrogen production applications. While LDHs present promising opportunities as electrocatalysts for hydrogen production, their utility is tempered by considerable challenges in catalytic activity, stability, and practical deployment. Addressing these concerns through innovative research and development is essential to realizing the potential of LDHs in contributing to sustainable hydrogen energy solutions.

7. Conclusions and Future Prospects

LDHs have emerged prominently as versatile and promising 2D materials for a wide array of energy applications, including batteries, supercapacitors, and hydrogen production. This review systematically outlines the foundational principles, synthesis methodologies, and application-specific advantages of LDHs, offering a comprehensive reference for re-

searchers within this domain. In battery-related applications, LDHs demonstrate significant potential driven by their remarkable structural stability, chemically adjustable composition, and advantageous electrochemical properties. Specifically, in LIBs, LDHs have been shown to enhance electrode performance through stabilization of electrode/electrolyte interfaces, mitigation of volumetric expansion, and improvement in electrical conductivity. LSBs benefit substantially from the inherent capability of LDHs to adsorb polysulfides, effectively reducing the shuttle effect, thereby enhancing cycle stability and capacity retention. Similarly, NIBs leverage LDHs' expanded interlayer spacing, facilitating efficient diffusion of larger sodium ions, which directly addresses critical challenges in electrode kinetics and rate capability. Beyond conventional systems, LDHs hold significant promise in emerging battery technologies, including LIBs, CIBs, ZIBs, LSBs, and ZABs. They provide innovative solutions to longstanding challenges, such as corrosion resistance, dendritic growth prevention, and enhancement of sluggish ion diffusion processes.

In supercapacitor technologies, LDHs offer a compelling combination of high specific capacitance, excellent pseudocapacitive behavior, and robust electrochemical stability. Their layered structures provide abundant active sites and pathways conducive to rapid ion transport and electron mobility, positioning LDHs as exceptionally suitable electrode materials. Further optimization through doping and composite formation allows tailored improvements in energy density and power output. Nevertheless, considerable challenges remain, including their inherently low electrical conductivity and mechanical instability during extended cycling, necessitating innovative synthetic strategies or composite structures to overcome these limitations. Regarding catalytic hydrogen production, LDHs have exhibited substantial promise, especially in electrocatalytic water splitting processes. Their adjustable layer compositions and diverse elemental combinations enable precise tuning of catalytic properties, significantly boosting both HER and OER. Despite these advances, achieving industrial-level efficiency and durability poses substantial challenges, primarily due to insufficient intrinsic conductivity, limited specific surface areas of bulk forms, and operational durability under prolonged and harsh conditions.

Addressing these challenges requires strategic and innovative approaches. Future research should explicitly focus on precise control and reproducibility of LDH morphologies and electrochemical properties through meticulous optimization of synthesis parameters. Advanced synthesis techniques such as exfoliation into ultrathin nanosheets, integration with conductive substrates, or hybridization with complementary catalysts must be systematically developed and standardized to enhance material performance consistently. One of the most pressing challenges is the scalable and economically feasible production of LDHs. Current advanced synthesis methods, such as exfoliation, sol-gel processes, or hydrothermal treatments, are typically complex, expensive, and challenging to scale. Future research must prioritize the development of simplified, cost-effective, and scalable manufacturing techniques. Techniques such as continuous-flow reactors, microwave-assisted synthesis, and scalable hydrothermal reactors warrant intensive exploration due to their potential to deliver LDHs on a commercially viable scale. Integration into commercial energy systems demands attention to the practical aspects of LDHs, including long-term cycling stability in energy storage applications and durability under harsh catalytic conditions. Detailed investigations into degradation mechanisms, especially under realistic operational scenarios, will be crucial. For instance, comprehensive studies addressing the interfacial stability of LDHs within electrode structures under extensive cycling are necessary to design robust materials for commercial applications. Furthermore, understanding and optimizing complex interactions within composite structures incorporating LDHs is another critical area requiring in-depth study. This includes evaluating the interfacial chemistry between LDHs and conductive additives like carbon nanotubes, graphene, and conductive polymers.

Advanced analytical and characterization techniques, including *in situ* microscopy and spectroscopy, are needed to elucidate interfacial phenomena and interactions at the atomic scale, facilitating targeted optimization of composite performance.

To expedite and streamline the development of advanced LDH materials, computational modeling and simulation represent potent tools for predicting optimal material compositions and structures. Employing DFT, molecular dynamics, and machine learning algorithms can dramatically reduce experimental iterations, guide synthetic strategies, and facilitate the rapid design of optimized LDH-based materials. Exploration of novel and hybrid battery chemistries involving LDHs, such as hybrid supercapacitors and dual-ion batteries, could further expand their applications, potentially delivering high-performance and safer energy storage solutions. This requires systematic exploration and validation of LDHs within these novel battery architectures to assess performance, reliability, and safety comprehensively. In hydrogen production, future research directions must center on enhancing intrinsic catalytic activities, addressing conductivity and stability constraints. Hybrid electrocatalysts, combining LDHs with high-conductivity materials such as graphene, carbon nanotubes, or conductive polymers, present promising pathways for significant enhancements in electron transport and catalytic efficiency. Research must also focus on developing novel support structures and protective coatings to improve catalyst durability under industrially relevant operating conditions.

While LDHs have been extensively explored in conventional liquid electrolyte-based batteries, their application in solid-state batteries (SSBs) remains largely untapped, presenting a promising future direction. SSBs, offering enhanced safety, higher energy density, and broader operating temperature ranges, require materials with excellent ionic conductivity, chemical stability, and favorable interfacial properties. The unique layered structure of LDHs, combined with their tunable composition and ion exchange capability, suggests their potential use as solid electrolytes, interfacial layers, or electrode additives in SSBs. For instance, modifying LDHs to create highly conductive, defect-rich structures or composite materials could help facilitate ion transport across solid interfaces, a critical bottleneck in current SSB technologies. Moreover, their intrinsic ability to incorporate various metal cations could be exploited to engineer multifunctional interfaces that enhance both mechanical stability and electrochemical performance. Therefore, future research focused on tailoring the structure, conductivity, and interface compatibility of LDHs could open new pathways for their integration into solid-state battery systems, contributing significantly to the next generation of safe and high-performance energy storage devices.

Critically, researchers should adopt a pragmatic approach to LDH development, balancing theoretical performance enhancements against practical economic and industrial constraints. This includes comprehensive lifecycle assessments, economic viability studies, and scalability analyses to align research trajectories closely with industry requirements and commercial realities. LDHs exhibit immense potential in addressing pivotal challenges across energy storage and conversion technologies. Nevertheless, realizing their commercial and practical utility demands targeted research efforts addressing synthesis reproducibility, scalability, material stability, and interfacial interactions within composites. By leveraging advanced computational techniques, innovative synthesis methods, and rigorous practical assessments, LDHs can significantly impact future energy technologies. This review provides a robust foundation, clearly identifying critical areas requiring deeper exploration and establishing a structured path toward innovative, efficient, and sustainable LDH-based solutions.

Funding: This research received no external funding.

Acknowledgments: The authors acknowledge the support from the Graduate School of Energy Science, Kyoto University, Japan.

Conflicts of Interest: The authors declare no conflict of interest.

References

- Chen, S.; Zhuo, Y.; Wang, X.; Li, S.; Lu, J.; Liu, D.; Pan, H.; Wang, Z. Advances of Layered Double Hydroxide Electrocatalysts for High-Current-Density Alkaline Water/Seawater Splitting. *Coord. Chem. Rev.* **2024**, *510*, 215832. [[CrossRef](#)]
- Long, X.; Wang, Z.; Xiao, S.; An, Y.; Yang, S. Transition Metal Based Layered Double Hydroxides Tailored for Energy Conversion and Storage. *Mater. Today* **2016**, *19*, 213–226. [[CrossRef](#)]
- Lin, Q.; Wang, L. Layered Double Hydroxides as Electrode Materials for Flexible Energy Storage Devices. *J. Semicond.* **2023**, *44*, 041601. [[CrossRef](#)]
- Yu, W.; Deng, N.; Cheng, K.; Yan, J.; Cheng, B.; Kang, W. Advances in Preparation Methods and Mechanism Analysis of Layered Double Hydroxide for Lithium-Ion Batteries and Lithium-Sulfur Batteries. *J. Energy Chem.* **2021**, *58*, 472–499. [[CrossRef](#)]
- Sahoo, D.P.; Das, K.K.; Mansingh, S.; Sultana, S.; Parida, K. Recent Progress in First Row Transition Metal Layered Double Hydroxide (LDH) Based Electrocatalysts towards Water Splitting: A Review with Insights on Synthesis. *Coord. Chem. Rev.* **2022**, *469*, 214666. [[CrossRef](#)]
- Hu, X.; Zheng, W.; Wu, M.; He, Q.; Zhan, F.; Chen, L. Ternary Layered Double Hydroxide Cathode Materials for Electrochemical Energy Storage: A Review and Perspective. *Sustain. Energy Fuels* **2022**, *6*, 4551–4581. [[CrossRef](#)]
- Zhou, D.; Li, P.; Lin, X.; McKinley, A.; Kuang, Y.; Liu, W.; Lin, W.F.; Sun, X.; Duan, X. Layered Double Hydroxide-Based Electrocatalysts for the Oxygen Evolution Reaction: Identification and Tailoring of Active Sites, and Superaerophobic Nanoarray Electrode Assembly. *Chem. Soc. Rev.* **2021**, *50*, 8790–8817. [[CrossRef](#)]
- Jing, C.; Tao, S.; Fu, B.; Yao, L.; Ling, F.; Hu, X.; Zhang, Y. Layered Double Hydroxide-Based Nanomaterials for Supercapacitors and Batteries: Strategies and Mechanisms. *Prog. Mater. Sci.* **2024**, *150*, 101410. [[CrossRef](#)]
- Zhang, D.; Guo, X.; Tong, X.; Chen, Y.; Duan, M.; Shi, J.; Jiang, C.; Hu, L.; Kong, Q.; Zhang, J. High-Performance Battery-Type Supercapacitor Based on Porous Biocarbon and Biocarbon Supported Ni-Co Layered Double Hydroxide. *J. Alloys Compd.* **2020**, *837*, 155529. [[CrossRef](#)]
- Antil, B.; Olhan, S.; Vander Wal, R.L. Production of Graphitic Carbon from Renewable Lignocellulosic Biomass Source. *Minerals* **2025**, *15*, 262. [[CrossRef](#)]
- Chaudhuri, H.; Yun, Y.S. A Critical Review on the Properties and Energy Storage Applications of Graphene Oxide/Layered Double Hydroxides and Graphene Oxide/MXenes. *J. Power Sources* **2023**, *564*, 232870. [[CrossRef](#)]
- Tomboc, G.M.; Kim, J.; Wang, Y.; Son, Y.; Li, J.; Kim, J.Y.; Lee, K. Hybrid Layered Double Hydroxides as Multifunctional Nanomaterials for Overall Water Splitting and Supercapacitor Applications. *J. Mater. Chem. A Mater.* **2021**, *9*, 4528–4557. [[CrossRef](#)]
- Fan, K.; Xu, P.; Li, Z.; Shao, M.; Duan, X. Layered Double Hydroxides: Next Promising Materials for Energy Storage and Conversion. *Next Mater.* **2023**, *1*, 100040. [[CrossRef](#)]
- Sherry, A.; Tahir, M. Recent Developments in Layered Double Hydroxide Structures with Their Role in Promoting Photocatalytic Hydrogen Production: A Comprehensive Review. *Int. J. Energy Res.* **2022**, *46*, 2093–2140. [[CrossRef](#)]
- Mohanty, U.A.; Sahoo, D.P.; Paramanik, L.; Parida, K. A Critical Review on Layered Double Hydroxide (LDH)-Derived Functional Nanomaterials as Potential and Sustainable Photocatalysts. *Sustain. Energy Fuels* **2023**, *7*, 1145–1186. [[CrossRef](#)]
- Zhao, Y.; Zhang, P.; Liang, J.; Xia, X.; Ren, L.; Song, L.; Liu, W.; Sun, X. Unlocking Layered Double Hydroxide as a High-Performance Cathode Material for Aqueous Zinc-Ion Batteries. *Adv. Mater.* **2022**, *34*, 2204320. [[CrossRef](#)] [[PubMed](#)]
- Aziz, M.A.; Shah, S.S.; Mahnashi, Y.A.; Mahfoz, W.; Alzahrani, A.S.; Hakeem, A.S.; Shaikh, M.N. A High-Energy Asymmetric Supercapacitor Based on Tomato-Leaf-Derived Hierarchical Porous Activated Carbon and Electrochemically Deposited Polyaniline Electrodes for Battery-Free Heart-Pulse-Rate Monitoring. *Small* **2023**, *19*, 2300258. [[CrossRef](#)]
- Jing, C.; Dong, B.; Zhang, Y. Chemical Modifications of Layered Double Hydroxides in the Supercapacitor. *Energy Environ. Mater.* **2020**, *3*, 346–379. [[CrossRef](#)]
- Antil, B.; Elkasabi, Y.; Strahan, G.D.; Vander Wal, R.L. Development of Graphitic and Non-Graphitic Carbons Using Different Grade Biopitch Sources. *Carbon* **2025**, *232*, 119770. [[CrossRef](#)]
- Yuan, Z.; Bak, S.M.; Li, P.; Jia, Y.; Zheng, L.; Zhou, Y.; Bai, L.; Hu, E.; Yang, X.Q.; Cai, Z.; et al. Activating Layered Double Hydroxide with Multivacancies by Memory Effect for Energy-Efficient Hydrogen Production at Neutral pH. *ACS Energy Lett.* **2019**, *4*, 1412–1418. [[CrossRef](#)]
- Khorshidi, M.; Asadpour, S.; Sarmast, N.; Dinari, M. A Review of the Synthesis Methods, Properties, and Applications of Layered Double Hydroxides/Carbon Nanocomposites. *J. Mol. Liq.* **2022**, *348*, 118399. [[CrossRef](#)]

22. Riaz, S.; Rehman, A.; Akhter, Z.; Najam, T.; Hossain, I.; Karim, M.R.; Assiri, M.A.; Shah, S.S.A.; Nazir, M.A. Recent Advancement in Synthesis and Applications of Layered Double Hydroxides (LDHs) Composites. *Mater. Today Sustain.* **2024**, *27*, 100897. [[CrossRef](#)]
23. Jijoe, P.S.; Yashas, S.R.; Shivaraju, H.P. Fundamentals, Synthesis, Characterization and Environmental Applications of Layered Double Hydroxides: A Review. *Environ. Chem. Lett.* **2021**, *19*, 2643–2661. [[CrossRef](#)]
24. Ali Khan, A.; Tahir, M.; Khan, N. Recent Developments in Titanium Carbide (Ti_3C_2)-Based Layered Double Hydroxide (LDH) Nanocomposites for Energy Storage and Conversion Applications: A Minireview and Perspectives. *Energy Fuels* **2022**, *36*, 9821–9843. [[CrossRef](#)]
25. Parsapour, F.; Moradi, M.; Bahadoran, A. Metal-Organic Frameworks-Derived Layered Double Hydroxides: From Controllable Synthesis to Various Electrochemical Energy Storage/Conversion Applications. *Adv. Colloid. Interface Sci.* **2023**, *313*, 102865. [[CrossRef](#)] [[PubMed](#)]
26. Li, C.; Zhao, J.; Xie, L.; Wu, J.; Ren, Q.; Wang, Y.; Li, G. Surface-Adsorbed Carboxylate Ligands on Layered Double Hydroxides/Metal–Organic Frameworks Promote the Electrocatalytic Oxygen Evolution Reaction. *Angew. Chem.* **2021**, *133*, 18277–18285. [[CrossRef](#)]
27. Bukhtiyarova, M.V. A Review on Effect of Synthesis Conditions on the Formation of Layered Double Hydroxides. *J. Solid. State Chem.* **2019**, *269*, 494–506. [[CrossRef](#)]
28. Wang, Q.; Ohare, D. Recent Advances in the Synthesis and Application of Layered Double Hydroxide (LDH) Nanosheets. *Chem. Rev.* **2012**, *112*, 4124–4155. [[CrossRef](#)]
29. Li, F.; Zhang, L.; Evans, D.G.; Duan, X. Structure and Surface Chemistry of Manganese-Doped Copper-Based Mixed Metal Oxides Derived from Layered Double Hydroxides. *Colloids Surf. A Physicochem. Eng. Asp.* **2004**, *244*, 169–177. [[CrossRef](#)]
30. Xu, J.; Liu, X.; Zhou, Z.; Deng, L.; Liu, L.; Xu, M. Surface Defects Introduced by Metal Doping into Layered Double Hydroxide for CO_2 Photoreduction: The Effect of Metal Species in Light Absorption, Charge Transfer and CO_2 Reduction. *Chem. Eng. J.* **2022**, *442*, 136148. [[CrossRef](#)]
31. Forano, C. Environmental Remediation Involving Layered Double Hydroxides. In *Interface Science and Technology*; Elsevier: Amsterdam, The Netherlands, 2004; Volume 1, pp. 425–458.
32. Perera-Solis, D.D.; Pimlott, M.; Fidment, E.; Whiting, A.; Greenwell, H.C. Adding Value to Waste Minerals in a Circular Economy Framework: Ochre-Derived Layered Double Hydroxide Catalysts in Fatty Acid Ketonisation. *Minerals* **2019**, *9*, 681. [[CrossRef](#)]
33. Roy Chowdhury, P.; Medhi, H.; Bhattacharyya, K.G.; Mustansar Hussain, C. Layered Double Hydroxides Derived from Waste for Highly Efficient Electrocatalytic Water Splitting: Challenges and Implications towards Circular Economy Driven Green Energy. *Coord. Chem. Rev.* **2024**, *501*, 215547. [[CrossRef](#)]
34. Chowdhury, P.R.; Medhi, H.; Bhattacharyya, K.G.; Hussain, C.M. Recent Developments in Ni-Based Layered Double Hydroxides Extracted from Waste for Oxygen Evolution Reactions: A Review on the Pursuit for Sustainable Green Hydrogen. *Sustain. Energy Fuels* **2025**, *9*, 1447–1463. [[CrossRef](#)]
35. Jerome, M.P.; Alahmad, F.A.; Salem, M.T.; Tahir, M. Layered Double Hydroxide (LDH) Nanomaterials with Engineering Aspects for Photocatalytic CO_2 Conversion to Energy Efficient Fuels: Fundamentals, Recent Advances, and Challenges. *J. Environ. Chem. Eng.* **2022**, *10*, 108151. [[CrossRef](#)]
36. Singha Roy, A.; Kesavan Pillai, S.; Ray, S.S. Layered Double Hydroxides for Sustainable Agriculture and Environment: An Overview. *ACS Omega* **2022**, *7*, 20428–20440. [[CrossRef](#)]
37. Zubair, M.; Daud, M.; McKay, G.; Shehzad, F.; Al-Harthi, M.A. Recent Progress in Layered Double Hydroxides (LDH)-Containing Hybrids as Adsorbents for Water Remediation. *Appl. Clay Sci.* **2017**, *143*, 279–292. [[CrossRef](#)]
38. Li, L.; Soyhan, I.; Warszawik, E.; van Rijn, P. Layered Double Hydroxides: Recent Progress and Promising Perspectives Toward Biomedical Applications. *Adv. Sci.* **2024**, *11*, 2306035. [[CrossRef](#)]
39. Nemček, L.; Hagarová, I.; Matúš, P. Layered Double Hydroxides as Next-Generation Adsorbents for the Removal of Selenium from Water. *Appl. Sci.* **2024**, *14*, 8513. [[CrossRef](#)]
40. Altalhi, A.A.; Mohamed, E.A.; Negm, N.A. Recent Advances in Layered Double Hydroxide (LDH)-Based Materials: Fabrication, Modification Strategies, Characterization, Promising Environmental Catalytic Applications, and Prospective Aspects. *Energy Adv.* **2024**, *3*, 2136–2151. [[CrossRef](#)]
41. Li, C.; Jing, H.; Wu, Z.; Jiang, D. Layered Double Hydroxides for Photo(Electro)Catalytic Applications: A Mini Review. *Nanomaterials* **2022**, *12*, 3525. [[CrossRef](#)]
42. Gao, J.; Jin, B.; Shao, M. Layered Double Hydroxides Functionalization toward Rechargeable Batteries. *Particuology* **2024**, *91*, 138–154. [[CrossRef](#)]
43. Lu, L.; Zheng, Y.; Yang, R.; Kakimov, A.; Li, X. Recent Advances of Layered Double Hydroxides-Based Bifunctional Electrocatalysts for ORR and OER. *Mater. Today Chem.* **2021**, *21*, 100488. [[CrossRef](#)]
44. Gaur, A.; Sharma, J.; Lim, D.; Lee, H.I.; Han, H. Recent Advances in Electronic Structure Modifications of Layered Double Hydroxide (LDH) for the Water Splitting Application. *ChemCatChem* **2025**, *17*, e202401584. [[CrossRef](#)]

45. Lin, Z.; Li, X.; Zhang, H.; Xu, B.B.; Wasnik, P.; Li, H.; Singh, M.V.; Ma, Y.; Li, T.; Guo, Z. Research Progress of MXenes and Layered Double Hydroxides for Supercapacitors. *Inorg. Chem. Front.* **2023**, *10*, 4358–4392. [[CrossRef](#)]
46. Li, X.; Ren, J.; Sridhar, D.; Xu, B.B.; Algadi, H.; El-Bahy, Z.M.; Ma, Y.; Li, T.; Guo, Z. Progress of Layered Double Hydroxide-Based Materials for Supercapacitors. *Mater. Chem. Front.* **2023**, *7*, 1520–1561. [[CrossRef](#)]
47. Luo, F.; San, X.; Wang, Y.; Meng, D.; Tao, K. Layered Double Hydroxide-Based Electrode Materials Derived from Metal–Organic Frameworks: Synthesis and Applications in Supercapacitors. *Dalton Trans.* **2024**, *53*, 10403–10415. [[CrossRef](#)] [[PubMed](#)]
48. Jafari, M.; Ganjali, F.; Eivazzadeh-Keihan, R.; Maleki, A.; Geranmayeh, S. Recent Advances in Applications of Graphene-Layered Double Hydroxide Nanocomposites in Supercapacitors and Batteries. *FlatChem* **2024**, *45*, 100658. [[CrossRef](#)]
49. Aman, M.; Konduparty, P.; Sharma, S.; Srivastava, R.P.; Bhattacharyya, S.; Sharma, V.; Balani, K.; Jha, S.K.; Omar, S. Layered Double Hydroxide Based Composites for Energy Storage Applications: Insights into Supercapacitors and Batteries. *J. Energy Storage* **2025**, *116*, 116093. [[CrossRef](#)]
50. Fan, G.; Li, F.; Evans, D.G.; Duan, X. Catalytic Applications of Layered Double Hydroxides: Recent Advances and Perspectives. *Chem. Soc. Rev.* **2014**, *43*, 7040–7066. [[CrossRef](#)]
51. Cardinale, A.M.; Carbone, C.; Consani, S.; Fortunato, M.; Parodi, N. Layered Double Hydroxides for Remediation of Industrial Wastewater from a Galvanic Plant. *Crystals* **2020**, *10*, 443. [[CrossRef](#)]
52. Tsuneishi, T.; Sakamoto, H.; Hayashi, K.; Kawamura, G.; Muto, H.; Matsuda, A. Preparation of Hydroxide Ion Conductive KOH-Layered Double Hydroxide Electrolytes for an All-Solid-State Iron–Air Secondary Battery. *J. Asian Ceram. Soc.* **2014**, *2*, 165–168. [[CrossRef](#)]
53. Leung, D.W.J.; Laney, K.R.; Kenyon, P.; Rees, N.H.; Buffet, J.-C.; Chen, C.; O'Hare, D. Optimising the Acid–Base Ratio of Mg–Al Layered Double Oxides to Enhance CO₂ Capture Performance: The Critical Role of Calcination Conditions. *Dalton Trans.* **2024**, *53*, 6200–6206. [[CrossRef](#)] [[PubMed](#)]
54. Xu, S.-M.; Zhu, Y.-Q.; Chen, Z.-R.; Yang, J.-R.; Chen, X.; Yan, H. Theoretical Prediction of the Carrier Mobilities for M^{II}₂M^{III}-Cl-Layered Double Hydroxides in Three-Dimensional Directions. *J. Mater. Chem. C Mater.* **2022**, *10*, 9573–9585. [[CrossRef](#)]
55. Xu, J.; Deng, H.; Song, J.; Zhao, J.; Zhang, L.; Hou, W. Synthesis of Hierarchical Flower-like Mg₂Al-Cl Layered Double Hydroxide in a Surfactant-Free Reverse Microemulsion. *J. Colloid. Interface Sci.* **2017**, *505*, 816–823. [[CrossRef](#)] [[PubMed](#)]
56. Memon, J.; Sun, J.; Meng, D.; Ouyang, W.; Memon, M.A.; Huang, Y.; Yan, S.; Geng, J. Synthesis of Graphene/Ni–Al Layered Double Hydroxide Nanowires and Their Application as an Electrode Material for Supercapacitors. *J. Mater. Chem. A Mater.* **2014**, *2*, 5060–5067. [[CrossRef](#)]
57. Palapa, N.R.; Taher, T.; Mohadi, R.; Lesbani, A. Removal of Anionic Direct Dye Using Zn/Al, Zn/Fe and Zn/Cr Layered Double Hydroxides Toward Interlayer Distance. *Sci. Technol. Indones.* **2019**, *4*, 70–76. [[CrossRef](#)]
58. Ibrahimova, K.A.; Azizov, A.A.; Bayayeva, O.O.; Alosmanov, R.M.; Abbasov, M.H. The sonochemical synthesis of PVA/Mg-Al-OH layered double hydroxide nanocomposite film. *Azerbaijan Chem. J.* **2023**, *1*, 141–148. [[CrossRef](#)]
59. Harada, K.; Nguyen, T.K.N.; Matsui, Y.; Fujii, K.; Grasset, F.; Ohashi, N.; Matsuda, M.; Uchikoshi, T. Observation of Stacking Faults and Photoluminescence of Laurate Ion Intercalated Zn/Al Layered Double Hydroxide. *Mater. Lett.* **2018**, *213*, 323–325. [[CrossRef](#)]
60. Kahl, M.; Golden, T.D. Corrosion Resistance of Electrochemically Synthesized Modified Zaccagnaite LDH-Type Films on Steel Substrates. *Materials* **2021**, *14*, 7389. [[CrossRef](#)]
61. Sun, X.; Neuperger, E.; Dey, S.K. Insights into the Synthesis of Layered Double Hydroxide (LDH) Nanoparticles: Part 1. Optimization and Controlled Synthesis of Chloride-Intercalated LDH. *J. Colloid. Interface Sci.* **2015**, *459*, 264–272. [[CrossRef](#)]
62. Geng, D.G. Removal of Nitrophenol from Water by Dodecyl Sulfate Modified Layered Double Hydroxides. *Asian J. Chem.* **2014**, *26*, 447–450. [[CrossRef](#)]
63. Mohadi, R.; Amri, A.; Badaruddin, M.; Ahmad, N.; Lesbani, A. Adsorption of Phenol from Aqueous Solution Using Zn/Al Layered Double Hydroxides-Cellulose Composite. *Sci. Technol. Indones.* **2023**, *8*, 123–128. [[CrossRef](#)]
64. Smalenskaite, A.; Sen, S.; Salak, A.N.; Ferreira, M.G.S.; Skaudzius, R.; Katelnikovas, A.; Kareiva, A. Sol-Gel Synthesis and Characterization of Non-Substituted and Europium-Substituted Layered Double Hydroxides Mg₃/Al_{1-x}Eu_x. *Curr. Inorg. Chem.* **2017**, *6*, 149–154. [[CrossRef](#)]
65. George, G.; Saravanakumar, M.P. Synthesising Methods of Layered Double Hydroxides and Its Use in the Fabrication of Dye Sensitised Solar Cell (DSSC): A Short Review. *IOP Conf. Ser. Mater. Sci. Eng.* **2017**, *263*, 032020. [[CrossRef](#)]
66. Yang, B.; Yang, Z.; Wang, R.; Feng, Z. Silver Nanoparticle Deposited Layered Double Hydroxide Nanosheets as a Novel and High-Performing Anode Material for Enhanced Ni–Zn Secondary Batteries. *J. Mater. Chem. A* **2014**, *2*, 785–791. [[CrossRef](#)]
67. Gong, M.; Li, Y.; Wang, H.; Liang, Y.; Wu, J.Z.; Zhou, J.; Wang, J.; Regier, T.; Wei, F.; Dai, H. An Advanced Ni–Fe Layered Double Hydroxide Electrocatalyst for Water Oxidation. *J. Am. Chem. Soc.* **2013**, *135*, 8452–8455. [[CrossRef](#)]
68. Shao, M.; Ning, F.; Zhao, J.; Wei, M.; Evans, D.G.; Duan, X. Hierarchical Layered Double Hydroxide Microspheres with Largely Enhanced Performance for Ethanol Electrooxidation. *Adv. Funct. Mater.* **2013**, *23*, 3513–3518. [[CrossRef](#)]

69. Jia, Z.; Wang, Y.; Qi, T. Hierarchical Ni–Fe Layered Double Hydroxide/MnO₂ Sphere Architecture as an Efficient Noble Metal-Free Electrocatalyst for Ethanol Electro-Oxidation in Alkaline Solution. *RSC Adv.* **2015**, *5*, 83314–83319. [CrossRef]
70. Gao, X.; Lei, L.; Chen, L.; Wang, Y.; He, L.; Lian, Y. Synthesis and Controlled Release of Vitamin C Intercalated Zn/Al Layered Double Hydroxide. *Asian J. Chem.* **2014**, *26*, 3471–3476. [CrossRef]
71. Iqbal, M.A.; Sun, L.; Fedel, M. Synthesis of Novel Cone-Shaped CaAl-LDH Directly on Aluminum Alloy by a Facile Urea Hydrolysis Method. *SN Appl. Sci.* **2019**, *1*, 1415. [CrossRef]
72. Liu, X.L. Chiral Recognition of Lysine by Cyclodextrin Intercalated Layered Double Hydroxides. *Asian J. Chem.* **2013**, *25*, 10277–10282. [CrossRef]
73. ABD MALEK, A.H.; YASIN, Y. Use of Layered Double Hydroxides to Remove Sunset Yellow FCF Dye from Aqueous Solution. *Chem. Sci. Trans.* **2012**, *1*, 194–200. [CrossRef]
74. Hanifa, Y.; Rahayu Palapa, N. Mg/Al Double Layer Hydroxides: Intercalation with H₃[α -PW₁₂O₄₀]•nH₂O. *Sci. Technol. Indones.* **2016**, *1*, 16–19. [CrossRef]
75. Rasouli, N. Application of a Novel, Efficient and Recyclable Photo Redox Catalyst (Zn–Al Layered Double Hydroxide/Eosin) for the Synthesis of Substituted Pyridine Derivatives under Visible Light Irradiation. *Appl. Organomet. Chem.* **2018**, *32*, e4585. [CrossRef]
76. Imron, M.; Said, M. Adsorption of Procion Red Using Layer Double Hydroxide Mg/Al. *Sci. Technol. Indones.* **2017**, *2*, 64–67. [CrossRef]
77. Mishra, G.; Dash, B.; Pandey, S. Layered Double Hydroxides: A Brief Review from Fundamentals to Application as Evolving Biomaterials. *Appl. Clay Sci.* **2018**, *153*, 172–186. [CrossRef]
78. Shin, J.; Kim, K.; Hong, J. Zn-Al Layered Double Hydroxide Thin Film Fabricated by the Sputtering Method and Aqueous Solution Treatment. *Coatings* **2020**, *10*, 669. [CrossRef]
79. Mattera, M.; Sorrenti, A.; De Gregorio Perpiñá, L.; Oestreicher, V.; Sevim, S.; Arteaga, O.; Chen, X.; Pané, S.; Abellán, G.; Puigmartí-Luis, J. “On-The-Fly” Synthesis of Self-Supported LDH Hollow Structures Through Controlled Microfluidic Reaction-Diffusion Conditions. *Small* **2024**, *20*, 2307621. [CrossRef]
80. Wang, C.; Xu, J.; Zhou, Z. A Mini-Review on CO₂ Photoreduction by MgAl-LDH Based Materials. *Energies* **2022**, *15*, 8117. [CrossRef]
81. Wang, L.; Yuan, Z.; Zhang, Y.; Guo, W.; Sun, X.; Duan, X. Sandwich Layered Double Hydroxides with Graphene Oxide for Enhanced Water Desalination. *Sci. China Mater.* **2022**, *65*, 803–810. [CrossRef]
82. Jaramillo-Hernández, C.; Oestreicher, V.; Mizrahi, M.; Abellán, G. Upscaling the Urea Method Synthesis of CoAl Layered Double Hydroxides. *Beilstein J. Nanotechnol.* **2023**, *14*, 927–938. [CrossRef] [PubMed]
83. Rosaiah, P.; Vadivel, S.; Prakash, N.G.; Dhananjaya, M.; Al-Asbahi, B.A.; Roy, S.; Chalapathi, U.; Park, S.-H. Fabrication of Porous Ni-Co LDH Nanocomposites as Efficient Electrodes for Supercapacitors. *Int. J. Energy Res.* **2023**, *2023*, 5793868. [CrossRef]
84. Cao, Y.; Zheng, D.; Li, X.; Lin, J.; Wang, C.; Dong, S.; Lin, C. Enhanced Corrosion Resistance of Superhydrophobic Layered Double Hydroxide Films with Long-Term Stability on Al Substrate. *ACS Appl. Mater. Interfaces* **2018**, *10*, 15150–15162. [CrossRef]
85. Kim, A.; Varga, I.; Adhikari, A.; Patel, R. Recent Advances in Layered Double Hydroxide-Based Electrochemical and Optical Sensors. *Nanomaterials* **2021**, *11*, 2809. [CrossRef] [PubMed]
86. Li, X.; Chen, F.; Zhao, B.; Zhang, S.; Zheng, X.; Wang, Y.; Jin, X.; Dai, C.; Wang, J.; Xie, J.; et al. Ultrafast Synthesis of Metal-Layered Hydroxides in a Dozen Seconds for High-Performance Aqueous Zn (Micro-) Battery. *Nanomicro Lett.* **2023**, *15*, 32. [CrossRef] [PubMed]
87. Xu, X.; Wang, J.; Zhou, A.; Dong, S.; Shi, K.; Li, B.; Han, J.; O’Hare, D. High-Efficiency CO₂ Separation Using Hybrid LDH-Polymer Membranes. *Nat. Commun.* **2021**, *12*, 3069. [CrossRef]
88. Belskaya, O.B.; Terekhova, E.N.; Gorbunova, O.V.; Muromtsev, I.V.; Trenikhin, M.V.; Salanov, A.N.; Likhobov, V.A. Synthesis of CuAl-LDHs by Co-Precipitation and Mechanochemical Methods and Selective Hydrogenation Catalysts Based on Them. *Inorganics* **2023**, *11*, 247. [CrossRef]
89. Shah, S.S.; Aziz, M.A.; Ali, M.; Hakeem, A.S.; Yamani, Z.H. Advanced High-Energy All-Solid-State Hybrid Supercapacitor with Nickel-Cobalt-Layered Double Hydroxide Nanoflowers Supported on Jute Stick-Derived Activated Carbon Nanosheets. *Small* **2024**, *20*, 2306665. [CrossRef]
90. Wu, F.; Liang, J.; Peng, Z.; Liu, B. Electrochemical Deposition and Characterization of Zn-Al Layered Double Hydroxides (LDHs) Films on Magnesium Alloy. *Appl. Surf. Sci.* **2014**, *313*, 834–840. [CrossRef]
91. Johnston, A.L.; Lester, E.; Williams, O.; Gomes, R.L. Understanding Layered Double Hydroxide Properties as Sorbent Materials for Removing Organic Pollutants from Environmental Waters. *J. Environ. Chem. Eng.* **2021**, *9*, 105197. [CrossRef]
92. Ibrahimova, K.A. The synthesis methods and applications of layered double hydroxides—A brief review. *NNC RK Bull.* **2022**, *4*, 16–29. [CrossRef]
93. Palapa, N.R.; Saria, Y.; Taher, T.; Mohadi, R.; Lesbani, A. Synthesis and Characterization of Zn/Al, Zn/Fe, and Zn/Cr Layered Double Hydroxides: Effect of M³⁺ Ions Toward Layer Formation. *Sci. Technol. Indones.* **2019**, *4*, 36–39. [CrossRef]

94. Huang, X.; Yang, X.; Li, G.; Ezeh, C.I.; Sun, C.; Snape, C. Hybrid Two-Step Preparation of Nanosized MgAl Layered Double Hydroxides for CO₂ Adsorption. In *Sorption in 2020s*; IntechOpen: Rijeka, Croatia, 2020.
95. G.Fouad, H.; Sayed Amin, A.; S.Ahmed, I.; A.Ali, A. Zinc-Aluminium Layered Double Hydroxides: Fabrication, Study and Adsorption Application for Removal Organic Dye from Aqueous Media. *Benza J. Appl. Sci.* **2022**, *7*, 53–61. [CrossRef]
96. Smalenskaite, A.; Kaba, M.M.; Grigoraviciute-Puroniene, I.; Mikoliunaite, L.; Zarkov, A.; Ramanauskas, R.; Morkan, I.A.; Kareiva, A. Sol-Gel Synthesis and Characterization of Coatings of Mg-Al Layered Double Hydroxides. *Materials* **2019**, *12*, 3738. [CrossRef]
97. Xu, Y.; Liu, T.; Li, Y.; Liu, Y.; Ge, F. Nanostructure Design and Catalytic Performance of Mo/ZnAl-LDH in Cationic Orchid X-BL Removal. *Materials* **2018**, *11*, 2390. [CrossRef]
98. Wijitwongwan, R.P.; Saothayanun, T.K.; Ogawa, M. Synthesis of NiFe Layered Double Hydroxides with Varied Layer Charge Densities: The Templatting Effect of Diethyl Sulfoxide. *Dalton Trans.* **2023**, *52*, 4692–4699. [CrossRef]
99. Zhang, J.-J.; Li, M.-Y.; Li, X.; Bao, W.-W.; Jin, C.-Q.; Feng, X.-H.; Liu, G.; Yang, C.-M.; Zhang, N.-N. Chromium-Modified Ultrathin CoFe LDH as High-Efficiency Electrode for Hydrogen Evolution Reaction. *Nanomaterials* **2022**, *12*, 1227. [CrossRef] [PubMed]
100. Cao, Y.; Zheng, D.; Luo, J.; Zhang, F.; Dong, S.; Pan, J.; Lin, C. Insight into the Fabrication of ZnAl Layered Double Hydroxides Intercalated with Organic Anions and Their Corrosion Protection of Steel Reinforced Concrete. *J. Electrochem. Soc.* **2019**, *166*, C617–C623. [CrossRef]
101. Fang, S.; Chen, K.; Yao, H.; Cao, Y.; Guo, S.; Wang, L.; Wang, Y.; Yu, S.; Wang, N. Preparation of Gallic Acid Intercalated Layered Double Hydroxide for Enhanced Corrosion Protection of Epoxy Coatings. *Coatings* **2023**, *13*, 128. [CrossRef]
102. Bani Hashemi, A.; Kasiri, G.; Glenneberg, J.; Langer, F.; Kun, R.; La Mantia, F. Electrochemical and Morphological Characterization of Zn–Al–Cu Layered Double Hydroxides as a Negative Electrode in Aqueous Zinc-Ion Batteries. *ChemElectroChem* **2018**, *5*, 2073–2079. [CrossRef]
103. Neethu, P.P.; Venkatachalam, G.; Venkatesha, N.J.; Joseph, D.; Sakthivel, A. Cobalt-Based Hydrotalcite: A Potential Non-Noble Metal-Based Heterogeneous Catalyst for Selective Hydrogenation of Aromatic Aldehydes. *Ind. Eng. Chem. Res.* **2023**, *62*, 4976–4986. [CrossRef]
104. Kitano, S.; Sato, Y.; Tagusari, R.; Zhu, R.; Kowalski, D.; Aoki, Y.; Habazaki, H. Facile Synthesis Approach of Bifunctional Co–Ni–Fe Oxyhydroxide and Spinel Oxide Composite Electrocatalysts from Hydroxide and Layered Double Hydroxide Composite Precursors. *RSC Adv.* **2023**, *13*, 10681–10692. [CrossRef]
105. Huang, L.; Megías-Sayago, C.; Bingre, R.; Zheng, Q.; Wang, Q.; Louis, B. Catalytic Performance of Layered Double Hydroxides (LDHs) Derived Materials in Gas-Solid and Liquid-Solid Phase Reactions. *ChemCatChem* **2019**, *11*, 3279–3286. [CrossRef]
106. Kovalenko, V.; Borysenko, A.; Kotok, V.; Nafeev, R.; Verbitskiy, V.; Melnyk, O. Determination of the Dependence of the Structure of Zn-Al Layered Double Hydroxides, as a Matrix for Functional Anions Intercalation, on Synthesis Conditions. *East.-Eur. J. Enterp. Technol.* **2022**, *1*, 12–20. [CrossRef]
107. Nyaba, L.; Munonde, T.S.; Mpupa, A.; Nomngongo, P.N. Magnetic Fe₃O₄@Mg/Al-Layered Double Hydroxide Adsorbent for Preconcentration of Trace Metals in Water Matrices. *Sci. Rep.* **2021**, *11*, 2302. [CrossRef] [PubMed]
108. Liu, J.; Yue, X.; Lu, X.; Guo, Y. Uptake Fluoride from Water by Starch Stabilized Layered Double Hydroxides. *Water* **2018**, *10*, 745. [CrossRef]
109. Yang, K.; Huang, Y.; Wang, P.; Tang, Y.; Zhu, Y.; Zhu, X.; Xu, Y.; Jiang, W.; Pan, L.; Li, Q.; et al. LDH Nanocrystal@amorphousness Core–Shell Structure Derived from LDH→LDO Transformation: Synergistically Enhanced Energy Stored for LIBs Anode. *Chem. Eng. J.* **2024**, *486*, 150416. [CrossRef]
110. Hwang, J.Y.; Park, H.; Kim, H.; Kansara, S.; Sun, Y.K. Advanced Cathodes for Practical Lithium-Sulfur Batteries. *Acc. Mater. Res.* **2025**, *6*, 245–258. [CrossRef]
111. Fortunato, M.; Sarapulova, A.; Schwarz, B.; Cardinale, A.M.; Dsoke, S. NiFe-NO₃ Layered Double Hydroxide as a Novel Anode for Sodium Ion Batteries. *Batter. Supercaps* **2024**, *8*, 2400451. [CrossRef]
112. Wu, Y.; Yuan, Q.; Wu, Z.; Zhao, Z.; Yin, Q.; Han, J. Interlayer-Spacing Regulation of NiFe LDH Nanosheets Cathode with High Rate Performance for Chloride Ion Battery. *J. Ind. Eng. Chem.* **2024**, *143*, 176–183. [CrossRef]
113. Li, J.; Li, M.; Xu, S.; Weng, H. Chloride Ion Batteries—Excellent Candidates for New Energy Storage Batteries Following Lithium-Ion Batteries. *Ionics* **2024**, *30*, 27–38. [CrossRef]
114. Song, Z.; Yin, Q.; Yang, S.; Miao, Y.; Wu, Y.; Li, Y.Z.; Ren, Y.; Sui, Y.; Qi, J.; Han, J. A High-Nickel Layered Double Hydroxides Cathode Boosting the Rate Capability for Chloride Ion Batteries with Ultralong Cycling Life. *Small* **2023**, *19*, 2302896. [CrossRef]
115. Chen, K.; Chen, C.; Long, J.; Zhou, G. MOF/LDH Cross Composites Derived Heterojunction Nanospheres as Highly Efficient Catalysts for ORR-OER and Rechargeable Zn-Air Batteries. *Appl. Surf. Sci.* **2024**, *657*, 159803. [CrossRef]
116. Allwyn, N.; Gokulnath, S.; Sathish, M. In-Situ Nanoarchitectonics of Fe/Co LDH over Cobalt-Enriched N-Doped Carbon Cookies as Facile Oxygen Redox Electrocatalysts for High-Rate Rechargeable Zinc–Air Batteries. *ACS Appl. Mater. Interfaces* **2024**, *16*, 20360–20374. [CrossRef] [PubMed]
117. Ogawa, M.; Asai, S. Hydrothermal Synthesis of Layered Double Hydroxide-Deoxycholate Intercalation Compounds. *Chem. Mater.* **2000**, *12*, 3253–3255. [CrossRef]

118. Jiang, F.; Xie, Y.; Zhang, H.; Zhang, L.; Gao, X.; Bai, H.; Yao, F.; Yue, H. Hierarchical Core-Shelled CoMo Layered Double Hydroxide@CuCo₂S₄ Nanowire Arrays/Nickel Foam for Advanced Hybrid Supercapacitors. *J. Colloid. Interface Sci.* **2025**, *677*, 150–157. [CrossRef]
119. Li, R.Y.; Shen, X.Y.; Li, J.; Zhao, D.P.; Zhao, R.D.; Wu, F.F. Enhanced Electrochemical Performance of NiCo-Layered Double Hydroxides: Optimal Synthesis Conditions and Supercapacitor Applications. *Adv. Sustain. Syst.* **2024**, *9*, 2400753. [CrossRef]
120. Zhi, P.X.; Guo, Q.L. Hydrothermal Synthesis of Layered Double Hydroxides (LDHs) from Mixed MgO and Al₂O₃: LDH Formation Mechanism. *Chem. Mater.* **2005**, *17*, 1055–1062. [CrossRef]
121. Ai, L.; Zhang, C.; Meng, L. Adsorption of Methyl Orange from Aqueous Solution on Hydrothermal Synthesized Mg-Al Layered Double Hydroxide. *J. Chem. Eng. Data* **2011**, *56*, 4217–4225. [CrossRef]
122. Knorpp, A.J.; Zawisza, A.; Huangfu, S.; Borzì, A.; Clark, A.H.; Kata, D.; Graule, T.; Stuer, M. Hydrothermal Synthesis of Multi-Cationic High-Entropy Layered Double Hydroxides. *RSC Adv.* **2022**, *12*, 26362–26371. [CrossRef]
123. Rybka, K.; Matusik, J. Exploring Synthesis Approaches, Properties and Applications of Layered Double Hydroxides Derived from Alternative Sources: A Comprehensive Review. *J. Clean. Prod.* **2025**, *498*, 145215. [CrossRef]
124. Sakai, M.; Imagawa, H.; Baba, N. Layered-Double-Hydroxide-Based Ni Catalyst for CO₂ Capture and Methanation. *Appl. Catal. A Gen.* **2022**, *647*, 118904. [CrossRef]
125. Liao, L.; Zhao, N.; Xia, Z. Hydrothermal Synthesis of Mg-Al Layered Double Hydroxides (LDHs) from Natural Brucite and Al(OH)₃. *Mater. Res. Bull.* **2012**, *47*, 3897–3901. [CrossRef]
126. Pan, Y.; Li, L.; Liu, D.; Wang, F.; Xia, M.; Wang, F. Macroscale Structures of Layered Double Hydroxides: A Review of Formation Strategies and Applications in Water Treatment. *J. Environ. Chem. Eng.* **2025**, *13*, 115284. [CrossRef]
127. Cheng, X.; Zhang, L.; Li, L.; Wu, H.; Zheng, J.; Sun, J.; Li, G. One-Step Hydrothermal Synthesis of Glucose-Induced Low Crystallinity NiCo-Based Layered Double Hydroxides for High-Performance Asymmetric Supercapacitors. *Chem. Eur. J.* **2024**, *31*, e202403439. [CrossRef]
128. Zhao, Y.; Xiao, F.; Jiao, Q. Hydrothermal Synthesis of Ni/Al Layered Double Hydroxide Nanorods. *J. Nanotechnol.* **2011**, *2011*, 646409. [CrossRef]
129. Zhang, F.; Du, N.; Song, S.; Liu, J.; Hou, W. Mechano-Hydrothermal Synthesis of Mg₂Al-NO₃ Layered Double Hydroxides. *J. Solid. State Chem.* **2013**, *206*, 45–50. [CrossRef]
130. Clark, I.; Dunne, P.W.; Gomes, R.L.; Lester, E. Continuous Hydrothermal Synthesis of Ca₂Al-NO₃ Layered Double Hydroxides: The Impact of Reactor Temperature, Pressure and NaOH Concentration on Crystal Characteristics. *J. Colloid. Interface Sci.* **2017**, *504*, 492–499. [CrossRef] [PubMed]
131. Wang, W.; Zhou, J.; Achari, G.; Yu, J.; Cai, W. Cr(VI) Removal from Aqueous Solutions by Hydrothermal Synthetic Layered Double Hydroxides: Adsorption Performance, Coexisting Anions and Regeneration Studies. *Colloids Surf. A Physicochem. Eng. Asp.* **2014**, *457*, 33–40. [CrossRef]
132. Tung, N.Q.; Van, D.T.C.; Thang, D.X.; An, N.T.K.; Trang, T.T.; Nhi, B.D.; Thao, N.P.; Son, L.T.; Huy, N.N.; Dung, N.T. Hydrothermal Synthesis of CuCoFe Layered Double Hydroxide and Its Performance in the Degradation of Antibiotics: Influencing Factors, Degradation Pathways, and Reaction Mechanism. *J. Environ. Chem. Eng.* **2023**, *11*, 110127. [CrossRef]
133. Prevot, V.; Caperaa, N.; Taviot-Guého, C.; Forano, C. Glycine-Assisted Hydrothermal Synthesis of NiAl-Layered Double Hydroxide Nanostructures. *Cryst. Growth Des.* **2009**, *9*, 3646–3654. [CrossRef]
134. Xiong, Q.; Li, X.; Zhou, M.; Chen, R.; Sun, C.; Zhou, Y.; Wang, S.; Qiu, X.; Song, M.; Wei, T. One-Pot Hydrothermal Synthesis of Flower-Shaped Zif-67@NiCo-LDH Heterostructure as Anode Materials for Lithium-Ion Batteries. *Ionics* **2023**, *29*, 1741–1749. [CrossRef]
135. Zhu, L.; Han, T.; Ding, Y.; Long, J.; Lin, X.; Liu, J. A Metal–Organic-Framework Derived NiFe₂O₄@NiCo-LDH Nanocube as High-Performance Lithium-Ion Battery Anode under Different Temperatures. *Appl. Surf. Sci.* **2022**, *599*, 153953. [CrossRef]
136. Luo, K.; Li, Y.; Yao, J.; Huang, B.; Zhu, Q.; Yang, J. Boosting the Lithium Storage Property of Nickel-Zinc Layered Double Hydroxides by Intercalation with Dodecyl Sulfate Anions. *Appl. Surf. Sci.* **2023**, *620*, 156850. [CrossRef]
137. Liu, Y.; Zhou, X.; Chen, P.; Cao, X.; Liu, D.; Wang, R. Properties of Hollow Yolk-Shell NiS₂/FeS₂@NC@NiFe LDH/FeO(OH) Nanoflower Microspheres as Anode Materials for Lithium-Ion Batteries. *J. Electroanal. Chem.* **2023**, *943*, 117606. [CrossRef]
138. Yang, T.; Zhang, Z.; Ma, P.; Li, H. Constructing 1D/2D NiCo-LDH Nanowire/MXene Composites for Efficient and Stable Lithium Storage. *Adv. Mater. Interfaces* **2024**, *11*, 2300962. [CrossRef]
139. Shah, S.S.; Aziz, M.A.; Rasool, P.I.; Mohmand, N.Z.K.; Khan, A.J.; Ullah, H.; Feng, X.; Oyama, M. Electrochemical Synergy and Future Prospects: Advancements and Challenges in MXene and MOFs Composites for Hybrid Supercapacitors. *Sustain. Mater. Technol.* **2024**, *39*, e00814. [CrossRef]
140. Yuan, Q.; Zhang, J.; Li, B.; Wu, Y.; Wu, Z.; Dou, Y.; Yin, Q.; Han, J. An MgAl Layered Double Hydroxide as a New Transition Metal-Free Anode for Lithium-Ion Batteries. *Chem. Commun.* **2023**, *59*, 13903–13906. [CrossRef]
141. Zhang, D.; Hua, Y.; Fu, X.; Cheng, C.; Kong, D.; Zhang, M.; Lei, B.; Liu, Z. Hierarchical Flower Array NiCoOOH@CoLa-LDH Nanosheets for High-Performance Supercapacitor and Alkaline Zn Battery. *Adv. Funct. Mater.* **2025**, *35*, e202414686. [CrossRef]

142. Yin, Q.; Song, Z.; Yang, S.; Zhao, Z.; Yuan, Q.; Qi, J.; Sui, Y.; Han, J. Heteroatoms Introduction via Temperature-Differential Doping Strategy Achieves Long-Cycle-Life NiCoMo-P LDH Cathode for Rechargeable Chloride-Ion Battery. *J. Electroanal. Chem.* **2023**, *951*, 117924. [[CrossRef](#)]
143. Zhao, G.; Deng, Z.; Wan, G.; Zhao, J.; Wang, G. Array Structured NiAl-Layered Double Hydroxides Grown on Graphene by Atomic Layer Deposition as Chloride-Ion Battery Cathode. *DeCarbon* **2025**, *8*, 100106. [[CrossRef](#)]
144. Yang, S.; Yin, Q.; Song, Z.; Xu, F.; Xie, Z.; Wu, Y.; Xu, S.; Li, Y.Z.; Zhao, D.; Xiao, B.; et al. Introducing High-Valence Molybdenum to Stimulate Lattice Oxygen in a NiCo LDH Cathode for Chloride Ion Batteries. *Mater. Horiz.* **2023**, *10*, 3429–3437. [[CrossRef](#)] [[PubMed](#)]
145. Wu, Z.; Wu, Y.; Yuan, Q.; Zhang, J.; Dou, Y.; Han, J. Aqueous Chloride-Ion Battery within a Neutral Electrolyte Based on a CoFe-Cl Layered Double Hydroxide Anode. *ACS Appl. Mater. Interfaces* **2023**, *15*, 38540–38549. [[CrossRef](#)]
146. Li, J.; Qin, Y.; Bai, Z.; Li, S.; Li, L.; Ouyang, B.; Kan, E.; Zhang, W. Investigating the Role of 3D Hierarchical Ni-CAT/NiFe-LDH/CNFs in Enhancing the Oxygen Evolution Reaction and Zn-Air Battery Performance. *Appl. Surf. Sci.* **2024**, *648*, 159080. [[CrossRef](#)]
147. Bhanuse, G.B.; Kumar, S.; Yu, C.C.; Fu, Y.P. Nanostructured ZnCo₂O₄@NiMn-LDH Electrodes for Supercapacitor and Zinc-Air Battery Application. *ACS Appl. Nano Mater.* **2024**, *7*, 13649–13663. [[CrossRef](#)]
148. Jia, Z.; Shang, J.; Xue, K.; Yang, X.; Wang, S.; Xu, C.; Wang, Q. N-doped Nanocarbon Inserted NiCo-LDH Nanoplates on NF with High OER/ORR Performances for Zinc-Air Battery. *ChemCatChem* **2023**, *15*, e202201469. [[CrossRef](#)]
149. Chen, J.; Liu, Z.; Liu, Y.; Cheng, Z.; Zhang, J.; Zhang, Q.; Li, Y.; Hou, C.; Li, K.; Wang, H. Efficient Bifunctional NiFe-LDH@Co₉S₈ Nanoflower Electrocatalysts Anchored with Pt Nanocrystal for Flexible Quasi-Solid Rechargeable Zinc Air Battery. *Energy Fuels* **2024**, *38*, 10264–10274. [[CrossRef](#)]
150. Liu, S.; Wan, R.; Lin, Z.; Liu, Z.; Liu, Y.; Tian, Y.; Qin, D.-D.; Tang, Z. Probing the Co Role in Promoting the OER and Zn–Air Battery Performance of NiFe-LDH: A Combined Experimental and Theoretical Study. *J. Mater. Chem. A Mater.* **2022**, *10*, 5244–5254. [[CrossRef](#)]
151. Dighe, P.S.; Redekar, R.S.; Tarwal, N.L.; Sarawade, P.B. Design and Development of the High-Performance Aqueous Asymmetric Supercapacitor Based on the Hydrothermally Grown Binder-Less Ni-Co LDH Nanosheets. *J. Energy Storage* **2024**, *88*, 111467. [[CrossRef](#)]
152. Chandra Sahoo, R.; Moolayadukkam, S.; Seok, J.H.; Lee, S.U.; Matte, H.S.S.R. Enhanced Charge Storage Capacity and High Rate Capabilities of Ni₂Co-Layered Double Hydroxides/Expanded-Graphite Composites as Anodes for Li-Ion Batteries. *J. Mater. Chem. A Mater.* **2023**, *11*, 7142–7151. [[CrossRef](#)]
153. Li, X.; Fortunato, M.; Cardinale, A.M.; Sarapulova, A.; Njel, C.; Dsoke, S. Electrochemical Study on Nickel Aluminum Layered Double Hydroxides as High-Performance Electrode Material for Lithium-Ion Batteries Based on Sodium Alginate Binder. *J. Solid. State Electrochem.* **2022**, *26*, 49–61. [[CrossRef](#)]
154. Du, P.; Xi, W.; Zhang, Y.; Wang, R.; Gong, Y.; He, B.; Wang, H.; Jin, J. Laser Induction of Hierarchically Micro/Nanostructured CoNi-LDH/C Composite for High-Performance Lithium-Sulfur Batteries. *J. Alloys Compd.* **2024**, *985*, 174043. [[CrossRef](#)]
155. Ye, Z.; Zhai, S.; Liu, R.; Liu, M.; Xu, Y.; Li, C.; Wang, X.; Mei, T. Sulfonate-Rich Polymer Intercalated LDH Artificial SEI Film to Enable High-Stability Li-S Batteries. *Chem. Eng. J.* **2024**, *479*, 147847. [[CrossRef](#)]
156. Zhen, M.; Meng, X.; Wang, X.; Zhang, Z.; Guo, S.-Q.; Hu, Z.; Shen, B. Layered Double Hydroxides-MXene Heterointerfaces with Abundant Anion Vacancies Expediting Sulfur Redox Kinetics for High-Performance Lithium–Sulfur Batteries. *Chem. Eng. J.* **2024**, *489*, 151285. [[CrossRef](#)]
157. Liu, Q.; Zhang, Y.; Zhou, Y.; Wang, M.; Li, R.; Yue, W. Layered Double Hydroxides Used as the Sulfur Hosts for Lithium-Sulfur Batteries and the Influence of Metal Composition on Their Performance. *J. Solid. State Electrochem.* **2023**, *27*, 797–807. [[CrossRef](#)]
158. Wang, H.Y.; Dai, Y.K.; Liao, K.M.; Deng, S.; Dai, G.P. Vertical Graphene Growth on LDH Nanosheets and Carbon Cloth Nanofibers with NiCo Nanoparticles as a Freestanding Host for High-Performance Lithium-Sulfur Batteries. *J. Phys. Chem. Lett.* **2025**, *16*, 1103–1113. [[CrossRef](#)]
159. Zhang, Y.; Zhang, Y.; Ma, L.; Yang, M.; Zhao, X. NiCr-Cl LDH/RGO Composite as Anode Material for Sodium-Ion Batteries. *J. Electron. Mater.* **2022**, *51*, 6067–6075. [[CrossRef](#)]
160. Li, B.; Li, J.; Li, P.; Zhang, N.; Shang, H.; Zhang, B. Sulfide Hollow ZIF-67 and NiCo-LDH Heterostructure for Superior Asymmetric Supercapacitors. *J. Alloys Compd.* **2025**, *1017*, 179128. [[CrossRef](#)]
161. He, L.; Cai, P.; Lai, H.; Lu, K.; Xu, Z.; Zeng, R.; Hao, C.; Wang, Z.; Gan, W. Sandwich-like NiFe-LDH/MnCO₃/MXene Ternary Nanocomposites Serve as Battery-Type Electrode for High-Performance Asymmetric Supercapacitor. *Chem. Eng. J.* **2025**, *504*, 159149. [[CrossRef](#)]
162. Liu, Y.; Wang, C.; Sun, H.; Duan, L.; Yang, Z.; Wang, X.; Liu, J. Construction of Flexible MnCo₂O₄@FeCoNi-LDH Electrode Materials with Nanoflower-like and Hierarchical Structure for High-Performance Asymmetric Supercapacitor. *J. Colloid. Interface Sci.* **2025**, *682*, 1051–1061. [[CrossRef](#)]

163. Tai, P.C.; Chung, R.J.; Wang, G.B.; Kongvarhodom, C.; Husain, S.; Yougbaré, S.; Chen, H.M.; Wu, Y.F.; Lin, L.Y. Polydopamine Derived Carbon Coated Cobalt Molybdenum Layered Double Hydroxide as Highly Stable Anode Materials of Sodium-Ion Battery. *J. Energy Storage* **2024**, *101*, 113961. [[CrossRef](#)]
164. Lin, Q.; Yuan, Z.; Wang, D.; Wei, W.; Wang, X.; Han, W.; Wang, L. Co-Co LDH-Derived CoSe₂ Anchored on N-Doped Carbon Nanospheres as High-Performance Anodes for Sodium-Ion Batteries. *Electrochim. Acta* **2022**, *432*, 141012. [[CrossRef](#)]
165. Ma, X.; Zhou, L.; Chen, T.; Sun, P.; Lv, X.; Yu, H.; Sun, X.; Leo Liu, T. High-Performance Aqueous Rechargeable NiCo//Zn Battery with Molybdate Anion Intercalated CoNi-LDH@CP Bilayered Cathode. *J. Colloid. Interface Sci.* **2024**, *658*, 728–738. [[CrossRef](#)]
166. Wang, C.; Han, L.; Yang, S.; Liu, Z.; Liu, M.; Li, B. Nanosheet-Structured ZnCo-LDH Microsphere as Active Material for Rechargeable Zinc Batteries. *J. Colloid. Interface Sci.* **2024**, *659*, 119–126. [[CrossRef](#)] [[PubMed](#)]
167. Zhang, Y.; Hu, S.; Li, C.; Yan, X.; Zhang, Y.; Yin, R.; Wei, Y.; Gao, K.; Gao, H. Advanced Strategies for Enhancing Electrochemical Performance of NiAl LDH Electrodes in Supercapacitors. *Coord. Chem. Rev.* **2025**, *531*, 216497. [[CrossRef](#)]
168. Jing, C.; Huang, L.; Tao, S.; Chen, Y.; Zhang, S.; Dong, W.; Ling, F.; Tang, X.; Li, Y.; Feng, L.; et al. Construction of MoB@LDH Heterojunction and Its Derivatives through Phase and Interface Engineering for Advanced Supercapacitor Applications. *J. Colloid. Interface Sci.* **2024**, *660*, 10–20. [[CrossRef](#)]
169. Tai, P.-Y.; Sakthivel, M.; Peng, Y.-J.; Kubendhiran, S.; Lin, L.-Y.; Ho, K.-C. In Situ Growing Te-Doped Ni-Mn Layered Double Hydroxide on a Cetyltrimethylammonium Bromide-Modified MXene Conductive Layer for Binder-Free Supercapacitors. *ACS Appl. Energy Mater.* **2025**, *8*, 4122–4133. [[CrossRef](#)]
170. Han, X.; Li, J.; Lu, J.; Luo, S.; Wan, J.; Li, B.; Hu, C.; Cheng, X. High Mass-Loading NiCo-LDH Nanosheet Arrays Grown on Carbon Cloth by Electrodeposition for Excellent Electrochemical Energy Storage. *Nano Energy* **2021**, *86*, 106079. [[CrossRef](#)]
171. He, T.-L.; Zhang, X.-R.; Ma, Q.-L.; Hua, W.-M.; Xiong, H.-M. Positive Carbon Dots Induced Electrodeposition of NiCo-LDH Nanosheets for High-Performance Supercapacitors. *ACS Appl. Energy Mater.* **2024**, *7*, 5508–5516. [[CrossRef](#)]
172. Niu, Y.; Chang, L.; Huang, Y.; Sun, Q.; Lu, X.; Cheng, H. Electrochemical Constructing Versatile ZnAl-LDH Artificial Interface Layer Coated (002)-Textured Zn for Highly Reversible Zinc Anodes. *Chem. Eng. J.* **2024**, *499*, 155813. [[CrossRef](#)]
173. Lashgari, M.; Yamini, Y. Fiber-in-tube Solid-phase Microextraction of Caffeine as a Molecular Tracer in Wastewater by Electrochemically Deposited Layered Double Hydroxide. *J. Sep. Sci.* **2018**, *41*, 2393–2400. [[CrossRef](#)]
174. Seumo Tchekwagep, P.M.; Banks, C.E.; Crapnell, R.D.; Farsak, M.; Kardaş, G. Electrochemical Synthesis of NiCo Layered Double Hydroxides on Nickel-Coated Graphite for Water Splitting: Understanding the Electrochemical Experimental Parameters. *RSC Adv.* **2025**, *15*, 3969–3978. [[CrossRef](#)] [[PubMed](#)]
175. Cysewska, K.; Zając, M.; Łapiński, M.; Karczewski, J.; Rybczyk, M.K.; Kamecki, B.; Jasiński, P.; Molin, S. The Effect of Cobalt Incorporation into Nickel–Iron Oxide/(oxy)Hydroxide Catalyst on Electrocatalytic Performance Toward Oxygen Evolution Reaction. *Energy Technol.* **2021**, *9*, 2100688. [[CrossRef](#)]
176. Wu, Q.; Li, F.; Sheng, H.; Qi, Y.; Yuan, J.; Bi, H.; Li, W.; Xie, E.; Lan, W. In Situ Fabrication of Hierarchical CuO@CoNi-LDH Composite Structures for High-Performance Supercapacitors. *ACS Appl. Mater. Interfaces* **2024**, *16*, 23241–23252. [[CrossRef](#)]
177. Kim, Y.; Jun, S.E.; Lee, G.; Nam, S.; Jang, H.W.; Park, S.H.; Kwon, K.C. Recent Advances in Water-Splitting Electrocatalysts Based on Electrodeposition. *Materials* **2023**, *16*, 3044. [[CrossRef](#)] [[PubMed](#)]
178. Pawar, S.A.; Yu, S.; Ju, E.; Seo, H.; Yeu, J.; Kim, J.; Patil, D.S.; Shin, J.C. Zinc Cobalt Layered Double Hydroxide Electrode for High-Performance Supercapacitor. *Appl. Sci. Converg. Technol.* **2019**, *28*, 164–168. [[CrossRef](#)]
179. Arbenin, A.Y.; Zemtsova, E.G.; Orehov, E.V.; Sokolova, D.N.; Baburova, P.I.; Petrov, A.A.; Gaishun, V.E.; Smirnov, V.M. Features of Fabrication of Titanium Dioxide Based Coatings for Non-Lithographic Template Electrochemical Synthesis of Micron Metal Particle Arrays. *Gels* **2021**, *7*, 202. [[CrossRef](#)] [[PubMed](#)]
180. Guo, H.; Guan, Y.; Zhang, M.; Qin, J.; Guo, X.; Li, Z.; Zhang, B.; Tang, J. Dynamic Morphological Evolution of Co-Based Layered Double Hydroxide Nanosheets Investigated by In Situ Electrochemical-Atomic Force Microscopy. *J. Phys. Chem. C* **2023**, *127*, 5219–5229. [[CrossRef](#)]
181. Wang, T.; Wang, W.; Shao, W.; Bai, M.; Zhou, M.; Li, S.; Ma, T.; Ma, L.; Cheng, C.; Liu, X. Synthesis and Electronic Modulation of Nanostructured Layered Double Hydroxides for Efficient Electrochemical Oxygen Evolution. *ChemSusChem* **2021**, *14*, 5112–5134. [[CrossRef](#)]
182. Ramachandran, R.; Lan, Y.; Xu, Z.X.; Wang, F. Construction of NiCo-Layered Double Hydroxide Microspheres from Ni-MOFs for High-Performance Asymmetric Supercapacitors. *ACS Appl. Energy Mater.* **2020**, *3*, 6633–6643. [[CrossRef](#)]
183. Shahid, N.F.; Jamal, A.; Haq, G.; Javed, M.; Saifullah, M.; Anjum, M.A.R. Cobalt–Iron Layered Double Hydroxide Nanosheet-Wrapped Nitrogen-Doped Graphite Felt as an Oxygen-Evolving Electrode. *Energy Adv.* **2023**, *2*, 2109–2118. [[CrossRef](#)]
184. Ren, B.; Zhang, B.Y.; Zhang, H.; Jiang, X.; Yi, Q.; Xu, K.; Yu, H.; Hu, Z.; Jeerapan, I.; Ou, J.Z. CoNi Layered Double Hydroxide Nanosheets Vertically Grown on Electrodeposited Dendritic Copper Substrates for Supercapacitor Applications. *ACS Appl. Nano Mater.* **2022**, *5*, 2395–2404. [[CrossRef](#)]

185. Zhang, H.; Li, X.; Hähnel, A.; Naumann, V.; Lin, C.; Azimi, S.; Schweizer, S.L.; Maijenburg, A.W.; Wehrspohn, R.B. Bifunctional Heterostructure Assembly of NiFe LDH Nanosheets on NiCoP Nanowires for Highly Efficient and Stable Overall Water Splitting. *Adv. Funct. Mater.* **2018**, *28*, 1706847. [[CrossRef](#)]
186. Iqbal, M.A.; Sun, L.; LaChance, A.M.; Ding, H.; Fedel, M. In Situ Growth of a CaAl-NO₃⁻-Layered Double Hydroxide Film Directly on an Aluminum Alloy for Corrosion Resistance. *Dalton Trans.* **2020**, *49*, 3956–3964. [[CrossRef](#)] [[PubMed](#)]
187. Gualandi, I.; Vlamilidis, Y.; Mazzei, L.; Musella, E.; Giorgetti, M.; Christian, M.; Morandi, V.; Scavetta, E.; Tonelli, D. Ni/Al Layered Double Hydroxide and Carbon Nanomaterial Composites for Glucose Sensing. *ACS Appl. Nano Mater.* **2019**, *2*, 143–155. [[CrossRef](#)]
188. Alsaç, E.P.; Zhou, K.; Rong, W.; Salamon, S.; Landers, J.; Wende, H.; Smith, R.D.L. Identification of Non-Traditional Coordination Environments for Iron Ions in Nickel Hydroxide Lattices. *Energy Environ. Sci.* **2022**, *15*, 2638–2652. [[CrossRef](#)]
189. Shi, Z.; Yuan, Y.; Xiao, Q.; Li, Z.; Zhu, J. Carbonate Doped NiCo-LDH Modified with PANI for High Performance Asymmetric Supercapacitors. *CrystEngComm* **2022**, *24*, 3546–3555. [[CrossRef](#)]
190. Tan, Z.; Luo, X.; Wei, T.; Zhang, F.; Lv, Y.; Chen, L.; Shi, Y. In Situ Formation of NiAl-Layered Double Hydroxide with a Tunable Interlayer Spacing in a Confined Impinging Jet Microreactor. *Energy Fuels* **2020**, *34*, 8939–8946. [[CrossRef](#)]
191. Yan, Z.; Sun, H.; Chen, X.; Liu, H.; Zhao, Y.; Li, H.; Xie, W.; Cheng, F.; Chen, J. Anion Insertion Enhanced Electrodeposition of Robust Metal Hydroxide/Oxide Electrodes for Oxygen Evolution. *Nat. Commun.* **2018**, *9*, 2373. [[CrossRef](#)]
192. Ghadimi, A.M.; Ghasemi, S.; Omrani, A.; Mousavi, F. Nickel Cobalt LDH/Graphene Film on Nickel-Foam-Supported Ternary Transition Metal Oxides for Supercapacitor Applications. *Energy Fuels* **2023**, *37*, 3121–3133. [[CrossRef](#)]
193. Cysewska, K.; Rybarczyk, M.K.; Cempura, G.; Karczewski, J.; Łapiński, M.; Jasinski, P.; Molin, S. The Influence of the Electrodeposition Parameters on the Properties of Mn-Co-Based Nanofilms as Anode Materials for Alkaline Electrolysers. *Materials* **2020**, *13*, 2662. [[CrossRef](#)] [[PubMed](#)]
194. Kumar, M.; Singh, R.P. Transforming Prussian Blue Analogues: The Future-Centric Pathway to Rise of Thin Layered Double Hydroxides for Superior Water Oxidation: An Overview. *Int. J. Multidiscip. Res.* **2024**, *6*, 240529213. [[CrossRef](#)]
195. Yang, Q.; Wang, Q.; Long, Y.; Wang, F.; Wu, L.; Pan, J.; Han, J.; Lei, Y.; Shi, W.; Song, S. In Situ Formation of Co₉S₈ Quantum Dots in MOF-Derived Ternary Metal Layered Double Hydroxide Nanoarrays for High-Performance Hybrid Supercapacitors. *Adv. Energy Mater.* **2020**, *10*, 1903193. [[CrossRef](#)]
196. Li, Z.; Han, F.; Li, C.; Jiao, X.; Chen, D. Multi-Anion Intercalated Layered Double Hydroxide Nanosheet-Assembled Hollow Nanoprisms with Improved Pseudocapacitive and Electrocatalytic Properties. *Chem. Asian J.* **2018**, *13*, 1129–1137. [[CrossRef](#)]
197. Li, S.; Mo, T.; Chen, L.; Zhang, F.; Jamil, S.; Lu, Y.; Cai, Q. Hierarchical MgAl-Layered Double Hydroxide Growth on Porous MgO Template for Pollution Removal. *Environ. Prog. Sustain. Energy* **2022**, *41*, e13907. [[CrossRef](#)]
198. Wei, M.; Huang, Q.; Zhou, Y.; Peng, Z.; Chu, W. Ultrathin Nanosheets of Cobalt-Nickel Hydroxides Hetero-Structure via Electrodeposition and Precursor Adjustment with Excellent Performance for Supercapacitor. *J. Energy Chem.* **2018**, *27*, 591–599. [[CrossRef](#)]
199. Chavan, H.S.; Lee, C.H.; Inamdar, A.I.; Han, J.; Park, S.; Cho, S.; Shreshta, N.K.; Lee, S.U.; Hou, B.; Im, H.; et al. Designing and Tuning the Electronic Structure of Nickel–Vanadium Layered Double Hydroxides for Highly Efficient Oxygen Evolution Electrocatalysis. *ACS Catal.* **2022**, *12*, 3821–3831. [[CrossRef](#)]
200. Zhai, P.; Xia, M.; Wu, Y.; Zhang, G.; Gao, J.; Zhang, B.; Cao, S.; Zhang, Y.; Li, Z.; Fan, Z.; et al. Engineering Single-Atomic Ruthenium Catalytic Sites on Defective Nickel-Iron Layered Double Hydroxide for Overall Water Splitting. *Nat. Commun.* **2021**, *12*, 4587. [[CrossRef](#)]
201. Wang, G.; Liu, G.; Jin, Z. In Situ Coupled Nickel-Based Layered Double Hydroxides with MXene to Enhance Supercapacitor Performance. *J. Mater. Chem. C Mater.* **2023**, *11*, 10547–10561. [[CrossRef](#)]
202. Laipan, M.; Yu, J.; Zhu, R.; Zhu, J.; Smith, A.T.; He, H.; O'Hare, D.; Sun, L. Functionalized Layered Double Hydroxides for Innovative Applications. *Mater. Horiz.* **2020**, *7*, 715–745. [[CrossRef](#)]
203. Chen, Z.; Zhu, J.; Yang, S.; Wei, Z.; Wang, Y.; Chen, A.; Huang, Z.; Zhi, C. MXene Supported Electrodeposition Engineering of Layer Double Hydroxide for Alkaline Zinc Batteries. *Angew. Chem. Int. Ed.* **2024**, *63*, e202411443. [[CrossRef](#)]
204. Cheng, X.; Wu, D.; Gao, H.; Wang, Q.; Lv, P.; Yoon, S.S.; Wei, Q. A Mild, Configurable, Flexible CoNi-LDH(v)/Zn Battery Based on H-Vacancy-Induced Reversible Zn²⁺ Intercalation. *J. Energy Chem.* **2025**, *100*, 498–508. [[CrossRef](#)]
205. Inamdar, A.I.; Chavan, H.S.; Jo, Y.; Im, H.; Kim, H. Nonprecious Bimetallic NiFe-layered Hydroxide Nanosheets as a Catalyst for Highly Efficient Electrochemical Water Splitting. *Int. J. Energy Res.* **2021**, *45*, 16963–16972. [[CrossRef](#)]
206. Li, H.; Zhao, R.; Zhou, W.; Wang, L.; Li, W.; Zhao, D.; Chao, D. Trade-off between Zincophilicity and Zincophobicity: Toward Stable Zn-Based Aqueous Batteries. *JACS Au* **2023**, *3*, 2107–2116. [[CrossRef](#)]
207. Meng, J.; Song, Y.; Qin, Z.; Wang, Z.; Mu, X.; Wang, J.; Liu, X.X. Cobalt–Nickel Double Hydroxide toward Mild Aqueous Zinc-Ion Batteries. *Adv. Funct. Mater.* **2022**, *32*, 2204026. [[CrossRef](#)]

208. Dai, L.; Peng, S.; Wang, X.; Chen, B.; Wu, Y.; Xie, Q.; Ruan, Y. Three-Dimensional NiCoS Nanotubes@NiCo-LDH Nanosheets Core–Shell Heterostructure for High-Rate Capability Alkaline Zinc-Based Batteries. *RSC Adv.* **2024**, *14*, 7999–8006. [CrossRef] [PubMed]
209. Zhou, K.; Wang, S.; Zhong, G.; Chen, J.; Bao, Y.; Niu, L. Hierarchical Heterostructure Engineering of Layered Double Hydroxides on Nickel Sulfides Heteronanowire Arrays as Efficient Cathode for Alkaline Aqueous Zinc Batteries. *Small* **2022**, *18*, 2202799. [CrossRef]
210. Cai, X.; Jiang, T.; Wu, M. Confined Growth of NiFe LDH with Hierarchical Structures on Copper Nanowires for Long-Term Stable Rechargeable Zn-Air Batteries. *Appl. Surf. Sci.* **2022**, *577*, 151911. [CrossRef]
211. Zhou, P.; Ji, Y.; Zhang, B.; Zhang, P.; Zhang, S.; Wang, S. Rational Construction of Tremella-like CuCo LDH@Ni₃S₂ Nanocomposites as High-Performance Supercapacitor Electrode Materials. *J. Alloys Compd.* **2025**, *1021*, 179586. [CrossRef]
212. Xing, H.; Deng, X.; Wang, X. Alkaline Capacity Decay Induced Vacancy-Rich LDH for High-Performance Magnesium Ions Hybrid Supercapacitor. *J. Colloid. Interface Sci.* **2025**, *679*, 43–53. [CrossRef]
213. Khalafallah, D.; Ibrahim, M.A.; Hou, H.; Wang, J.; Liu, C.; Zhang, Q. Configuring Cations–Doped Cobalt Lanthanum LDH Nanoarray-on-Nanoarray Platforms for Supercapacitors. *Sustain. Mater. Technol.* **2025**, *43*, e01286. [CrossRef]
214. Duddi, R.; Shivani; Dhiman, S.; Kumar Singh, A.; Kamboj, N.; Kumar, S. Superior Cycle Stability and Enhanced Pseudocapacitive Performance of NiAl-LDH Decorated Carbon Cloth for Supercapacitor Application. *Appl. Surf. Sci.* **2025**, *679*, 161298. [CrossRef]
215. Mazloum-Ardakani, M.; Mozaffari, S.A.; Rasche, B.; Ebrahimi, F. Bio-Inspired Coral Reef-like NiCo-LDH Nanostructure Fabricated on Carbon Felt for High Performance Flexible Supercapacitor. *Sci. Rep.* **2025**, *15*, 10542. [CrossRef] [PubMed]
216. Klydziate, G.; Gliaudyte, L.; Sokol, D.; Vasiliauskiene, D.; Yang, T.C.-K.; Kareiva, A. Layered Double Hydroxides: Sol-Gel Synthesis, Characterization and Application. *Preprint* **2024**. [CrossRef]
217. Valente, J.S.; Lima, E.; Toledo-Antonio, J.A.; Cortes-Jacome, M.A.; Lartundo-Rojas, L.; Montiel, R.; Prince, J. Comprehending the Thermal Decomposition and Reconstruction Process of Sol–Gel MgAl Layered Double Hydroxides. *J. Phys. Chem. C* **2010**, *114*, 2089–2099. [CrossRef]
218. Mallakpour, S.; Dinari, M.; Behranvand, V. Ultrasonic-Assisted Synthesis and Characterization of Layered Double Hydroxides Intercalated with Bioactive N,N’-(Pyromellitoyl)-Bis-L-α-Amino Acids. *RSC Adv.* **2013**, *3*, 23303–23308. [CrossRef]
219. Sokol, D.; Vieira, D.E.L.; Zarkov, A.; Ferreira, M.G.S.; Beganskiene, A.; Rubanik, V.V.; Shilin, A.D.; Kareiva, A.; Salak, A.N. Sonication Accelerated Formation of Mg-Al-Phosphate Layered Double Hydroxide via Sol-Gel Prepared Mixed Metal Oxides. *Sci. Rep.* **2019**, *9*, 10419. [CrossRef]
220. Butenko, E.; Malyshev, A.; Kapustin, A. LDHs as Adsorbents of Phenol and Their Environmental Applications. *Am. J. Environ. Prot.* **2014**, *2*, 11–15. [CrossRef]
221. Mahjoubi, F.Z.; Khalidi, A.; Abdennouri, M.; Barka, N. Zn–Al Layered Double Hydroxides Intercalated with Carbonate, Nitrate, Chloride and Sulphate Ions: Synthesis, Characterisation and Dye Removal Properties. *J. Taibah Univ. Sci.* **2017**, *11*, 90–100. [CrossRef]
222. Shan, X.; Guo, Z.; Zhang, C.; Wang, W.; Zhao, L. Nickel Aerogel @ Ultra-Thin NiCo-LDH Nanosheets Integrated Freestanding Film as a Collaborative Adsorption and Accelerated Conversion Cathode to Improve the Rate Performance of Lithium Sulfur Batteries. *Chem. Eng. J.* **2024**, *488*, 151105. [CrossRef]
223. Yang, Y.; Ma, S.; Xia, M.; Guo, Y.; Zhang, Y.; Liu, L.; Zhou, C.; Chen, G.; Wang, X.; Wu, Q.; et al. Elaborately Converting Hierarchical NiCo-LDH to Rod-like LDH-Decorated MOF as Interlayer for High-Performance Lithium–Sulfur Battery. *Mater. Today Phys.* **2023**, *35*, 101112. [CrossRef]
224. Li, J.; Qiu, W.; Liu, X.; Zhang, Y.; Zhao, Y. NiCo-Layered Double Hydroxide to Composite with Sulfur as Cathodes for High-Performance Lithium-Sulfur Batteries. *ChemElectroChem* **2022**, *9*, e202101211. [CrossRef]
225. Chen, Q.; Zhou, J.; Zhu, Y.; Jin, C.; Zhang, J.; Wu, Y.; Tang, W. In Situ Transformation of LDH into NiCo₂S₄-NiS₂ Nano-Heterostructures on Hollow Carbon Boxes to Promote Sulfur Electrochemistry for High-Performance Lithium-Sulfur Batteries. *Energy Fuels* **2023**, *37*, 4711–4719. [CrossRef]
226. Li, M.; Li, Y.; Cu, Q.; Li, Y.; Li, H.; Li, Z.; Li, M.; Liao, H.; Li, G.; Li, G.; et al. Hollow and Hierarchical CuCo-LDH Nanocatalyst for Boosting Sulfur Electrochemistry in Li-S Batteries. *Energy Mater. Adv.* **2023**, *4*, 0032. [CrossRef]
227. Dong, H.; Qi, S.; Wang, L.; Chen, X.; Xiao, Y.; Wang, Y.; Sun, B.; Wang, G.; Chen, S. Conductive Polymer Coated Layered Double Hydroxide as a Novel Sulfur Reservoir for Flexible Lithium-Sulfur Batteries. *Small* **2023**, *19*, 2300843. [CrossRef]
228. Wu, Y.; Yang, S.; Liu, K.; Li, Q.; Wang, H.; Jiang, J. New Anode Materials for Sodium-Ion Batteries: Ni_xCa_{2-x}Al-Cl LDH and Co_yCa_{2-y}Al-Cl LDH Prepared from Dechlorination Wastes. *J. Energy Storage* **2024**, *101*, 113991. [CrossRef]
229. Li, Y.; Xu, C.; Li, D.; Zhang, Y.; Ni, G.; Xu, S.; Liu, B.; Huo, P. Sodium-Ion Batteries Enabled by CoSn-LDH Microspheres Anchored on Few-Layer Ti₃C₂ MXene. *ACS Appl. Nano Mater.* **2024**, *7*, 20598–20608. [CrossRef]
230. Yin, Q.; Wang, T.; Song, Z.; Yang, S.; Miao, Y.; Wu, Y.; Sui, Y.; Qi, J.; Li, Y.; Zhao, D.; et al. Computational High-Throughput Screening of Layered Double Hydroxides as Cathodes for Chloride Ion Batteries. *Chem. Eng. J.* **2023**, *459*, 141545. [CrossRef]

231. Zhang, G.; Xing, J.; Zhao, Y.; Yang, F. Hierarchical N,P Co-Doped Graphene Aerogels Framework Assembling Vertically Grown CoMn-LDH Nanosheets as Efficient Bifunctional Electrocatalyst for Rechargeable Zinc-Air Battery. *J. Colloid. Interface Sci.* **2021**, *590*, 476–486. [[CrossRef](#)]
232. Bao, E.; Ren, X.; Wang, Y.; Zhang, Z.; Luo, C.; Liu, X.; Xu, C.; Chen, H. Advanced Hybrid Supercapacitors Assembled with CoNi LDH Nanoflowers and Nanosheets as High-Performance Cathode Materials. *J. Energy Storage* **2024**, *82*, 110535. [[CrossRef](#)]
233. Wu, S.; Cai, D.; Tian, Z.; Guo, L.; Wang, Y. One-Step Synthesis of NiCo-MOF@LDH Hybrid Nanosheets for High-Performance Supercapacitor. *J. Energy Storage* **2024**, *89*, 111670. [[CrossRef](#)]
234. Owusu, K.A.; Wang, Z.; Saad, A.; Boakye, F.O.; Mushtaq, M.A.; Tahir, M.; Yasin, G.; Liu, D.; Peng, Z.; Cai, X. Room Temperature Synthesis of Vertically Aligned Amorphous Ultrathin NiCo-LDH Nanosheets Bifunctional Flexible Supercapacitor Electrodes. *Energy Environ. Mater.* **2024**, *7*, e12545. [[CrossRef](#)]
235. Zhang, Y.; Yao, Y.; Ye, H.; Chen, J.; Wan, L.; Du, C.; Zhang, Y.; Xie, M. Gradually Sulfurized Co-Ni LDH as Electrode for Highly-Stable Asymmetric Supercapacitor. *J. Energy Storage* **2024**, *91*, 112117. [[CrossRef](#)]
236. Hu, J.; Pan, Y.; Zhang, Q.; Dong, Z.; Han, S. Constructing Flower-Shaped NiCo₂S₄ @CoAl-LDH Heterojunction Nanosheets Exhibits Extraordinary Electrochemical Behavior for a Light-Assisted Asymmetric Supercapacitor. *Energy Fuels* **2024**, *38*, 6459–6470. [[CrossRef](#)]
237. Zhao, W.; Deng, J.; Li, M.; Du, G.; Fan, M.; Gao, H.; Yuan, Z. Rational Synthesis of Sea Urchin-like NiCo-LDH/Tannin Carbon Microsphere Composites Using Microwave Hydrothermal Technique for High-Performance Asymmetric Supercapacitor. *Adv. Compos. Hybrid. Mater.* **2025**, *8*, 215. [[CrossRef](#)]
238. Kovalenko, V.; Kotok, V.; Murashevych, B. Layered Double Hydroxides as the Unique Product of Target Ionic Construction for Energy, Chemical, Foods, Cosmetics, Medicine and Ecology Applications. *Chem. Rec.* **2024**, *24*, e202300260. [[CrossRef](#)] [[PubMed](#)]
239. Luo, Y.; Yang, Y.; Tian, Y.; Wu, Q.; Lin, W.-F.; Wen, M. Collaborative Reconstruction of FeOOH/FeNiCo-LDH Heterogeneous Nanosheets for Enhancing Anion Exchange Membrane Seawater Electrolysis. *J. Mater. Chem. A Mater.* **2025**, *13*, 7136–7148. [[CrossRef](#)]
240. Yang, L.; Lin, Q.; Guo, D.; Wu, L.; Guan, Z.; Jin, H.; Fang, G.; Chen, X.; Wang, S. Nitrogen Plasma Activates CoMn-Layered Double Hydroxides for Superior Electrochemical Oxygen Evolution. *Inorg. Chem.* **2023**, *62*, 17565–17574. [[CrossRef](#)]
241. Shankar Naik, S.; Theerthagiri, J.; Nogueira, F.S.; Lee, S.J.; Min, A.; Kim, G.-A.; Maia, G.; Pinto, L.M.C.; Choi, M.Y. Dual-Cation-Coordinated CoFe-Layered Double-Hydroxide Nanosheets Using the Pulsed Laser Ablation Technique for Efficient Electrochemical Water Splitting: Mechanistic Screening by In Situ/Operando Raman and Density Functional Theory Calculations. *ACS Catal.* **2023**, *13*, 1477–1491. [[CrossRef](#)]
242. Wu, K.; Shi, L.; Wang, Z.; Zhu, Y.; Tong, X.; He, W.; Wang, J.; Zheng, L.; Kang, Y.; Shan, W.; et al. A General Strategy to Generate Oxygen Vacancies in Bimetallic Layered Double Hydroxides for Water Oxidation. *Chem. Commun.* **2023**, *59*, 3138–3141. [[CrossRef](#)]
243. Zhou, J.; Wang, Y.; Chen, L.; Zhao, W.; Han, L. Precise Design and in Situ Synthesis of Hollow Co₉S₈ @CoNi-LDH Heterostructure for High-Performance Supercapacitors. *Dalton Trans.* **2023**, *52*, 12978–12987. [[CrossRef](#)] [[PubMed](#)]
244. Li, N.; Yang, T.; Huang, L.; Jiang, H.; Xiao, J.; Ma, X.; Lou, H.; Xie, C.; Yang, Y. Interfacial Coupling Engineering Boosting Electrocatalytic Performance of CoFe Layered Double Hydroxide Assembled on N-Doped Porous Carbon Nanosheets for Water Splitting and Flexible Zinc-Air Batteries. *ACS Appl. Mater. Interfaces* **2023**, *15*, 52530–52541. [[CrossRef](#)] [[PubMed](#)]
245. Jiang, H.; Ke, Q.; Qiu, X.; Chen, J.; Chen, P.; Wang, S.; Luo, X.; Rao, B. NiCo Layered Double Hydroxide Nanocages for High-Performance Asymmetric Supercapacitors. *Inorg. Chem. Front.* **2023**, *10*, 2154–2164. [[CrossRef](#)]
246. Zhai, H.; Wu, L.; Yu, L.; Li, L.; Wan, G.; Zhang, Y.; Yuan, X.; Wang, J.; Wang, G. Polypyrrole/NiFe-Layered Double Hydroxide Composite as an Anticorrosive Microwave Absorber. *J. Mater. Chem. C Mater.* **2024**, *12*, 11001–11011. [[CrossRef](#)]
247. Zhang, W.; Zhang, B.; Wang, Y.; Cao, X.; Wang, J.; Lu, W.; Guo, Y. Gelatin-Based Hydrogel Functionalized with Dopamine and Layered Double Hydroxide for Wound Healing. *Gels* **2024**, *10*, 318. [[CrossRef](#)] [[PubMed](#)]
248. Mohammadi Zardkhoshouei, A.; Arian, R.; Hosseiny Davarani, S.S. Tunable Construction of CuS Nanosheets@flower-like ZnCo-Layered Double Hydroxide Nanostructures for Hybrid Supercapacitors. *Ind. Chem. Mater.* **2023**, *1*, 443–457. [[CrossRef](#)]
249. Wang, L.; Li, J.; Meng, Q.; Xiao, M.; Liu, C.; Xing, W.; Zhu, J. Facilitating Active NiOOH Formation via Mo Doping towards High-Efficiency Oxygen Evolution. *Catal. Sci. Technol.* **2024**, *14*, 4166–4173. [[CrossRef](#)]
250. Lin, X.; Wang, Z.; Cao, S.; Hu, Y.; Liu, S.; Chen, X.; Chen, H.; Zhang, X.; Wei, S.; Xu, H.; et al. Bioinspired Trimesic Acid Anchored Electrocatalysts with Unique Static and Dynamic Compatibility for Enhanced Water Oxidation. *Nat. Commun.* **2023**, *14*, 6714. [[CrossRef](#)]
251. Das, J.P.; Nardekar, S.S.; Kesavan, D.; Bhunia, K.; Ravichandran, V.; Kim, S.-J. Unveiling the Effect of Growth Time on Bifunctional Layered Hydroxide Electrodes for High-Performance Energy Storage and Green Energy Conversion. *J. Mater. Chem. A Mater.* **2024**, *12*, 20179–20190. [[CrossRef](#)]
252. Chen, S.; Zheng, Z.; Li, Q.; Wan, H.; Chen, G.; Zhang, N.; Liu, X.; Ma, R. Boosting Electrocatalytic Water Oxidation of NiFe Layered Double Hydroxide via the Synergy of 3d–4f Electron Interaction and Citrate Intercalation. *J. Mater. Chem. A Mater.* **2023**, *11*, 1944–1953. [[CrossRef](#)]

253. Matsuda, K.; Okuda, A.; Kawashimo, M.; Fukuzaki, R.; Iio, N.; Tarutani, N.; Katagiri, K.; Inumaru, K. Molecular-Level Pictures of Chemical and Structural Transformations of Mg–Al Layered Double Hydroxide Crystals ($Mg/Al = 2$) at Elevated Temperatures. *J. Phys. Chem. C* **2023**, *127*, 12599–12605. [[CrossRef](#)]
254. Dillenburger, J.D.; Schulte, L.; Mahale, P.; Suleiman, M.; Mallouk, T.E. Anion-Dependent Structure, Dehydration, and Hydroxide Ion Conductivity of Magnesium Aluminum Layered Double Hydroxides. *Chem. Mater.* **2023**, *35*, 6437–6446. [[CrossRef](#)]
255. Fang, J.; Wen, D.; Zhang, Z.; Zheng, D.; Meng, A.; Su, Y.; Zhou, S. CoNiMn-Layered Double Hydroxide/Ti₃C₂T_x Nanosheet Composites for Enhanced Pseudocapacitive Performance. *J. Phys. Conf. Ser.* **2023**, *2566*, 012004. [[CrossRef](#)]
256. Zou, L.; Sun, S.; Zhang, C.; Zhao, X. NiTi-Layered Double Hydroxide@Carbon Nanotube as a Cathode Material for Chloride-Ion Batteries. *Nanomaterials* **2023**, *13*, 2779. [[CrossRef](#)] [[PubMed](#)]
257. Bai, X.; Liu, Q.; Lu, Z.; Liu, J.; Chen, R.; Li, R.; Song, D.; Jing, X.; Liu, P.; Wang, J. Rational Design of Sandwiched Ni-Co Layered Double Hydroxides Hollow Nanocages/Graphene Derived from Metal-Organic Framework for Sustainable Energy Storage. *ACS Sustain. Chem. Eng.* **2017**, *5*, 9923–9934. [[CrossRef](#)]
258. Xu, J.; Tang, R.; Liu, M.; Xie, S.; Zhang, D.; Kong, X.; Jin, S.; Ji, H.; Zhang, T. Enhancing the Catalytic Activity of Layered Double Hydroxide Supported on Graphene for Lithium–Sulfur Redox Reactions. *Batteries* **2022**, *8*, 200. [[CrossRef](#)]
259. Hu, J.; Yuan, C.; Zhi, L.; Zhang, H.; Yuan, Z.; Li, X. In Situ Defect-Free Vertically Aligned Layered Double Hydroxide Composite Membrane for High Areal Capacity and Long-Cycle Zinc-Based Flow Battery. *Adv. Funct. Mater.* **2021**, *31*, 2102167. [[CrossRef](#)]
260. Zhang, D.; Cao, J.; Zhang, X.; Insin, N.; Wang, S.; Han, J.; Zhao, Y.; Qin, J.; Huang, Y. Inhibition of Manganese Dissolution in Mn₂O₃ Cathode with Controllable Ni²⁺ Incorporation for High-Performance Zinc Ion Battery. *Adv. Funct. Mater.* **2021**, *31*, 2009412. [[CrossRef](#)]
261. Yan, Z.; Wang, E.; Gao, J.; Yang, J.; Wu, C.; Jiang, L.; Zhu, M.; Sun, G. An Exceptionally Facile Synthesis of Highly Efficient Oxygen Evolution Electrodes for Zinc-Oxygen Batteries. *ChemElectroChem* **2017**, *4*, 2190–2195. [[CrossRef](#)]
262. Gao, Z.; Wang, J.; Li, Z.; Yang, W.; Wang, B.; Hou, M.; He, Y.; Liu, Q.; Mann, T.; Yang, P.; et al. Graphene Nanosheet/Ni²⁺/Al³⁺ Layered Double-Hydroxide Composite as a Novel Electrode for a Supercapacitor. *Chem. Mater.* **2011**, *23*, 3509–3516. [[CrossRef](#)]
263. Zhang, D.; Cao, J.; Zhang, X.; Zeng, Z.; Insin, N.; Qin, J.; Huang, Y. Modification Strategies of Layered Double Hydroxides for Superior Supercapacitors. *Adv. Energy Sustain. Res.* **2022**, *3*, 2100183. [[CrossRef](#)]
264. Malak-Polaczyk, A.; Vix-Guterl, C.; Frackowiak, E. Carbon/Layered Double Hydroxide (LDH) Composites for Supercapacitor Application. *Energy Fuels* **2010**, *24*, 3346–3351. [[CrossRef](#)]
265. Zhang, C.; Zhu, Z.; Zhang, Y.; Shao, W.; Wu, D.; Peng, G.; Liu, Z. Introduction of Bimetallic Oxide-Modified Carbon Nanotubes for Boosting the Energy Storage Performance of NiCo-LDH Based in-Plane Micro-Supercapacitors on Paper. *Chem. Eng. J.* **2024**, *494*, 153242. [[CrossRef](#)]
266. Wang, J.; Ding, Q.; Bai, C.; Wang, F.; Sun, S.; Xu, Y.; Li, H. Synthesis of CNTs/CoNiFe-LDH Nanocomposite with High Specific Surface Area for Asymmetric Supercapacitor. *Nanomaterials* **2021**, *11*, 2155. [[CrossRef](#)] [[PubMed](#)]
267. Chen, H.; Hu, L.; Chen, M.; Yan, Y.; Wu, L. Nickel–Cobalt Layered Double Hydroxide Nanosheets for High-performance Supercapacitor Electrode Materials. *Adv. Funct. Mater.* **2014**, *24*, 934–942. [[CrossRef](#)]
268. Li, L.; Hui, K.S.; Hui, K.N.; Xia, Q.; Fu, J.; Cho, Y.-R. Facile Synthesis of NiAl Layered Double Hydroxide Nanoplates for High-Performance Asymmetric Supercapacitor. *J. Alloys Compd.* **2017**, *721*, 803–812. [[CrossRef](#)]
269. Shah, S.S. Biomass-Derived Carbon Materials for Advanced Metal-Ion Hybrid Supercapacitors: A Step Towards More Sustainable Energy. *Batteries* **2024**, *10*, 168. [[CrossRef](#)]
270. Jayababu, N.; Kim, D. CuCo LDHs Coated CuCoTe Honeycomb-Like Nanosheets as a Novel Anode Material for Hybrid Supercapacitors. *Small* **2021**, *17*, 2102369. [[CrossRef](#)]
271. Zhao, R.; Wang, M.; Zhao, D.; Li, H.; Wang, C.; Yin, L. Molecular-Level Heterostructures Assembled from Titanium Carbide MXene and Ni–Co–Al Layered Double-Hydroxide Nanosheets for All-Solid-State Flexible Asymmetric High-Energy Supercapacitors. *ACS Energy Lett.* **2018**, *3*, 132–140. [[CrossRef](#)]
272. Yang, J.; Yu, C.; Fan, X.; Qiu, J. 3D Architecture Materials Made of NiCoAl-LDH Nanoplates Coupled with NiCo-Carbonate Hydroxide Nanowires Grown on Flexible Graphite Paper for Asymmetric Supercapacitors. *Adv. Energy Mater.* **2014**, *4*, 1400761. [[CrossRef](#)]
273. Jia, H.; Wang, M.; Feng, M.; Li, G.; Li, L.; Liu, Y. Synergistic Enhancement of Supercapacitor Performance: Modish Designation of BPQD Modified NiCo-LDH/NiCo₂S₄ Hybrid Nanotube Arrays with Improved Conductivity and OH[−] Adsorption. *Chem. Eng. J.* **2024**, *484*, 149591. [[CrossRef](#)]
274. Luo, C.-W.W.; Zhang, K.; Zeng, H.-Y.Y.; Yan, W.; Lv, S.-B.B.; Wu, G.-Z.Z. Engineering ZnNi-LDH with Improved Wettability by N-Direct-Doping for High-Performance Supercapacitor. *J. Alloys Compd.* **2025**, *1010*, 177406. [[CrossRef](#)]
275. Wei, X.; Li, M.; Li, L.; Feng, W.; Wu, H. Black Phosphorus Quantum Dots Embedded NiCoCu-LDH with Porous Structure for High-Performance Hybrid Supercapacitor. *Appl. Surf. Sci.* **2025**, *686*, 162203. [[CrossRef](#)]

276. Moradi, M.; Afkhami, A.; Madrakian, T.; Moazami, H.R.; Tirandaz, A. Partial Hydrothermal Sulfidation of Electrosynthesized Co-Mn Layered-Double-Hydroxide as an Active Material for Supercapacitor Applications. *J. Power Sources* **2025**, *629*, 235993. [[CrossRef](#)]
277. Wang, J.; Li, J.; Wang, F.; Zhang, X.; Wu, X.; Zhang, J.; Niu, S.; Chen, L. Introducing Ce into the Interface of NiCo LDH@PBAs to Build Multi Core–Shell Electrode with Superior Stability of Supercapacitor. *Chem. Eng. J.* **2024**, *488*, 150932. [[CrossRef](#)]
278. Hu, W.; Hu, B.; Wu, Z.; Zuo, M.; Song, Y.; Zheng, Q.; Shan, G.; Du, M. Exceeding 50 000 Cycle Durability of Layered Hydroxide-Based Hybrid Supercapacitor Through Scandium Doping-Induced Superlong Activation Process. *Small Struct.* **2024**, *5*, 2300574. [[CrossRef](#)]
279. Chen, R.X.; Cheng, L. Preparation of Flower-Like Layered Double Hydroxides Supercapacitor Cathode Based on Biominerization Strategy. *Key Eng. Mater.* **2024**, *993*, 3–8. [[CrossRef](#)]
280. Bhandari, R.; Shah, R.R. Hydrogen as Energy Carrier: Techno-Economic Assessment of Decentralized Hydrogen Production in Germany. *Renew. Energy* **2021**, *177*, 915–931. [[CrossRef](#)]
281. Terlouw, T.; Bauer, C.; McKenna, R.; Mazzotti, M. Large-Scale Hydrogen Production via Water Electrolysis: A Techno-Economic and Environmental Assessment. *Energy Environ. Sci.* **2022**, *15*, 3583–3602. [[CrossRef](#)]
282. Haque, M.A.; Kawakami, T.; Negishi, Y. Navigating Challenges and Possibilities for Improving Polymer Electrolyte Membrane Fuel Cells via Pt Electrocatalyst, Support and Ionomer Advancements. *Int. J. Hydrogen Energy* **2024**, *85*, 30–47. [[CrossRef](#)]
283. Zhang, B.; Ma, C.; Wang, J.; Zhang, X.; Tu, J. Layered Hydroxides as Electrocatalysts for Water Splitting. In *Metal Oxides and Related Solids for Electrocatalytic Water Splitting*; Elsevier: Amsterdam, The Netherlands, 2022; pp. 241–272, ISBN 9780323857352.
284. Ye, S.; Xu, Y.; Bai, X.; Liang, Z.; Liu, Q.; Wei, Q.; Yang, D.; Yang, W.; Gao, F.; Shi, Q. Efficient Bifunctional Water Splitting Catalysts Enabled by Crystalline-Amorphous Ni_xSy@NiFe LDH Heterojunctions. *J. Mater. Chem. A Mater.* **2025**. [[CrossRef](#)]
285. Xia, X.; Wang, S.; Liu, D.; Wang, F.; Zhang, X.; Zhang, H.; Yu, X.; Pang, Z.; Li, G.; Chen, C.; et al. Electronic Modulation in Cu Doped NiCo LDH/NiCo Heterostructure for Highly Efficient Overall Water Splitting. *Small* **2024**, *20*, 2311182. [[CrossRef](#)]
286. Huo, J.M.; Ma, Z.L.; Wang, Y.; Cao, Y.J.; Jiang, Y.C.; Li, S.N.; Chen, Y.; Hu, M.C.; Zhai, Q.G. Monodispersed Pt Sites Supported on NiFe-LDH from Synchronous Anchoring and Reduction for High Efficiency Overall Water Splitting. *Small* **2023**, *19*, 2207044. [[CrossRef](#)] [[PubMed](#)]
287. Tucker-Quiñónez, A.M.; Rivadeneira-Mendoza, B.F.; Gorozabel-Mendoza, M.L.; Pérez-Almeida, I.B.; García-Guerrero, A.J.; Dueñas-Rivadeneira, A.A.; Yadav, K.K.; Zambrano-Intriago, L.A.; Rodríguez-Díaz, J.M. Challenges and Potential of Layered Double Hydroxides as Electrocatalytic Materials for Hydrogen Production from Water: A Review of Recent Advances and Applications. *Energy Nexus* **2025**, *17*, 100399. [[CrossRef](#)]
288. He, H.; Xiao, J.; Liu, Z.; Yang, B.; Wang, D.; Peng, X.; Zeng, L.; Li, Z.; Lei, L.; Qiu, M.; et al. Boosting the Hydrogen Evolution of Layered Double Hydroxide by Optimizing the Electronic Structure and Accelerating the Water Dissociation Kinetics. *Chem. Eng. J.* **2023**, *453*, 139751. [[CrossRef](#)]
289. Jia, Q.; Liu, E.; Jiao, L.; Li, J.; Mukerjee, S. Current Understandings of the Sluggish Kinetics of the Hydrogen Evolution and Oxidation Reactions in Base. *Curr. Opin. Electrochem.* **2018**, *12*, 209–217. [[CrossRef](#)]
290. Wang, S.; Lu, A.; Zhong, C.J. Hydrogen Production from Water Electrolysis: Role of Catalysts. *Nano Converg.* **2021**, *8*, 4. [[CrossRef](#)]
291. de Chialvo, M.R.G.; Chialvo, A.C. Hydrogen Evolution Reaction: Analysis of the Volmer–Heyrovsky–Tafel Mechanism with a Generalized Adsorption Model. *J. Electroanal. Chem.* **1994**, *372*, 209–223. [[CrossRef](#)]
292. You, H.; Wu, D.; Si, D.; Cao, M.; Sun, F.; Zhang, H.; Wang, H.M.; Liu, T.F.; Cao, R. Monolayer NiIr-Layered Double Hydroxide as a Long-Lived Efficient Oxygen Evolution Catalyst for Seawater Splitting. *J. Am. Chem. Soc.* **2022**, *144*, 9254–9263. [[CrossRef](#)]
293. Jadhav, H.S.; Roy, A.; Desalegan, B.Z.; Seo, J.G. An Advanced and Highly Efficient Ce Assisted NiFe-LDH Electrocatalyst for Overall Water Splitting. *Sustain. Energy Fuels* **2019**, *4*, 312–323. [[CrossRef](#)]
294. Shivakumar, P.; Monika, M.N.; Deepu, M.; Manjunatha Kumara, K.S.; Budagumpi, S.; Nagaraju, D.H. Amorphous and Crystalline Heterostructure MoSe₂/NiFe-LDH through p-n Junction Formation for Electrochemical Water Splitting–Synergistic Back Bonding Effect. *Int. J. Hydrogen Energy* **2024**, *65*, 74–82. [[CrossRef](#)]
295. Liu, G.; Huang, C.; Yang, Z.; Su, J.; Zhang, W. Ultrathin NiMn-LDH Nanosheet Structured Electrocatalyst for Enhanced Electrocatalytic Urea Oxidation. *Appl. Catal. A Gen.* **2021**, *614*, 118049. [[CrossRef](#)]
296. Cao, H.; Liu, B.; Bai, J.; Li, C.; Xu, G. Interfacial Engineering of Hierarchical Ultra-Thin NiCo-LDH Nanosheet Superstructures Nanofiber for Water Cracking Electrocatalysis. *J. Alloys Compd.* **2025**, *1010*, 178041. [[CrossRef](#)]
297. Yan, F.; Guo, D.; Kang, J.; Liu, L.; Zhu, C.; Gao, P.; Zhang, X.; Chen, Y. Fast Fabrication of Ultrathin CoMn LDH Nanoarray as Flexible Electrode for Water Oxidation. *Electrochim. Acta* **2018**, *283*, 755–763. [[CrossRef](#)]
298. Bodhankar, P.M.; Sarawade, P.B.; Singh, G.; Vinu, A.; Dhawale, D.S. Recent Advances in Highly Active Nanostructured NiFe LDH Catalyst for Electrochemical Water Splitting. *J. Mater. Chem. A Mater.* **2021**, *9*, 3180–3208. [[CrossRef](#)]
299. Fu, X.; Liao, H.; Zhang, Z.; Zheng, Y.; Lu, J.; Cheng, S.; Jiang, Y.; Gao, Y. Medium-Entropy Heterostructure of Crystalline NiCoFeP @ Amorphous NiCoFe-LDH for Industrial-Current Density and Ultrastable Overall Water Splitting. *Chem. Eng. J.* **2025**, *505*, 159520. [[CrossRef](#)]

300. Hong, C.; Ji, J.; Huang, J.; Zhang, Y.; Li, L. NiMo/NiFe-LDH Heterostructured Electrocatalyst for Hydrogen Production from Water Electrolysis. *Mater. Lett.* **2025**, *379*, 137664. [[CrossRef](#)]
301. Hou, Y.; Lu, Q.; Guo, Z.; Zhang, Y.; Zhang, Y.; Wan, X.; Lei, L. One-Step Electrodeposition Synthesis of Composites of NiFeMn Alloy and Its Hydroxide as an Efficient Bifunctional Water Splitting Catalyst. *J. Solid. State Chem.* **2025**, *348*, 125356. [[CrossRef](#)]
302. Ye, Z.; Wang, P.; Zhong, W.; Zheng, X.; Cai, W. Active-Site-Enriched Cu-Doped Ni-Fe Layered Double Hydroxide Nanosheets for Boosting the Oxygen Evolution Reaction. *New J. Chem.* **2023**, *47*, 9536–9539. [[CrossRef](#)]
303. Guo, J.; Wang, K.; Zhang, H.; Zhang, H. Enhanced Electrocatalytic Activity of Mo-Doped NiFe Layered Double Hydroxide Nanosheet Arrays for the Hydrogen Evolution Reaction. *ACS Appl. Nano Mater.* **2023**, *6*, 379–389. [[CrossRef](#)]
304. Ding, L.; Li, K.; Xie, Z.; Yang, G.; Yu, S.; Wang, W.; Cullen, D.A.; Yu, H.; Zhang, F.Y. W-Induced Morphological Modification of NiFe Layered Double Hydroxides as Efficient Electrocatalysts for Overall Water Splitting. *Electrochim. Acta* **2021**, *395*, 139199. [[CrossRef](#)]
305. Wang, T.; Zhang, X.; Yu, X.; Li, J.; Wang, K.; Niu, J. Interfacial Interaction in NiFe LDH/NiS₂/VS₂ for Enhanced Electrocatalytic Water Splitting. *Molecules* **2024**, *29*, 951. [[CrossRef](#)] [[PubMed](#)]
306. Udayakumar, A.; Dhandapani, P.; Ramasamy, S.; Angaiah, S. Layered Double Hydroxide (LDH)—MXene Nanocomposite for Electrocatalytic Water Splitting: Current Status and Perspective. *ES Energy Environ.* **2023**, *20*, 902. [[CrossRef](#)]
307. Jia, Y.; Zhang, L.; Gao, G.; Chen, H.; Wang, B.; Zhou, J.; Soo, M.T.; Hong, M.; Yan, X.; Qian, G.; et al. A Heterostructure Coupling of Exfoliated Ni-Fe Hydroxide Nanosheet and Defective Graphene as a Bifunctional Electrocatalyst for Overall Water Splitting. *Adv. Mater.* **2017**, *29*, 1700017. [[CrossRef](#)]
308. Yao, L.; Li, R.; Zhang, H.; Humayun, M.; Xu, X.; Fu, Y.; Nikiforov, A.; Wang, C. Interface Engineering of NiTe@CoFe LDH for Highly Efficient Overall Water-Splitting. *Int. J. Hydrogen Energy* **2022**, *47*, 32394–32404. [[CrossRef](#)]
309. Wang, J.; Lv, G.; Wang, C. A Highly Efficient and Robust Hybrid Structure of CoNiN@NiFe LDH for Overall Water Splitting by Accelerating Hydrogen Evolution Kinetics on NiFe LDH. *Appl. Surf. Sci.* **2021**, *570*, 151182. [[CrossRef](#)]
310. Kalusulingam, R.; Mariyaselvakumar, M.; Antonyraj, C.A.; Mathi, S.; Mikhailova, T.S.; Khubezhov, S.A.; Pankov, I.V.; Srinivasan, K.; Myasoedova, T.N. Highly Efficient Water Splitting with Pd-Integrated NiAl-LDH Nanosheets as Bifunctional Electrocatalysts. *Energy Fuels* **2023**, *37*, 13319–13330. [[CrossRef](#)]
311. Zhai, P.; Zhang, Y.; Wu, Y.; Gao, J.; Zhang, B.; Cao, S.; Zhang, Y.; Li, Z.; Sun, L.; Hou, J. Engineering Active Sites on Hierarchical Transition Bimetal Oxides/Sulfides Heterostructure Array Enabling Robust Overall Water Splitting. *Nat. Commun.* **2020**, *11*, 5462. [[CrossRef](#)]
312. Das, M.; Khan, Z.B.; Biswas, A.; Dey, R.S. Inter-Electronic Interaction between Ni and Mo in Electrodeposited Ni-Mo-P on 3D Copper Foam Enables Hydrogen Evolution Reaction at Low Overpotential. *Inorg. Chem.* **2022**, *61*, 18253–18259. [[CrossRef](#)]
313. Govind Rajan, A.; Carter, E.A. Microkinetic Model for pH- And Potential-Dependent Oxygen Evolution during Water Splitting on Fe-Doped β -NiOOH. *Energy Environ. Sci.* **2020**, *13*, 4962–4976. [[CrossRef](#)]
314. Wang, Y.; Zhang, M.; Liu, Y.; Zheng, Z.; Liu, B.; Chen, M.; Guan, G.; Yan, K. Recent Advances on Transition-Metal-Based Layered Double Hydroxides Nanosheets for Electrocatalytic Energy Conversion. *Adv. Sci.* **2023**, *10*, 2207519. [[CrossRef](#)] [[PubMed](#)]
315. Ge, Z.Q.; Li, J.; Zhang, H.J.; Liu, C.; Che, G.; Liu, Z.Q. p-d Orbitals Coupling Heterosites of Ni₂P/NiFe-LDH Interface Enable O-H Cleavage for Water Splitting. *Adv. Funct. Mater.* **2024**, *34*, 2411024. [[CrossRef](#)]
316. Zheng, K.; Ren, J.; Li, X.; Li, G.; Jiao, L.; Xu, C. Engineering Crystalline CoMP-Decorated (M = Mn, Fe, Ni, Cu, Zn) Amorphous CoM LDH for High-Rate Alkaline Water Splitting. *Chem. Eng. J.* **2022**, *441*, 136031. [[CrossRef](#)]
317. Feng, Y.; Smith, R.L.; Shen, F.; Qi, X. Structure-Oriented Electrochemical Synthesis of Layered Double Hydroxide Electrocatalytic Materials for 5-Hydroxymethylfurfural Oxidation. *ACS Sustain. Chem. Eng.* **2024**, *12*, 16905–16913. [[CrossRef](#)]
318. Yi, W.; Yu, R.; Jiang, H.; Wu, J.; Cheng, G.J. Unveiling the Synergistic Potential of Laser Chemical Solid-Phase Deposition of Atomic Platinum-Metal Layer on 2D Materials for Bifunctional Catalysts. *Adv. Funct. Mater.* **2024**, *34*, 2308575. [[CrossRef](#)]
319. Xiong, T.; Zhu, Z.; He, Y.; Balogun, M.-S.; Huang, Y. Phase Evolution on the Hydrogen Adsorption Kinetics of NiFe-Based Heterogeneous Catalysts for Efficient Water Electrolysis. *Small Methods* **2023**, *7*, 2201472. [[CrossRef](#)]
320. Zhai, Z.; Li, H.; Zhou, C.; Zheng, H.; Liu, Y.; Yan, W.; Zhang, J. Anisotropic Strain Boosted Hydrogen Evolution Reaction Activity of F-NiCoMo LDH for Overall Water Splitting. *J. Electrochem. Soc.* **2023**, *170*, 036509. [[CrossRef](#)]
321. Rosely, C.V.S.; John, H. Role of Surfactants on Electrocatalytic Activity of Co/Al Layered Double Hydroxides for Hydrogen and Oxygen Generation. *ChemCatChem* **2025**, *17*, 2401377. [[CrossRef](#)]
322. Wang, J.; Wei, X.; Song, W.; Shi, X.; Wang, X.; Zhong, W.; Wang, M.; Ju, J.; Tang, Y. Plasmonic Enhancement in Water Splitting Performance for NiFe Layered Double Hydroxide-N₁₀TC MXene Heterojunction. *ChemSusChem* **2021**, *14*, 1948–1954. [[CrossRef](#)]
323. Xi, C.; Ding, W.; Jiang, J.; Wang, Y.; Wang, S.; Zhang, Z.; Han, S. Unveiling the CoFe LDH Generated by Partial in Situ Conversion Strategy: Synergistic Effect of Modified MXene and Cationic Vacancies for Overall Water Splitting. *Fuel* **2024**, *370*, 131844. [[CrossRef](#)]
324. Shen, B.; Huang, H.; Jiang, Y.; Xue, Y.; He, H. 3D Interweaving MXene–Graphene Network–Confined Ni–Fe Layered Double Hydroxide Nanosheets for Enhanced Hydrogen Evolution. *Electrochim. Acta* **2022**, *407*, 139913. [[CrossRef](#)]

325. Luo, H.; Liu, C.; Chen, N.; Xue, K.; Yu, L.; Zhu, H.; Zhang, Y. Metal-Organic Frameworks Derived NiFe-Hydroxides for Efficient Electrocatalytic Hydrogen Evolution. *Adv. Comput. Mater. Sci. Res.* **2024**, *1*, 192. [[CrossRef](#)]
326. Lee, E.; Jeong, S.; Jeong, Y.; Kim, B.; Lee, K. Nanoscale-Confining Synthesis of 2D Metal Compounds for Electrochemical Applications. *Small Methods* **2025**, *9*, 2301782. [[CrossRef](#)] [[PubMed](#)]
327. Liu, J.; Zheng, K.; Hua, Y.; Peng, L.; Meng, X.; Zhang, C.; Su, R.; Tao, X.; Hu, H.; Guo, Y.; et al. LDHs and Their Derivatives for Electrochemical Energy Storage and Conversion Systems: Design, Insights and Applications. *ChemElectroChem* **2024**, *11*, e202400156. [[CrossRef](#)]
328. Yao, Y.; Zou, C.; Sun, S.; Guo, Y.; Hong, S.; Cai, Z.; Yang, C.; Zhuang, W.; Luo, F.; Hamdy, M.S.; et al. Ultrastable Seawater Oxidation at Ampere-level Current Densities with Corrosion-resistant $\text{CoCO}_3/\text{CoFe}$ Layered Double Hydroxide Electrocatalyst. *Small* **2025**, *21*, 2409627. [[CrossRef](#)]
329. Ding, L.; Shen, Z.; Pan, H.; Chen, Y.; Hu, Y.; Zhao, G.; Hai, G.; Huang, X. Regulating Intermediate Adsorption and Promoting Charge Transfer of CoCr-LDHs by Ce Doping for Enhancing Electrooxidation of 5-Hydroxymethylfurfural. *Small* **2025**, *21*, 2409343. [[CrossRef](#)]
330. Chen, Y.; Zhang, Y.; Bai, X.; Zhao, J.; Yang, L.; Wang, X.; Wu, Q.; Hu, Z. Interlayer Engineering of Layered Double Hydroxides for Advanced Energy Storage and Conversion. *FlatChem* **2024**, *48*, 100775. [[CrossRef](#)]
331. Wang, Y.; Ying, Z.; Gao, Y.; Shi, L. Layered Double Hydroxide Nanosheets: Synthesis Strategies and Applications in the Field of Energy Conversion. *Chem. Eur. J.* **2024**, *30*, e202303025. [[CrossRef](#)]
332. Zhou, X.; Hou, Z.; Zhang, H.-Y.; Yu, J. Synergistic Coupling of NiVAl-Layered Double Hydroxide with Few-Layered $\text{Ti}_3\text{C}_2\text{T}_x$ -MXene Nanosheets for Superior Asymmetric Supercapacitor Performance. *J. Mater. Chem. C Mater.* **2023**, *11*, 15571–15580. [[CrossRef](#)]
333. Jaramillo Hernández, C.; Oestreicher, V.; Mizrahi, M.; Abellán, G. An In-Situ Study of the Transformation of Hybrid Layered Hydroxides into Metallic Nanocomposites with Interest in Energy Storage Systems. In Proceedings of the ECS Meeting Abstracts 2023, Boston, MA, USA, 28 May–2 June 2023; Volume MA2023-01, p. 1322. [[CrossRef](#)]
334. Sun, X.; Chen, H.; Li, Y.; Zeng, D.; Qiu, P.; Zeng, H.; Ji, X.; Chen, L.; Shi, X. Efficient Harvesting Waste Heat by Zn-Ion Battery Under Thermally Regenerative Electrochemical Cycles. *Adv. Mater.* **2025**, *37*, 2418482. [[CrossRef](#)]
335. Abu Nayem, S.M.; Hardianto, Y.P.; Shuaibu, A.D.; Shah, S.S.; Islam, S.; Jafar Mazumder, M.A.; Aziz, M.A.; Saleh Ahammad, A.J. Biomass Derived Amino Acid Assisted Synthesis of FeNi Layered Double Hydroxide for Efficient Oxygen Evolution Reaction. *Inorg. Chem. Commun.* **2025**, *171*, 113574. [[CrossRef](#)]

Disclaimer/Publisher’s Note: The statements, opinions and data contained in all publications are solely those of the individual author(s) and contributor(s) and not of MDPI and/or the editor(s). MDPI and/or the editor(s) disclaim responsibility for any injury to people or property resulting from any ideas, methods, instructions or products referred to in the content.